THE ROLE OF CILIARY VORTICES ON THE CORAL'S OXYGEN EXCHANGE AND FOOD CAPTURE

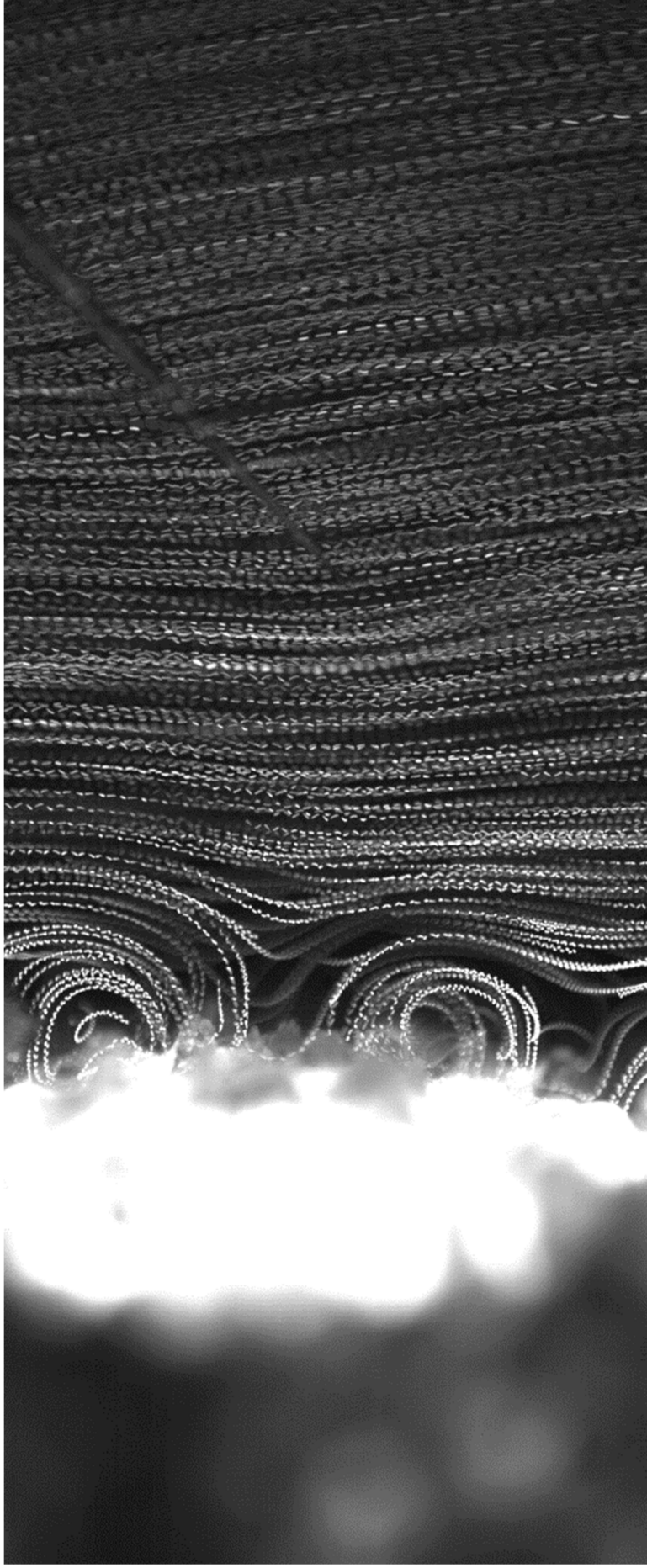

Cesar O. **Pacherres**

Universität Bremen

Universität Bremen

The role of ciliary vortices on the coral's oxygen exchange and food capture

Dissertation

In partial fulfilment of the requirements for the degree of

Doctor of natural sciences

– Dr. rer. nat. –

Faculty of Biology / Chemistry

University of Bremen

Submitted by

Cesar Omar Pacherres Reaño

July - 2021

The present study was carried out from January 2017 to July 2021 at the Alfred-Wegener-Institute, Helmholtz Center for Polar and Marine Research (AWI), Bremerhaven, Germany. Additional logistical and instrumental support was given by the Max Planck Institute for Marine Microbiology, Bremen, Germany. It was financed by the AWI and FONDECYT, initiative from the *Consejo Nacional de Ciencia, Tecnología e Innovación Tecnológica* (CONCYTEC), *Perú*.

Date of the doctoral colloquium: 22.09.2021

Examination committee

1st Examiner:	Prof. Dr. Claudio Richter Bentho-Pelagic Processes, Alfred Wegener Institute, Helmholtz Center for Polar and Marine Research Bremerhaven, Germany
2nd Examiner:	Prof. Dr. Michael Kühl Marine Biological Laboratory, University of Copenhagen Helsingør, Denmark
3rd Examiner:	Dr. Eva-Maria Zetsche Ludwig-Maximilians-Universität München Munich, Germany
1st Additional Examiner:	Prof. Dr. Tilmann Harder Department of Marine Chemistry, University of Bremen Bremen, Germany
2nd Additional Examiner:	Dr. Andreas Kunzmann WG Experimental Aquaculture, Leibniz Center for Tropical Marine Research Bremen, Germany
1st student member:	M.Sc. Nur Garcia Herrera Dr. candidate, Alfred Wegener Institute, Helmholtz Center for Polar and Marine Research Bremerhaven, Germany
2nd student member:	Alexandra Lago M.Sc. Marine Biology student, University of Bremen Bremen, Germany

A mis padres...

Table of contents

Summary

Tropical shallow corals live in a highly dynamic environment dominated by wave action with water currents ruling over their physiological processes. Due to their relatively small size and lack of mobility, they will interact with the water column via a so called diffusive boundary layer (DBL), a layer of water located at the immediate surface of the coral and where molecular diffusion is the dominant transport mechanism for solutes. All elements needed to ensure the functioning of the coral, and its symbiotic algae, must traverse this layer in order to either reach or leave the coral tissue. Thus, the recent discovery that corals possess the ability to enhance mass transport in the DBL by the generation of vortices caused by the beating of epidermal cilia, opened several questions as of the extent of their effect on the coral's ecophysiological processes. **The aim of this thesis** is to better understand the role which ciliary vortices play on the dynamics of the coral boundary layer by studying how these currents intervene in elemental and particle transport processes along the autotrophic and heterotrophic pathways of the coral holobiont.

For this purpose, and using a flow-through chamber specifically created for this project (**Chapter 2**), oxygen (using electrochemical microsensors) and flow dynamics (by Particle image Velocimetry – PIV – and Particle Tracking Velocimetry) were measured at the boundary layer of the massive coral *Porites lutea* under different flow speeds and light conditions (**Chapter 3**). Results show that, regardless of the flow speed of the water column, ciliary vortices mitigate extreme oxygen concentrations close to the tissue surface during both oxygen production and consumption. Moreover, the ciliary redistribution of oxygen had no effect on the oxygen flux across the upper DBL further proving that the benefit of vortex mixing is the reduction of oxygen as part of a homeostatic control mechanism, which may play a crucial role in the coral's relationship with its symbionts and response to environmental stress. However, the ability of ciliary vortices to enhance mass transport was not homogeneous along the coral surface as it depended upon the characteristics of the vortex itself and their location along the coral surface (**Chapter 3**). In order to better observe and understand these heterogeneities, PIV (using oxygen sensitive nanoparticles –sensPIV **Chapter 4**), together chlorophyll-sensitive hyperspectral imaging (used to map the μ-metric distribution of chlorophyll inside the coral tissue) were applied for the first time on a coral colony (**Chapter 5**). Results showed that high chlorophyll areas (septa and coenosarc) were situated outside the vortex structures, while low chlorophyll areas (mouth openings) were situated underneath the vortex suggesting the coupling of ciliary beatings with these areas of high chlorophyll as means to ventilate them and consequently promote the efflux of oxygen out of the tissue (**Chapter 5**). A mechanism that might be of particular importance in order to mitigate oxygen accumulation inside the tissue containing high chlorophyll concentrations, thus preventing the detrimental consequences of oxygen accumulation (i.e. inhibition of photosynthesis).

These small surface currents played important roles not only by boosting chemical mass transport towards and away from the tissue but also by intervening in the coral's interaction with suspended prey elements. As described in **Chapter 6**, the vortices generated by the beating of cilia are also key to the coral's heterotrophic nutrition. These currents enhanced the capture of tiny particles by mucus filaments, providing the first mechanistic explanation for ultraplankton capture in scleractinian corals. Given that heterotrophic feeding provides a safe route in the recovery of corals to bleaching events, their ability to enhance the capture of a highly abundant food source might therefore have important implications when facing climatic stressors. Moreover, the creation of these feeding currents by cilia beating call for a review on the trophic classification of corals – long considered passive suspension feeders – as the results presented here showed they could rather be classified as filter feeders together with mollusks and sponges.

Overall, this thesis contributes to the understanding of small-scale variations in the physicochemical and hydrodynamic microenvironment of corals created by the interaction of ciliary vortices and the surrounding water, providing essential mechanistic insights in areas such as symbiotic relationships, micro-heterotrophy and stress response. The complex symbiont-host relationships and the internal and external physicochemical heterogeneities observed here may well represent a source of buffering and acclimation for corals, and thus resilience to environmental stresses. The question that now arises is: how – or rather if – these mechanisms will contribute to the adaptation of coral reefs to an accelerated anthropogenic climate change. The novel tools developed and uniquely combined here proved suitable to address such a question and can in the future shed new light on the underlying processes of stress exposure.

Zusammenfassung

Tropische Flachwasserkorallen leben in einer sehr dynamischen Umwelt, die von Wellenbewegungen und Wasserströmung dominiert wird. Beides hat einen starken Einfluss auf die physiologischen Prozesse der Korallen. Aufgrund ihrer relativ geringen Größe und mangelnden Mobilität interagieren sie mit der Wassersäule über eine sogenannte diffusive Grenzschicht (DBL). Die DBL ist eine Wasserschicht, die sich an der unmittelbaren Oberfläche der Koralle befindet und in der die molekulare Diffusion der dominierende Transportmechanismus für gelöste Stoffe ist. Alle Elemente, die für das Funktionieren der Koralle und ihrer symbiotischen Algen benötigt werden, müssen diese Schicht durchqueren, um entweder das Korallengewebe zu erreichen oder dieses zu verlassen. Die neuste Entdeckung, dass Korallen die Fähigkeit besitzen, den Stofftransport innerhalb der DBL durch das Schlagen von Zilien effektiv zu verändern, warf daher einige Fragen über das Ausmaß ihrer Wirkung auf die ökophysiologischen Prozesse der Koralle auf. **Das Ziel dieser Arbeit** ist es besser zu verstehen welche Rolle die Zilienwirbel auf die Dynamik der Korallengrenzschicht spielen, indem untersucht wird, wie diese Strömungen in Element- und Partikeltransportprozesse entlang der autotrophen und heterotrophen Pfade des Korallenholobionten eingreifen.

Zu diesem Zweck und unter Verwendung einer speziell für dieses Projekt gebauten Durchflusskammer (**Kapitel 2**) wurde die Sauerstoffkonzentration (mit elektrochemischen Mikrosensoren) und die Strömungsdynamik (mittels ‚Particle Image Velocimetry' – PIV – und ‚Particle Tracking Velocimetry') an der Grenzschicht der massiven Koralle Porites lutea unter verschiedenen Strömungsgeschwindigkeiten und Lichtbedingungen gemessen (**Kapitel 3**). Die Ergebnisse zeigen, dass, unabhängig von der Strömungsgeschwindigkeit des Wasserkörpers, Wirbelströmungen die extremen Sauerstoffkonzentrationen nahe der Gewebeoberfläche infolge der Sauerstoffproduktion als auch beim Sauerstoffverbrauch abmildern. Darüber hinaus hatte die Umverteilung des Sauerstoffs durch die Zilien keine Auswirkung auf den Sauerstofffluss in den oberen DBL Schichten. Dies beweist, dass der Nutzen der Wirbelmischung in der Reduktion des Sauerstoffs als Teil eines homöostatischen Kontrollmechanismus besteht. Dieser kann somit eine entscheidende Rolle in der Beziehung der Koralle zu ihren Symbionten sowie in der Reaktion auf Umweltstress spielen. Die Fähigkeit der Zilien, den Stofftransport zu verbessern, war jedoch nicht homogen entlang der Korallenoberfläche verteilt. Sie hing einerseits von den Eigenschaften des Wirbels selbst und andererseits ihrer Position entlang der Korallenoberfläche ab (**Kapitel 3**). Um diese Heterogenitäten besser zu beobachten und zu verstehen, wurde die PIV (unter Verwendung von sauerstoffsensitiven Nanopartikeln -sensPIV **Kapitel 4**), zusammen mit Chlorophyll-sensitiver Hyperspektral-Bildgebung (verwendet, um die µ-metrische Verteilung von Chlorophyll innerhalb des Korallengewebes abzubilden) zum ersten Mal auf eine

Korallenkolonie angewendet (**Kapitel 5**). Die Ergebnisse zeigten, dass Bereiche mit hohem Chlorophyllgehalt (Septen und Coenosark) außerhalb der Wirbelstrukturen lagen, während Bereiche mit niedrigem Chlorophyllgehalt (Mundöffnungen) unterhalb des Wirbels lagen, was auf die Kopplung von Zilienschlägen mit den Bereichen mit hohem Chlorophyllgehalt hindeutet, um diese zu belüften und folglich den Abfluss von Sauerstoff aus dem Gewebe zu fördern (**Kapitel 5**). Ein Mechanismus, der von besonderer Bedeutung sein könnte, um die Sauerstoffanreicherung innerhalb des Gewebes mit hohen Chlorophyllkonzentrationen abzuschwächen und so die schädlichen Folgen der Sauerstoffanreicherung und damit Hemmung der Photosynthese zu verhindern.

Diese kleinen Oberflächenströmungen können zudem eine wichtige Rolle in der Energiegewinnung durch Beutefang spielen. Es ist anzunehmen, dass sie nicht nur den chemischen Massentransport zum Gewebe hin und weg fördern, sondern auch in die Interaktion der Koralle mit schwebenden Beuteteilchen eingreifen. Wie in **Kapitel 6** beschrieben, sind die Wirbel, die durch das Schlagen der Zilien erzeugt werden, auch der Schlüssel zur heterotrophen Ernährung der Korallen. Diese Strömungen verstärkten das Einfangen von winzigen Partikeln durch Schleimfilamente und lieferten die erste mechanistische Erklärung für das Einfangen von Ultraplankton in skelettbildenden Korallen. In Anbetracht der Tatsache, dass heterotrophe Fütterung maßgebend für die Erholung von Korallen nach Bleichereignissen ist, wird ihre Fähigkeit eine reichhaltige Nahrungsquelle zu beschaffen wichtige Implikationen im Hinblick auf klimatischen Stressoren haben. Darüber hinaus erfordert die Erzeugung dieser Futterströme durch das Schlagen der Cilien eine Überprüfung der trophischen Klassifizierung von Korallen. Lange Zeit wurden sie als passive Suspensionsfresser betrachtet. Die hier vorgestellten Ergebnisse zeigen jedoch, dass sie auch als Filterfresser zusammen mit Mollusken und Schwämmen klassifiziert werden könnten.

Insgesamt trägt diese Arbeit zum Verständnis der kleinskaligen Variationen in der physikochemischen und hydrodynamischen Mikroumgebung von Korallen bei, die durch die Interaktion von Zilienströmen und dem sie umgebenden Wasser entstehen. Sie liefert wesentliche mechanistische Erkenntnisse in Bereichen der Interkation zwischen Korallen und ihrer Symbionten, der Nahrungsbeschaffung sowie Stressreaktion. Die komplexen Beziehungen zwischen Symbionten und Wirt und die beobachteten internen und externen physikochemischen Heterogenitäten der Koralle könnten sehr wohl die Quelle für Pufferung und Akklimatisierung und damit Widerstandsfähigkeit gegenüber Umweltbelastungen sein. Die Frage, die sich nun stellt, ist: Wie, oder vielmehr ob, diese Mechanismen zur Akklimatisierung und Anpassung von Korallenriffen an einen beschleunigten anthropogenen Klimawandel beitragen können? Die hier entwickelten und einzigartig kombinierten Methoden erweisen sich als geeignet, dieser aktuellen Frage nachzugehen und können zukünftig neues Licht auf die zugrunde liegenden Prozesse unter Stressbedingungen werfen.

Resumen

Los corales tropicales de aguas someras viven en un entorno muy dinámico dominado por la acción de las olas y en el que las corrientes de agua rigen sus procesos fisiológicos. Debido a su tamaño relativamente pequeño y a su falta de movilidad, interactúan con la columna de agua a través de la llamada capa límite difusiva (DBL-por sus siglas en ingles), una capa de agua situada en la superficie inmediata del coral donde la difusión molecular es el mecanismo de transporte dominante para los solutos. Todos los elementos necesarios para el funcionamiento del coral y de sus algas simbióticas deben atravesar esta capa para llegar o salir del tejido coralino. Es por esto que el reciente descubrimiento de que los corales poseen la capacidad de mejorar el transporte de masa en la DBL mediante la generación de vórtices causados por el batido de los cilios epidérmicos, abrió varios interrogantes sobre el alcance de su efecto en los procesos ecofisiológicos del coral. **El objetivo de esta tesis** es comprender mejor el papel que desempeñan los vórtices ciliares en la dinámica de la capa límite del coral, estudiando cómo estas corrientes intervienen en los procesos de transporte de elementos y partículas a lo largo de las vías autotróficas y heterotróficas del holobionte coralino.

Para ello, y utilizando una cámara de flujo creada específicamente para este proyecto (**Capítulo 2**), se midió el oxígeno (mediante microsensores electroquímicos) y la dinámica del flujo (mediante Velocimetría de Imagen de Partículas – PIV por sus siglas en inglés – y Velocimetría de Seguimiento de Partículas) en la capa límite del coral masivo *Porites lutea* bajo diferentes velocidades de flujo y condiciones de luz (**Capítulo 3**). Los resultados muestran que, independientemente de la velocidad de flujo en la columna de agua, los flujos vorticales mitigan las concentraciones extremas de oxígeno cerca de la superficie del tejido tanto durante la producción como el consumo de oxígeno. Además, la redistribución ciliar del oxígeno no tuvo ningún efecto sobre el flujo de oxígeno que atraviesa la parte superior de la DBL, lo que demuestra que el beneficio de la mezcla vortical es la reducción del oxígeno como parte de un mecanismo de control homeostático, que puede desempeñar un papel crucial en la relación del coral con sus simbiontes y la respuesta al estrés ambiental. Sin embargo, la capacidad de los cilios para mejorar el transporte de masa no fue homogénea a lo largo de la superficie del coral, ya que dependía de las características propias del vórtice y de su ubicación a lo largo de la superficie del coral (**capítulo 3**). Para observar y comprender mejor estas heterogeneidades, se aplicó por primera vez en una colonia de coral la PIV (utilizando nanopartículas sensibles al oxígeno -sensPIV **Capítulo 4**), junto con imágenes hiperespectrales sensibles a la clorofila (utilizadas para cartografiar la distribución μ-métrica de la clorofila en el interior del tejido coralino) (**Capítulo 5**). Los resultados mostraron que las zonas de alta clorofila (septos y coenosarcos) estaban situadas fuera de las estructuras de vórtice, mientras que las zonas de baja clorofila (aberturas bucales) estaban situadas debajo del vórtice, lo que sugiere el acoplamiento de los batidos. ciliares con las zonas de alta clorofila como medio para ventilarlas y, en consecuencia, promover el eflujo

de oxígeno fuera del tejido Este mecanismo podría ser de especial importancia para mitigar la acumulación de oxígeno dentro del tejido que contenga altas concentraciones de clorofila, evitando así las consecuencias perjudiciales de la acumulación de oxígeno (es decir, la inhibición de la fotosíntesis).

Estas pequeñas corrientes superficiales desempeñan un papel importante no sólo al impulsar el transporte de elementos químicos hacia y desde el tejido, sino también al intervenir en la interacción del coral con su presa en suspensión. Como se describe en el **capítulo 6**, los vórtices generados por el batir de los cilios también son clave para la nutrición heterótrofa de los corales. Estas corrientes potencian la captura de partículas diminutas por parte de los filamentos de mucus, lo que proporciona la primera explicación mecanicista de la captura de ultraplancton en los corales escleractinios. Dado que la alimentación heterótrofa proporciona una vía segura en la recuperación de los corales ante eventos de blanqueamiento, la capacidad de estos para fomentar la captura de una fuente de alimento muy abundante tendrá, por tanto, importantes consecuencias cuando se enfrenten a estresores climáticos. Además, la creación de estas corrientes de alimentación mediante el batido de los cilios exige una revisión de la clasificación trófica de los corales – considerados durante mucho tiempo como suspensívoros pasivos – dado que los resultados presentados aquí demuestran que más bien podrían clasificarse como filtradores junto con los moluscos y las esponjas.

En conjunto, esta tesis contribuye a la comprensión de las variaciones a pequeña escala en el microambiente físico-químico e hidrodinámico de los corales, creadas por la interacción de los flujos ciliares y el agua que los rodea, proporcionando conocimientos mecanísticos esenciales en áreas como las relaciones simbióticas, la micro-heterotrofia y la respuesta al estrés. Las complejas relaciones entre los simbiontes y el huésped y las heterogeneidades fisicoquímicas internas y externas aquí observadas podrían, muy bien, representar una fuente de amortiguación y aclimatación para los corales, y por tanto de resistencia a las presiones ambientales. La pregunta que deberíamos plantearnos ahora es: De qué manera – o más bien sí – estos mecanismos contribuirán a la adaptación de los arrecifes de coral al acelerado cambio climático al que están expuestos. Las herramientas desarrolladas y combinadas de forma única para la realización de esta tesis han demostrado ser adecuadas para abordar esta pregunta y de esta manera tener los medios para, en el futuro, arrojar nueva luz sobre los procesos subyacentes de la exposición al estrés.

Résumé

Les coraux tropicaux peu profonds vivent dans un environnement très dynamique dominé par l'action des vagues où les courants d'eau régissent leurs processus physiologiques. En raison de leur taille relativement petite et de leur manque de mobilité, ils interagissent avec la colonne d'eau par l'intermédiaire de la couche limite diffusive (DBL pour *Diffuse Boundary Layer*), une couche d'eau située à la surface immédiate du corail, où la diffusion moléculaire est le mécanisme de transport dominant pour les solutés. Tous les éléments nécessaires au fonctionnement du corail, et de ses algues symbiotiques, doivent traverser cette couche pour atteindre ou quitter le tissu corallien. Ainsi, la découverte récente que les coraux possèdent la capacité d'améliorer le transport de masse dans la DBL par la génération de tourbillons causés par le battement des cils épidermiques, a ouvert plusieurs questions quant à l'étendue de leur effet sur les processus écophysiologiques du corail. **L'objectif de cette thèse** est de mieux comprendre le rôle que jouent les tourbillons ciliaires sur la dynamique de la couche limite du corail en étudiant comment ces courants interviennent dans les processus de transport d'éléments et de particules le long des voies autotrophes et hétérotrophes de l'holobionte corallien.

Dans ce but, et grâce à une chambre d'écoulement spécialement créée pour ce projet (**chapitre 2**), l'oxygène (à l'aide de micro-capteurs électrochimiques) et la dynamique des fluides (par vélocimétrie d'image de particules – PIV pour *Particle Image Velocimetry* – et vélocimétrie de suivi des particules) ont été mesurés au niveau de la couche limite du corail massif *Porites lutea* sous différentes vitesses d'écoulement et conditions de lumière (**chapitre 3**). Les résultats montrent que, quelle que soit la vitesse d'écoulement de la colonne d'eau, les flux tourbillonnaires atténuent les concentrations extrêmes d'oxygène près de la surface des tissus, tant pendant la production que pendant la consommation d'oxygène. En outre, la redistribution ciliaire de l'oxygène n'a eu aucun effet sur le flux d'oxygène à travers la partie supérieure de la DBL, ce qui prouve que l'avantage du mélange tourbillonnaire est la réduction de l'oxygène dans le cadre d'un mécanisme de contrôle homéostatique, qui peut jouer un rôle crucial dans la relation du corail avec ses symbiotes et dans sa réponse au stress environnemental. Cependant, la capacité des cils à améliorer le transport de masse n'est pas homogène le long de la surface du corail car elle dépend des caractéristiques du vortex lui-même et de leur emplacement le long de la surface du corail (**chapitre 3**). Afin de mieux observer et comprendre ces hétérogénéités, la PIV (utilisant des nanoparticules sensibles à l'oxygène -sensPIV **Chapitre 4**), ainsi que l'imagerie hyperspectrale sensible à la chlorophylle (utilisée pour cartographier la distribution µ-métrique de la chlorophylle à l'intérieur du tissu corallien) ont été appliquées pour la première fois sur une colonie corallienne (**Chapitre 5**). Les résultats ont montré que les zones à forte teneur en chlorophylle (septa et coenosarc) étaient situées à l'extérieur des structures tourbillonnaires, tandis que les zones à faible teneur en chlorophylle (ouvertures de la bouche) étaient situées sous le tourbillon, suggérant le couplage des battements ciliaires avec les zones à forte teneur

en chlorophylle comme moyen de les ventiler et par conséquent de favoriser l'efflux d'oxygène hors du tissu (**Chapitre 5**). Un mécanisme qui pourrait être particulièrement important pour atténuer l'accumulation d'oxygène à l'intérieur du tissu contenant de fortes concentrations de chlorophylle, prévenant ainsi les conséquences néfastes de l'accumulation d'oxygène (c'est-à-dire l'inhibition de la photosynthèse).

Ces petits courants de surface joueront un rôle important non seulement en stimulant le transport de masse chimique vers et depuis le tissu, mais aussi en intervenant dans l'interaction du corail avec les éléments proies en suspension. Comme décrit au **chapitre 6**, les tourbillons générés par le battement des cils sont également essentiels à la nutrition hétérotrophe des coraux. Ces courants ont favorisé la capture de minuscules particules par les filaments de mucus, fournissant ainsi la première explication mécaniste de la capture de l'ultraplankton chez les coraux scléractiniaires. Étant donné que l'alimentation hétérotrophe constitue pour les coraux une voie sûre de récupération après des événements de blanchiment, leur capacité à améliorer la capture d'une source de nourriture très abondante aura donc des implications importantes face aux facteurs de stress climatiques. De plus, la création de ces courants alimentaires par le battement des cils appelle à une révision de la classification trophique des coraux - longtemps considérés comme des suspensivores passifs - les résultats présentés ici ont montré qu'ils pourraient plutôt être classés comme des filtreurs avec les mollusques et les éponges.

Globalement, cette thèse contribue à la compréhension des variations à petite échelle du microenvironnement physico-chimique et hydrodynamique des coraux, créées par l'interaction des flux ciliaires et de l'eau environnante, fournissant des informations essentielles dans des domaines tels que les relations symbiotiques, la micro-hétérotrophie et la réponse au stress. Les relations symbiotes-hôtes complexes et les hétérogénéités physico-chimiques internes et externes observées ici pourraient bien représenter une source d'amortissement et d'acclimatation pour les coraux, et donc de résilience aux stress environnementaux. La question qui se pose maintenant est la suivante : comment ces mécanismes contribueront-t-ils à l'adaptation des récifs coralliens à un changement climatique anthropique accéléré? Les nouveaux outils développés et combinés de manière unique ici se sont avérés appropriés pour répondre à cette question et peuvent à l'avenir apporter un nouvel éclairage sur les processus sous-jacents à l'exposition au stress.

1

General Introduction

Tropical shallow coral reefs are among the most productive ecosystems on the planet (Grigg et al. 1984) and, as such, they sustain a complex web of interactions that extends far beyond the coastal oceans (Wild et al. 2004, de Goeij et al. 2013, Brandl et al. 2019). It is because of their association with dinoflagellate algae (see Box 1 for an understanding of the coral's biology) that they are positioned at the base of the food web, as their symbionts convert carbon dioxide into biomass via photosynthesis (Yonge et al. 1932). Although light provides the energy that fuels reef productivity, other important elements, such as carbon dioxide, oxygen, nutrients, trace elements, must either reach or leave the coral tissue in order to ensure the functioning of the coral-algae association (also known as holobiont) (Muscatine 1973, Crawley et al. 2010). In this extent, the rate of transfer of these essential elements, towards and away from the colony, can have profound effects not only on the coral's productivity, but also on its health and, by extension, on the health of the communities that depend on the reefs. At a colony level, and due to the lack of respiratory organs, the mass transfer of elements is believed to be at the mercy of environmental water currents (a highly fluctuating factor) acting on passive diffusion (Kühl et al. 1995, de Beer et al. 2000). However, corals also possess a series of hair-like structures, located at the surface of their tissue, called cilia. Their rapid movement have the ability to stir the adjacent water with profound implications on mass transfer (Shapiro et al. 2014) and possibly food capture. The aim of this introduction is to provide information on the coral's environment with an emphasis on water flow and how it influences processes such as oxygen production/consumption and food capture by the coral. Finally, the known role of cilia and their generated vortices is explained in order to introduce their hypothesized significance on the aforementioned coral processes.

Box 1 Coral Biology

Scleractinian corals (Cnidaria: Anthozoa) are sessile animals, mainly colonial, that secrete a calcium carbonate skeleton outside of their bodies (Veron 2011). The body plan of a coral's polyp is relatively simple (Fig. 1.1), it is composed of two tissue layers, epi- and endodermis (also known as gastrodermis), surrounding a sac-like cavity called coelenteron. Tubular tentacles, that have the same tissue arrangement as the rest of the polyp, encircle the polyp's single opening, the mouth. As in all cnidarians, coral tentacles are armed with a series of stinging cells, called nematocysts, used to capture plankton for heterotrophic nutrition (Sebens et al. 1996). The single polyps of a colony are linked together by the coenosarc, which possess a similar tissue arrangement as the polyps. Fluids and nutrients are shared between polyps via the gastrovascular canal, which is an extension of the coelenteron (Ruppert et al. 2004).

Most shallow water tropical corals live in close symbiosis with dinoflagellate algae (Zooxanthellae) located in varying numbers within the cells of the endodermis (Goreau et al. 1971, Brown et al. 1995). This association starts at the earliest stage of coral development (Yonge 1940, Baird et al. 2009) and provides both organisms with essential metabolites that would not be produced by either of them separately and that helps them withstand environmental stressors (Muscatine and Porter 1977).

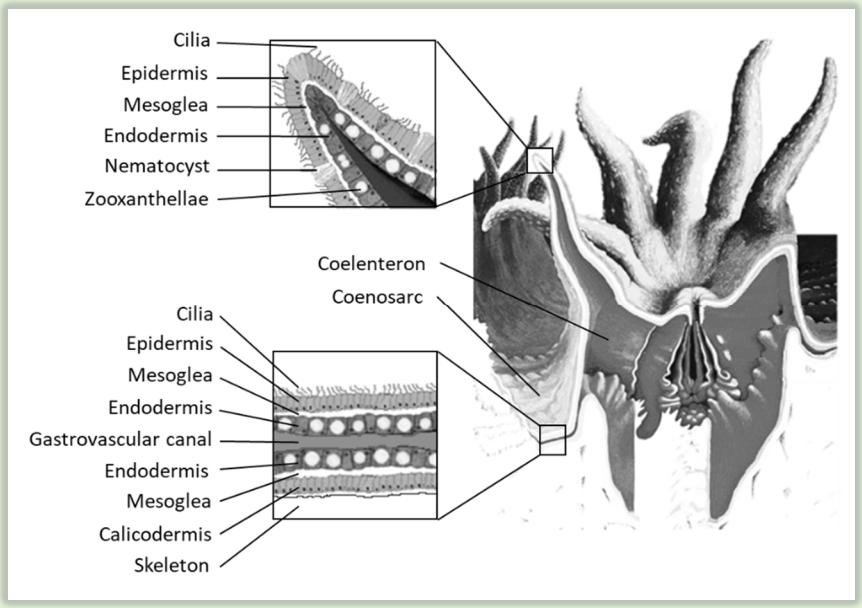

Figure 1.1. General structure of a coral polyp and tissue arrangements (Modified fromVeron 2000).

1.1 The coral's fluctuating environment

The environment around tropical coral reefs is not, and has never been, stable (Brown 1997). Over millennia and across oceans, corals have experienced and survived extreme variations in: sea surface temperature (SSTs): ~5°C (Anderson et al. 1989, Beck et al. 1992, Lea et al. 2000), dissolved carbon concentration: ~2000 ppm (Pearson and Palmer 2000), and drastic oscillations in sea level and currents (Pandolfi 1996), which have marked their geographical

distribution and evolution (Veron 1995). On higher temporal resolution (inter-annual, monthly, daily), the observed variations in SST, current speed and sedimentation are mostly a product of diurnal and seasonal changes (Coles and Fadlallah 1991, Brown et al. 1994, Lough 1994). If, above that, storms (Naseer and Hatcher 2000), as well as regional oceanographic phenomena such as internal waves (Schmidt et al. 2012, Wall et al. 2012) and upwelling (Andrews and Gentien 1982) are taken into account, the scenario becomes much more complex. On even smaller temporal (hours to milliseconds) and spatial scales (centimeters to microns) corals experience strong fluctuations in the physicochemical characteristics of the water around them as well, mostly due to their complex interaction with water currents (de Beer et al. 2000, Gardella and Edmunds 2001, Fabricius 2006). Their surface roughness and, in many cases, intricate shapes can create a series of microenvironments around the polyps with characteristics that may differ substantially from those found in the free circulating water column (Chang et al. 2009, Jimenez et al. 2011, Ong et al. 2019). A branching coral colony, for example, can experience strong water flows on the leading edges of the colony and nearly stagnant conditions in the interior (Chamberlain and Graus 1975, Chang et al. 2009, Hossain and Staples 2019) with corresponding variations in, for instance, oxygen and pH due to the depletion or accumulation of solutes in the stagnated water zones.

Water flow is, therefore, a fundamental component of the aquatic environment irrespective of the scale (Nowell and Jumars 1984, Shashar et al. 1996). Not only will it affect the behavior of the different organism present in the reef, but also modulate the interaction between coral species (Genin and Karp 1994). Enhanced circulation can modify many important environmental factors ruling over the reefs, such as plankton availability (Alldredge and King 2009), turbidity (Jones et al. 2016), salinity and temperature (Brown 1997), while diminished water movement can decrease coral growth, recruitment and mortality (Jokiel 1978). On a polyp level, water flow plays an important role in the expansion/contraction behavior of corals indirectly controlling its heterotrophic success (Sebens and Johnson 1991, Levy et al. 2001). At the same time, water flow is a fundamental element, equivalent to light and nutrients, in determining rates of photosynthesis (Mass 2010), respiration (Patterson et al. 1991) and calcification (Dennison and Barnes 1988) by enhancing the provision and/or removal of solutes to and from the coral tissue (Chamberlain and Graus 1975, Finelli et al. 2006). High flow has been proven to be of importance in the susceptibility and recovery of corals to heat stress and subsequent bleaching as well (Fifer et al. 2021). Field observations and laboratory experiments have shown that corals

experiencing higher flow regimes are more likely to survive bleaching events compared to the ones exposed to low water currents (Nakamura et al. 2003, Nakamura et al. 2005). While corals are affected by water motion, they will affect the currents as well, interacting with the water column in an area of water also called boundary layer (BL) (Shashar et al. 1996). The characteristics of this layer are, therefore, of extreme importance to the coral ecosystem as they rule over the coral's processes and responses to the environment.

1.2 The coral boundary layer

In aquatic environments, the boundary layer (BL) is the part of the marine environment surrounding all submerged solid surfaces (see Box 2 for its definition). In the case of sediments and organisms on the seafloor it is termed Benthic Boundary Layer (BBL) (Shashar et al. 1996, Dade et al. 2001). The BBL can have several decimeters or meters in height and it is the layer in which currents influence and are influenced by the surface topography (Reidenbach et al. 2006, Stocking et al. 2016). The BBL itself consists on several sublayers:

- The turbulent BL, comprising most of the BBL's height where turbulent motion shapes the mean velocity gradient and turbulent diffusion controls the vertical exchange of mater (Dade et al. 2001).

- Closer to the solid, surface vertical motions of turbulence die out, leaving a region dominated by viscous transport of momentum, the laminar BL. This layer is a few mm to cm in height, where water movement is parallel to the surface and viscosity shapes the mean velocity gradient (Dade et al. 2001). In the case of corals

Box 2 Boundary Layer

A so-called Boundary Layer (BL) surrounds all submerged surfaces. This layer is formed as the surrounding fluid adheres to the surface of the solid (due to water´s viscosity) and where frictional processes retard the motion of the fluid (Fig. 1.2). Inside this layer, the velocity of the fluid increases from zero at the surface to its full value, which corresponds to the external frictionless flow (Schlichting and Gersten 2017).

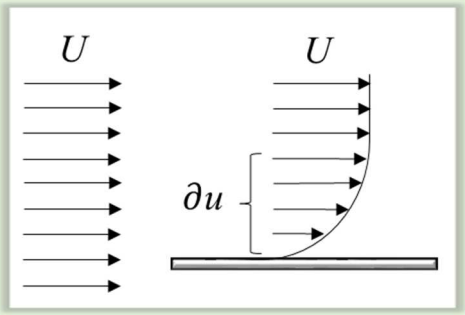

Figure 1.2. Water velocity (U) distribution without and with a solid surface. In front of the surface (left), the velocity is uniform, denoted by the length of the arrows. With the introduction of the solid (right) the water velocity is retarded (∂u) forming a Boundary Layer (bracket).

it is also referred as Momentum Boundary Layer (MBL) (Shashar et al. 1996) and is related to the fine currents surrounding each coral and is influenced by the 3D structure of the coral colony skeleton (Chamberlain and Graus 1975) and by tentacle expansion (Sebens and Johnson 1991).

- Finally, the Diffusive Boundary Layer (DBL), which occupies the lower part of the BBL where molecular diffusion is the dominant transport mechanism for solutes. The DBL is best visualized when the production or consumption of dissolved compounds by the organism creates a linear concentration gradient starting from its surface to the water column promoting the transport of solutes by diffusion (Jørgensen 2001). The DBL's upper limit is demarcated by the distance, where the turbulent diffusion coefficient, *K*, which governs the turbulent region of the water column, approaches the molecular diffusion coefficient, *D* (Jørgensen and Revsbech 1985, Hondzo et al. 2005). In practical terms, the thickness of the DBL is usually defined as the distance from the surface to where the concentration of the dissolved substance under study deviates ± 10% of the concentration in the free medium (Jørgensen and Des Marais 1990). In the case of corals, for most small molecules and ions of biological interest (e.g. O_2, CO_2, etc.), the thickness of the DBL is expected to be around $1/8^{th}$ times the thickness of the MBL (Patterson et al. 1991) and it is controlled by surface roughness and flow speed (Schlichting and Gersten 2017, Hossain and Staples 2020). Fick's first law characterizes mass transport across the DBL:

$$J = -D\ \Delta C/\Delta z \qquad \text{[Eq. 1.1]}$$

where *J* is the flux rate, *D* is the molecular diffusion coefficient of the substance of interest at a specific temperature and salinity, *C* the concentration and *z* the distance perpendicular to the surface. A reduction in the diffusional distance (z) from the free water flow to the coral tissue will have important consequences: For a given concentration difference (ΔC) it will increase *J* by increasing the concentration gradient ($\Delta C/\Delta z$). For a given *J* it will decrease the concentration difference between coral and environment reducing the time needed to equilibrate changes in the concentration of the dissolved species (Patterson et al. 1991). Due to these reasons the DBL will act as a bottleneck for the exchange of solutes between corals and their

environment with the different factors altering its height having important consequences upon the organism and its processes.

1.2.1 Oxygen in the coral BL

Oxygen is fundamental to many aspects of the reef functions as it acts as mediator in the interaction between corals and the organisms around them, e.g. algae (Haas et al. 2009, Jorissen et al. 2016), fish (Nilsson et al. 2010) and microorganism vectors of diseases (Barott and Rohwer 2012). At this scale, variations of oxygen concentration around reefs are not only influenced by sea-air interactions and mass transport by currents (Talley 2011), but also by photosynthesis and respiration of the corals, algae and animals inhabiting the reef (Kraines et al. 1996, Niggl et al. 2010).

On a colony level, oxygen will drive many key physiological processes of the coral holobiont, i.e. rates of respiration (Shick 1990), photosynthesis (Harland and Davies 1995, Gardella and Edmunds 1999) and calcification (Rinkevich and Loya 1984) are enhanced during the day as photosynthesis and subsequent oxygen production peaks. While most of the photo-derived oxygen is immediately consumed by the coral (78-90 %) (Kühl et al. 1995), the excess is released out of the tissue where it will accumulate creating a concentration gradient with the water column (Shick 1990, Patterson 1992). Under dark conditions or reduced light, the opposite is the case, as the coral's consumption is combined with that of the zooxanthella, reverting the direction of the oxygen flux from the water column towards the coral tissue (Finelli et al. 2006). Nevertheless, and even though oxygen is essential for the coral-algae association, the accretion of oxygen above a certain level during the day is detrimental to the coral holobiont as well. Excess oxygen has been proven to inhibit calcification of the coral (Wijgerde et al. 2014) and photosynthesis of the zooxanthellae (Dykens and Shick 1984, Lesser and Shick 1989), hypothetically due to the formation of Reactive Oxygen Species (ROS) (Lesser 1997, Nielsen et al. 2018), a process which can lead to the expulsion of the symbionts causing the bleaching of the coral colony (Glynn 1983). Facing oxygen accumulation at their tissue surface during the day, corals must, optimize the removal in order to reduce the detrimental consequences. As the DBL is a bottleneck for mass transfer, the different factors that shape the DBL, and by extension the efflux of photo-derived oxygen, are thus of great significance for the health of the coral holobiont (Nakamura and van Woesik 2001, Nakamura et al. 2005).

Oxygen mass transfer between the coral and the water column depends on a variety of factors, from environmental to the characteristics of the coral itself (de Beer et al. 2000). Flow speed of external water currents is the most important element controlling mass transfer in aquatic environments (Jørgensen and Revsbech 1985, Dennison and Barnes 1988, Patterson et al. 1991) as higher flow regimes reduce the thickness of the DBL (Finelli et al. 2006) increasing the flux or decreasing the gradient at constant flux (Eq. 1). However, coral morphology (Gardella and Edmunds 2001, van Woesik et al. 2012), as well as polyp expansion (Sebens and DeRiemer 1977) and epidermal cilia (Shapiro et al. 2014) can play important roles in enhancing mass transfer as well. In the leaf lettuce coral *Acropra tenuifolia* the space in between branches has significant effects upon mass flux (Helmuth et al. 1997), while in massive corals the thickness of the DBL negatively correlates with the size of the polyps (Shashar et al. 1993). On the other hand, polyp tentacle expansion at night has been suggested as a mean to increase the coral's surface area, thus increasing exchange rates between coral and environment and reducing oxygen limitation during darkness (Shick et al. 1979). Inside the DBL, oxygen concentrations are reported to decrease lineally from high to low concentration (Kühl et al. 1995, de Beer et al. 2000) assuming that no other processes, except for diffusion, are involved in mass transport inside the layer (Schlichting and Gersten 2017). However, inside the coral DBL other features have recently emerged, showing that, under stagnant conditions, corals are not entirely enslaved to ambient flows and diffusion limitations. Instead, they have the ability to actively manipulate the conditions of diffusive mass transport by the beating of epidermal cilia, which generates vortices that enhance the transport of elements (Shapiro et al. 2014). If vortices may reduce the thickness of the DBL, are they also increasing the flux, or rather decrease the oxygen gradient under a constant flux? What are the consequences of vortex activity towards the physiological processes of the coral and its symbionts? Are vortices acting homogenously along the coral surface? Or are they specifically localized at certain areas, possibly related to the chlorophyll content inside the tissue? This thesis aims at answering those questions (see section 1.4).

1.2.2 Food capture in the coral BL

All corals are considered passive suspension-feeders (Goreau et al. 1971, Muscatine 1973) as they depend on ambient currents to drive water past their nematocyst-bearing stinging tentacles, which immobilize and kill their suspended prey (Yonge 1930, Ben-Ari et al. 2018). The importance of heterotrophy in the coral metabolism is known to vary between coral species (Anthony and Fabricius 2000), reef habitats (Lesser et al. 2010) and seasons (Ferrier-

Pagès et al. 2011) ranging between 15 and 35% of the daily metabolic requirements (Houlbrèque and Ferrier-Pagès 2009). Despite being small, that percentage contribution is of extreme importance for the coral in order to replenish the losses of inorganic nitrogen, phosphorus, and other nutrients that cannot be adequately supplied by their symbiotic algae (Farrant et al. 1987, Anthony 1999). Several studies have shown the influence of higher food availability on many physiological parameters of scleractinian corals (Clayton and Lasker 1982, Houlbrèque et al. 2004a, Ferrier-Pagès et al. 2010). Photosynthetic rates (Houlbrèque et al. 2004a) as well as skeletal growth rates (Anthony and Fabricius 2000, Ferrier-Pagès et al. 2003) are higher in fed corals as the amount of zooxanthellae and chlorophyll per zooxanthellae is enhanced compared to their unfed counterparts(Houlbrèque et al. 2003). Yet, in most cases the contribution of large zooplankton (i.e. mesozooplankton, >200 µm lenght) feeding does not appear to be adequate to sustain the coral's metabolic need for growth and reproduction (Clayton and Lasker 1982). Studies have shown that nanoflagellates (<20 µm diameter) can represent up to 94% of the total ingested carbon and up to 85% of the total ingested nitrogen (Houlbrèque et al. 2004b). On the other hand, phosphorus is mostly supplied by organic matter, i.e. picoplankton (<2 µm) (Sorokin 1973a, D'Elia 1977, Anthony 1999), highlighting the plasticity of corals in regard to their nutrient suppliers. The coral's ability to capture its suspended nutrient sources, irrespective the size of the food, is, in part, the key to its capacity to thrive in oligotrophic waters (Porter 1976, Muscatine and Porter 1977, Houlbrèque and Ferrier-Pagès 2009).

Coral feeding is facilitated as currents carrying food particles are retarded when they reach the coral colonies (LaBarbera 1984, Patterson 1984, Patterson 1991, Sebens and Johnson 1991). Corals have the ability to increase the chances of trapping food by extending their tentacles into the BL, thus increasing the area exposed to currents (Yonge 1940, Lewis and Price 1975). At the same time, the differentiation in local exposure to flow, due to coral morphology and micro currents around the polyps, are known to affect coral prey capture (Abelson et al. 1993, Helmuth and Sebens 1993, Sebens et al. 1998, Wijgerde et al. 2012). Mesozooplankton by virtue of its relative large size lay at the interception of the viscous and inertial worlds (Naganuma 1996). As such, they possess the inertia needed to short-cut the flow lines around the tentacles, impact the coral surface and trigger nematocyst discharge, which is the mechanistic basis for an efficient food capture by the tentacles (Yonge 1930, Hentschel and Shimeta 2008). However, for smaller organisms, such as pico- and nanoplankton (<2µm, <20µm, Cushing et al. 1958), this sieving technique is ineffective,

since the viscous forces dominate the inertial forces at very low Reynolds numbers and particles no longer escape the streamlines to cause physical impact (Vogel 1996). If corals are to profit from these food size ranges, other means of prey capture must be used.

Mucus released by corals into the water column has been reported to act as a trap for small cyanobacteria and other suspended elements (Stafford-Smith and Ormond 1992, Wild et al. 2004, Naumann et al. 2009). Corals have long been known to use mucus to get rid of inorganic particles settling on their surface using epidermal cilia to move the mucus strings (Yonge 1930, Stafford-Smith 1993). While it was noted early that these organelles are present in most corals, they were long considered unimportant in the coral's food capture (Carlgren 1905, Carpenter 1910, Yonge 1928, Mariscal 1974). This notion was overturned by Lewis and Price (1976) who proposed that the cilia play a role in lifting the mucus layer, exposing the sticky strands to the ambient currents, thus facilitating the scavenging of particles to be subsequently drawn into the mouth (Lewis and Price 1976). Nevertheless, the mechanistic explanation of particle entrapment by coral mucus has never been fully explained. The recent discovery of the ability of ciliary vortices to enhance mass transport at the lower DBL leads to the question if they are also involved in the transport of other elements, i.e. pico-, ultra and nanoplankton, consequently intervening in coral's heterotrophic nutrition.

1.3 The coral's epidermal cilia

As mentioned before, the coral tissue is heterogeneously covered with a series of hair-like structures called cilia – usually 10 to 20 μm in length (see Box 3, for an understanding of the cilia structure and its movement) – with regions of dense and scarce cilia presence (Eppard et al. 1989, Tambutté et al. 2020). Their occurrence is not only restricted to the epidermis facing the water column (Mariscal 1974) and endodermis facing the gastrovascular canal (Eppard et al. 1989), but they have also been found in the calicoblastic epitelium (calicodermis) responsible for skeletal formation (Tambutté et al. 2020).

Though, a ubiquitous element of the coral anatomy, the role of cilia in the physiological processes of the coral has seldom been recognized. They were known to be indirectly involved in feeding (Yonge 1930, Lewis and Price 1976). First, in the movement of mucus, (Yonge 1930, Brown and Bythell 2005), and second, by the reception of mechanistic clues

and subsequent discharge of their nematocyst, triggered as zooplankton prey touches the tentacles (Mariscal 1974, Fautin and Mariscal 1991).

Box 3 Cilia: structure, function and movement

Cilia are evolutionary conserved organelles found in almost all Eukaryotes from microorganisms to animals alike (Mitchell 2007). They are thin membrane-covered contractile structures that extend from the body of a variety of cells and are responsible – among other functions – for the propulsion of the organism in the fluid or the propulsion of the fluid around the organism (Brennen and Winet 1977). Exactly how cilia beat is, up to this day, a long-standing mystery (Gilpin et al. 2020). Nevertheless some insights are well known: the motion of cilia originates from chemical and mechanical processes coupled in a tube-shaped structure called Axoneme, which is composed of nine microtubule doublets arranged in a circle and usually a central pair of microtubules (Manton and Clarke 1952). The outer doublets are attached to one other via nexin links while protein complexes (radial spokes) extend towards the central pair (Fig. 1.3). Beating is driven by dynein, a protein attached at regular intervals along the length of the doublets (Mitchison and Mitchison 2010). In order to bend the Axoneme, dyneins on one side must be active – using ATP as energy source (Summers and Gibbons 1971) – while those on the other side must be inactive generating a sliding motion among the doublets. Movement propagation is achieved by switching dynein activity in a controlled manner (therein lies the mystery) not only spatially, but also temporally (Brokaw 2009). This movement powers the swimming of many small organisms and sperm as well as the movement of fluids and mucus in the brain and lung of mammals (Wan 2018).

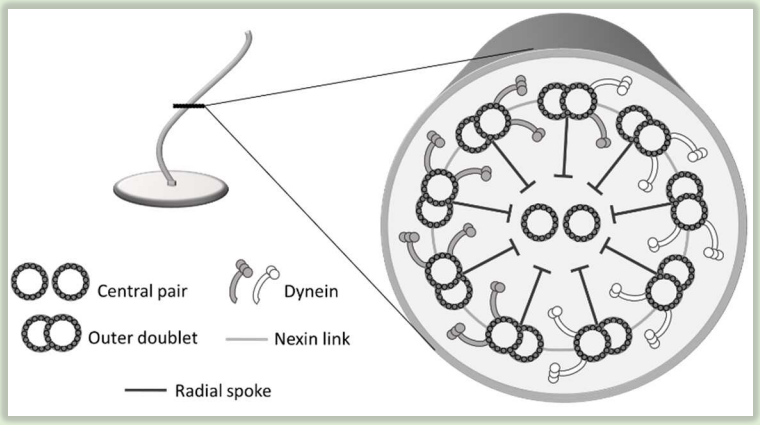

Figure 1.3. A cross-sectional scheme of a typical axoneme of cellular cilia showing the arrangements of microtubule doublets and in-between linkages. The axoneme bends, when dyneins on one side (gray) are active, while those on the other side are inactive (white) (Modified from Mitchison and Mitchison 2010).

Nevertheless, the sensory and mechanistic role of cilia might also be important for other processes, such as calcification and BL dynamics. Tambutté et al. (2020) found a primary form of cilia (named as such since they possess a simpler structure than regular cilia and are found in post-mitotic cells) in the calicoblastic cells and suggested their involvement in

sensing the characteristics of the extracellular calicoblastic medium triggering calcification. On the other hand, and as described before, the beating of cilia also gives the coral the ability to stir the lower BL by the formation of vortices, allowing the movement of water parcels towards and away from the surface subsequently enhancing mass transport (Shapiro et al. 2014). The discovery of such a feature marked a milestone in the study of the dynamics of the coral BL, leading to several questions that paved the foundations of this thesis (see next).

1.4 Research questions of the thesis

The aim of this thesis is to better understand the role which ciliary vortices play on the dynamics of the coral BL by studying how these currents intervene in elemental and particle transport processes along the autotrophic and heterotrophic pathways of the coral holobiont. Given that the characteristics of the BL and its drivers can have profound repercussions on the coral's physiological processes, the newly discovered role of cilia (Shapiro et al. 2014) lead to the research questions:

1. How do ciliary vortices behave under various flow and light conditions?
2. By thinning the DBL, what happens with the diffusive flux and how is the coral profiting on the effects of a reduced DBL thickness?
3. Is the removal of oxygen by ciliary vortices, homogeneous along the surface of the coral?

   Or

4. Are ciliary vortices at the tissue surface related to the amount of chlorophyll inside the tissue?
5. Are the vortices able to transport not only dissolved chemical elements, but also small particles, effectively intervening in the coral's heterotrophic nutrition?

In order to answer these questions four main objectives are proposed:

1. Create and test novel methods necessary for the detailed visualization of ciliary vortices and the parallel recording of oxygen concentrations of the coral diffusive boundary layer (DBL) (**Chapter 2, and 4**).

2. Quantify the oxygen gradients and fluxes on the disturbed and undisturbed BL of tropical corals under different flow and light regimes in order to better understand vortex effect in the coral-symbiont relationship (**Chapter 3, 4, 5**).

3. Unveil the role of ciliary vortices in the coupling of DBL dynamics and chlorophyll concentrations inside the coral tissue (**Chapter 5**).

4. Reveal the role of ciliary vortices in the heterotrophic nutrition of corals (**Chapter 6**).

Based on these objectives, the following research hypotheses are suggested:

H1 Cilia induced vortices enhance oxygen mass transport regardless of the light regime and flow speed of the water aloft, relaxing the excess O_2 at the surface of their tissue.

So far, the influence of ciliary vortices on the mass transport of oxygen has been identified only under stagnant conditions by Shapiro et al. (2014) with a model extension for different flow regimes. **Chapter 3** expands on that previous work by introducing flow into a newly designed flow-through chamber (described in **Chapter 2**) holding the coral *Porites lutea*, testing the effect of ciliary flows not only during oxygen production, but also during consumption and further exploring the role of cilia in corals homeostasis.

H2 Oxygen reagent nanoparticles can be used for the simultaneous characterization of oxygen concentrations and flow dynamics of the coral DBL.

Currently available methods are sometimes insufficient, when mapping oxygen fluxes as they are often invasive or too slow, which hampers our ability to accurately map biotic and abiotic interactions in the DBL resulting in a limited understanding of its characteristics and inner process. **Chapter 4** is a detailed protocol for the use of oxygen reagent nanoparticles (sensPIV) in the study of microfluidics with its application – among others – on a coral colony.

H3 Cilia-induced vortical flows are used by the coral to ventilate areas of oxygen accumulation at the surface of their tissue.

Zooxanthellae distribution is not homogeneous along the coral tissue and some areas along the colony might become hotspots of oxygen production. If that is the case, these areas need to be actively ventilated in order not to accumulate oxygen that will,

eventually, affect the coral. **Chapter 5** describes the linkage between clusters of chlorophyll (identified by using Hyperspectral technology) and oxygen transport promoted by ciliary vortices. Oxygen concentrations and the flow field at the coral DBL are measured by using oxygen reagent nanoparticles (SensPIV) described in **Chapter 4**.

H4 Ciliary vortices help alleviate the inhibition of photosynthesis due to high oxygen concentrations.

High oxygen concentrations may lead to the inhibition of photosynthesis and, eventually, to the bleaching of the coral colony. To prevent this, corals use ciliary vortices to alleviate oxygen accumulation at their surface and thus reduce the detrimental consequences inside the tissue. By applying a numerical model (**Chapter 5**), oxygen concentrations and fluxes inside the DBL were simulated in the presence of constant and heterogeneous oxygen production rates by the coral. This model is applied for two scenarios, one taking into account the inhibition of photosynthesis with increasing oxygen concentrations, and one assuming no inhibitory properties of high oxygen concentrations. Results are quantified as a function of the magnitude of ciliary flow speeds.

H5 Cilia and their generated vortices enhance the ability of corals to capture suspended prey.

Corals are voracious heterotrophic suspension feeders, displaying an array of tools, depending on the size of their suspended prey, with cilia and their generated currents believed to act purely as stimuli receptors and mucus transporters. **Chapter 6** further explores the role of cilia in the capture success of corals, exposed to different particle sizes. A modified micro Particle Image Velocimetry (PIV) set-up with a LED light sheet was used to observe ciliary vortices interacting with the mucus on the coral surface, and quantify the capture rate of ultraparticles (5 µm) with and without cilia activity. In addition, incubation experiments were conducted with suspensions of *Artemia franciscana*-naupii (~740 µm length), in order to determine whether the capture rate of mesozooplankton by corals varies depending on their cilia state.

1.5 Manuscript outline

Chapter 3: Ciliary vortex flows and oxygen dynamics in the coral boundary layer.

Cesar O. Pacherres, Soeren Ahmerkamp, Gertraud M. Schmidt-Grieb, Moritz Holtappels and Claudio Richter.

Published in Scientific Reports, **10**, 7541. Doi:10.1038/s41598-020-64420-7

The experiments for this study were designed by C.O.P., S.A., G.M.S., M.H. and C.R., C.O.P. conducted all experiments. C.O.P. and S.A. analyzed the PIV and PTV data. C.O.P. and M.H. analyzed the oxygen data. C.O.P., S.A. and M.H. created all figures. C.O.P., S.A., G.M.S., M.H. and C.R. contributed to the interpretation of the collected data, and conceived and wrote the manuscript.

Chapter 4: sensPIV: simultaneous visualization of flow fields and oxygen concentrations to unravel metabolic exchange fluxes.

Soeren Ahmerkamp, Farooq Moin Jalaluddin, Yuan Cui, Cesar O. Pacherres, Jasmine Berg, Roman Stocker, Marcel MM Kuypers, Klaus Koren and Lars Behrendt

Manuscript ready to be submitted

S.A., L.B., K.K, M.M.M.K., J.B., R.S. conceived the study and interpreted data. K.K. synthesized sensor particles. Y.C. and L.B. performed experiments with microfluidic chips and processed data. F.M.J. and S.A. performed experiments with laboratory particles and processed data. S.A. developed and built optical setups. C.O.P. and S.A. developed flow-chamber setup, performed experiments with coral fragments and processed data. C.O.P. performed microsensor measurement. All authors edited and approved the paper.

Chapter 5: Ciliary currents and symbiont heterogeneity segregate sites of oxygen production and accumulation in the coral boundary layer

Cesar O. Pacherres, Soeren Ahmerkamp, Klaus Koren, Claudio Richter and Moritz Holtappels.

Manuscript ready to be submitted

The experiments for this study were designed by C.O.P., S.A., C.R and M.H., C.O.P. conducted all experiments. C.O.P. and S.A. analyzed the sensPIV and hyperspectral data and generated the figures. M.H. and S.A worked on the model and its figures. K.K. created and supplied the sensPIV particles, necessary for the oxygen experiments. C.O.P., S.A., K.K., C.R. and M.H. contributed to the interpretation of the collected data, and conceived and wrote the manuscript.

Chapter 6: The role of cilia in coral suspension feeding.

Cesar O. Pacherres, Soeren Ahmerkamp, Moritz Holtappels, Gertraud M. Schmidt-Grieb and Claudio Richter.

Manuscript in preparation

The experiments for this study were designed by C.O.P., S.A., M.H., G.M.S. and C.R. C.O.P. conducted all the experiments. S.A. provided the Matlab algorithm for particle counting. C.O.P. extracted and processed all data and created all figures. C.O.P. and C.R. contributed to the interpretation of the collected data, and conceived and wrote the manuscript.

1.6 References

Abelson, A., T. Miloh, and Y. Loya. 1993. Flow patterns induced by substrata and body morphologies of benthic organisms, and their roles in determining availability of food particles. Limnol Oceanogr **38:** 1116-1124.

Alldredge, A. L., and J. M. King. 2009. Near-surface enrichment of zooplankton over a shallow back reef: implications for coral reef food webs. Coral Reefs **28:** 895-908.

Anderson, D. M., W. L. Prell, and N. J. Barratt. 1989. Estimates of Sea Surface Temperature in the Coral Sea at the Last Glacial Maximum. Paleoceanography **4:** 615 - 627.

Andrews, J. C., and P. Gentien. 1982. Upwelling as a source of nutrients for the Great Barrier Reef ecosystems: A solution to Darwin's question? Mar Ecol Prog Ser **8:** 257-269.

Anthony, K. R. N. 1999. Coral suspension feeding on fine particulate matter. J Exp Mar Biol Ecol **232:** 85-106.

Anthony, K. R. N., and K. E. Fabricius. 2000. Shifting roles of heterotrophy and autotrophy in coral energetics under varying turbidity. J Exp Mar Biol Ecol **252:** 221-253.

Baird, A. H., J. R. Guest, and B. L. Willis. 2009. Systematic and biogeographical patterns in the reproductive biology of scleractinian corals. Annu Rev Ecol Evol Syst **40:** 551-571.

Barott, K. L., and F. L. Rohwer. 2012. Unseen players shape benthic competition on coral reefs. Trends Microbiol **20:** 621-628.

Beck, J. W. and others 1992. Sea-surface temperature from coral skeletal strontium/calcium ratios. Science **257:** 644-647.

Ben-Ari, H., M. Paz, and D. Sher. 2018. The chemical armament of reef-building corals: inter- and intra-specific variation and the identification of an unusual actinoporin in *Stylophora pistilata*. Sci Rep **8:** 251.

Brandl, S. J. and others 2019. Demographic dynamics of the smallest marine vertebrates fuel coral reef ecosystem functioning. Science **364:** 1189-1192.

Brennen, C., and H. Winet. 1977. Fluid mechanics of propulsion by cilia and flagella. Annu Rev Fluid Mech **9:** 339-398.

Brokaw, C. J. 2009. Thinking about flagellar oscillation. Cell Motility **66:** 425-436.

Brown, B. E. 1997. Adaptations of reef corals to physical environmental stress, p. 221-299. *In* J. H. S. Blaxter and A. J. Southward [eds.], Adv Mar Biol. Academic Press.

Brown, B. E., and J. C. Bythell. 2005. Perspectives on mucus secretion in reef corals. Mar Ecol Prog Ser **296:** 291-309.

Brown, B. E., R. P. Dunne, T. P. Scoffin, and M. D. A. Le Tissier. 1994. Solar damage in intertidal corals. Mar Ecol Prog Ser **105:** 219-230.

Brown, B. E., M. D. A. Le Tissier, and J. C. Bythell. 1995. Mechanisms of bleaching deduced from histological studies of reef corals sampled during a natural bleaching event. Mar Biol **122:** 655-663.

Carlgren, O. 1905. Über die Bedeutung der Flimmerbewegung für den Nahrungstransport bei den Actinarien und Madreporarien. Biol. Zbl. **25:** 308-322.

Carpenter, F. W. 1910. Feeding reactions of the rose coral (*Isophyllia*). Proc Am Acad Arts Sci **46:** 149-162.

Chamberlain, J. J. A., and R. R. Graus. 1975. Water flow and hydromechanical adaptations of branched reef corals. Bull Mar Sci **25:** 112-125.

Chang, S., C. Elkins, M. Alley, J. Eaton, and S. Monismitha. 2009. Flow inside a coral colony measured using magnetic resonance velocimetry. Limnol Oceanogr **54:** 1819-1827.

Clayton, W. S., Jr, and H. R. Lasker. 1982. Effects of light and dark treatments on feeding by the reef coral *Pocillopora damicornis* (Linnaeus). J Exp Mar Biol Ecol **63:** 269-279.

Coles, S. L., and Y. H. Fadlallah. 1991. Reef coral survival and mortality at low temperatures in the Arabian Gulf: new species-specific lower temperature limits. Coral Reefs **9:** 231-237.

Crawley, A., D. I. Kline, S. Dunn, K. Anthony, and S. Dove. 2010. The effect of ocean acidification on symbiont photorespiration and productivity in *Acropora formosa*. Glob. Change Biol. **16:** 851-863.

Cushing, D. H., G. F. Humphrey, K. Banse, and T. Laevastu. 1958. Report of the committee on terms and equivalents. Rapp. P.-V. Réun. Cons. perm. int. Explor. Mer **144:** 15-16.

D'Elia, C. F. 1977. The uptake and release of dissolved phosphorus by reef corals. Limnol Oceanogr **22:** 301-315.

Dade, W. B., A. J. Hogg, and B. P. Boudreau. 2001. Physics of flow above the sediment-water interface, p. 4-43. *In* B. P. Boudreau and B. B. Jørgensen [eds.], The benthic boundary layer: transport processes and biogeochemistry. Oxford University Press.

de Beer, D., M. Kühl, N. Stambler, and L. Vaki. 2000. A microsensor study of light enhanced Ca^{2+} uptake and photosynthesis in the reef-building hermatypic coral *Favia* sp.†. Mar Ecol Prog Ser **194:** 75-85.

de Goeij, J. M. and others 2013. Surviving in a marine desert: The sponge loop retains resources within coral reefs. Science **342:** 108-110.

Dennison, W. C., and D. J. Barnes. 1988. Effect of water motion on coral photosynthesis and calcification. J Exp Mar Biol Ecol **115:** 67-77.

Dykens, J. A., and J. M. Shick. 1984. Photobiology of the symbiotic sea anemone, *Anthopleura elegantissima*: Defenses against photodynamic effects, and seasonal photoacclimatization. Biol Bull **167:** 683-697.

Eppard, R. A., G. J. Highison, and R. W. Mead. 1989. Scanning electron microscopy of epithelial surfaces of the sea anemone *Acontiophorum niveum* (Phylum Cnidaria): Class anthozoa. J Morphol **200:** 63-69.

Fabricius, K. E. 2006. Effects of irradiance, flow, and colony pigmentation on the temperature microenvironment around corals: Implications for coral bleaching? Limnol Oceanogr **51:** 30-37.

Farrant, P. A., M. A. Borowitzka, R. Hinde, and R. J. King. 1987. Nutrition of the temperate Australian soft coral *Capnella gaboensis*. Mar Biol **95:** 575-581.

Fautin, D., and R. N. Mariscal. 1991. Cnidaria: Anthozoa, p. 267-358. *In* F. W. Harrison and J. A. Westfall [eds.], Microscopic anatomy of invertebrates: Placozoa, Porifera, Cnidaria and Ctenophora. Microscopic anatomy of invertebrates. Wiley-Liss.

Ferrier-Pagès, C. and others 2011. Summer autotrophy and winter heterotrophy in the temperate symbiotic coral *Cladocora caespitosa*. Limnol Oceanogr **56:** 1429-1438.

Ferrier-Pagès, C., C. Rottier, E. Beraud, and O. Levy. 2010. Experimental assessment of the feeding effort of three scleractinian coral species during a thermal stress: Effect on the rates of photosynthesis. J Exp Mar Biol Ecol **390:** 118-124.

Ferrier-Pagès, C., J. Witting, E. Tambutté, and K. P. Sebens. 2003. Effect of natural zooplankton feeding on the tissue and skeletal growth of the scleractinian coral *Stylophora pistillata*. Coral Reefs **22:** 229-240.

Fifer, J., B. Bentlage, S. Lemer, A. G. Fujimura, M. Sweet, and L. J. Raymundo. 2021. Going with the flow: How corals in high-flow environments can beat the heat. Mol Ecol **30:** 2009-2024.

Finelli, C. M., B. S. T. Helmuth, N. D. Pentcheff, and D. S. Wethey. 2006. Water flow influences oxygen transport and photosynthetic efficiency in corals. Coral Reefs **25:** 47-57.

Gardella, D. J., and P. J. Edmunds. 1999. The oxygen microenvironment adjacent to the tissue of the scleractinian *Dichocoenia stokesii* and its effects on symbiont metabolism. Mar Biol **135:** 289-295.

---. 2001. The effect of flow and morphology on boundary layers in the scleractinians *Dichocoenia stokesii* (Milne-Edwards and Haime) and *Stephanocoenia michilini* (Milne-Edwards and Haime). J Exp Mar Biol Ecol **256:** 279-289.

Genin, A., and L. Karp. 1994. Effects of flow on competitive superiority in scleractinian corals. Limnol Oceanogr **39:** 913-924.

Gilpin, W., M. S. Bull, and M. Prakash. 2020. The multiscale physics of cilia and flagella. Nat Rev Phys **2:** 74-88.

Glynn, P. W. 1983. Extensive 'bleaching' and death of reef corals on the pacific coast of Panamá. Environ Conserv **10:** 149-154.

Goreau, T. F., N. I. Goreau, and C. M. Yonge. 1971. Reef corals: Autotrophs or heterotrophs? Biol Bull **141:** 247-260.

Grigg, R., J. Polovina, and M. Atkinson. 1984. Model of a coral reef ecosystem. Coral Reefs **3:** 23-27.

Haas, A., M. Al-Zibdah, and C. Wild. 2009. Effect of inorganic and organic nutrient addition on coral–algae assemblages from the Northern Red Sea. J Exp Mar Biol Ecol **380:** 99-105.

Harland, A. D., and P. S. Davies. 1995. Symbiont photosynthesis increases both respiration and photosynthesis in the symbiotic sea anemone *Anemonia viridis*. Mar Biol **123:** 715-722.

Helmuth, B., and K. Sebens. 1993. The influence of colony morphology and orientation to flow on particle capture by the scleractinian coral *Agaricia agaricites* (Linnaeus). J Exp Mar Biol Ecol **165:** 251-278.

Helmuth, B. S. T., K. P. Sebens, and T. L. Daniel. 1997. Morphological variation in coral aggregations: branch spacing and mass flux to coral tissues. J Exp Mar Biol Ecol **209:** 233-259.

Hentschel, B. T., and J. Shimeta. 2008. Suspension Feeders, p. 3437-3442. *In* S. E. Jørgensen and B. D. Fath [eds.], Encyclopedia of Ecology. Academic Press.

Hondzo, M., T. Feyaerts, R. Donovan, and B. L. O'Connor. 2005. Universal scaling of dissolved oxygen distribution at the sediment-water interface: A power law. Limnol Oceanogr **50:** 1667-1676.

Hossain, M. M., and A. E. Staples. 2019. Passive vortical flows enhance mass transport in the interior of a coral colony. Phys Fluids **31:** 061701.

---. 2020. Mass transport and turbulent statistics within two branching coral colonies. Fluids **5:** 153.

Houlbrèque, F., and C. Ferrier-Pagès. 2009. Heterotrophy in tropical scleractinian corals. Biol Rev (Camb) **84:** 1-17.

Houlbrèque, F., E. Tambutté, D. Allemand, and C. Ferrier-Pagès. 2004a. Interactions between zooplankton feeding, photosynthesis and skeletal growth in the scleractinian coral *Stylophora pistillata*. J. Exp. Biol. **207:** 1461-1469.

Houlbrèque, F., E. Tambutté, and C. Ferrier-Pagès. 2003. Effect of zooplankton availability on the rates of photosynthesis, and tissue and skeletal growth in the scleractinian coral *Stylophora pistillata*. J Exp Mar Biol Ecol **296:** 145-166.

Houlbrèque, F., E. Tambutté, C. Richard, and C. Ferrier-Pagès. 2004b. Importance of a micro-diet for scleractinian corals. Mar Ecol Prog Ser **282:** 151-160.

Jimenez, I. M., M. Kühl, A. W. D. Larkum, and P. J. Ralph. 2011. Effects of flow and colony morphology on the thermal boundary layer of corals. J R Soc Interface **8:** 1785-1795.

Jokiel, P. L. 1978. Effects of water motion on reef corals. J Exp Mar Biol Ecol **35:** 87-97.

Jones, R., P. Bessell-Browne, R. Fisher, W. Klonowski, and M. Slivkoff. 2016. Assessing the impacts of sediments from dredging on corals. Mar Pollut Bull **102:** 9-29.

Jørgensen, B. B. 2001. Life in the diffusive boundary layer, p. 348-373. *In* B. P. Boudreau and B. B. Jørgensen [eds.], The benthic boundray layer: Transport processes and biogeochemistry. Oxford University Press.

Jørgensen, B. B., and D. J. Des Marais. 1990. The diffusive boundary layer of sediments: Oxygen microgradients over a microbial mat. Limnol Oceanogr **35:** 1343-1355.

Jørgensen, B. B., and N. P. Revsbech. 1985. Diffusive boundary layers and the oxygen uptake of sediments and detritus1. Limnol Oceanogr **30:** 111-122.

Jorissen, H., C. Skinner, R. Osinga, D. de Beer, and M. M. Nugues. 2016. Evidence for water-mediated mechanisms in coral - algal interactions. Proc R Soc B **283:** 20161137.

Kraines, S., Y. Suzuki, K. Yamada, and H. Komiyama. 1996. Separating biological and physical changes in dissolved oxygen concentration in a coral reef. Limnol Oceanogr **41:** 1790-1799.

Kühl, M., Y. Cohen, T. Dalsgaard, B. B. Jørgensen, and N. P. Revsbech. 1995. Microenvironment and photosynthesis of zooxanthellae in scleractinian corals studied with microsensors for O_2, pH and light. Mar Ecol Prog Ser **117:** 159-172.

LaBarbera, M. 1984. Feeding currents and particle capture mechanisms in suspension feeding animals. Am Zool **24:** 71-84.

Lea, D. W., D. K. Pak, and H. J. Spero. 2000. Climate impact of late quaternary equatorial pacific sea surface temperature variations. Science **289:** 1719-1724.

Lesser, M. P. 1997. Oxidative stress causes coral bleaching during exposure to elevated temperatures. Coral Reefs **16:** 187-192.

Lesser, M. P., and J. M. Shick. 1989. Effects of irradiance and ultraviolet radiation on photoadaptation in the zooxanthellae of *Aiptasia pallida* primary production, photoinhibition, and enzymic defenses against oxygen toxicity. Mar Biol **102:** 243-255.

Lesser, M. P., M. Slattery, M. Stat, M. Ojimi, R. D. Gates, and A. Grottoli. 2010. Photoacclimatization by the coral *Montastraea cavernosa* in the mesophotic zone: light, food, and genetics. Ecology **91:** 990-1003.

Levy, O., L. Mizrahi, N. E. Chadwick-Furman, and Y. Achituv. 2001. Factors controlling the expansion behavior of *Favia favus* (Cnidaria: Scleractinia): Effects of light, flow, and planktonic prey. Biol Bull **200:** 118-126.

Lewis, J. B., and W. S. Price. 1975. Feeding mechanisms and feeding strategies of Atlantic reef corals. J Zool (Lond) **176:** 527-544.

---. 1976. Patterns of ciliary currents in Atlantic reef corals and their functional significance. J Zool (Lond) **178:** 77-89.

Lough, J. M. 1994. Climate variation and El Niño-Southern Oscillation events on the Great Barrier Reef: 1958 to 1987. Coral Reefs **13:** 181-185.

Manton, I., and B. Clarke. 1952. An electron microscope study of the spermatozoid of *sphagnum*. J Exp Bot **3:** 265-275.

Mariscal, R. N. 1974. Scanning electron microscopy of the sensory surface of the tentacles of sea anemones and corals. Zeitschrift für Zellforschung und Mikroskopische Anatomie **147:** 149-156.

Mitchell, D. R. 2007. The evolution of eukaryotic cilia and flagella as motile and sensory organelles, p. 130-140. Eukaryotic membranes and cytoskeleton: Origins and evolution. Springer New York.

Mitchison, T. J., and H. M. Mitchison. 2010. How cilia beat. Nature **463:** 308-309.

Muscatine, L. 1973. Nutrition of corals p. 77-115. *In* O. A. Jones and R. Endean [eds.], Biology and Geology of Coral Reefs. Academic Press.

Muscatine, L., and J. W. Porter. 1977. Reef corals: Mutualistic symbioses adapted to nutrient-poor environments. Bioscience **27:** 454-460.

Naganuma, T. 1996. Calanoid copepods: Linking lower-higher trophic levels by linking lower-higher Reynolds numbers. Mar Ecol Prog Ser **136:** 311-313.

Nakamura, T., and R. van Woesik. 2001. Water-flow rates and passive diffusion partially explain differential survival of corals during the 1998 bleaching event. Mar Ecol Prog Ser **212:** 301-304.

Nakamura, T., R. van Woesik, and H. Yamasaki. 2005. Photoinhibition of photosynthesis is reduced by water flow in the reef-building coral *Acropora digitifera*. Mar Ecol Prog Ser **301:** 109-118.

Nakamura, T., H. Yamasaki, and R. van Woesik. 2003. Water flow facilitates recovery from bleaching in the coral *Stylophora pistillata*. Mar Ecol Prog Ser **256:** 287-291.

Naseer, A., and B. G. Hatcher. 2000. Assessing the integrated growth response of coral reefs to monsoon forcing using morphometric analysis of reefs in Maldives. Proc 9th Int Coral Reef Symp **1:** 75-80.

Naumann, M. S., C. Richter, M. el-Zibdah, and C. Wild. 2009. Coral mucus as an efficient trap for picoplanktonic cyanobacteria: implications for pelagic–benthic coupling in the reef ecosystem. Mar Ecol Prog Ser **385:** 65-76.

Nielsen, D. A., K. Petrou, and R. D. Gates. 2018. Coral bleaching from a single cell perspective. ISME J **12:** 1558-1567.

Niggl, W., A. F. Haas, and C. Wild. 2010. Benthic community composition affects O_2 availability and variability in a Northern Red Sea fringing reef. Hydrobiologia **644:** 401-405.

Nilsson, G. E., S. Östlund-Nilsson, and P. L. Munday. 2010. Effects of elevated temperature on coral reef fishes: Loss of hypoxia tolerance and inability to acclimate. Comp Biochem Physiol A **156:** 389-393.

Nowell, A. R. M., and P. A. Jumars. 1984. Flow environments of aquatic benthos. Annu Rev Ecol Syst **15:** 303-328.

Ong, R. H., A. J. C. King, B. J. Mullins, and M. J. Caley. 2019. The effect of small-scale morphology on thermal dynamics in coral microenvironments. J Therm Biol **86:** 102433.

Pandolfi, J. M. 1996. Limited membership in pleistocene reef coral assemblages from the Huon Peninsula, Papua New Guinea: Constancy during global change. Paleobiology **22:** 152-176.

Patterson, M. R. 1984. Patterns of whole colony prey capture in the octocoral, *Alcyonium siderium*. Biol Bull **167:** 613-629.

---. 1991. The effects of flow on polyp-level prey capture in an octocoral, *Alcyonium siderium*. Biol Bull **180 1:** 93-102.

---. 1992. A mass transfer explanation of metabolic scaling relations in some aquatic invertebrates and algae. Science **255:** 1421-1423.

Patterson, M. R., K. P. Sebens, and R. Randolph Olson. 1991. *In situ* measurements of flow effects on primary production and dark respiration in reef corals. Limnol Oceanogr **36:** 936-948.

Pearson, P. N., and M. R. Palmer. 2000. Atmospheric carbon dioxide concentrations over the past 60 million years. Nature **406:** 695-699.

Porter, J. W. 1976. Autotrophy, heterotrophy, and resource partitioning in caribbean reef-building coral. Am Nat **110:** 731-742.

Reidenbach, M. A., S. G. Monismith, J. R. Koseff, G. Yahel, and A. Genin. 2006. Boundary layer turbulence and flow structure over a fringing coral reef. Limnol Oceanogr **51:** 1956-1968.

Rinkevich, B., and Y. Loya. 1984. Does light enhance calcification in hermatypic corals? Mar Biol **80:** 1-6.

Ruppert, E. E., R. S. Fox, and B. R. D. 2004. Invertebrate zoology: A functional evolutionary approach, 7th ed. Thomson, Brooks/Cole.

Schlichting, H., and K. Gersten. 2017. Boundary-layer Theory, 9th ed. Springer -Verlag.

Schmidt, G. M., N. Phongsuwan, C. Jantzen, C. Roder, S. Khokiattiwong, and C. Richter. 2012. Coral community composition and reef development at the Similan Islands,

Andaman Sea, in response to strong environmental variations. Mar Ecol Prog Ser **456:** 113-126.

Sebens, K. P., and K. DeRiemer. 1977. Diel cycles of expansion and contraction in coral reef anthozoans. Mar Biol **43:** 247-256.

Sebens, K. P., S. P. Grace, B. Helmuth, E. J. Maney Jr, and J. S. Miles. 1998. Water flow and prey capture by three scleractinian corals, *Madracis mirabilis, Montastrea cavernosa* and *Porites porites*, in a field enclosure. Mar Biol **131:** 347-360.

Sebens, K. P., and A. S. Johnson. 1991. Effects of water movement on prey capture and distribution of reef corals. Hydrobiologia **226:** 91-101.

Sebens, K. P., K. S. Vandersall, L. A. Savina, and K. R. Graham. 1996. Zooplankton capture by two scleractinian corals *Madracis mirabilis* and *Montastrea cavernosa*, in a field enclosure. Mar Biol **127:** 303-317.

Shapiro, O. H. and others 2014. Vortical ciliary flows actively enhance mass transport in reef corals. PNAS **111:** 13391-13396.

Shashar, N., Y. Cohen, and Y. Loya. 1993. Extreme diel fluctuations of oxygen in diffusive boundary layers surrounding stony corals. Biol Bull **185:** 455-461.

Shashar, N., S. Kinane, P. L. Jokiel, and M. R. Patterson. 1996. Hydromechanical boundary layers over a coral reef. J Exp Mar Biol Ecol **199:** 17-28.

Shick, J. M. 1990. Diffusion limitation and hyperoxic enhancement of oxygen consumption in zooxanthellate sea anemones, zoanthids, and corals. Biol Bull **179:** 148-158.

Shick, J. M., W. I. Brown, E. G. Dolliver, and S. R. Kayar. 1979. Oxygen uptake in sea anemones: Effects of expansion, contraction, and exposure to air and the limitations of diffusion. Physiol Zool **52:** 50-62.

Sorokin, Y. I. 1973a. Microbial aspects of the productivity of coral reefs, p. 17-46. *In* O. A. Jones and R. Endean [eds.], Biology and Geology of Coral Reefs. Academic Press.

Stafford-Smith, M. G. 1993. Sediment–rejection efficiency of 22 species of Australian scleractinian corals. Mar Biol **115:** 229-243.

Stafford-Smith, M. G., and R. F. G. Ormond. 1992. Sediment–rejection mechanisms of 42 species of Australian scleractinian corals. Mar. Freshw. Res. **43:** 683-705.

Stocking, J. B., J. P. Rippe, and M. A. Reidenbach. 2016. Structure and dynamics of turbulent boundary layer flow over healthy and algae-covered corals. Coral Reefs **35:** 1047-1059.

Summers, K. E., and I. R. Gibbons. 1971. Adenosine triphosphate–induced sliding of tubules in trypsin-treated flagella of sea-urchin sperm. PNAS **68:** 3092-3096.

Talley, L. 2011. Descriptive physical oceanography, 6th ed. Academic Press.

Tambutté, E., P. Ganot, A. A. Venn, and S. Tambutté. 2020. A role for primary cilia in coral calcification? Cell Tissue Res.

van Woesik, R., A. Irikawa, R. Anzai, and T. Nakamura. 2012. Effects of coral colony morphologies on mass transfer and susceptibility to thermal stress. Coral Reefs **31:** 633-639.

Veron, J. E. N. 1995. Corals in space and time, 1st ed. UNSW Press.

---. 2000. Corals of the world. Australian Institute of Marine Science.

---. 2011. Corals: Biology, skeletal deposition, and reef-building, p. 275-281. *In* D. Hopley [ed.], Encyclopedia of modern coral reefs: Structure, form and process. Springer Netherlands.

Vogel, S. 1996. Life in moving fluids, 2nd ed. Princeton Univ. Press.

Wall, M., G. M. Schmidt, P. Janjang, S. Khokiattiwong, and C. Richter. 2012. Differential impact of monsoon and large amplitude internal waves on coral reef development in the Andaman Sea. PLoS ONE **7:** e50207.

Wan, K. Y. 2018. Coordination of eukaryotic cilia and flagella. Essays Biochem **62:** 829 - 838.

Wijgerde, T., C. I. F. Silva, V. Scherders, J. van Bleijswijk, and R. Osinga. 2014. Coral calcification under daily oxygen saturation and pH dynamics reveals the important role of oxygen. Biology Open **3:** 489-493.

Wijgerde, T., P. Spijkers, E. Karruppannan, J. A. J. Verreth, and R. Osinga. 2012. Water flow affects zooplankton feeding by the scleractinian coral *Galaxea fascicularis* on a polyp and colony level. J Mar Biol **2012:** 854849.

Wild, C., M. Huettel, A. Klueter, S. G. Kremb, M. Y. M. Rasheed, and B. B. Jørgensen. 2004. Coral mucus functions as an energy carrier and particle trap in the reef ecosystem. Nature **428:** 66-70.

Yonge, C. M. 1928. Feeding mechanisms in the invertebrates. Biol Rev **3:** 21-76.

---. 1930. Studies on the physiology of corals: I. Feeding mechanisms and food. Scientific Reports / Great Barrier Reef Expedition 1928-29. **1:** 13-57.

---. 1940. The Biology of reef–building corals. Scientific Reports / Great Barrier Reef Expedition 1928-29. **1:** 352-391.

Yonge, C. M., M. J. Yonoe, and A. G. Nicholls. 1932. Studies on the physiology of corals: VI. The relationship between respiration in corals and the production of oxygen by their zooxanthellae. Scientific Reports / Great Barrier Reef Expedition 1928-29. **1:** 213-251.

2

Method development: Flow-through chamber

Processes occurring in and around corals at µ- to millimetric scales, such as oxygen production and consumption, calcification, etc. have long been a matter of intense scrutiny, as those processes are the first ones responding to environmental pressures (Jokiel 1978, Dennison and Barnes 1988). The later development and use of precise µ- and millimetric methods such as microsensors, image pulse amplitude fluorometry, etc. allowed the scientific community to gain a deeper understanding of such processes and their importance (Kühl et al. 1995, Ralph et al. 2005). However, obtaining data in such scales is not trivial and requires the exact determination and monitoring of the external experimental conditions, such as microcurrents, bulk oxygen, pH, etc. in order to avoid unwanted external influences in the parameters under study. Flow-through chambers have long been used for such purposes as they allow the control of all desired parameters, while keeping the organism alive and unstressed (Patterson et al. 1991, de Beer et al. 2000, Al-Horani et al. 2003, Carpenter and Patterson 2007, Shapiro et al. 2016). Nevertheless, small flow-through chambers that can be used in novel configurations are not commercially available, which arouse the need to create a chamber with enough plasticity to accommodate the needs of this project and fulfill its objectives (see Chapter 1, section 1.4).

The scales of the processes this thesis focuses on are in the range of micrometers and milliseconds, which required the use of specialized equipment such as microsensors and high magnification light- sheet-optics on living coral colonies. In order to keep the corals alive and unstressed for the duration of the experiments, they had to be kept in a chamber with

constant water exchange, oxygen permeability, temperature stability and a predictable flow regime while allowing experiments to be performed in parallel. Therefore, the flow-through chamber needed to fulfilled several requirements:

1) Transparency for external optics and light experiments.

2) Accessibility for sensors from above.

3) Stable and unidirectional flow.

For these reasons, a chamber (4.6 cm long × 1.3 cm wide × 1.6 cm high) of transparent polydimethylsiloxane (PDMS) was designed to be built using common microscope glass slides as bottom and front screens. An important feature of the chamber was the absence of a lid, which permitted free access from above to microsensors and syringes. (Fig. 2.1).

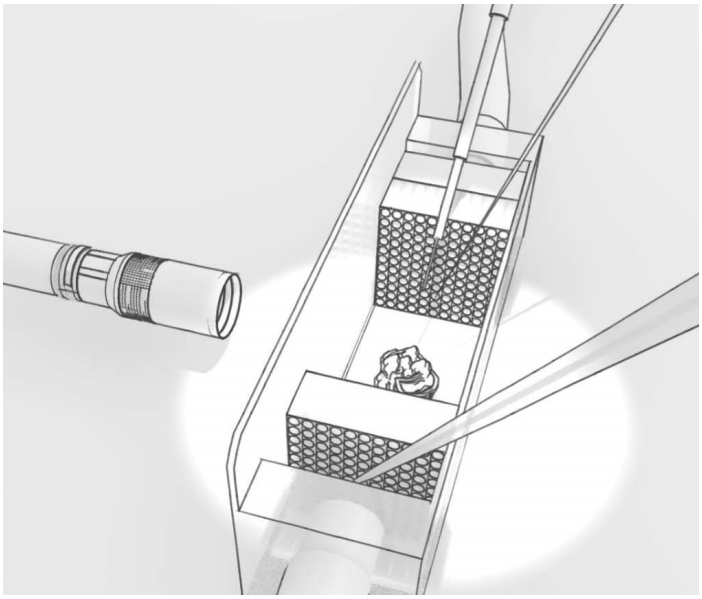

Figure 2.1. Schematic flow-through chamber.

2.1. Materials and Methods

A 3-D negative model of the chamber was derived using the online software THINKERCAD® from AUTODESK® (Fig. 2.2 a). The model was not a simple cubic rectangular but contained two protrusions that were to be used as diffuser fixers. The chamber was created by placing the 3D-printed model on top and next to 2 common

microscope glass slides and by pouring liquid PDMS around but not covering it, so that the model and glass wall protrude above the PDMS.

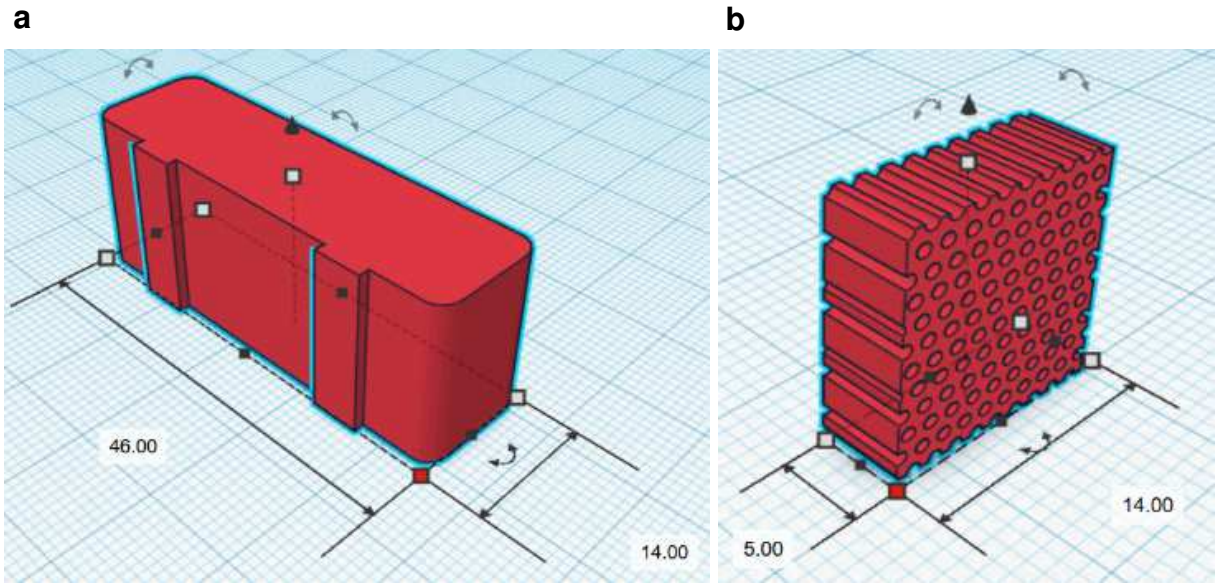

Figure 2.2. 3D-printed elements of the flow-through chamber. **a** Volumetric structure which later became the chamber. **b** Details of the diffuser. Appearing numbers are in millimeters (Forms were created using the free online software THINKERCAD® from AUTODESK®).

After 24 hours, and once the PDMS was dry, the model was carefully removed leaving a volumetric print with three sides (two of them made out of glass) and no lid. Plasma bonding between the PDMS and the glass slides (Kim et al. 2008) was not necessary as the liquid PDMS was poured directly onto the glass allowing an automatic bonding in the drying process.

The presence of a constant flow of water inside the chamber enables the maintenance and continuous control over water chemistry in the system. Thus, observations under constant conditions were facilitated by the introduction of flow via inlet and outlet tubes. The introduction of flow is also critical to prevent undesirable changes in the organism microenvironment due to the accumulation of waste products during the acclimation and observation phases. For this purpose, two 0.5 mm Ø silicon hoses were placed at the sides of the future chamber before the pouring of the liquid PDMS and were later connected to a water pump (REGLO Z, ISMATEC, Germany) (Fig. 2.3). The total operating volume of water fitting in the system was ~20 mL, which included the chamber and hoses internal volumes.

For the purpose of this thesis not only the speed of water entering the chamber needed to be constant, but the direction of the flow inside the chamber needed to be as homogeneous and stable as possible as well. This allowed us to observe the regular flow of the water inside the chamber and identify processes which could alter its regular behavior. Homogeneous water flow was achieved by placing a sponge in front of the water inlet followed by a diffuser created using a 3D printer – with a series of 1 mm holes at regular intervals (Fig. 2.2, b) and by placing a second diffuser of similar characteristics before the outlet (Fig. 2.3, a). Only under such circumstances it will be possible to observe fluid dynamic processes that occur in the water column created by the organism that alter regular flow in the chamber. For instance, coral cilia may form vortices by their active movement altering not only flow but also their chemical microenvironment.

To resolve the flow field inside the chamber, Particle Image Velocimetry (PIV) was used and monitored at two different pump rates (4 and 10 mL min^{-1}). First it was applied with the empty chamber (containing only water) to validate that the designed chamber set-up created laminar conditions inside the chambers. Only afterwards, a microcolony of the target species (*Porites lutea*) was introduced into the chamber in order to observe how the corals modulate their environment. PIV is based on the detection of small particles moving inside the flow, therefore the water in the system was seeded with 5 µm fluorescent particles (Exc: 468 nm, Emi: 530 nm) (Applied Microspheres, The Netherlands). Particle density was adjusted to approx. 50×10^6 particles L^{-1}, to allow a good map of the flow field. Illumination was achieved using a LED Pulsing System PIV V2 (ILA_5150, Germany) connected to led light sheet optics (Willert et al. 2010) (Fig. 2.3). The light sheet was 1 mm thick and intensity reached 5500 µmol quanta m^{-2} s^{-1} (LI-COR LI-192, USA) at a wavelength of around 468 nm. Images were captured using a ILA.PIV.µEYE camera (ILA_5150, Germany) recording pictures at 25 frames per second (fps) with an exposure time of 26 ms. A long distance microscope lens (Optem FUSION, Germany) with a bandpass filter of 532 nm was used for all trials. Video frames were processed using PIV software (PIVview2C, PIVTech GmbH). To obtain velocity fields the image sample size was set to 64 × 64 px with a 50% overlap and a multigrid sampling window of 128 × 128. For all experiments temperature and oxygen of the water inside the chamber were monitored every 30 seconds, using an optical sensor (PyroScience, Germany) positioned at different places inside the chamber (Fig. 2.1 & 2.3 b).

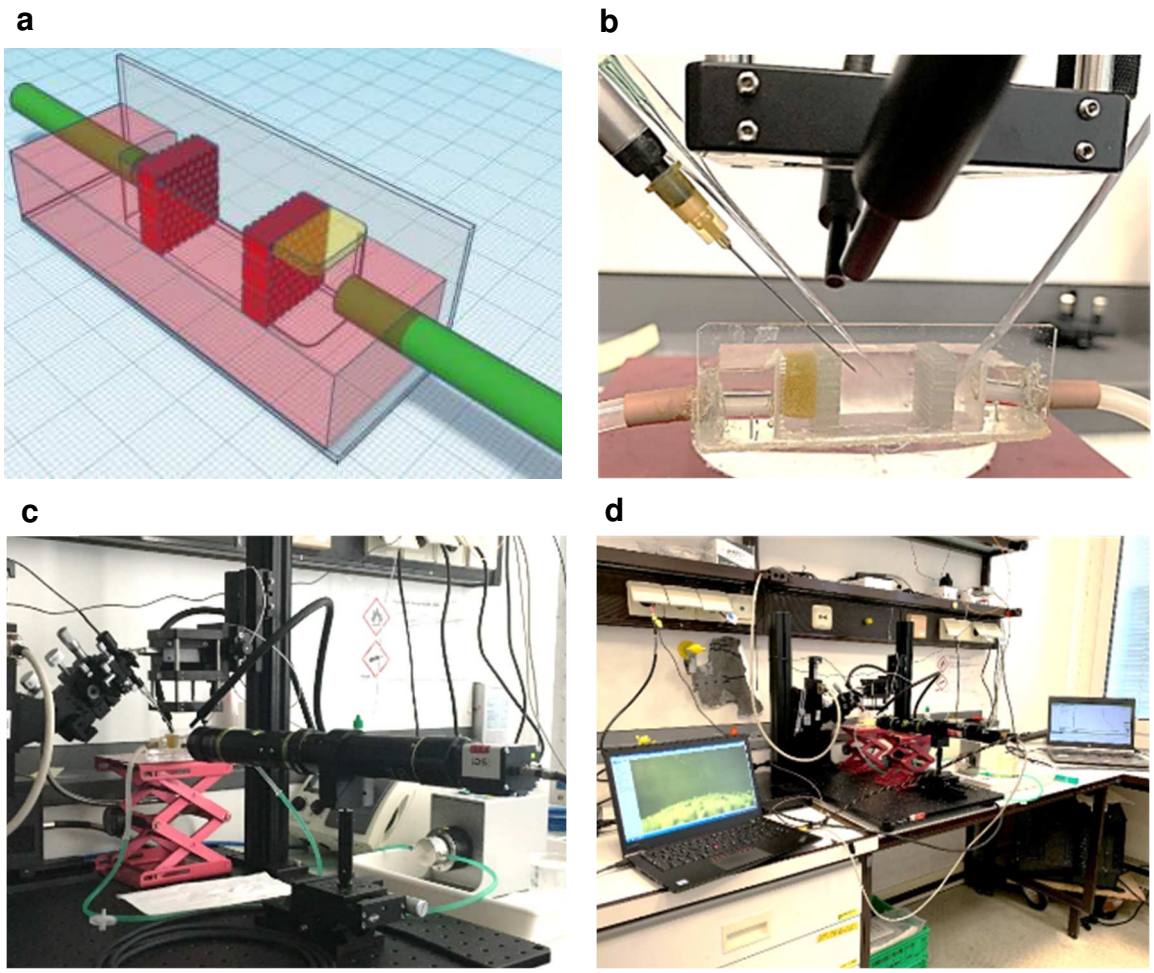

Figure 2.3. The flow-through chamber and experimental set-up from design to reality. **a** Initial 3D model of the chamber used as blueprint for 3D printing and building. **b** Fully realized chamber showing the accessibility and arrangement of the external equipment (for details of the different elements see Chapter 3 - Figure 3.1). **c** & **d** Final set-up with the chamber connected to the pump, image acquisition equipment and computers.

2.2. Results and Discussion

The unique buildup of the flow-through chamber presented here allowed the instantaneous and reliable visualization of the flow regime inside at different inflow velocities following expected behaviors (Fig 2.4). Particle Image Velocimetry (PIV) measurements showed a horizontal and stable movement of water with expected boundary layers being formed at all borders of the chamber (Fig. 2.4a & c). The overall direction of the flow inside was mainly horizontal with an overall stronger contribution of the horizontal compared to the vertical flow as measured across a section of the chamber, in particular under elevated flow rates

(Fig. 2.4, b & d). The open space on top plus the low thermal capacity and oxygen permeability of the different elements used in the construction of the chamber (glass and silicone), allowed the maintenance of the water temperature – which mimicked the external ambient temperature (25 ± 0.5 °C) – and of constant oxygen saturation values (100%).

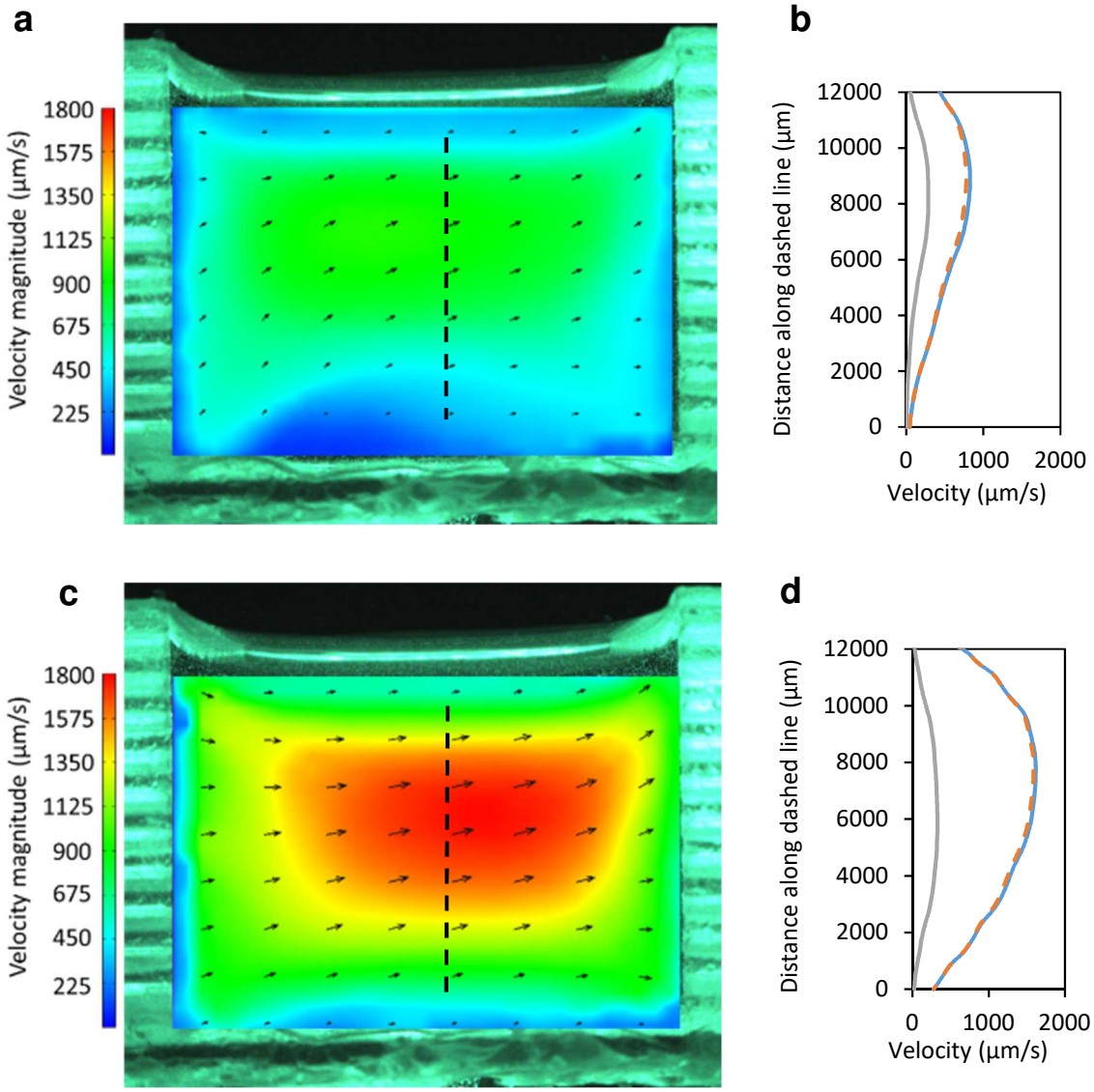

Figure 2.4. **a** & **c**Velocity maps (µm s^{-1}) inside the empty chamber at two different pump speeds: 4 and 10 mL min^{-1} respectively, extracted from PIV analysis. Arrows represent the direction of the flow. **b** & **d** Velocity components along the respective dashed lines inserted in **a** & **c**: Overall velocity magnitude (blue), horizontal component of the velocity (dashed orange), vertical component of the velocity (grey).

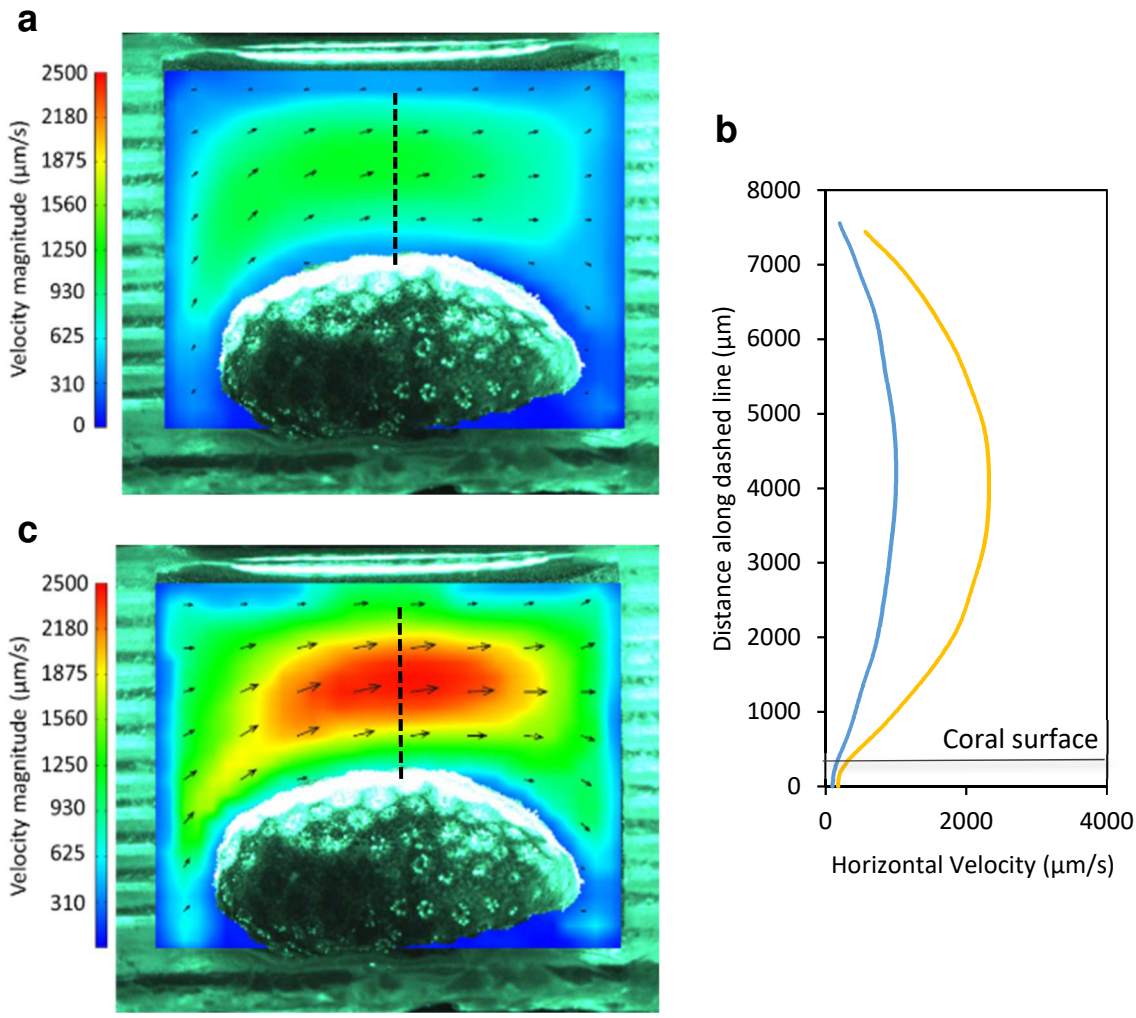

Figure 2.5. **a** & **c** Velocity maps (µm s^{-1}) inside chamber with a coral colony at two different pump speeds: 4 and 10 mL min^{-1} respectively, extracted from PIV analysis. Arrows represent the direction of the flow. **b** Horizontal velocity along the respective dashed lines inserted in **a** & **c**: 4 mL min^{-1} (blue), 10 mL min^{-1} (orange).

In order to demonstrate the applicability of the chamber in the study of boundary layer processes of corals, a *Porites lutea* micro-colony was introduced (Fig. 2.5) and PIV measurements were conducted at the same pump speeds as previously used with the empty chamber. The presence of the coral colony had the expected effect on the water flow with the building of a momentum boundary layer on top of he colony (Fig. 2.5b). For both tested pump rates (4 & 10 mL min^{-1}) the direction of the flow on top of the colony, the area of designated physiological measurements, showed a clear horizontal flow, as can be seen from the direction of the arrows inserted in Fig 2.5 (a-c). Higher flow rates of the pump were also tested however in these cases the flow inside the chamber became highly turbulent and rather

unpredictable. These fast and turbulent flows proved not to be ideal for PIV measurements using the above described equipment as faster high speed cameras would be required in order to map particle movemet (Liao et al. 2009, Gemmell et al. 2014). Nevertheless the relatively smooth flow imposed here yielded velocities that correspond to flow velocities of 1-2 cm s^{-1} in a benthic boundary layer above estimated from Van Driest (1956) which compare well with the flow velocities measured in the immediate vicinity of coral colonies (Chang et al. 2009).

It is important to acknowledge that the, here designed, closed circulating system is not sustainable for exceedingly long observation periods, as the water chemistry will start to change due to evaporation coupled with the metabolic activity of the coral itself. Therefore, such a chamber was only used for rather short-term experimental procedures that lasted for a few hours. Irrespective, the chamber proved highly capable to address pertinent questions on microscale physiological process in corals and the interaction with the surrounding water column. Its proven capacity to allow a tight control and monitoring of a range of physicochemical parameters will further help us to decipher coral responses to various external factors, e.g. light, temperature extreme conditions, etc. Furthermore, the system can be coupled with newly developed high-resolution techniques such as oxygen reagent nanoparticles (sensPIV – see chapter 4), and linear hyperspectral imaging (see chapter 5) enabling novel insights into the physiology of corals.

2.3. References

Al-Horani, F. A., S. M. Al-Moghrabi, and D. de Beer. 2003. Microsensor study of photosynthesis and calcification in the scleractinian coral, *Galaxea fascicularis*: active internal carbon cycle. J Exp Mar Biol Ecol **288:** 1-15.

Carpenter, L. W., and M. R. Patterson. 2007. Water flow influences the distribution of photosynthetic efficiency within colonies of the scleractinian coral *Montastrea annularis* (Ellis and Solander, 1786); implications for coral bleaching. J Exp Mar Biol Ecol **351:** 10-26.

Chang, S., C. Elkins, M. Alley, J. Eaton, and S. Monismitha. 2009. Flow inside a coral colony measured using magnetic resonance velocimetry. Limnol Oceanogr **54:** 1819-1827.

de Beer, D., M. Kühl, N. Stambler, and L. Vaki. 2000. A microsensor study of light enhanced Ca^{2+} uptake and photosynthesis in the reef-building hermatypic coral *Favia* sp.†. Mar Ecol Prog Ser **194:** 75-85.

Dennison, W. C., and D. J. Barnes. 1988. Effect of water motion on coral photosynthesis and calcification. J Exp Mar Biol Ecol **115:** 67-77.

Gemmell, B. J., H. Jiang, and E. J. Buskey. 2014. A new approach to micro-scale particle image velocimetry (μPIV) for quantifying flows around free-swimming zooplankton. J Plankton Res **36:** 1396-1401.

Jokiel, P. L. 1978. Effects of water motion on reef corals. J Exp Mar Biol Ecol **35:** 87-97.

Kim, P., K. W. Kwon, Park, Min Cheol , S. H. Lee, S. M. Kim, and K. Y. Suh. 2008. Soft Lithography for Microfluidics: a Review. Biochip Journal **2:** 1-11.

Kühl, M., Y. Cohen, T. Dalsgaard, B. B. Jørgensen, and N. P. Revsbech. 1995. Microenvironment and photosynthesis of zooxanthellae in scleractinian corals studied with microsensors for O_2, pH and light. Mar Ecol Prog Ser **117:** 159-172.

Liao, Q. and others 2009. Development of an *in situ* underwater particle image velocimetry (UWPIV) system. Limnol Oceanogr Methods **7:** 169-184.

Patterson, M. R., K. P. Sebens, and R. Randolph Olson. 1991. *In situ* measurements of flow effects on primary production and dark respiration in reef corals. Limnol Oceanogr **36:** 936-948.

Ralph, P. J., U. Schreiber, R. Gademann, M. Kühl, and A. W. D. Larkum. 2005. Coral photobiology studied with a new imaging pulse amplitude modulated fluorometer. J Phycol **41:** 335-342.

Shapiro, O. H., E. Kramarsky-Winter, A. R. Gavish, R. Stocker, and A. Vardi. 2016. A coral–on–a–chip microfluidic platform enabling live-imaging microscopy of reef-building corals. Nat Commun **7:** 10860.

Van Driest, E. R. 1956. On turbulent flow near a wall. AIAA J. **23:** 1007-1011.

Willert, C., B. Stasicki, J. Klinner, and S. Moessner. 2010. Pulsed operation of high-power light emitting diodes for imaging flow velocimetry. Meas Sci Technol **21:** 075402.

3

Ciliary vortex flows and oxygen dynamics in the coral boundary layer

Cesar O. Pacherres[1,2,*], Soeren Ahmerkamp[3,4], Gertraud M. Schmidt-Grieb[1], Moritz Holtappels[1,4,a], Claudio Richter[1,2,a]

1 Alfred Wegener Institute, Helmholtz Centre for Polar and Marine Research, Bremerhaven, Germany

2 University of Bremen, Germany

3 Max Planck Institute for Marine Microbiology, Bremen, Germany

4 Marum, Bremen, Germany

a These authors share senior authorship

* Corresponding author

Published in Scientific Reports 10, 7541 (2020)

DOI: 10.1038/s41598-020-64420-7

Received: 16 – Jan – 2020

Accepted: 15 – Apr – 2020

3.1 Abstract

The exchange of metabolites between environment and coral tissue depends on the flux across the diffusive boundary layer (DBL) surrounding the tissue. Cilia covering the coral tissue have been shown to create vortices that enhance mixing in the DBL in stagnant water. To study the role of cilia under simulated ambient currents, we designed a new light-sheet microscopy based flow chamber setup. Microparticle velocimetry was combined with high-resolution oxygen profiling in the coral *Porites lutea* under varying current and light conditions with natural and arrested cilia beating. Ciliary vortices in the lower DBL mitigated extreme oxygen concentrations close to the tissue surface. Under light and arrested cilia, oxygen surplus at the tissue surface increased to 350 µM above ambient, in contrast to 25 µM under ciliary beating. Oxygen shortage in darkness decreased from 120 µM (cilia arrested) to 86 µM (cilia active) below ambient. Ciliary redistribution of oxygen had no effect on the photosynthetic efficiency of the photosymbionts and overall oxygen flux across the DBL indicating that oxygen production and consumption was not affected. We found that corals actively change their environment and suggest that ciliary flows serve predominantly as a homeostatic control mechanism which may play a crucial role in coral stress response and resilience.

Author contributions

C.O.P., S.A., G.M.S., M.H. and C.R. designed the setup for the experiments. C.O.P. conducted all the experiments. C.O.P. and S.A. analyzed the PIV and PTV data. C.O.P. and M.H. analyzed the oxygen data. C.O.P., S.A. and M.H. created all figures. C.O.P., S.A., G.M.S., M.H. and C.R. contributed to the interpretation of the collected data, and conceived and wrote the manuscript.

3.2 Introduction

It is commonly perceived that sessile aquatic organisms are subjected to the physicochemical conditions of their environment, and that their capacity to cope and adapt determines their survival (Bayne 1985). It is less known, however, that sedentary animals may also shape their environment physically and chemically (Odling-Smee et al. 1996, Laland and Sterelny 2006), in these cases active responses through adaptation or modifications of the environment may entail large energetic costs, particularly in small organisms operating at small Reynolds numbers where energy reserves are low. In the case of coral colonies, which individuals have limited or no motility, modifying the characteristics of their immediate surrounding, i.e. the Diffusive Boundary Layer (DBL), might be crucial for their survival (Shapiro et al. 2014).

The DBL is the thin layer of water adjacent to all submerged surfaces where molecular diffusion is the dominant mechanism of transport for dissolved substances. The flow in the DBL is laminar and parallel to the boundary surface, so that vertical advective fluxes approach zero and diffusive fluxes dominate. The DBL is generally between 0.2-1 mm thick (Jørgensen and Revsbech 1985) and varies depending on the flow speed of the ambient water (Patterson and Sebens 1989, Jørgensen and Des Marais 1990, Wang et al. 2012). Its upper boundary is defined by the distance where the eddy diffusion coefficient, K, which governs the turbulent free-flow region of the water column, approaches the molecular diffusion coefficient, D (Hondzo et al. 2005). Therefore, and according to classic boundary layer theory, assuming that there is no production or consumption of the compound within the DBL itself, the concentration gradient across the DBL should be linear (Barry and Diamond 1984, Schlichting and Gersten 2017).

In most coral colonies, the individual polyps are small (cm to mm) and surrounded by a DBL, the thickness of which depends on ambient water flow and colony morphology (Gardella and Edmunds 2001, Chang et al. 2009). Any exchange or transport of dissolved substances between organism and surrounding water column has to happen via diffusion through this DBL, a process that in turn will depend on the molecules' diffusivity and concentration gradients (Cussler 2007). For tropical corals living in symbiosis with unicellular dinoflagellate algae (Zooxanthellae), oxygen is of particular importance. During the day, the photosynthetic algae produce a surplus of oxygen, as a function of light intensity (Levy et al. 2003, Ferrier-Pagès et al. 2013), zooxanthellae density (Hoegh-Guldberg and

Smith 1989), ambient flow speed (Finelli et al. 2006, Mass et al. 2010), and dissolved inorganic carbon (Langdon and Atkinson 2005). This excess of oxygen accumulates in the tissue and diffuses across the DBL into the water column aloft (Kühl et al. 1995). During the night, oxygen is consumed reversing the direction of the diffusive flux from the water column towards the tissue (Shashar et al. 1993). The characteristics of the DBL, therefore, have a strong influence on coral physiology and its ability to respond to ambient conditions.

The water flow in the DBL is laminar and parallel to the surface of the solid (Vogel 1996). However, in corals the cilia covering the tissue have the ability to enhance the mixing in this layer by generating vortices (Shapiro et al. 2014). These cilia are present in most Scleractinian corals (Mariscal and Bigger 1977) and considered to be important as feeding and cleaning mechanisms, where they transport particles towards and/or away from the oral openings (Yonge 1930, Lewis and Price 1976, Stafford-Smith and Ormond 1992). So far, the mixing-effect of ciliary vortices have been described by carrying out PIV and microsensor measurements under stagnant flow conditions and constant light, and extending the findings to natural flow conditions by modelling (Shapiro et al. 2014). Here, we extend this study to measure the changes in oxygen across the DBL at different flow speeds, light regimes and under active and arrested cilia activity (the latter achieved using sodium orthovanadate (Shapiro et al. 2014 – see M&M), using the reef-building coral *Porites lutea* as a model organism. Particle Image Velocimetry (PIV) and Particle Tracking Velocimetry (PTV) were used to map the microscale flow regime at the coral surface and to identify vortex locations when present. Microsensor probes were used to obtain oxygen profiles across the DBL and vortices. Chlorophyll fluorescence quenching was used to measure the effect of ciliary flows on coral health.

3.3 Material and Methods

3.3.1 Coral fragments

Colonies of the massive coral *Porites lutea* reared at the aquaria facilities of the Alfred Wegener Institute (AWI) under conditions mimicking those found at the depth of their origin (15 m) were used as fragment source (Roder et al. 2010, Schmidt et al. 2012). They were kept in artificial seawater (salinity 32.6 ± 0.26) (Dupla Marin Premium Reef Salt Natural Balance) at 25.2 ± 0.07 °C on a 12-h light-dark cycle. Light intensities fluctuated between

75 and 80 µmol quanta m^{-2} s^{-1} (LI-COR LI-192, USA) and pH was kept at 7.9 ± 0.09 (YSI, USA). Food was provided in the form of freshly hatched *Artemia* nauplii every second day. Before the start of the experiments small fragments, (1.5 cm long, 1 cm wide) bearing 60 to 80 polyps were cut out from 4 of the source colonies and allowed to heal for at least two weeks in the same culturing tanks their original colonies were kept. Survival of the fragments was >90%

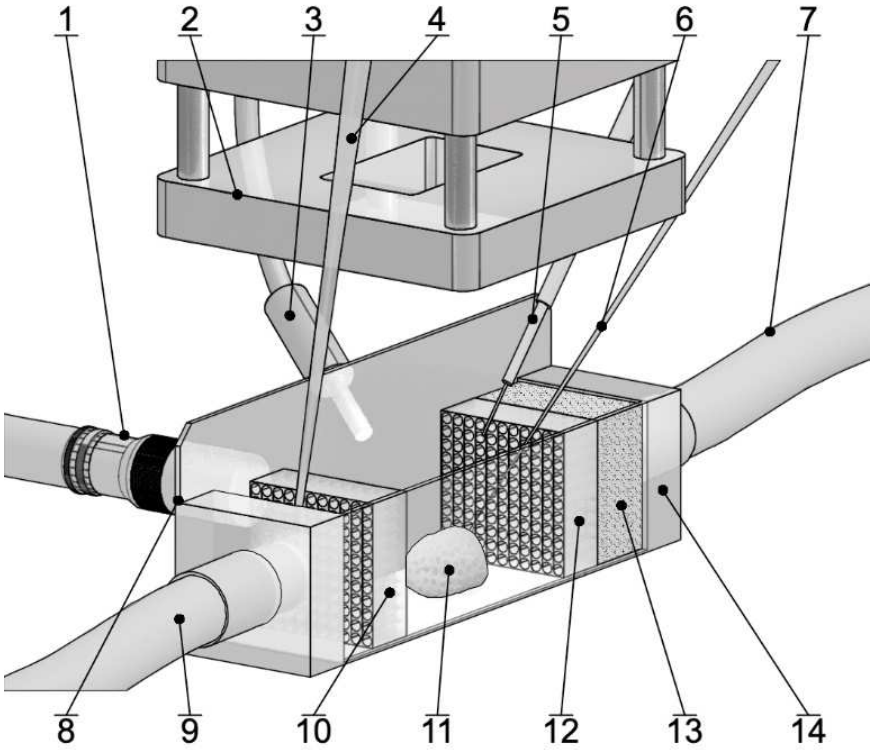

Figure 3.1 Schematic illustration of the light-sheet-microscopy based flow chamber setup. The coral fragment (11) was placed at the center of the PDMS chamber (14) with microscopy glass slides as walls (8). Homogeneous water flow was achieved by placing a sponge (13) and a diffuser (12) at the inlet (7) and a diffuser (10) at the outlet (9). A fiber optic lamp (3) was used as light source for all experiments under light conditions. The LED lens (2) projected a 1 mm thick light sheet on top of the coral colony for the PIV and PTV measurements carried out by a camera pointing sideways and equipped with a long distance microscope lens (1). An electrochemical sensor (6) was used for the oxygen profiles. Temperature (4) and optical oxygen (5) sensors were used to monitor water characteristics inside the chamber. Figure not drawn to scale.

3.3.2 Experimental set up

A polydimethylsiloxane (PDMS) flow-through chamber (2 cm long × 1.5 cm wide × 1.5 cm high) was built over microscope glass slides to allow a side view of the coral colony while leaving an open space on top to allow access for the microsensors (Fig. 3.1). The chamber was connected to a water pump (REGLO Z, ISMATEC, Germany) by 0.5 mm ⌀ silicon hoses. Homogeneous water flow inside the chamber was achieved by placing a sponge on the water inlet followed by a diffuser with a series of 1 mm holes and by placing a second diffuser on the outlet of the chamber.

The coral fragment was placed in the chamber filled with Filtered Artificial Sea Water (FASW) (0.2 pore size) from the coral´s culturing tank. It was allowed to acclimate to the chamber conditions under a low flow regime (water replacement in the chamber every 2 minutes) for at least an hour under dark conditions before experiments started.

To arrest cilia activity we used the fully reversible ATPase inhibitor sodium orthovanadate (Na_3VO_4; Sigma Aldrich). Prior to the experiment, the coral fragment was kept for an hour on FASW containing Na_3VO_4 at a concentration of 0.1 mM (Gibbons et al. 1978). Arrest of cilia activity was verified visually under a stereo microscope before the fragment was transferred into the experimental flow-through chamber supplied with Na_3VO_4–treated FASW for the duration of the experiment.

Oxygen and temperature of the water inside the chamber were monitored every 30 seconds using optical sensors (microoptodes, PyroScience, Germany) positioned at the inlet and outlet of the chamber respectively (Fig. 3.1). For all experiments, temperature was kept constant at 25 °C ± 0.5 and oxygen at 100% saturation.

3.3.3 Particle Velocimetry

To resolve the flow field around the coral fragment, Particle Image Velocimetry (PIV) and Particle Tracking Velocimetry (PTV) were used. Water inside the flow through system was first seeded with 5 μm fluorescent particles (Exc: 468 nm, Emi: 530 nm) (Applied Microspheres, The Netherlands). Particle density was adjusted to approx. 50×10^6 particles L^{-1}, to allow a good map of the flow field without inducing mucus production, a natural response in corals to suspended sediments (Stafford-Smith and Ormond 1992). Illumination was achieved using a LED Pulsing System PIV V2 (ILA_5150, Germany) connected to led

light sheet optics (Willert et al. 2010). The light sheet was 1 mm thick and intensity reached 5500 µmol quanta m^{-2} s^{-1} (LI-COR LI-192, USA) at a wavelength of around 468 nm. Images were captured using a ILA.PIV.µEYE camera (ILA_5150, Germany) recording pictures at 25 frames per second (fps) with an exposure time of 26 ms. A long distance microscope lens (Optem FUSION, Germany) with a bandpass filter of 532 nm was used for all experiments. To avoid photoinhibition of the zooxanthellae from the intense illumination, light exposure was < 5 s for each experiment.

Video frames were processed using PIV software (PIVview2C, PIVTech GmbH). To obtain velocity fields the image sample size was set to 64 × 64 px with a 50% overlap and a multigrid sampling window of 128 × 128. The velocity map was smoothed using a 3 × 3 median filter. PIV output was then post-processed using custom-built Matlab (MathWorks, R2018b) algorithms to obtain the averaged velocity components. Particle trajectories (PTV) were obtained by superimposing consecutive images and the corresponding velocities were calculated by implementing a particle tracking algorithm (Matlab).

3.3.4 Oxygen profiles

Dissolved oxygen profiles in the DBL were carried out using OX10 oxygen microelectrodes (Unisense, Denmark) connected to an OXY-meter amplifier (Unisense, Denmark). Values were recorded using the SensorTrace-PRO software (Unisense, Denmark). Each day microelectrodes were 2-point calibrated in oxygen-free (bubbling pre-filtered seawater with nitrogen gas for 10 min) and air-saturated FASW of known salinity and temperature (Kühl et al. 1995). The tip of the sensor was carefully placed at the surface of the coral. A micromanipulator (Unisense, Denmark) was programmed to move the sensor up in 10 µm steps. The range of the vertical profile was 1000 µm. At each step, dissolved oxygen was measured three times with a sampling interval of 2 s. Oxygen profiles were processed using R Studio Version 1.1.4.

3.3.5 Determination of oxygen flux and DBL thickness

The oxygen flux across the DBL was calculated from the measured oxygen profiles using Fick's first law of diffusion:

$$J = -D\,\Delta C/\Delta z \qquad \text{[Eq. 3.1]}$$

where D is the molecular diffusion coefficient of oxygen at a specific temperature and salinity, in our case: 2.13×10^{-9} m^{-2} s^{-1} (Boudreau 1997) and $\Delta C/\Delta z$ is the vertical oxygen concentration gradient, calculated by linear regression, where C is the concentration and z the vertical distance.

Commonly, the upper boundary of the DBL is determined by the intercept between the linear concentration gradient and the constant part of the O_2 profile, representing the bulk concentration in the free-stream water aloft (Jørgensen and Revsbech 1985). The lower boundary in this study was the coral surface, but only for the case of no cilia activity. Shapiro et al. (Shapiro et al. 2014) showed that ciliary vortices modified the oxygen transport in the lower boundary layer, creating curved or S-shaped profiles that indicate an effective mass transport coefficient significantly larger than the molecular diffusion coefficient. For flux calculations we therefore used the linear part of the profiles above the vortices, a layer we refer to as upper DBL, where particle tracks indicate a laminar, plane parallel flow (see results below) and in which a predominantly diffusive transport can be assumed. We further assume that oxygen is neither produced/consumed in the vortex layer nor in the upper DBL so that the oxygen flux across the two adjacent layers is equal and ultimately represents the flux between coral and ambient water.

3.3.6 Photosynthetic efficiency

The kinetics of chlorophyll fluorescence is commonly used to assert the efficiency of the photosynthetic apparatus, which is susceptible to environmental stress (Warner et al. 1996, Ulstrup et al. 2005) by measuring the maximum quantum yield (MQY) of the Photosystem II complex (PSII) (*Fv/Fm*). We evaluated the response of the coral´s PSII to the experimental manipulation of flow and light under active and arrested ciliary motion by Pulse Amplitude Modulation (PAM) chlorophyll a fluorometry (Schreiber et al. 1986), using a diving PAM fluorometer (Walz, Germany). For this purpose, three coral fragments were subjected to all experimental conditions and the maximum quantum yield of PSII measured for each treatment combination allowing a 15 min adaptation of the coral fragment to the light/dark conditions. PAM data was processed using R Studio.

3.3.7 Experimental design

To identify the relative importance of light, flow speed and cilia activity on the oxygen profiles of *Porites*, their effects were tested in combination. All experiments were performed

in random order and with different coral fragments. Different flow rates from the pump were chosen resulting in flow velocities of 300, 425, 750 and 1300 µm s^{-1} at 2 mm above the coral tissue (Supp. Inf. Fig. S3.1). Such velocities in the laminar boundary layer correspond to flow velocities of 1-2 cm s^{-1} in a turbulent boundary layer above estimated from Van Driest (Van Driest 1956) which compare with the flow velocities measured in the immediate vicinity of coral colonies (Chang et al. 2009).

For all experiments under light, a fiber optic lamp (Schott 1500, USA) was used as light source to maintain constant illumination of 165 µmol quanta m^{-2} s^{-1}. For the experiments under dark conditions (< 1 µmol quanta m^{-2} s^{-1}), all lights were turned off 15 minutes prior to the start of the oxygen profiles. Oxygen profiles were recorded 15 min after the PIV measurement.

3.4 Results

3.4.1 Flow field and DBL

The particle trajectories of the PIV measurements revealed laminar flow conditions in the boundary layer of the coral with water flowing parallel to the tissue surface. These conditions prevailed throughout the entire boundary layer whenever cilia activity was suppressed (Fig. 3.2b+d). When cilia were active, vortices near the tissue were detected, under light exposure and in the dark (Fig. 3.2a+c). The vortex diameters, as approximated from the particle trajectories, were 200 µm under high flow velocities (1300 µm s^{-1}, Fig. 3.2a+c) and 500 µm under low flow velocities (300 µm s^{-1}, Supp. Inf. Fig. S3.2a+c). The upper boundary of the DBL varied inversely with flow. At low flow velocities, the DBL extended up to 1000 µm above the coral surface, while at high velocities it was reduced to 500 µm.

3.4.2 Oxygen gradients and fluxes

With arrested cilia and under light, photosynthetic oxygen production caused very high oxygen concentrations near the coral surface (300 µM above saturation), which decreased linearly from the surface to the upper boundary of the DBL (Fig. 3.2b). When cilia were actively beating, the induced vortices were mixing the lower boundary layer thereby reducing and partly reversing the oxygen gradients (Fig. 3.2a). Vortex mixing caused a decrease of oxygen concentrations at the coral surface by about 110 µM. Above the vortex

layer, the plane parallel particle trajectories and the linear oxygen gradients indicated a diffusive transport. The oxygen gradient in the upper DBL was comparable to the gradient measured under arrested cilia (Fig. 3.3d), suggesting that the flux across the DBL did not change by cilia activity.

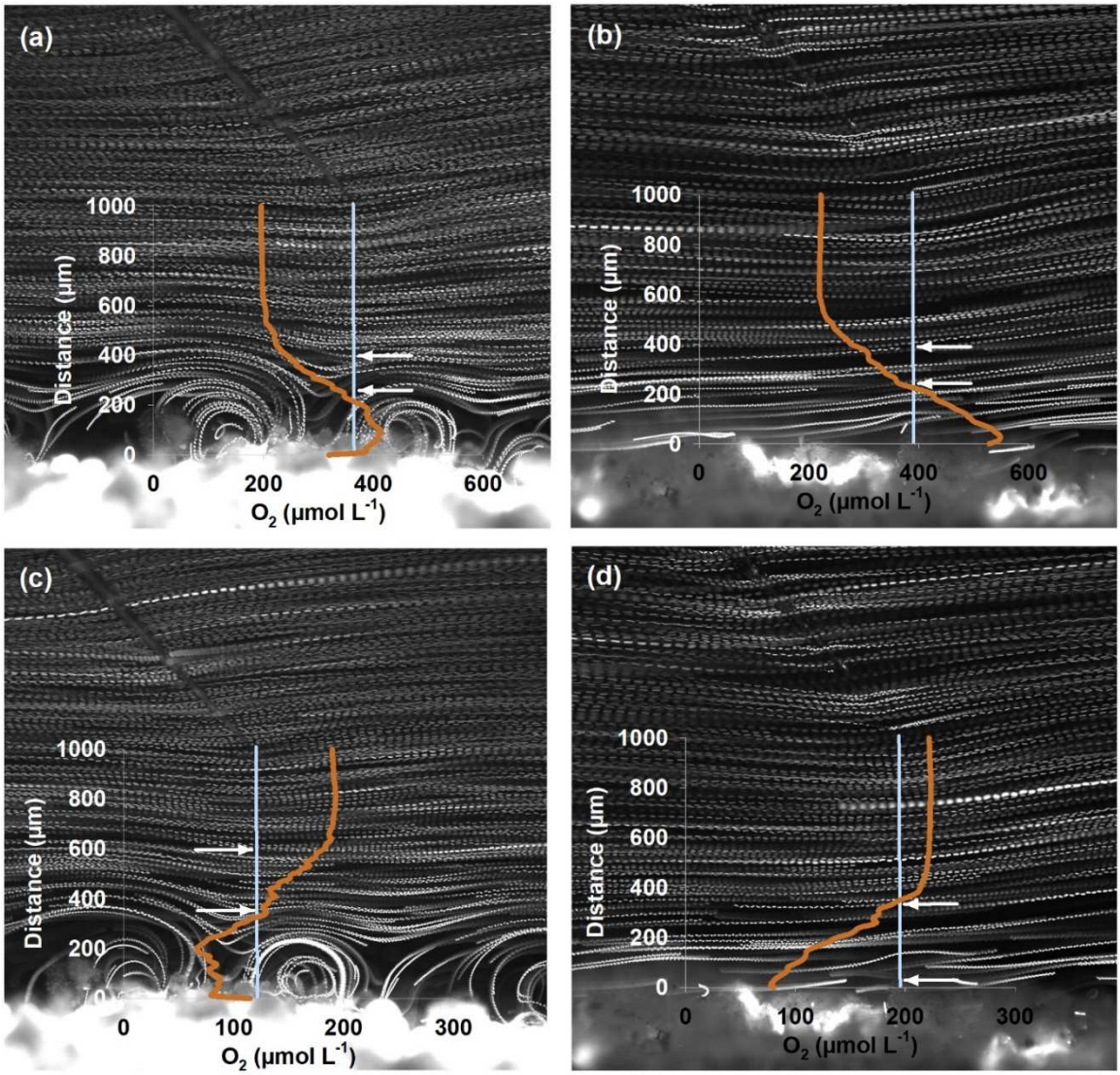

Figure 3.2. Pathline image and oxygen profiles of the coral *Porites lutea* under active (**a** & **c**) and arrested (**b** & **d**) cilia activity as well as under light (**a** & **b**) and dark (**c** & **d**) conditions. Pathlines indicate particle trajectories. Orange lines indicate oxygen concentration along the light blue line measured with a microsensor (also seen in the images). Flow speed of water in this case was 1300 µm s^{-1} measured at 2 mm from the coral surface (see text for more details). Arrows indicate the part of the diffusive boundary layer (DBL) that was considered for oxygen flux calculations.

For the other flow velocities (Fig. 3.2a+b+c), the oxygen gradients in the upper DBL were similar with and without cilia activity, but in all cases the total oxygen content in the DBL was strongly reduced, thus decreasing the extreme oxygen concentrations near the coral surface.

The oxygen extremes were less pronounced in the dark than in light. With arrested cilia and under dark conditions (Fig. 3.2d), we found a linear oxygen decrease by 140 µM between the upper boundary of the DBL and the tissue surface. Under cilia activity (Fig. 3.2c), vortices were again mixing the lower boundary layer. The generation of vortices was associated with a reduced oxygen shortage near the coral surface (only 75 µM below ambient concentrations).

For the lower flow velocities (Supp. Inf. Fig. S3.2b+d & Fig. S3.3), the arrested cilia condition caused a linear decrease in oxygen concentration towards the tissue surface. The oxygen respiration in the dark caused much less deviation from ambient concentrations compared to oxygen production under light exposure. During cilia activity, the vortices caused a redistribution of the oxygen in the vortex layer, which however was not always related to a significant relaxation of oxygen condition towards ambient concentrations.

The oxygen concentration gradient above the vortices was used to calculate the oxygen flux across the upper DBL. The undisturbed upper DBL started where the particle trajectories were quasi-parallel to the tissue surface and extended until the oxygen concentration reached that one of the bulk water (see Fig. 3.2a+c). If possible, the oxygen gradients measured under arrested and active cilia were taken from the same length interval to calculate the flux across the upper DBL (hatched layers in Fig. 3.3). Under light exposure, the calculated fluxes ranged between 5 and 10 µmol cm^{-2} d^{-1} and appeared to show no relation to flow velocities (Fig. 3.3, inserts). The fluxes were comparable between arrested and active cilia conditions with no significant difference at low and high flow velocities (300 and 1300 µm s^{-1}) and only small differences for the intermediate velocities (425 and 750 µm s^{-1}).

When oxygen was consumed by the holobiont in the dark, the oxygen profiles show less overlap between arrested and active cilia conditions (Supp. Inf. Fig. S3.3). Again, only those concentration gradients were considered for flux calculations that were situated in the plane parallel flow, either above the vortices or closer to the tissue surface where a linear gradient was established during arrested cilia conditions. The resulting fluxes ranged between -3.7 and -7.3 µmol cm^{-2} d^{-1}. Except for the low flow velocity, the fluxes were significantly

different between arrested and active cilia conditions. However, no trend was found as only in two cases the flux was enhanced by the cilia activity (Supp. Inf. Fig. S3.3).

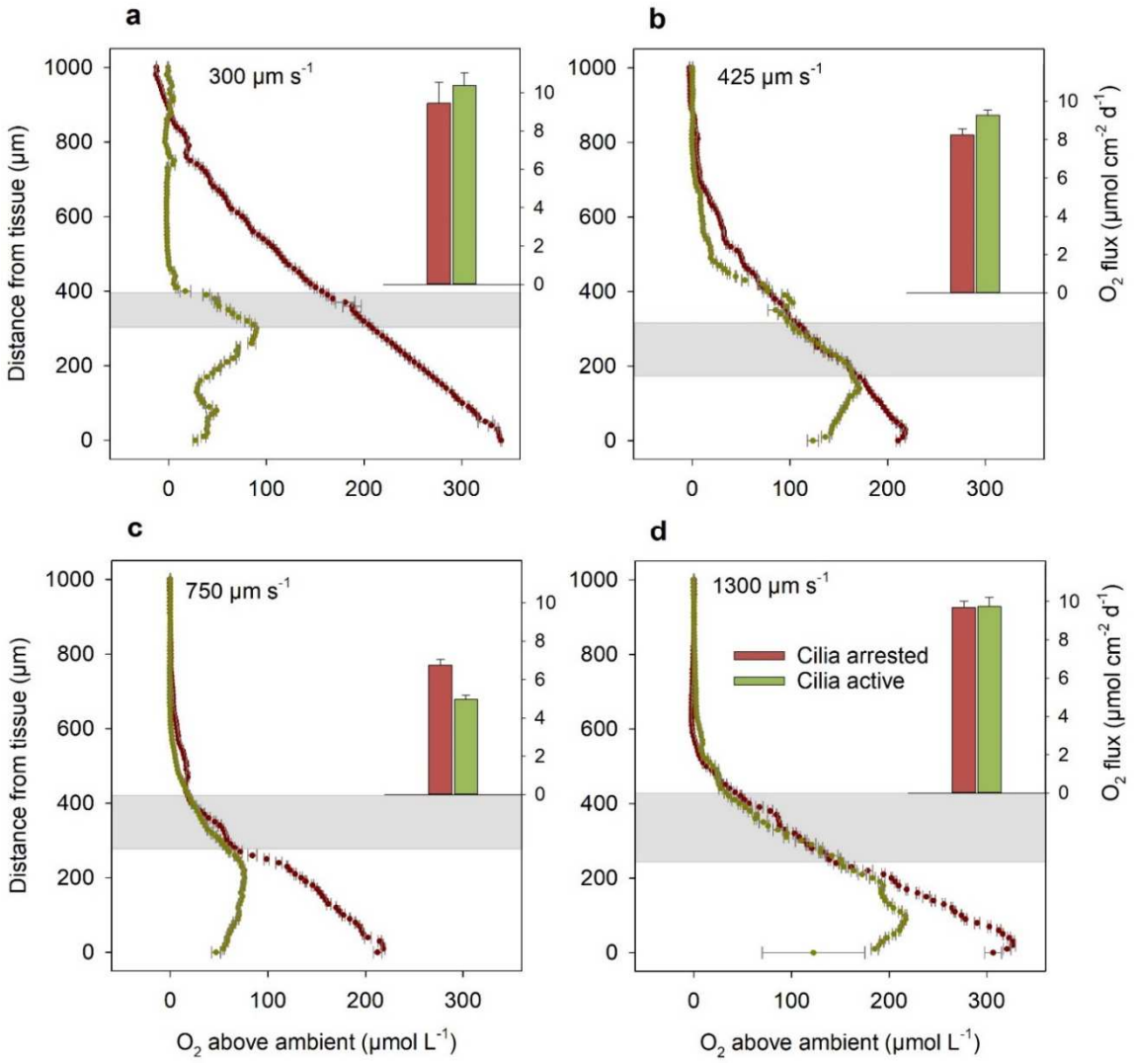

Figure 3.3. Oxygen concentrations along a perpendicular 1000 µm transect from the tissue of *Porites lutea* to the water column under light exposure, at flow speeds of **a**: 300, **b**: 425, **c**: 750 and **d**: 1300 µm s^{-1}, and for arrested and active cilia conditions. Inserted bar plots show the flux of oxygen as calculated from oxygen gradients in the upper DBL (hatched layer). Error bars represent ± standard error of the linear regression.

3.4.3 Oxygen concentrations in the vortex layer

In the vortex layer close to the coral tissue, the shape of the oxygen profile was dependent on the position of the microsensor relative to the 2-dimensional vortex geometry. For profile interpretation, the vortex mixing is briefly described (Fig. 3.4a). The cilia-generated vortices can be seen as stationary features that enhance the exchange between the coral tissue and the

upper DBL where the ambient water is flowing plane parallel. When the coral's photosymbionts are producing oxygen, the lower part of the vortex is exposed to high oxygen concentrations at the coral tissue so that oxygen diffuses into the lower vortex. As the vortex revolves, elevated oxygen concentrations are transported to the upper part of the vortex, which is exposed to the relatively low oxygen concentration in the upper DBL, so that oxygen diffuses out of the upper vortex. On the downturn, the vortex brings again relatively low oxygen to the coral tissue. This revolving distribution mechanism is reflected in the shape of the oxygen profiles (Fig. 3.4b+c).

The largest dissimilarity to the arrested state was seen for profiles that cut in the downward flow and close to the middle of the vortex where relatively low oxygen concentrations are transported downwards, while the least change was found in the upward flow of the vortex where relatively high concentrations are transported upwards. The flow speeds in the boundary layer did not seem to affect the overall pattern.

While the effect of cilia activity on the oxygen fluxes across the upper DBL is minor, vortices strongly affect the oxygen concentrations close to the tissue. The differences in oxygen concentrations were strongest during light conditions, where a decrease of up to several hundred micromoles per liter was caused by cilia activity (Fig. 3.3). In order to quantify the oxygen mitigation close to the tissue, the oxygen concentrations in the lower 50 µm, i.e. below the vortex center and above 10 µm from the tissue (to avoid any boundary artifacts), were averaged for arrested and active cilia conditions. Subsequently the deviations from ambient oxygen concentrations were compared (averaging over the lower 100 µm shows similar results). Under light conditions, cilia activity reduced the above-ambient concentration at the tissue by 34-89% (Fig. 3.4d). The average reduction over the three vortex positions (middle position, downward and upward flow position) was 60%.

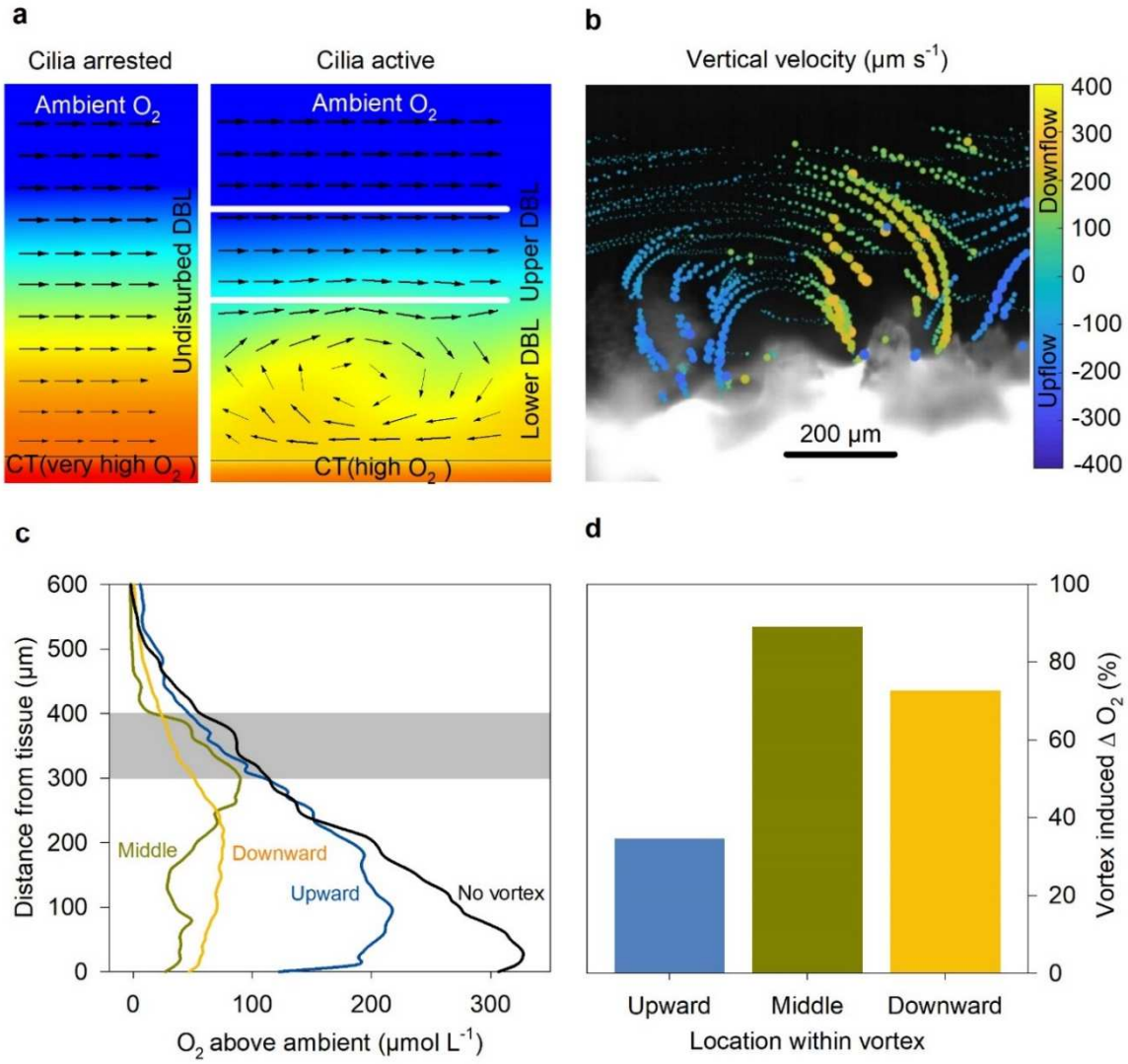

Figure 3.4. **a** Schematic drawing of the enhanced transport mechanism within the vortex layer. Colors denote oxygen concentrations, arrows indicate the flow field. The oxygen gradient close to the tissue is undisturbed when cilia are arrested (left). A revolving vortex (right) destabilizes the gradient by advecting high concentrations upwards and low concentration downwards. Just above the vortex, the exchange is again dominated by diffusion. We define this layer as upper DBL. The enhanced transport by the vortex causes decreased oxygen concentrations close to the coral tissue (CT). **b** Detailed vertical velocity component of a vortex extracted from the PIV results under 1300 µm s^{-1} flow speed, positive values indicate movement towards the coral while negative values indicate water moving away from the coral. **c** Compilation of the oxygen profiles plotted by their location within the vortex: blue -upward section (Fig. 3.3d - Flow speed 1300 µm s^{-1}); green - middle section (Fig. 3.3a - Flow speed 300 µm s^{-1}) and yellow - downward section (Fig. 3.3c - Flow speed 750 µm s^{-1}), black line represents the profile under arrested cilia activity (Fig. 3.3d - Flow speed 1300 µm s^{-1}). Gray area shows the slope similarities of the profiles regardless of flow speed and cilia activity. Vortex extension must be taken under consideration when interpreting the graph. **d** Vortex induced delta O_2 under light conditions for the different locations within the vortex. The reduction of oxygen concentration in the first 50 µm of the DBL under active cilia is shown in percent of the above-ambient oxygen concentrations measured under arrested cilia.

3.4.4 Photosynthetic efficiency

The photosynthetic efficiency was measured for three coral fragments to assess the environmental stress due to the various experimental conditions. *Fv/Fm* values were similar across all experiments (Fig. 3.5). No differences were detected due to light regimes, flow speeds or cilia activity, tested neither as single factors nor in interactions (ANOVA, Supp. Inf. Table S3.1). Moreover, there was no effect of the ciliary inhibitor on the photosynthetic efficiency of the zooxanthellae as can be seen on the similar MQY values when compared active and arrested cilia activity under light (Fig. 3.5) (For the MQY values in the dark, see Supp. Inf. Fig. S3.4).

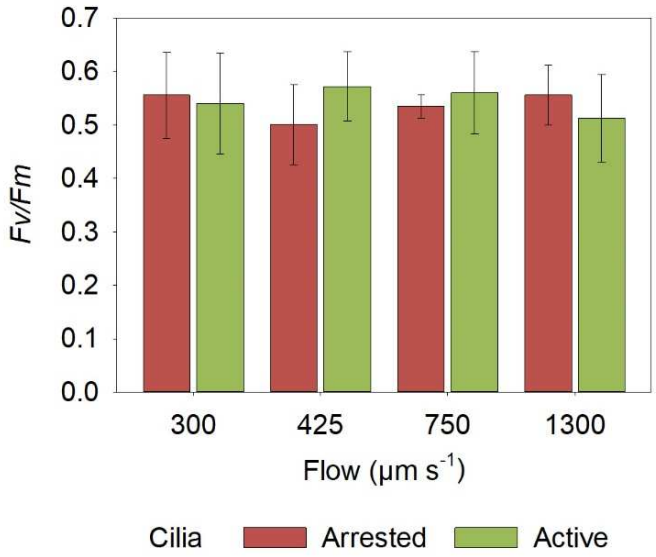

Figure 3.5. Maximum quantum yield (MQY) of photosystem II (*Fv/Fm*) of zooxanthellae within *Porites lutea* in relation to the flow speed of the water (µm s^{-1}) and cilia activity (active and arrested) after 15 min light adaptation (165 µmol quanta m^{-2} s^{-1}). Error bars represent ± s.d.

3.5 Discussion

Corals have the ability to create a microhabitat around them with characteristics that can be considerably different from those of the water column (Schiller and Herndl 1989). The flow and oxygen measurements revealed a clear effect of cilia induced vortex flow on oxygen concentration in the boundary layer of the coral *Porites lutea* under natural flow and light conditions. The vortices enhanced the mixing of oxygen in the lower boundary layer

regardless of the ambient flow speed and therefore significantly changed the oxygen concentrations close to the coral tissue compared to the diffusion-controlled transport without cilia activity. Vortex mixing is a complex transport process in which advection and diffusion are intertwined. If vortices are assumed stable over time, the water parcels revolve permanently without an effective advection out of the vortex. However, as the water parcels in a vortex revolve they are brought to layers of different oxygen concentrations so that steep concentration gradients enhance the diffusive exchange. The transport across the vortex layer is thus a mixture of diffusion and advection which, on average, results in an increased effective mass transport coefficient larger than the molecular diffusion coefficient. Above the vortex layer, the laminar flow was oriented plane parallel so that diffusive transport was again dominating the vertical flux. The vortex layer was thus topped by an upper diffusive boundary layer in which oxygen gradients could be measured and fluxes determined. Since we assume no oxygen production or consumption in the vortex layer and in the upper DBL, the flux across the two layers is equal and ultimately represents the flux between coral and ambient water. In the light exposure experiments, the gradients and thus the fluxes in the (upper) DBL were similar with and without cilia activity (Fig. 3.3) suggesting for both cases a constant flux and thus a constant oxygen production in the coral tissue. The enhanced mass transport coefficient in the vortex layer did not result in enhanced fluxes, indicating that photosynthetic oxygen production of the endosymbionts was neither down- nor up-regulated upon vortex mixing but remained constant, seen also in the PAM results, and probably depended only on light intensity and symbiont density (Hoegh-Guldberg and Smith 1989, Ferrier-Pagès et al. 2013).

In our study, the main benefit of the generated vortices is the reduction of elevated oxygen concentrations at the immediate surface of the coral. The vortex mixing had thus a different outcome in our measurements compared to the Shapiro-Fernandez model (Shapiro et al. 2014). The reason is that the Shapiro-Fernandez model assumed constant oxygen concentration at the coral tissue, which results in increased oxygen fluxes upon cilia activity, whereas we observed constant fluxes which results in reduced concentrations. Nevertheless, the relative increase of the mass transport coefficient due to cilia activity is comparable in both studies. In our study, the effect of vortices can roughly be estimated from the reduction in oxygen concentrations close to the tissue. Upon vortex mixing, the oxygen concentrations at the coral surface decreased on average to 40% of the above-ambient concentration without vortex mixing. Applying Fick's law for the entire boundary layer (i.e. vortex layer and upper

BL) and assuming a constant flux (*J*), a reduction of concentrations by a factor of 0.4 suggests a reciprocal enhancement of the effective mass transport coefficient (*D*) by a factor of 2.5 (=1/0.4). This compares well with the 2-3 fold flux enhancement that was modeled for a small-polyped plate under similar flow conditions (Shapiro et al. 2014). Under the observed constant oxygen production, the role of vortex mixing is predominantly the mitigation of excessive oxygen concentrations at the coral tissue. A change of oxygen concentrations at the tissue surface has several physiological consequences. Oxygen is the essential element for all aerobic organisms. However, as in the case of corals, excess of oxygen can also be detrimental to living tissues (Dykens and Shick 1984, Lesser and Shick 1989). The higher affinity of Rubisco Form II to oxygen over CO_2 will cause photorespiration, which has a high metabolic cost (Crawley et al. 2010). On the other hand, the production and accumulation of oxygen radicals after photosynthesis have proved to cause cellular damage and a subsequent bleaching reaction in corals (Lesser et al. 1990, Lesser 1997, Yakovleva et al. 2009). Vortex formation caused the mitigation of the high oxygen values seen under arrested cilia activity, improving the conditions at the tissue surface by promoting the efflux of oxygen out of the tissue and reducing its detrimental consequences inside the coral. We suggest that cilia induced flows change the chemical environment of corals as part of a homeostatic control mechanism. This mechanism may be of particular importance for buffering the activity of the photosynthetic endosymbionts whose oxygen production may not be downregulated by the host organism itself.

The cilia mediated mitigation should be also effective for other substrates and products that are exchanged with the ambient water. Assuming the same ratio between the fluxes of oxygen and pH as found by Chan, et al. (2016) (12 µmol O_2 cm^{-2} d^{-1} and -7.28 10^{-10} mol H^+ cm^{-2} d^{-1}), we calculated that for an ambient pH of 7.9: the expected pH at the tissue surface in our experiments would have been 8.53 pH units without vortex mixing. Cilia induced vortices would have effectively reduced the pH to 8.06 units. Photosynthesis, respiration and calcification influence proton concentration at the surface of the coral (Al-Horani et al. 2003) with higher pH values during light regimes. Cilia activity will cause the mitigation of extreme proton depletion at surface levels, enhancing their flux towards the tissue, which in turn might favor coral´s growth rates.

The results were less conclusive when oxygen was consumed by the holobiont in the dark. Although the vortex flows clearly effect oxygen gradients in the lower DBL, the calculated fluxes were neither similar between active and arrested cilia conditions nor was there a clear

trend suggesting an enhancement of the flux. The mitigation of oxygen depletion by active cilia was less obvious and found only in 2 out of 4 flow velocities. We suggest two possible reasons for the deviating results under dark conditions. First, different from the oxygen production which was controlled mostly by light intensity and endosymbiont density, the consumption of the holobiont may be diffusion limited within the tissue, depending on the tissue thickness and the oxygen demand therein. Enhanced oxygen concentrations under active cilia conditions would result in enhanced fluxes. The other factor is the potential heterogeneity within the investigated coral tissue and between different coral fragments. Different coral fragments were used for each flow field and oxygen measurement, and the tissue itself, its thickness and oxygen demand may be less homogenous compared to the endosymbiont distribution (Hill et al. 2004). The oxygen demand of the holobiont may also depend on temporal aspects such as day-night rhythm or the time period since the last feeding. Nevertheless, it is likely that the enhanced vortex mixing is also beneficial in the dark during oxygen consumption. Corals living in reef flats and lagoons can experience periods of minimum water flow (Nakamura and van Woesik 2001) which can lead to frequent and prolonged periods of hypoxia (Kühl et al. 1995) causing bleaching and death of the coral colony (Altieri et al. 2017). Cilia beating at night might therefore help to alleviate detrimental low oxygen concentrations, which together with other mechanisms such as polyp expansion, triggered by low light (Pacherres et al. 2013) will promote the exchange of oxygen with the water column (Shashar et al. 1993).

For the interpretation of the results we assume that the experimental treatments did not affect the photosynthetic efficiency as the *Fv/Fm* of the coral colonies during the experiments was in the range of the response of healthy corals in the field (0.5 -0.9) (Jones and Hoegh-Guldberg 2001). There was not a significant change of the photosynthetic efficiency of PSII as a result of the exposure of the coral fragments to neither sodium orthovanadate (used to inactivate cilia movements), nor to light. Corals under high light conditions tend to present lower yield values reflecting the stress the PSII is being exposed to (Levy et al. 2004) however in our case, light intensity was not as strong as to produce a detectable stress signal in the PSII efficiency, which, at the same time, excludes photoinhibition due to oxygen radical production (Lesser 1997).

Further research is needed to study the response of cilia activity to different boundary conditions under elevated heat, increased pH, or high particle concentrations. Ideally, the 1-dimensional oxygen profiling should be supported by 2-D or 3-D visualization of oxygen

concentrations such as shown by Koren et al. (2016) who captured the oxygen dynamic on the tissue surface of a larger coral fragment. Moreover, the possible involuntary arrestment of cilia beating by different stressors requires as well in-depth understanding, since elemental accumulation or depletion at tissue level might have detrimental consequences to coral physiology. Understanding the physico-chemical conditions of the coral´s DBL and the way the organism interacts with that layer is essential if we want to elucidate its response to a changing environment. The proven ability of corals to alter their DBL and by doing so interfere with diffusion processes consequently shaping their environment, might be the missing key when trying to understand processes such as selective bleaching and recovery in the face of warming and acidifying oceans.

Acknowledgements

We thank Esther Lüdtke and Nils Owsianowski for their advice and prompt help. This research was conducted in the frame of the Ph.D. project of Cesar O. Pacherres at the University of Bremen and the Alfred Wegener Institute. It was supported and financed by Cienciactiva, initiative from the Consejo Nacional de Ciencia, Tecnología e Innovación Tecnológica (CONCYTEC), Perú. Contrato 086-2016-FONDECYT and the Alfred Wegener Institute (PACES II programme, Topic 2, WP 3). MPI Bremen provided logistic and instrumental support. S.A. acknowledges funding from the Max Planck Society (MPG) for the "Multiscale Approach on the Role of Marine Aggregates (MARMA)" project.

3.6 References

Al-Horani, F. A., S. M. Al-Moghrabi, and D. de Beer. 2003. Microsensor study of photosynthesis and calcification in the scleractinian coral, *Galaxea fascicularis*: active internal carbon cycle. J Exp Mar Biol Ecol **288:** 1-15.

Altieri, A. H., S. B. Harrison, J. Seemann, R. Collin, R. J. Diaz, and N. Knowlton. 2017. Tropical dead zones and mass mortalities on coral reefs. PNAS **114:** 3660-3665.

Barry, P. H., and J. M. Diamond. 1984. Effects of unstirred layers on membrane phenomena. Physiol. Rev. **64:** 763-872.

Bayne, B. L. 1985. Response to environmental stress: tolerance, resistance and adaptation, p. 331 - 349. *In* J. S. Gray and M. E. Christiansen [eds.], Marine Biology of Polar Regions and Effects of Stress in Marine Organisms: Proceedings of the 18th European Marine Biology Symposium, University of Oslo, Norway. John Wiley & Sons.

Boudreau, B. P. 1997. Diagenetic models and their implementation, 1st ed. Springer.

Chan, N. C. S., D. Wangpraseurt, M. Kühl, and S. R. Connolly. 2016. Flow and coral morphology control coral surface ph: Implications for the effects of ocean acidification. Front Mar Sci **3**.

Chang, S., C. Elkins, M. Alley, J. Eaton, and S. Monismitha. 2009. Flow inside a coral colony measured using magnetic resonance velocimetry. Limnol Oceanogr **54:** 1819-1827.

Crawley, A., D. I. Kline, S. Dunn, K. Anthony, and S. Dove. 2010. The effect of ocean acidification on symbiont photorespiration and productivity in *Acropora formosa*. Glob. Change Biol. **16:** 851-863.

Cussler, E. L. 2007. Diffusion: Mass transfer in fluid systems, 3rd ed. Cambridge University Press.

Dykens, J. A., and J. M. Shick. 1984. Photobiology of the symbiotic sea anemone, *Anthopleura elegantissima*: Defenses against photodynamic effects, and seasonal photoacclimatization. Biol Bull **167:** 683-697.

Ferrier-Pagès, C. and others 2013. In situ assessment of the daily primary production of the temperate symbiotic coral *Cladocora caespitosa*. Limnol Oceanogr **58:** 1409-1418.

Finelli, C. M., B. S. T. Helmuth, N. D. Pentcheff, and D. S. Wethey. 2006. Water flow influences oxygen transport and photosynthetic efficiency in corals. Coral Reefs **25:** 47-57.

Gardella, D. J., and P. J. Edmunds. 2001. The effect of flow and morphology on boundary layers in the scleractinians *Dichocoenia stokesii* (Milne-Edwards and Haime) and *Stephanocoenia michilini* (Milne-Edwards and Haime). J Exp Mar Biol Ecol **256:** 279-289.

Gibbons, I. R. and others 1978. Potent inhibition of dynein adenosinetriphosphatase and of the motility of cilia and sperm flagella by vanadate. PNAS **75:** 2220-2224.

Hill, R., U. Schreiber, R. Gademann, A. W. D. Larkum, M. Kühl, and P. J. Ralph. 2004. Spatial heterogeneity of photosynthesis and the effect of temperature-induced bleaching conditions in three species of corals. Mar Biol **144:** 633-640.

Hoegh-Guldberg, O., and G. J. Smith. 1989. Influence of the population density of zooxanthellae and supply of ammonium on the biomass and metabolic characteristics of the reef corals *Seriatopora hystrix* and *Stylophora pistillata*. Mar Ecol Prog Ser **57:** 173-186.

Hondzo, M., T. Feyaerts, R. Donovan, and B. L. O'Connor. 2005. Universal scaling of dissolved oxygen distribution at the sediment-water interface: A power law. Limnol Oceanogr **50:** 1667-1676.

Jones, R. J., and O. Hoegh-Guldberg. 2001. Diurnal changes in the photochemical efficiency of the symbiotic dinoflagellates (*Dinophyceae*) of corals: photoprotection, photoinactivation and the relationship to coral bleaching. Plant Cell Environ **24:** 89-99.

Jørgensen, B. B., and D. J. Des Marais. 1990. The diffusive boundary layer of sediments: Oxygen microgradients over a microbial mat. Limnol Oceanogr **35:** 1343-1355.

Jørgensen, B. B., and N. P. Revsbech. 1985. Diffusive boundary layers and the oxygen uptake of sediments and detritus1. Limnol Oceanogr **30:** 111-122.

Koren, K., S. L. Jakobsen, and M. Kühl. 2016. In-vivo imaging of O_2 dynamics on coral surfaces spray-painted with sensor nanoparticles. Sens. Actuators B Chem. **237:** 1095-1101.

Kühl, M., Y. Cohen, T. Dalsgaard, B. B. Jørgensen, and N. P. Revsbech. 1995. Microenvironment and photosynthesis of zooxanthellae in scleractinian corals studied with microsensors for O_2, pH and light. Mar Ecol Prog Ser **117:** 159-172.

Laland, K. N., and K. Sterelny. 2006. Perspective: Seven reasons (not) to neglect niche construction. Evolution **60:** 1751-1762.

Langdon, C., and M. J. Atkinson. 2005. Effect of elevated pCO_2 on photosynthesis and calcification of corals and interactions with seasonal changes in temperature/irradiance and nutrient enrichment. J. Geophys. Res. **110:** 1-16.

Lesser, M. P. 1997. Oxidative stress causes coral bleaching during exposure to elevated temperatures. Coral Reefs **16:** 187-192.

Lesser, M. P., and J. M. Shick. 1989. Effects of irradiance and ultraviolet radiation on photoadaptation in the zooxanthellae of *Aiptasia pallida* primary production, photoinhibition, and enzymic defenses against oxygen toxicity. Mar Biol **102:** 243-255.

Lesser, M. P., W. R. Stochaj, D. W. Tapley, and J. M. Shick. 1990. Bleaching in coral reef anthozoans: effects of irradiance, ultraviolet radiation, and temperature on the activities of protective enzymes against active oxygen. Coral Reefs **8:** 225-232.

Levy, O., Z. Dubinsky, and Y. Achituv. 2003. Photobehavior of stony corals: responses to light spectra and intensity. J. Exp. Biol. **206:** 4041-4049.

Levy, O., Z. Dubinsky, K. Schneider, Y. Achituv, D. Zakai, and M. Y. Gorbunov. 2004. Diurnal hysteresis in coral photosynthesis. Mar Ecol Prog Ser **268**.

Lewis, J. B., and W. S. Price. 1976. Patterns of ciliary currents in Atlantic reef corals and their functional significance. J Zool (Lond) **178:** 77-89.

Mariscal, R. N., and C. H. Bigger. 1977. Possible ecological significance of octocoral epithelial ultrastructure. Proc 3rd Int Coral Reef Symp **1:** 127-134.

Mass, T., A. Genin, U. Shavit, M. Grinstein, and D. Tchernov. 2010. Flow enhances photosynthesis in marine benthic autotrophs by increasing the efflux of oxygen from the organism to the water. PNAS **107:** 2527-2531.

Nakamura, T., and R. van Woesik. 2001. Water-flow rates and passive diffusion partially explain differential survival of corals during the 1998 bleaching event. Mar Ecol Prog Ser **212:** 301-304.

Odling-Smee, F. J., K. N. Laland, and M. W. Feldman. 1996. Niche construction. Am Nat **147:** 641-648.

Pacherres, C. O., G. M. Schmidt, and C. Richter. 2013. Autotrophic and heterotrophic responses of the coral *Porites lutea* to large amplitude internal waves. J. Exp. Biol. **216:** 4365-4374.

Patterson, M. R., and K. P. Sebens. 1989. Forced convection modulates gas exchange in cnidarians. PNAS **86:** 8833-8836.

Roder, C., L. Fillinger, C. Jantzen, G. M. Schmidt, S. Khokiattiwong, and C. Richter. 2010. Trophic response of corals to large amplitude internal waves. Mar Ecol Prog Ser **412:** 113-128.

Schiller, C., and G. J. Herndl. 1989. Evidence of enhanced microbial activity in the interstitial space of branched corals: possible implications for coral metabolism Coral Reefs **7:** 179-184.

Schlichting, H., and K. Gersten. 2017. Boundary-layer Theory, 9th ed. Springer -Verlag.

Schmidt, G. M., N. Phongsuwan, C. Jantzen, C. Roder, S. Khokiattiwong, and C. Richter. 2012. Coral community composition and reef development at the Similan Islands, Andaman Sea, in response to strong environmental variations. Mar Ecol Prog Ser **456:** 113-126.

Schreiber, U., U. Schliwa, and W. Bilger. 1986. Continuous recording of photochemical and non-photochemical chlorophyll fluorescence quenching with a new type of modulation fluorometer. Photosynth. Res. **10:** 51-62.

Shapiro, O. H. and others 2014. Vortical ciliary flows actively enhance mass transport in reef corals. PNAS **111:** 13391-13396.

Shashar, N., Y. Cohen, and Y. Loya. 1993. Extreme diel fluctuations of oxygen in diffusive boundary layers surrounding stony corals. Biol Bull **185:** 455-461.

Stafford-Smith, M. G., and R. F. G. Ormond. 1992. Sediment–rejection mechanisms of 42 species of Australian scleractinian corals. Mar. Freshw. Res. **43:** 683-705.

Ulstrup, K. E., R. Hill, and P. J. Ralph. 2005. Photosynthetic impact of hypoxia on in hospite zooxanthellae in the scleractinian coral *Pocillopora damicornis*. Mar Ecol Prog Ser **286:** 125-132.

Van Driest, E. R. 1956. On turbulent flow near a wall. AIAA J. **23:** 1007-1011.

Vogel, S. 1996. Life in moving fluids, 2nd ed. Princeton Univ. Press.

Wang, J., L. Zhao, and H. Wei. 2012. Variable diffusion boundary layer and diffusion flux at sediment-water interface in response to dynamic forcing over an intertidal mudflat. Chin. Sci. Bull. **57:** 1568-1577.

Warner, M. E., W. K. Fitt, and G. W. Schmidt. 1996. The effects of elevated temperature on the photosynthetic efficiency of zooxanthellae in hospite from four different species of reef coral: a novel approach. Plant Cell Environ **19:** 291-299.

Willert, C., B. Stasicki, J. Klinner, and S. Moessner. 2010. Pulsed operation of high-power light emitting diodes for imaging flow velocimetry. Meas Sci Technol **21:** 075402.

Yakovleva, I. M., A. H. Baird, H. H. Yamamoto, R. Bhagooli, M. Nonaka, and M. Hidaka. 2009. Algal symbionts increase oxidative damage and death in coral larvae at high temperatures. Mar Ecol Prog Ser **378:** 105-112.

Yonge, C. M. 1930. Studies on the physiology of corals: I. Feeding mechanisms and food. Scientific Reports / Great Barrier Reef Expedition 1928-29. **1:** 13-57.

3.7 Supplementary information

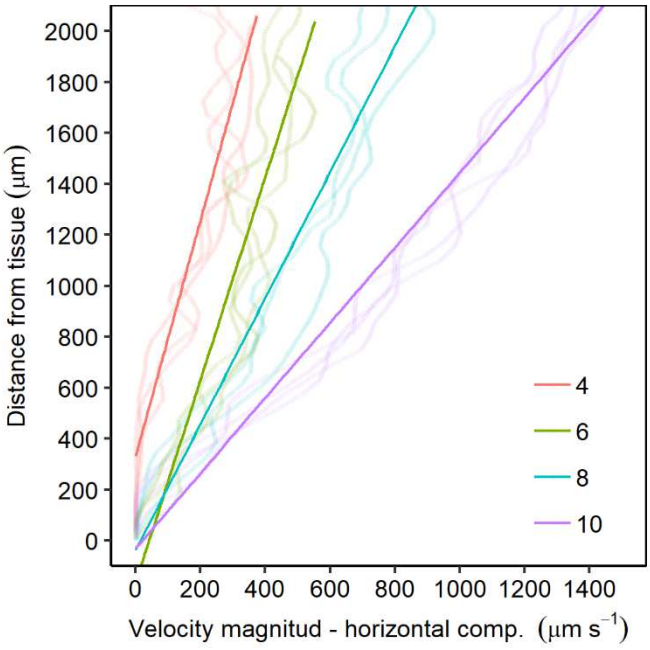

Fig. S3.1 Horizontal flow speeds (µm s^{-1}) parallel to the coral surface according to the four pump rates chosen for the experiments: 4, 6, 8, 10 (mL min^{-1}). Solid line represents the linear fit of the different flow speeds profiles. Background curves correspond to the individual velocity profiles extracted from the PIV of the different experiments under arrested cilia activity.

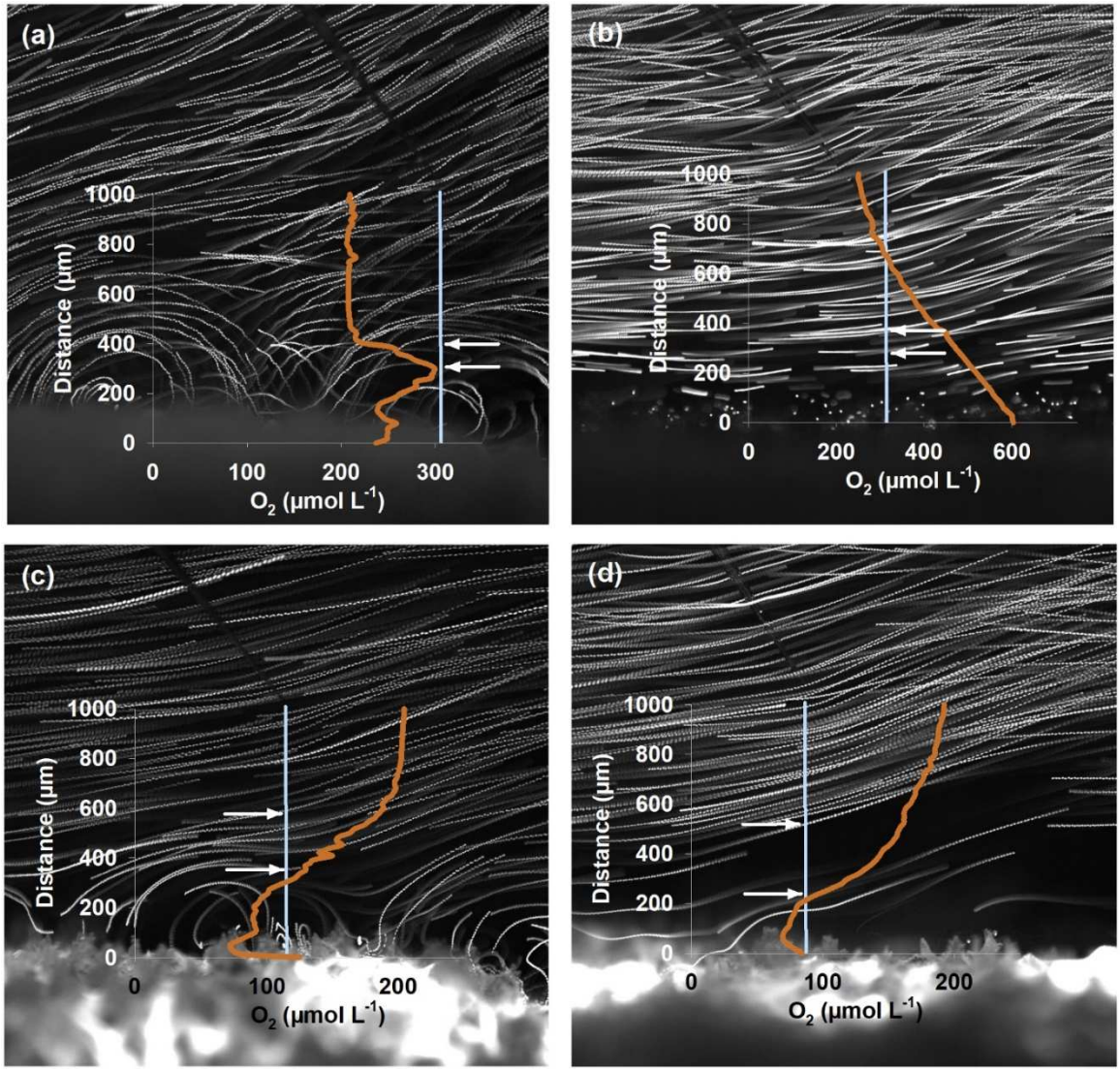

Fig. S3.2. PIV image and oxygen profiles of the coral *Porites lutea* under active (**a**, **c**) and arrested (**b**, **d**) cilia activity as well as under Light (**a**, **b**) and Dark (**c**, **d**) conditions. Pathlines show particle trajectories. Orange lines indicate oxygen concentration along the light blue line measured with a microsensor (also seen in the images). Flow speed of water in this case was 300 µm s^{-1} measured at 2 mm from the coral surface (see text for more details). Arrows indicate the part of the DBL that was considered for oxygen flux calculations.

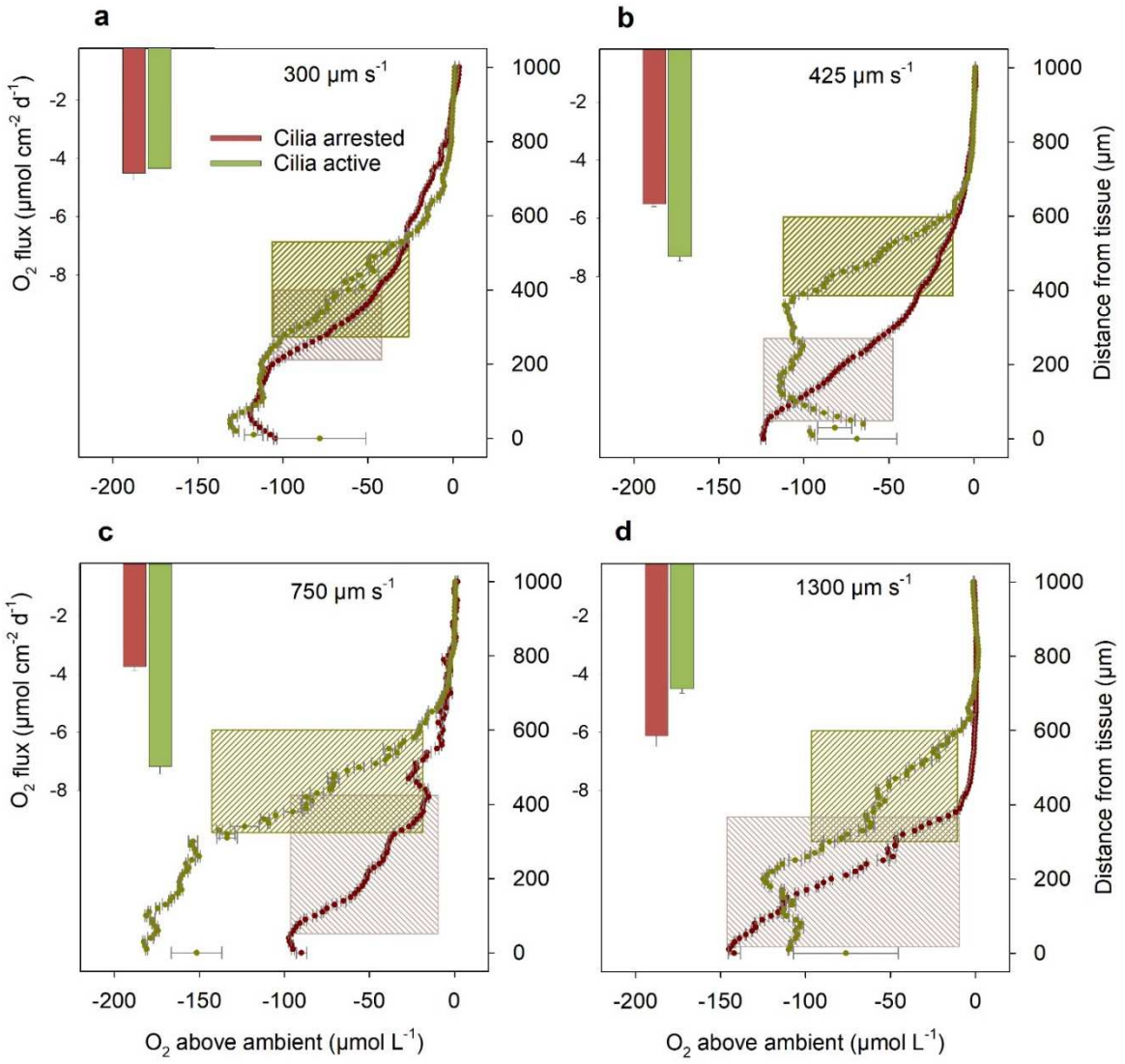

Fig. S3.3. Oxygen concentrations along a perpendicular 1000 µm transect from the tissue of *Porites lutea* to the water column in the dark, at flow speeds of (**a**) 300, (**b**) 425, (**c**) 750 and (**d**) 1300 µm s^{-1}, and for arrested and active cilia conditions. Inserted bar plots show the flux of oxygen in the DBL as calculated from oxygen gradients, either in the upper DBL (active cilia profile, green hatched background) or across a linear part of the DBL (arrested cilia profile, red hatched background). Error bars represent ± standard error of the linear regression.

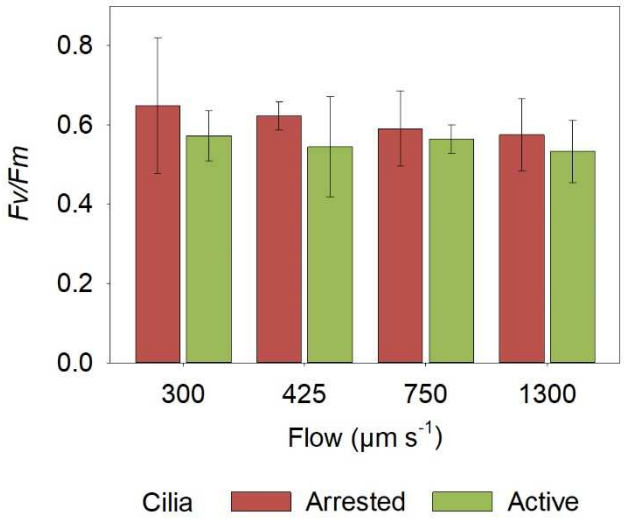

Fig. S3.4. Maximum quantum yield (MQY) of photosystem II (*Fv/Fm*) of zooxanthellae within *Porites lutea* in relation to the flow speed of the water (µm s^{-1}) and cilia activity (active and arrested) after 15 min of dark adaptation (0 µmol quanta m^{-2} s^{-1}). Error bars represent ±s.d.

Table S3.1. ANOVA results on the maximum quantum yield of photosystem II (*Fv/Fm*) of zooxanthellae within *Porites lutea* exposed to different treatment conditions regarding flow speed (µm s^{-1}), cilia activity (active and arrested) and light regime (dark, light).

Source of variation	Sum of squares	d.f.	Mean square	*F*	*P*
Light	19160	1	19160	2.627	0.115
Flow	7528	3	2509	0.344	0.794
Cilia	6604	1	6604	0.905	0.349
Light x Flow	3273	3	1091	0.150	0.929
Light x Cilia	12708	1	12708	1.742	0.196
Flow x Cilia	5336	3	1779	0.244	0.865
Light x Flow x Cilia	8853	3	2951	0.405	0.751

4

sensPIV: Simultaneous visualization of flow fields and oxygen concentrations to unravel metabolic exchange fluxes

Soeren Ahmerkamp[1,*], Farooq Moin Jalaluddin[1,*], Yuan Cui[2,*], Cesar O. Pacherres[3], Jasmine Berg[4], Roman Stocker[5], Marcel MM Kuypers[1], Klaus Koren[6,***] and Lars Behrendt[2***]

1 Max Planck Institute for Marine Microbiology, Bremen, Germany

2 Science for Life Laboratory, Department of Environmental Toxicology, Uppsala University, Sweden

3 Alfred Wegener Institute, Helmholtz Centre for Polar and Marine Research, Bremerhaven, Germany

4 University of Lausanne, Lausanne, Switzerland

5 Institute for Environmental Engineering, Department of Civil, Environmental and Geomatic Engineering, ETH Zurich, Switzerland

6 Aarhus University Centre for Water Technology, Department of Biology, Section for Microbiology, Aarhus University, Denmark

* Authors contributed equally

*** Joint senior scientists

Manuscript ready to be submitted

4.1 Abstract

Transport of oxygen (O_2) is vital for most life on earth as it sustains aerobic respiration. While the consumption of O_2 leads to a local sink the re-supply is governed by diffusion on advection. These transport processes typically unfold across scales of micrometer to millimeter and can change in response to hydrodynamic flow in milliseconds to seconds. This spatio-temporal complexity makes the accurate assessment of O_2 fluxes via currently available methods either difficult, laborious or unreliable. Here, we combined ratiometric and lifetime based imaging methods of phosphorescence quenching with particle velocimetry to measure O_2 concentrations and flow fields at the same time. This new method- 'sensPIV'- now enables non-invasive measurements of O_2 exchange fluxes across a wide-range of spatial scales at an unprecedented accuracy and speed. Here we document three proof-of-concept applications of sensPIV to measure O_2 fluxes, i) within simple microfluidic devices, ii) sinking model particles and iii) complex colony forming corals. sensPIV is a new technology for quantitatively linking metabolic rates and transport processes in a range of biological- and engineering applications.

Author contributions

S.A., L.B., K.K, M.M.M.K., J.B., R.S. conceived the study and interpreted data. K.K. synthesized sensor particles. Y.C. and L.B. performed experiments with microfluidic chips and processed data. F.M.J. and S.A. performed experiments with laboratory particles and processed data. S.A. developed and built optical setups. C.O.P. and S.A. developed flow-chamber setup, performed experiments with coral fragments and processed data. C.O.P. performed microsensor measurement. All authors edited and approved the paper.

4.2 Introduction

The production of oxygen (O_2) by photosynthesis began 2.5 billion years ago and the high energy yield of its respiration enabled the development and proliferation of multicellular life on Earth. Nevertheless, the poor solubility of O_2 in water poses a fundamental constraint on life in aquatic environments where diffusive and advective transport thus govern metabolic fluxes and the interaction of organisms with their environment. Across the kingdoms of life, a multitude of biological ventilation mechanisms have evolved, ranging from symbiotic relationships to cell-specific adaptations that enable the transport of O_2 away from producing cells to minimize its toxicity and towards consuming cells to optimize respiration. Understanding the fundamental role of O_2 in regulating biogeochemical processes in aquatic environments thus requires untangling the complex relationship between consumption, production as well as diffusive and advective transport processes. Until now, existing methods to visualize the transport of O_2 on microscales are largely limited to diffusive processes. Here, we expand the set of available powerful O_2 sensing methods with 'sensPIV', which can provide simultaneous and instantaneous information on flow fields and O_2 concentrations on microscales.

Our current understanding of transport on microscales is largely based on particle image velocimetry and particle tracking velocimetry (PIV and PTV, respectively), two key experimental technologies that use tracer particles to track fluid flows. Naturally occurring, or artificially added, particles with typical sizes between 0.1 µm - 10 µm are sequentially imaged in order to obtain information about local flow dynamics (velocity, direction). Based on this, the flow field can be reconstructed in 2D or, using stereoscopic or tomographic approaches, even in 3D (Westerweel et al. 2013, Raffel et al. 2018) The increasing number of commercially available PIV systems and ever improving image processing toolboxes has made particle velocimetry an integral part of medical and biological studies that deal with transport phenomena. In medical applications, PIV has enabled scientists to measure blood flow through cardiovascular systems in vitro (e.g. Yousif et al. 2011) and even in vivo (e.g. Kheradvar et al. 2010). In biological applications, PIV has been used to measure the interaction of individual organisms e.g., small crustacea (Gemmell et al. 2014), flocs or particles (Drescher et al. 2010, Zetsche et al. 2020, Nielsen and Kiørboe 2021), jellyfish (Gemmell et al. 2015, Costello et al. 2021) and microswimmers such as planktonic protists (Drescher et al. 2010, Gilpin et al. 2017, Nielsen and Kiørboe 2021) with the surrounding flow field. Additionally, PIV was successfully applied to study jellyfish movement *in situ*

(Katija and Dabiri 2008) revealing the importance of entrainment-based mixing processes that substantially contribute to ocean mixing (Katija and Dabiri 2009). On microscales, PIV has further enabled fascinating insights into foraging trade-offs in planktonic organisms (Drescher et al. 2010, Zetsche et al. 2020, Nielsen and Kiørboe 2021). While these studies focus on the interaction of organisms with surrounding flow fields, the focus has been on flow optimization, propulsion mechanisms or foraging behavior. Very little is known how the flow field surrounding the organisms control the exchange of O_2.

Historically, spatially resolved O_2 measurements on microscales have been performed using amperometric electrodes (Clark et al. 1953). The accuracy of these sensors, the ability to measure microbial activity and their high spatial resolution, limited only by the small sensor-tip diameter (~10 µm), has decisively influenced our understanding of the role of microbial communities in biogeochemical processes (e.g Revsbech and Jørgensen 1986), human physiology (e.g. Sheffield 1998) and plant physiology (e.g. Pedersen et al. 1998). Three decades ago, the adaptation of pressure sensitive paints (dyes) - that actually measure partial pressures of O_2 via O_2- dependent phosphorescence quenching - to monitor O_2 concentrations has led to the development of a new optical sensor-type: optodes (Morris et al. 1993, Klimant et al. 1995). Since their invention, optodes have emerged as indispensable and extremely powerful tools for measuring O_2. Examples are planar optodes (Glud et al. 2001) that have been used to map the millimeter-scale heterogeneity in O_2 within sediments (Frederiksen and Glud 2006, Stockdale et al. 2009, Meysman et al. 2010) or dental biofilms (Khosravi et al. 2020). With the invention of O_2-sensitive sensor particles and the ability to directly coat surfaces inhabited by microorganisms, new insights have been gained into how microorganisms interact with their microenvironment (Koren et al. 2016, Moßhammer et al. 2019). For example, sensor particles were used to determine O_2 concentrations in bone marrow of live animals (Spencer et al. 2014) respiration of individual prokaryotic cells (Scilipoti et al. 2021) or in combination with hyperspectral imaging to visualize the distribution of chlorophyll f-containing cyanobacteria and to quantify their contribution to photosynthetic O_2 production in a complex natural sample (Kühl et al. 2020). However, owing to low temporal resolution, the invasiveness and associated exclusion of advective transport have constrained the applications to measurements of O_2 concentrations and, derived from O_2 gradients, the one-dimensional diffusional transport. There are no spatially resolved measurements that simultaneously combine advective and diffusive fluxes which limits our understanding on the transport of O_2 on microscales.

It is important to emphasize the limitations of separate O_2 and flow measurements. Studies combining particle image velocimetry with microsensors to measure the microscale interaction between O_2 and flow dynamics have revealed the effects of ciliary flow on O_2 exchange processes in the coral boundary layer (Shapiro et al. 2014, Pacherres et al. 2020). While these studies provided strong evidence for enhanced mass transport through advection induced by ciliary movement, they insufficiently mapped the dynamic interaction between photosynthetic activity and flow fields. Although steps have been taken to demonstrate the potential of combining O_2 -sensitive sensor particles with flow measurements (Abe et al. 2004, Kim et al. 2013), these studies have been limited by problems associated with inhomogeneous light intensities and bleaching of O_2 -sensitive sensor particles. Heterogeneous illumination in one study reduced the accuracy of the O_2 measurements which therefore could only be performed at strong O_2 gradients in microfluidic devices. In a second study, next to a complex measuring setup and slow imaging speed (4 Hz), the measured signals could not be uniquely associated with specific O_2 concentrations leading to inaccurate interpretations of O_2 gradients. It is clear that a standardized, reliable and reproducible approach combining flow measurements with O_2 sensing is needed for the systematic study of biological systems and their metabolic exchange fluxes at micrometer scales.

To address these shortcomings, we present ‘sensPIV’, a new method that expands the powerful ability of optodes to measure O_2 with the possibility to measure flow fields at the same time and at high spatial resolution. This is achieved through the combination of state-of-the-art O_2-sensitive sensor particles with rapid lifetime imaging and ratiometric fluorescence imaging. Using sensPIV, the interaction of transport processes and biological reactions can now be investigated at an unprecedented temporal and spatial resolution using readily available experimental setups. We demonstrate the versatility of sensPIV by measuring combined flow and O_2 concentrations in microfluidic devices, settling particle analogs, and live coral fragments. The preliminary measurements reveal new insight into how flow fields amplify exchange processes and how corals shape their microenvironment to optimize metabolic fluxes.

4.3 Results

SensPIV enables the simultaneous visualization of flow fields and O_2 concentrations by combining methods available in most laboratories performing ‘classic’ PIV. In the following

we will discuss the necessary steps for other researchers to successfully implement sensPIV. These steps are i) the synthesis of O_2-sensitive (optode) sensor particles ii) the illumination of sensor particles and iii) the detection of O_2 sensing particles via imaging systems. After a detailed discussion on these steps we will then explore the use of sensPIV across three test cases relevant to engineering and environmental questions.

4.3.1 Method development

Synthesis of O2-sensitive (optode) sensor particles

Although many O_2 sensitive compounds fulfill the requirements for sensPIV (see for example Quaranta et al. 2012, Wang and Wolfbeis 2014 for chemistry overview) we recommend the use of Platinum(II) meso- (2,3,4,5,6-pentafluoro)phenyl porphyrin (PtTFPP) which is commercially available, mostly unaffected by temperature and exhibits a good sensitivity across a broad O_2 concentration range (Fig. 4.1.i and ii). The dynamic-quenching of PtTFPP by O_2 leads to an O_2 dependent and reversible luminescence intensity as well as luminescence lifetime. This relationship is described by the Stern-Volmer relationship:

$$I_0/I - 1 = K_{sv} \, . [O_2] \qquad \text{[Eq. 4.1]}$$

Where K_{sv} is the Stern-Volmer constant, $[O_2]$ is the dissolved- O_2 concentration, I is the luminescence-intensity at a given dissolved- O_2 concentration and I_0 the luminescence intensity in absence of O_2. I and I_0 can be replaced by the luminescence-lifetime τ and luminescence-lifetime in absence of O_2: τ_0, respectively. From equation (1) it follows that the calibration of sensPIV particles can readily be performed based on measured luminescence -intensities of the O_2 -sensitive dyes at known dissolved- O_2 concentrations. In many cases a simple two-point calibration is sufficient for accurate O_2 measurements via sensPIV.

To synthesize suitable particles for sensPIV we explored the use of two methods ensuring that the linearity of the Stern-Volmer relationship would not be affected: i) a precipitation method (Mistlberger et al. 2010) and ii) a staining method for commercially available particles (diameter of 2.3 µm, Fig. 4.1.i). Precipitation is a straightforward process in which an indicator dye (PtTFPP), a reference dye (fluorescence yellow 10GN) and a polymer are dissolved in a solvent (tetrahydrofuran) that is well miscible with water (see methods for details). As dyes and polymer components are not soluble in water, dye- containing particles

with sizes between 200 nm and 1800 nm spontaneously nucleate upon mixing with water (Fig. 4.1.i a-c). To prevent further growth through aggregation we used a copolymer of styrene and maleic anhydride. During precipitation the anhydride groups are hydrolysed and the resulting carbonic acid groups on the surface stabilize the particles against aggregation (see also Mistlberger et al. 2010 for tuning possibilities of nano-particles). The staining method uses commercially available particles and the sensor chemicals (indicator and reference dye) are introduced at a later stage (Borisov et al. 2008). The synthetic particles swell upon addition to a mixture of an organic solvent (here acetone) and water containing the sensor chemical. Removal of the organic solvent by evaporation results in the entrapment of the lipophilic dyes within the particles. After this step the particles are ready for sensor applications. Both methods have the advantage that large quantities of sensor particles can be prepared with minimal effort and virtually no specialized equipment. This is an essential aspect as it enables a wide range of laboratories to prepare the particles required for sensPIV. However, for both fabrication methods, we identified a heterogeneous dispersity and particle size distribution which could be reduced via sonication, centrifugation, and subsequent filtration. These procedures are described in detail in the methods section to facilitate reproduction.

Illumination of sensor particles

The basic measuring principle of sensPIV is based on the excitation of sensor particles and the subsequent emission that is altered by the increased quenching under increasing O_2 concentrations. sensor particles can be excited with a variety of light sources and illumination methods. We report on two techniques which allow us to illuminate a wide range of luminescence-based sensing dyes. i) Standard epi-fluorescence microscopes ii) Light sheet microscopy . Epi-fluorescence microscopes can readily be used for sensPIV measurements using existing light sources that cover the excitation wavelengths for PtTFPP (~ 390 nm) or by retrofitting with filter cubes equipped with long pass filters (~ 490 nm). These standard microscopes enable the straight-forward integration of sensPIV in, e.g., microfluidic applications with well-defined geometries. On the other hand, light-sheet microscopy techniques are advantageous for imaging sensPIV particles around larger objects or in experimental setups that require a combination of instruments, such as flow-chambers. Light sheet microscopy requires high light intensities in combination with a homogeneous illumination field, which is achievable with commercially available light-emitting diode

(LED) systems with a power output ranging between 2.5 W to 5 W (em: 450 nm, see methods section for details).

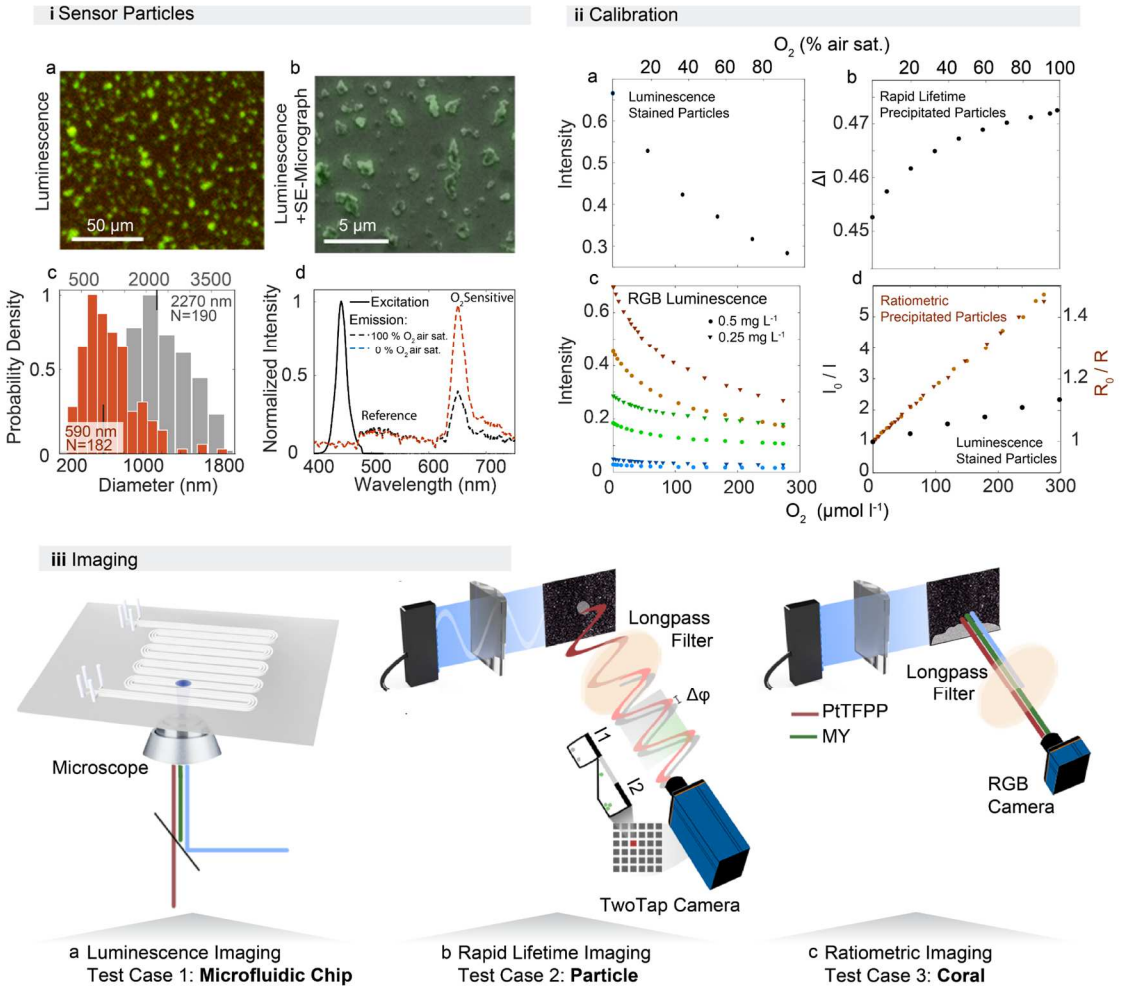

Figure 4.1. SensPIV allows for combined measurements of dynamic flow and O_2 by three imaging methods of increasing complexity. **i.a** O_2-sensitive sensor particles excited by blue wavelengths (365-440 nm) emitting in the green and red (500- 650nm). **b** Scanning electron micrographs of the nano-particles overlaid with the fluorescent signal. **c** Size spectrum analysis reveals that sensor particle sizes range between 200 and 1800 nm with a median of 590 nm for the precipitated particles (orange) and 500-4000 nm with a median of 2270 nm for stained particles (gray). **d** Excitation and emission spectra of the oxygen-sensitive dye (PtTFPP). **ii.a** The luminescence intensity and **b** estimated lifetime as a function of the O_2 concentration. **c** Luminescence imaging with a RGB camera, notice that as a result of the spectral overlap, the green channel has a slight O_2 dependency. **d** calibration curve for ratiometric imaging at different concentrations of O_2 and sensor particles. **iii** Conceptual illustration of the three imaging methods compatible with sensPIV and used within this study. (i) Luminescence intensity imaging: here blue light (~430-480 nm) is used to excite the antenna dye MY that then transfers energy to excite the O_2 -sensitive dye (PtTFPP at ~500-550 nm) on sensPIV particles. The resulting red-shifted (>650 nm) luminescence intensity depends on ambient O_2 concentrations. (ii) Ratiometric imaging: here blue light

(~450 nm) is used to excite both (PtTFPP) and the reference as well as antenna dye (MY). The emission of the PtTFPP (red, R, ~650 nm) is normalized by MY (green, G, ~500 nm) which compensates for inhomogeneous illumination and simplifies calibration. LF indicates a long pass filter that separates excitation and emission. (iii) Rapid lifetime imaging: here sensPIV particles are excited with an intensity modulated light sheet (~450 nm) and the luminescence emitted (~650 nm) by the sensor particles is phase shifted. The resulting phase shift $\Delta\varphi$ depends on the O_2 concentration and is estimated based on a two-tap camera chip (see text).

SensPIV detection

To detect sensPIV particles, we used three different detection modes that have been proven to be sufficiently rapid to track particles (> 10 Hz) and are relatively easy to use: i) luminescence imaging, ii) ratiometric imaging and iii) rapid lifetime imaging. In its most simple form, sensPIV can be executed by recording the luminescence intensity of the sensor particles using a simple monochromatic camera. Such cameras have the advantage of high quantum efficiencies which allows for working at lower excitation intensities and faster recording frequencies (> 100 Hz). However, the accuracy of measurements is usually limited by the homogeneity of illumination and topographical features of the investigated objects or the sensor particles themselves. This detection method therefore requires a time-intensive and challenging measurement of the illumination field, especially if objects are moving or the biological specimens are fluorescent themselves. Calibrations accounting for sensor particle size and concentration must also be performed (Fig.4.1.i a). In our test cases, we show that the additional measurement of the background illumination can be avoided by either performing in situ calibrations of sensor particles in simplified environments (such as microfluidic devices, see test case 1), or by using alternative imaging methods (such as ratiometric or rapid lifetime imaging) that record the excitation light field at the same time as the emission light field enabling instantaneous referencing.

Ratiometric imaging takes advantage of two fluorescent dyes, one having an O_2-sensitive emission intensity and a second acting as a reference dye. The intensity of an O_2-sensitive dye is normalized by the O_2 insensitive dye to compensate for inhomogeneous illumination fields. This simplifies system calibration and avoids artefact induced by topographic features (see also Koren et al. 2019 and references therein). Ratiometric imaging for sensPIV must be performed with a rapid color camera rather than the (time consuming) switching of specific filter cubes or beam splitting. Here it is of importance to select ratiometric dyes that

optimally cover the RGB spectra from the color filter array (bayer-filter) installed in commercially-available cameras. We found that the O_2-sensitive compound PtTFPP in combination with the reference dye Macrolex fluorescent yellow 10GN (MY, emission peak at ~480 nm) yields optimal performance measurements in combination with standard commercially available RGB cameras (see also Koren et al. 2015). The combination of PtTFPP with MY also results in a significant increase in sensor brightness through the so-called light-harvesting (Mayr et al. 2009) effect. MY acts not only as a reference dye, but also as an antenna molecule that transfers excitation energy effectively to the indicator (PtTFPP). It is therefore possible to work with very powerful blue LEDs contrary to using an array of less powerful green or UV LEDs that target the specific absorbance spectra of PtTFPP. In our experiments, we adapted and optimized the synthesis of PtTFPP sensor particles for ratiometric SensPIV (see above and supplementary information, see test case 3 for application).

In order to measure dissolved- O_2 concentrations without addition of a reference dye, luminescent lifetime imaging is the method of choice (Murniati et al. 2016). The intrinsically referenced lifetime of the O_2-sensitive dye (~60 µs in the absence of O_2) can be estimated via repetitive imaging of the declining luminescence intensity after light exposure (see for example Koren et al. 2019). However, for shutter-modulated cameras the temporal resolution is on the order of 10-100 s due to relatively slow sensor readout times and low light intensities during measurements. Recent technical advances allow for estimating the lifetime τ in the frequency domain based on the frequency-shift $\Delta\Phi$. This method improves temporal resolution and lifetime images can be recorded in less than 10s (Koren et al. 2019). In order to improve the temporal resolution further and to meet the requirements for particle velocimetry (which in most applications requires recording frequencies above 10 Hz), we performed rapid lifetime measurements with a camera-chip (QMFLIM2, pco) that has an in-pixel charge swing separating two taps within each pixel (Chen et al. 2015). The in-pixel charge swing allows quasi-instantaneous recording of two sequential images (I_{T1}, I_{T2}) where each image covers a quarter of modulation frequency (5 kHz, see Figure 4.1). The normalized intensity difference of the two images: $\Delta I = (I_{T1} - I_{T2}) / (I_{T1} + I_{T2})$ is related to $\Delta\Phi$ and, thus, the dissolved- O_2 concentration (see Figure 4.1iii b). The major advantage of this method is that only one O_2-sensitive dye is needed and highly accurate luminescence measurements can be achieved even in heterogeneous samples (see test case 2 for application).

In summary, the three basic steps of sensPIV ((i) sensor particle synthesis, (ii) illumination and (iii) detection) are easy to implement in non-specialized set-ups and enable a wide range of applications in laboratory and environmental settings. In the following, we present three test-cases with increasing complexity that illustrate the advantages and disadvantages of the different illumination and detection techniques, the range of spatial scales that can be covered with sensPIV (from micrometer to millimeter) and the different possibilities of data processing as well as analysis.

4.3.2 Applications of sensPIV

SensPIV under well-defined O_2 gradients within microfluidic devices

Microfluidic chambers provide an ideal testing arena for sensPIV due to the high level of control over fluid flow and chemical environments, i.e. specific O_2 concentrations, in addition to easy imaging of microscale processes (Son et al. 2015). In a microfluidic device, fluid flows laminarly through microscopic channels owing to the importance of viscosity at such small scales. Exact mathematical solutions are known for the robust calibration of flow measurements in prototypical geometries such as rectangular channels (Batchelor 2000). Moreover, specific chemical gradients (e.g. in O_2 concentrations) can be controlled and varied over time (Garren et al. 2014, Rusconi et al. 2014a, Yawata et al. 2014). These features have made microfluidic devices useful in a wide range of biological and medical applications from the study of anaerobiosis to cellular responses to O_2. We performed O_2 - manipulation experiments within a microfluidic device to carefully calibrate sensPIV particles and to validate the sensor particles for simultaneous visualization of flow fields and O_2 concentrations on microscales.

For initial calibration, we introduced PtTFPP stained sensor particles into the central channel of a simple PDMS microfluidic device consisting of a main fluid channel and two adjacent gas-channels through which O_2 concentration could be controlled (Fig. 4.2a, see methods section for chip production). To determine the oxygen specific signal of the sensor particle we i) identified individual particles from brightfield images (via intensity thresholding), ii) measured the luminescence intensity of a given particle and performed a two-point calibration iii) based on the luminescence intensity per-particle at 100% and 0% O_2 (degassing via N_2). We performed a first experiment with changing gas conditions and no fluid flow by generating an O_2 gradient by applying a compressed air flow (100% O_2) to one of the gas channels and 0% O_2 to the other. The changing O_2 concentrations were determined

following steps i) and ii) and relating the per-particle luminescence intensity to the two-point calibration curve. This procedure allowed us to observe the evolution of O_2 concentrations and compare the results at the specific locations to a time-resolved numerical model solving the scalar transport equations (Fig. 4.2b, see methods section for numerical methods). After initiation of the experiments, the O_2 gradient was steepening and the O_2 concentration increased rapidly. The experimental O_2 concentration reached full diffusive-relaxation after a time period between 160-205 seconds which is consistent with the model-derived diffusion time scale for the microfluidic channel size used. Deviations between model and experiments were found immediately after experiments were initialized, which we attribute to the short offset between initialization of the model and experiments due to the gas permeability and capacity of PDMS to retain gases. In a second experiment, we again manipulated O_2 concentrations in a PDMS device but this time under a simple pressure-drive flow regime with a constant velocity of 10 $\mu m\ s^{-1}$. The visualization of the O_2 gradient as described above was extended by the visualization of the laminar flow field using PIV techniques applied to the moving sensor particles. The flow field had a characteristic parabolic shape with maximum flow velocities in the central section (Fig. 4.2c), declining towards the wall. The changing O_2 profiles demonstrate a similar pattern as observed for no-flow conditions. However, O_2 concentrations in experiments and predicted from models match better as the constant flow stabilizes O_2 concentrations within the microfluidic chip. Together these experiments verified the capability of sensPIV to resolve spatially defined O_2 concentrations and flow fields simultaneously.

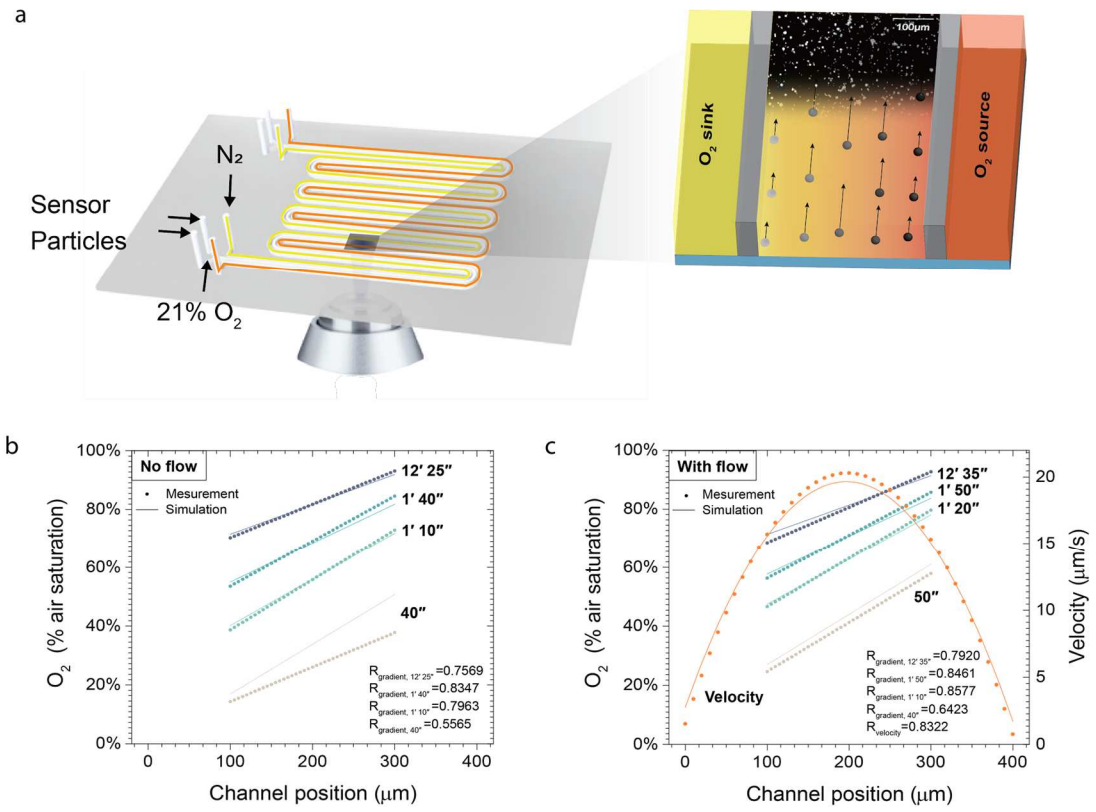

Figure 4.2. The behavior of sensPIV particles in a simple microfluidic device with a well-defined linear O_2 profile. **a** Conceptual cross-section view of the simple microfluidic device used in this study. A central fluid-containing channel is surrounded by two (gas) side channels which work as O_2 source and sink, respectively. By injecting 100% N_2 into one of the gas channels and compressed air (21% O_2) into the other, a linear O_2 gradient develops in the central channel where sensPIV particles are introduced to concurrently detect the resulting O_2 gradient and evolution of flow fields. **b** sensPIV results under quiescent conditions: Comparison between sensPIV measurements and model simulations in the case of no flow conditions. **c** sensPIV results under flow conditions: Comparison between sensPIV measurements and model simulations under flow conditions. The microfluidic device is adopted from (Rusconi et al. 2014b).

SensPIV for measuring the dynamic O_2 exchange around a model laboratory particle

Sedimentation of particles, flocs or aggregates is a key element of natural and technical processes including particulate matter transport in the ocean and wastewater treatment. In these systems, the high content of organic carbon in particles and associated microbial activity leads to the formation of microenvironments. A prime example is the exhaustion of O_2 inside particles through aerobic respiration. Anoxic microenvironments in particles favor anaerobic processes such as denitrification and anammox leading to the efficient removal of nutrients in the ocean (Bianchi et al. 2018, Karthäuser et al. 2021) and wastewater treatment

plants (Speth et al. 2016). The extent of O_2 depleted volumes inside the settling particles and the duration for which these microenvironments are sustained is strongly dependent on the O_2 supply through the particle boundary layer and the surrounding water. We tested whether sensPIV can concurrently visualize microscale O_2 gradients and flow to quantitatively assess the O_2 exchange processes on micrometer-scales. For this, we synthesized a porous agarose particle (φ =0.97 ± 0.01, with φ the porosity, n = 6, r = 2.7 ± 0.1, with r the radius) with embedded sensor particles (produced via precipitation). The agarose particles were degassed and placed into a temperature-compensated flow chamber (Fig. 4.3a) to simulate sinking. Two separate experiments were performed in which the particle was exposed to a flow of 2.1 mm s^{-1}, representing a Reynolds number of approx. 1, and a reference experiment with no flow.

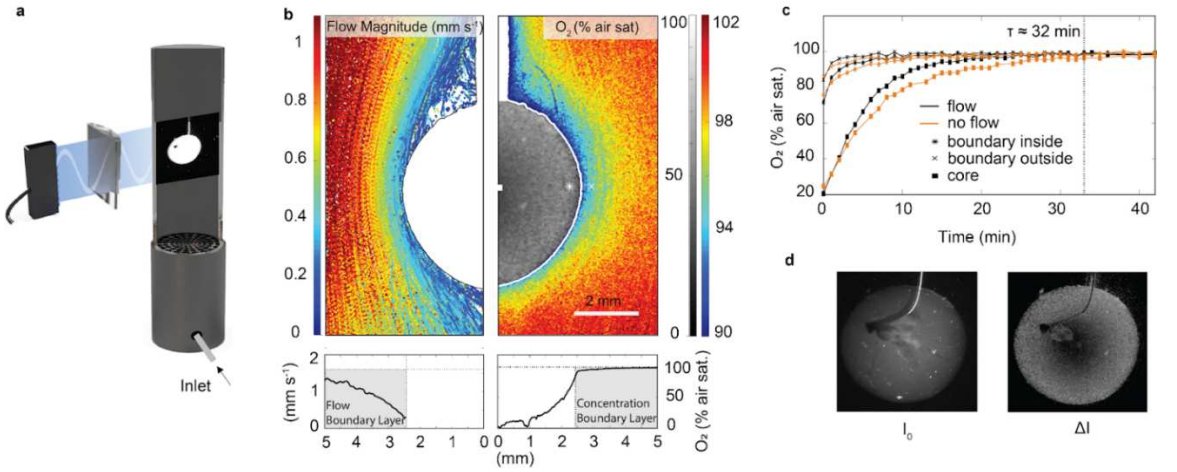

Figure 4.3: SensPIV visualizes flow and O_2 gradients around and inside a porous particle. **a** Conceptual illustration of the experimental setup consisting of a flow chamber, agarose sphere with embedded sensor-particles and imaging setup. **b** Reconstruction of the flow field (left panel) and O_2 concentration inside and around the particle (right panel). Note the different scale bars for the O_2 concentration inside and outside the particle (see also text). Lower Panels indicate flow and O_2 profile along the equator of the particle. **c** Transient O_2 concentrations in the core of the particle, at the surface and in the boundary layer for flow and no flow conditions. Diffusion timescale τ is estimated from the radius of the particle and the diffusion of O_2 (see text). **d** Luminescence intensity of a snapshot before and after referencing via the two taps of the camera chip. Even though the intensity I_0 is O_2 dependent, many brighter spots are visible which would be falsely interpreted as regions of low O_2 concentrations. The normalized intensity mostly compensates for these effects despite a very short exposure of 100 ms.

In both experiments, the O_2 boundary layer surrounding the particle and the O_2 concentration inside the particle was visualized by taking a total of 100 images via rapid lifetime imaging at a frequency of 10 Hz. The O_2 concentration was reconstructed by calculating the normalized difference of the two intensity images recorded with the two-tap camera and relating the value to the calibration curve (Fig 4.1.ii b). For the flow experiment, the flow field was reconstructed based on particle tracking velocimetry (PTV) (Extended Data Fig. 4.1). The images clearly reveal the O_2 boundary layer and flow boundary layer surrounding the agarose particle (Fig. 4.2b). The O_2 boundary layer surrounding the particle extends 2.5 mm outwards into the flow field whereas the O_2 concentration increases rapidly in the vicinity of the surface. The shape is asymmetric, confirming previous measurements with a microsensor (Ploug 2001). However, we were able to obtain the sensPIV results for the similar sized particle 100-times faster in comparison to microsensor measurements. This allowed us to resolve the O_2 dynamics temporally and to simultaneously visualize the flow fields which was achieved for the first time. The sensPIV method enables high-resolution visualization of O_2 gradients and flow, which are a prerequisite to study the spatial organisation of O_2 fluxes on microscales. The ability to do these measurements will allow to better understand remineralization inside and around particles and their impact on carbon sequestration in the ocean. Further, the particle test-case was chosen as analog of a microswimmer, for which an increasing amount of studies show active and passive interactions with the surrounding flow which increase nutrient and O_2 transport (e.g. Guasto et al. 2012, Kanso et al. 2021).

We next examined the impact of flow on the dynamic exchange processes between the particle interior and the ambient water. This was done by extracting the measured O_2 concentration in the core of the particle and at the particle-water interface (inside and outside) (Fig. 4.3c). After initialization of the experiments, O_2 diffused from the boundary layer into the particle core. The diffusion timescale of O_2 into the particle was estimated as which matches experimental results. Under flow, the diffusion of O_2 into the particle core was strongly enhanced and after 10 min the O_2 concentrations were increased by more than 8% compared to no-flow conditions indicating a strong enhancement of O_2 uptake. To quantitatively assess this enhancement in O_2 uptake, we evaluated the fluxes through the surface of the particle by calculating the concentration gradient along the surface in direction of the particle core at flow and no-flow conditions. To account for the asymmetry of the O_2

concentrations, we averaged all oxygen gradients along the whole surface of the particle following the equation:

$$J = -D/A \int \vec{n} \,.\nabla C \,.\, dA \qquad \text{[Eq. 4.2]}$$

where *D* is the diffusion coefficient of O_2, the O_2 concentration gradient perpendicular to the surface of the particle and A is the particle surface. The fluxes of O_2 into the particle were initially between 77-107 nmol cm^{-2} h^{-1} but declined over time as a result of the gradually decreasing concentration (compare Fig. 4.3c). In order to account for this O_2 flux variability, we extracted the fluxes for a given O_2 concentration and expressed the flow-dependent uptake enhancement as the Sherwood number, which is the ratio of the flux with flow to the flux in absence of flow. For the present case, we found an average Sherwood number of 1.75, implying that the presence of flow increased O_2 exchange by 75% compared to no-flow conditions. However, this number only represents a single test-case and strongly depends on the ratio of (settling-) velocity timescales and diffusion timescales. While this is the first measured simultaneous visualization of the flow field as well as surrounding and interstitial O_2 concentration of a particle, previous modelling studies have addressed this problem and found a vastly greater Sherwood number (Sh = 10 Kiørboe and Thygesen 2001). We attribute this difference to a failure of most models to take into account the particle porosity through simplified boundary conditions, a notation that is supported by a recent modelling study where no enhanced O_2 uptake was found when particles are porous (Moradi et al. 2018). The discrepancy between experiments and modelling studies underlines that the exchange between particles and microswimmers with the ambient flow needs further investigation, particularly, with regards to flow conditions and the spatial organization of microbial processes inside the particle. Such combinations of numerical simulations with sensPIV experiments have to be taken into account to gain new insights into the tight coupling between flow, metabolic rates and exchange fluxes.

SensPIV for the visualization of O_2 dynamics and vortical flows around the coral Porites lutea

sensPIV was used to investigate the interaction of a living reef-building coral fragment with its hydrodynamic environment. While previous studies on coral-flow fields have provided data with high spatial and temporal resolution (Shapiro et al. 2014), O_2 measurements consisted only of a few selected profiles obtained with microprofilers which were performed

independently of the flow measurements. The results showed that the beating of epidermal cilia constantly stir the boundary layer and enhance transport where the endosymbionts are located. However, due to the methodological limitations, it is not conclusively understood how the flow field caused by the cilia affects the O_2 concentrations within the coral boundary layer and what mutualistic benefit the coral derives from this.

We selected the stony coral species *Porites lutea* as a model organism, to i) demonstrate the integration of sensPIV into existing light-sheet based experimental setup and to ii) test the biocompatibility of sensor particles and illumination in a living photosensitive organism. To measure sensPIV particles around the surface of a *P. lutea* fragment, we adapted a newly developed light sheet microscope in combination with a recirculating flow chamber (Pacherres et al. 2020). Biocompatibility of sensPIV particles was tested by adding particles (produced via precipitation) and observing coral cilia beating for 5 minutes. The excitation light source was triggered by the camera resulting in short stroboscopic light exposures (20 ms). Following the introduction of sensPIV particles and imaging, we did not observe bleaching or changes in the cilia beating but substantial mucus production started after ~1 min in line with previous observations (Fabricius-Dyg et al. 2012, Koren et al. 2016). After finishing the experiments, the coral fragment was observed over the next few days and no substantial release of zooxanthellae was detected. In a dedicated additional experiment, the continuous illumination for a duration of two minutes led to the release of the endosymbionts and bleaching along light-exposed coral parts. We conclude that good biocompatibility can be ensured as long as light and sensor particle exposure are minimized. In all subsequent experiments, this was achieved by using short light strobes (<= 20 ms) and removing sensor particles after finishing experiments (~1 min).

To visualize the dynamic O_2 concentrations around *P. lutea*, we introduced sensPIV particles and recorded 100 color images within a time window of two seconds. Based on this image ensemble, we reconstructed the O_2 concentration using a ratiometric-referencing approach based on the R and G channel of the color image (Fig. 4a+b). Individual images are sufficient to reconstruct the O_2 concentrations with an error of approx 10%, but further imaging can improve the raw ratiometric signal which stabilizes after an ensemble of approx. 40 images (Supp. Inf. Fig. S4.2). This averaging procedure under flow conditions represents repeated measurements with different optodes at one location, increasing the accuracy of the O_2 measurements. To determine the accuracy, individual vertical profiles were extracted and O_2 concentrations were determined to be $\Delta C = 1.5\ \mu mol\ L^{-1}$ at a spatial resolution of ~ Δz =

20 µm (Supp. Inf. Fig. S4.3) which is close to the spatial resolution of commercially available O_2 microsensors. The experiments were performed at environmentally realistic O_2 concentration of 240 µmol L^{-1} (Nelson and Altieri 2019), a concentration where we expect O_2 sensor particles to be already substantially quenched. Lower O_2 concentration will enhance the ratiometric signal which would increase the accuracy of the O_2 measurements further.

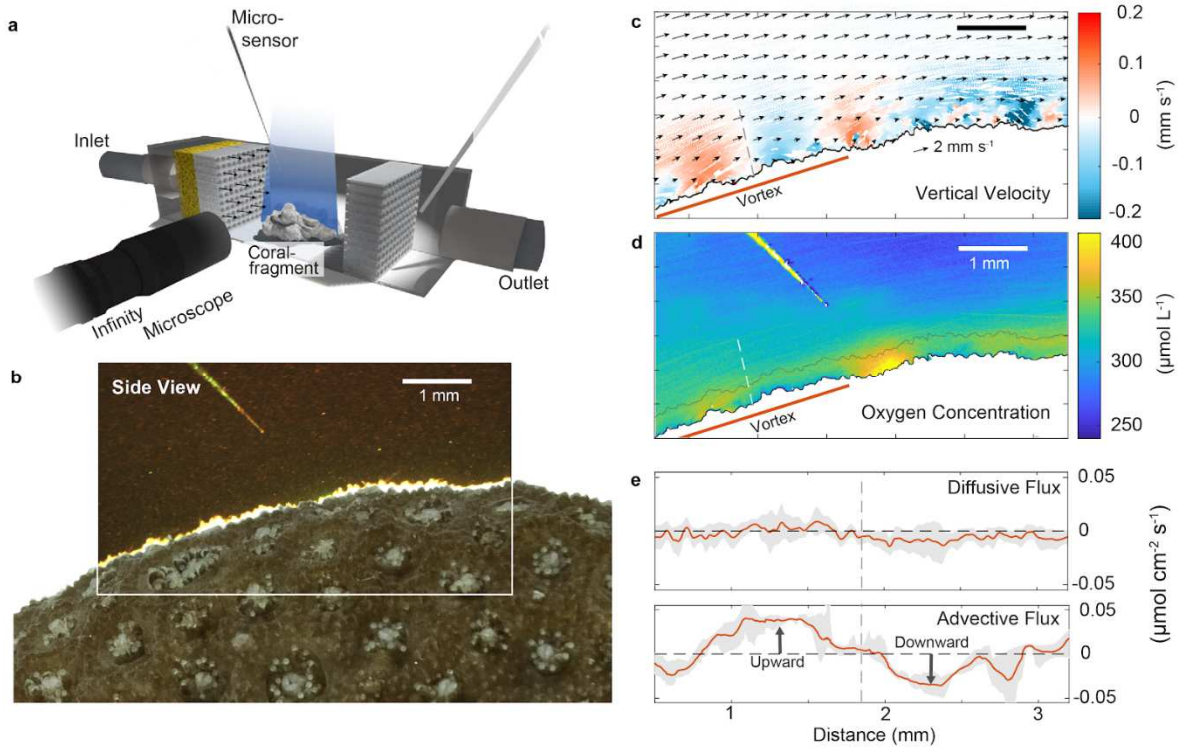

Figure 4.4: SensPIV permits the sensing of flow and O_2 around complex biological structures, here the coral *Porites lutea.* **a** sensPIV Particles were visualized using a light-sheet microscope connected to a flow chamber. The coral is actively stirring the boundary layer with cilia (see SV1 for video). **b** Color image of the sensor-particles around the coral surface. Note the O_2 microsensor in the top left corner which is used to reference the measurements. **c** Combined particle image velocimetry (PIV) and particle tracking velocimetry PTV) of sensPIV particles. Arrows indicate the flow along the coral´s surface determined by conventional PIV based on the red channel of the RGB image. Colored dots represent single tracked particles and the color indicates the velocity normal to the coral surface. Here red and blue depict upward and downward flow of particles, respectively and the size of the dots was scaled by the magnitude of the vertical velocity. **d** O_2 concentrations inside the boundary layer of the coral extracted from sensPIV. **e** Diffusive and advective O_2 fluxes along the vortex area highlighted in d with a red line.

Our 2-dimensional analyses of O_2 concentrations revealed a boundary layer along the coral surface of approx. 700 µm width along the coral surface with high degree of heterogeneity in, both, the horizontal and vertical directions. Two distinct semi-circular shaped structures (vortices) with O_2 supersaturation were indicative of localized increased O_2 production at the coral surface (Fig 4.4d). The width of the vortices varied between 800 µm and 1500 µm and extended up to 500 µm into the flow field therefore traversing almost the entire boundary layer (Fig. 4.4d). From the same image ensemble, we reconstructed the averaged flow field based on PIV (indicated by white arrows). To increase the accuracy of our flow measurement we additionally applied particle tracking velocimetry (PTV). In PTV individual particles are tracked instead of an ensemble (typical for PIV, Supp. Inf. Fig. S4.1), which allows measurements at a higher spatial and temporal resolution. To further improve the visualization of the vortical flow, the velocity perpendicular to the coral surface was calculated (Fig. 4.4c). In accordance with previous PTV data, vertical velocities ranged between -0.1 and 0.1 mm s^{-1} and also revealed two vortices along the coral surface with sizes between 1000 - 1250 µm.

Comparing O_2 concentrations with the concurrently resolved flow fields, sugests that upward directed particle velocities, induced by cilia, coincide with zones of increased O_2 production. This implies that cilia are not stirring the entire boundary layer homogeneously as assumed previously (Shapiro et al. 2014), but organize their beating pattern to increase the upward transport of O_2 where production at the surface is high, a first-time observation. To quantify this transport effect, we calculated the advective flux of O_2 as:

$$J_{adv} = u_{\perp} C \qquad \text{[Eq. 4.3]}$$

and diffusive flux as:

$$J_{dif} = -D \underset{n}{\rightarrow} . \nabla C \qquad \text{[Eq. 4.4]}$$

The advective flux of O_2 ranges between -36 nmol cm^{-2} s^{-1} and 38 nmol cm^{-2} s^{-1} and when averaging along the vortex the net upward flux is 1.5 nmol cm^{-2} s^{-1}. In comparison, the net diffusive flux (averaged along the whole surface of the coral fragment) is 0.4 nmol cm^{-2} s^{-1}. The net advective flux thus exceeds the diffusive flux. This process will need further attention in future studies. Previously, heterogeneous nutrient and O_2 concentrations within the boundary layer of corals were attributed to a change in coral topography and the resulting variations in boundary layer thicknesses (de Beer et al. 2000). Instead, and by using sensPIV,

we uncovered that coral topography acts in tandem with local ciliary flow to efficiently ventilate coral tissues and at the same time to optimize the coral metabolism. While further research is needed to disentangle the complex interactions occurring within a few mm's along coral surfaces, our first proof-of-concept results emphasize the power of sensPIV to provide new insights into mass-flow exchange around complex biological structures.

4.4 Discussion

SensPIV links measurements of flow, traditionally performed via PIV, with measurements of O_2 concentrations, normally measured by microsensors or immobilized optodes. Here we present three test cases that illustrate the versatility of sensPIV for the rapid and simultaneous measurement of flow fields and O_2 concentrations in microfluidic devices, model particles and live corals. To date, most studies that provided estimates of flow and O_2 on exchange fluxes have been conducted using numerical modeling approaches. Models are inherently simplified versions of reality and the in silico approaches rely on simplified geometries, tethering of objects and do not take into account microscale heterogeneities in flow and concentration which are very likely important for biological tissues and cells. In the coral test-case we demonstrated the importance of the advective ciliary flow of the coral which linked heterogeneous zones of consumption and production within the coral boundary layer. The three test cases presented here and the novel findings associated with them indicate the gap of missing instrumentation to study advective and diffusive fluxes on microscales which is now closed with sensPIV. Notably, sensPIV (in its most basic form) only requires simple experimental setups and off-the-shelf instruments (Supp. Inf. Table S4.1) which makes this technology accessible to a broader research community at minimal costs.

sensPIV will enable in-depth investigations of in vitro and in situ mass-transport phenomena across a wide range of research areas. The simplicity of ratiometric sensPIV will allow for an straight-forward integration into existing microscopy platforms (e.g. Krzic et al. 2012) or in laser scanning instruments developed for aquatic systems (e.g. Katija and Dabiri 2008, Liao et al. 2009, Ahmerkamp et al. 2017, Katija et al. 2017) enabling non-invasive measurements of O_2. The model particle is a proof-of-principle case resembling particle sedimentation, but it is also intended as an analog of a microswimmer - which can be artificial (e.g. Volpe et al. 2011) or natural (e.g. Kanso et al. 2021). Further potential areas

of application for sensPIV include complex flow setups to study planktonic organisms (Krishnamurthy et al. 2020), the single cell heterogeneity in O_2 production of microalgae (Behrendt et al. 2020), or more general in medical applications such as the transfer of O_2 to tissue cells (Bein et al. 2018). Moreover, research fields that focus on engineering problems may also profit from sensPIV as a new tool to study transport of O_2 in bioreactors for pharmaceutical applications (Seidel et al. 2021) and for pressure measurements via the partial pressure of O_2 (Gregory et al. 2008).

SensPIV is not limited to O_2 measurements but can also be used in combination with other analystes. The coral test-case suggests the important role of heterogeneous zones of production and consumption which will likely affect nutrient distributions. *In situ*, the exchange between the coral's endosymbionts and the coral is likely not limited to O_2 but will also affect nutrient distributions and other analytes. An increasing number of analytes including - pH, CO_2, temperature and NH_3 (Moßhammer et al. 2019, Merl and Koren 2020)- can now be optically monitored through fluorescent lifetime or ratiometric measurements. The application of sensPIV with new chemical sensors promises to reveal important insights into remineralization processes and flow at the scale of individual organisms. We thus anticipate a wide range of applications for sensPIV, as it is a powerful imaging method for studying transport dynamics and metabolic activity in biological and medical systems.

4.5 Methods

4.5.1 Sensor-particle Production

For ratiometric and lifetime imaging, sensor particles (SPs) were prepared as described earlier (Mistlberger et al. 2010, Koren et al. 2015, Koren et al. 2016) with minor specific modifications as described in the following. In short, 100 mg of the polymer PSMA (styrene maleic anhydride copolymer with 8% MA, Mw: 250000 g mol^{-1}; generously provided by Polyscope), 1.5 mg of the reference dye Macrolex fluorescence yellow 10GN (MY) obtained from Lanxess (Köln, Germany) and 1.5 mg of the O_2 indicator Platinum(II) meso- (2,3,4,5,6-pentafluoro)phenyl porphyrin (PtTFPP, Frontier Scientific) were dissolved in 10 g of tetrahydrofuran (THF). This solution was then rapidly poured into 200 mL of vigorously stirred milliQ water. After evaporating the THF under an airstream, the particle suspension was further concentrated at elevated temperature (around 60 °C) until a concentration of 5

mg mL^{-1} was reached. The final concentration was measured by drying and subsequent weighing of 1 mL of the particle suspension. A small sample was then dried on a indium tin oxide coated glass slide for further inspection using a scanning electron microscope (Quanta 250 FEG scanning electron microscope) combined with an fluorescent microscope (Seacom). It was ensured that fluorescent signals based on a 392 nm excitation did strongly correlate with the particles on the glass side (Supp. Inf. Fig. S4.1).

Alternatively particles were prepared by staining existing particles. In this case FluoSpheres™ Polystyrene Microspheres (Thermo Scientific; catalogue number F13080) were treated as follows. 1 mL of the bead suspension was mixed with 1 mL of acetone (Sigma Adldrich) for a duration of 2 min. Afterwards 0.5 mL of 0.5 mg PtTFPP dissolved in acetone were added and mixed for another 2 min. Subsequently, the acetone was slowly removed from the solution by gently blowing nitrogen over the stirred solution. While the acetone evaporates the dye gets entrapped within the particles.

In all test-cases, before each use particles were centrifuged. For the microfluidic chip, the supernatant was replaced with a 0.05% surfactant Tween 20 (Sigma-Aldrich Co., Germany) in Mili-Q water. In the case of the coral experiments, the sensor particles were repeatedly centrifuged in the seawater medium at a salinity of 33 PSU. Afterwards the particle sample was ultrasonic vibrated for 15 minutes to eliminate remaining particle aggregations. Next to this study, biocompatibility of similar sensor particles was previously tested for algae, colony-forming corals and seagrass roots (Koren et al. 2015, Koren et al. 2016, Trampe et al. 2018).

4.5.2 Excitation of the oxygen-sensitive sensor-particles

In order to meet the requirements for sensPIV imaging (>=10 Hz), high light intensities are required. In the past, such requirements were only fulfilled by high-energy continuous-wave or pulsed laser diodes, however, those limit the applicability as the costs are high, special requirements for safe operation are needed and experimental designs can become very complex. These methodological limitations can be overcome with new ultra-bright light emitting diode (LED) systems that can reach light intensities similar to laser diodes. The commercially available LED systems applied in this study have powers ranging between 2.5 W (Wavelength dependent, Omicron, LedHUB, here used for rapid lifetime imaging) up to 5 W (LPS3, ILA5150 GmbH, here used for ratiometric imaging). Collimation of LED light is challenging but using state-of-the-art optics, light sheets with widths of 500 µm - 1000

µm can be generated 72. To achieve this, the LED light was directed via a fiber bundle into the light sheet optics. In front of a cylindrical lense the fiber bundle was aligned in a linear arrangement resulting in a light-sheet thickness of ~1000 µm (Fig. 4.1). A second cylindrical lens was applied to yield a converging light sheet that minimizes the light sheet to a thickness of < 500 µm over a depth of ~ 2 mm.

4.5.3 Luminescence imaging in a microfluidic chip

A published microfluidic device design (Rusconi et al. 2014b) was adapted to generate linear O_2 gradients and apply sensor particles. Briefly, the device consists of two parallel side channels that act as the O_2 source and sink, respectively, and a central channel where the O_2 gradient develops. See the device dimension and channel system cross-section in Fig. 4.2.

The micro-channel system was designed with AutoCAD software and printed on a plastic photolithography mask (microlitho.co.uk). Then a silicon wafer was spin coated with SU-8 photoresist (SU-8 2150, MicroChem company, US) and baked according to manufacturer recommendations to allow the formation of a cross-link between the photoresist and the silicon substrate. This step was repeated until the desired photoresist thickness (here 750 µm) was achieved. The photolithography mask was put on top of the photoresist-wafer complex in an alignment machine and exposed to UV light. After removing the mask from the photoresist and submerging the whole wafer in an organic solvent (e.g. mr-DEV 600, micro resist technology) to dissolve the portions of the photoresist which were not cross-linked. A master was formed with the features of the device imprinted onto the silicon wafer.

The device was fabricated using standard PDMS replica molding procedures. Briefly, a 1:10 vacuum degassed PDMS solution consisting of curing agent (SYLGARD 184 Silicon Elastomer Curing Agent, Sigma-Aldrich Co., US): PDMS base (SYLGARD 184 Silicon Elastomer Base, Sigma-Aldrich Co., US) was poured onto the mold and thermally cured for at least 15 min at 80 °C. After curing, devices were cut using a scalpel and peeled away. The PDMS device was plasma treated for 30 s (Zepto low cost plasma laboratory unit, Diener electronic GmbH, Germany) and bonded onto a 75 mm × 50 mm micro slide (2947-75×50, Corning Inc., US). The resulting device was placed onto a heating plate set to 80 °C for 5 hours to improve bonding. Inlet and outlet ports were punched using a biopsy punch (AG15110-15, Miltex Biopsy Punch with Plunger, Integra LifeSciences Co., US). Final channel widths and heights were 400 µm and 750 µm, respectively. The PDMS wall thickness was adjusted to 400 µm. The overall length of the channels was 53 cm.

PtTFPP sensor particles were calibrated under two O_2 levels within the microfluidic device. Before experiments, the two side channels were connected to gas flow controllers through Tygon tubing (Z685585, Sigma-Aldrich, Germany). The inlet of the central channel was connected to a 1 mL syringe (Sigma-Aldrich, Germany) mounted onto a neMESYS Syringe Pump (Base Module BASE 120, CETONI GmbH, Germany) in order to control particle flow rates. First N_2 was supplied into both side channels for 40 minutes to reach 0% air saturation within the gas permeable PDMS device. After this equilibration, a solution of sensor particles was introduced into the central channel filled with MQ water and thereafter the flow was stopped to keep particles still. Particles in the main channel were then equilibrated to 0 % air saturation for 20 minutes and imaged using an inverted Nikon Ti-E microsope and a Zyla sCMOS camera; first by phase contrast using a LED white-light illuminator and secondly by fluorescence excitation via blue excitation ~450 nm (Spectra X light engine). This was repeated for several locations along the central channel and the resulting images were analyzed (below) to obtain calibration images for 0% O_2. To obtain calibration images of particles under 100% air saturation, compressed air (CA) was supplied to both side channels while keeping the rest of the calibration procedure the same.

Experiments were performed under flow and no-flow conditions. In order to study the predictability of the dissolved-O_2 concentration evolution, model simulations of the dissolved-O_2 transport inside the microfluidic chips were performed. For that, a multiphysics COMSOL model was set up based on the 3-dimensional microfluidic channel geometry. The flow field was simulated by solving laminar navier-stokes equations:

$$\rho\,(u\,.\nabla)u = -\nabla p + \mu\,\nabla^2 u \qquad \text{[Eq. 4.5]}$$

where u is the velocity vector, p the pressure, μ dynamics viscosity and ∇ the del-operator. The continuity equation for incompressible fluids reads:

$$\nabla\,.\,u = 0 \qquad \text{[Eq. 4.6]}$$

The oxygen distribution in the microfluidic chip was then calculated solving the advection-diffusion equation:

$$0 = -D\,\nabla^2\,C + u\,.\,\nabla\,C \qquad \text{[Eq. 4.7]}$$

where D is the diffusion coefficient for oxygen and PDMS ($D_{PDMS,water}$=3.25·10^{-9} m^2 s^{-1} (Markov et al. 2014), $D_{O2,water}$=2.01·10^{-9} m^2 s^{-1}, T = 293.15 K (Welty et al. 2000) and C is

the O_2 concentration. For all walls we assumed no slip conditions and the flow field was driven based on the pressure as imposed in the experiments. For the O_2 distribution, the gas concentration of the outer channels was imposed at the boundary and saturated O_2 concentrations at the inlet were assumed.

4.5.4 Rapid lifetime imagine of a particle in flow

The model laboratory particle used for the experiment was prepared by mixing 2.48 mg mL^{-1} of sensor particles with a 0.7% agarose matrix. Agarose (Biozym) was mixed with Mili-Q (MQ) water by boiling the mixture in a microwave. Subsequently the solution was cooled down to ~40°C and the sensor particle solution was added and thoroughly mixed to homogenize. In order to form spherical particles the prepared agarose solution was pipetted into a glass beaker, containing MQ water overlaid with cold plant oil. The oil causes the solution to form spherical shapes while cooling before the model laboratory particles drop out of the oil layer into the MQ water. Laboratory particles were then sieved, washed and stored immersed in MQ water in the dark. The laboratory particles were then used to visualize the O_2 concentration and flow field of a particle in flow.

The experiments with the laboratory particles were performed in a recirculating glass flow chamber (height: 10.7cm; diameter: 2.5cm). The glass chamber was connected via a 3D-printed Peek inlet with 1 mm capillaries to a gear pump (ISMATEC ISM901B). The capillaries are intended to provide a homogeneous flow field. The pump volume was adjusted to achieve a flow velocity of 2.1 mm s^{-1} inside the flow chamber. The entire chamber was immersed in an aquarium filled with MQ water (dimensions: 18.4 x 9.7 x 9.7cm) to stabilize the temperature. The particle was degassed overnight using N_2 gas and was attached to a needle connected to a motorized linear drive (Faulhaber, T-LSR75A), to precisely adjust the position of the agarose particle. The anoxic agarose particle was then placed in the center of the glass chamber.

To image dissolved O_2 concentrations at a high spatial resolution, luminescent lifetime imaging is a method of choice (Murniati et al. 2016). Here, the lifetime of the O_2-sensitive dye (~100 µs) can be estimated via repetitive imaging of the declining fluorescence intensity after light exposure (see for example Koren et al. 2019). However, for shutter-modulated cameras the temporal resolution is of order 10-100 s due to relatively slow sensor readout times and low light intensities employed in most experiments. Recent technical advances, namely a two-tap QMFLIM2 image sensor (pco.FLIM, PCO AG) allows to estimate the

lifetime τ (~100 µs) in the frequency domain based on the frequency-shift, ΔΦ, induced by the quencher (O_2) which allows to keep light-intensities at a high level. Lifetime and frequency-shift are directly related through the equation $\tau=\tan(\Delta\Phi)/(2\pi\ fmod)$, where fmod is the modulation frequency (~ 5 kHz). This method improves temporal resolution and lifetime images can be recorded in less than 10s (Koren et al. 2019). In order to improve the temporal resolution further and to meet the requirements for particle velocimetry (frequencies above 10 Hz), we adapted the two-tap QMFLIM2 camera chip (pco.FLIM), which has in each pixel an in-pixel charge swing separating two taps per pixel. The in-pixel charge swing allows quasi-instantaneous recording of two sequential images (IT1, IT2) where each image covers a quarter of fmod (Fig. 4.1). Owing the Nyquist-Shannon theorem, the frequency shift ΔΦ cannot be directly estimated based on the two sequential images along half the phase, however the normalized intensity difference of the two images: $\Delta I = (I_{T1} - I_{T2}) / (I_{T1} + I_{T2})$ is related to ΔΦ and, thus, the dissolved- O_2 concentration (Fig. 4.1b). It is important to ensure that ΔI is maximized when imaging the fluorescent dye in absence of O_2. Further, the in-pixel swing leads to an asymmetry of the two in-pixel taps that is intensity dependent. This asymmetry was corrected by recording a homogeneously illuminated object with a wavelength matching the emission wavelength of the O_2-sensitive dye. A telecentric lense (Computar, TEC – v7x) was fitted to the camera and Lee filter 101 Yellow was used to filter the blue excitation light. sensor particle excitation was achieved through a light sheet using LedHUB attached to customized light sheet optics (see above).

Calibration of the sensor particles was performed in the flow chamber via a custom build degassing setup that allows to precisely adjust O_2 concentrations. The Stern-Volmer plot (Fig 4.1.ii b) indicates that the measured signal does not scale linearly which is why we applied a second order polynom for fitting. The O_2 concentration was reconstructed by decomposing the field of view into the interior of the particle and the outside of the particle. Care has to be taken that the darker image I_{T2} does not fall below the noise level of the camera chip tap. In that case the normalized intensity will not be uniquely associated with one O_2 concentration. However, in that case we found substantial improvements of the intensity by subtracting I_{T2} from I_{T1}. Flow fields were determined using an in-house developed kinematic prediction algorithm. In each image, 1154 ± 23 sensor particles were tracked and the reconstructed PTV tracks ranged between 5 - 463 individual data points. The tracks were colorized based on the determined velocity.

4.5.5 Flow and oxygen visualization through ratiometric imaging of a coral

We adapted a custom built light sheet microscopy recirculating flow chamber setup (see Pacherres et al. 2020 for details, schematic in Fig. 4.1) with which we performed ratiometric oxygen measurements, particle image velocimetry and particle tracking velocimetry. A coral fragment of roughly 2 cm size was placed into the flow chamber and free-flow velocities of 1500 µm s^{-1} were imposed. After an equilibration time of 10 min, 1 mL of 0.5 mg mL^{-1} sensor particle stock solution was added to the flow-chamber resulting in a final concentration of 0.025 mg per mL. In order to minimize mucus production, the coral was only exposed for short time periods (< 2 min) with the sensor particles before filtering the particles using a syringe filter (0.22 µm) that was placed into the recirculation system. The experiments were performed in a temperature controlled room at 25° C. The sensor particles were illuminated with a blue LED (450 nm, LPS3 ILA) using light sheet optics as described above (see also Fig 4.4a). Imaging was performed using an RGB camera (Grasshopper3, SONY ICX625, FLIR) through a custom-build microscopic lense array (Optem-Fusion). Exposure times were reduced to 20 ms and the light was triggered by the camera to minimize light exposure to the coral. The blue channel was used to determine the surface of the coral using an in-house developed tracking algorithm. Particle image velocimetry was performed based on the red channel using standard cross-correlation techniques of two subsequent images using the software PIVView (Pivtech, see also Extended Data 1), and particle tracking velocimetry was performed based on a in-house developed kinematic prediction algorithm. O_2 concentrations were determined based on ratiometric measurements of the red and green channel: IR = R/G after calibration at various oxygen concentrations using eq. 4.1. All image post-processing was performed in Matlab (2018b, Mathworks). It should be noted, that during the calibration procedure, we observed an emission of schott-glass filters that can affect the ratiometric measurements and corrections that would require an additional light-dependent referencing of the applied filter. However, the problem can be overcome by using non-invasive plastic filters (e.g. Lee filters). In addition to the sensPIV measurements, an electrochemical microsensor (Unisense) was used for comparison and to reference the measurements.

Acknowledgements

We thank Volker Meyer, Paul Faerber and Gerhard Holst for technical support. We thank Sina Schorn, Bram Vekeman and Juliane Schoetz for support in the laboratory. We thank Dirk de Beer for valuable discussion and comments. The study was funded by the Max Planck Society (MPG) through the "Multiscale Approach on the Role of Marine Aggregates" (MARMA) project. C.O.P. acknowledges funding from the Helmholtz Association (Alfred Wegener Institute, Helmholtz Centre for Polar and Marine Research). F.M.J received funding from the Cluster of Excellence "The Ocean Floor—Earth's Uncharted Interface" (Germany's Excellence Strategy—EXC-2077-390741603 of the DFG). L.B. and Y.C. were supported by grants from the Swedish Research Council (2019-04401) and the Science for Life Laboratory. R.S. acknowledges funding from the Simons Foundation through the Principles of Microbial Ecosystems (PriME) Collaborative (grant 542395). K.K. acknowledges financial support by research grants from the Grundfos Foundation and a Sapere Aude grant from the Independent Research Fund Denmark (IRFD): DFF-8048-00057B.

4.6 References

Abe, S., K. Okamoto, and H. Madarame. 2004. The development of PIV–PSP hybrid system using pressure sensitive particles. Meas Sci Technol **15:** 1153-1157.

Ahmerkamp, S. and others 2017. Regulation of benthic oxygen fluxes in permeable sediments of the coastal ocean. Limnol Oceanogr **62:** 1935-1954.

Batchelor, G. K. 2000. An Introduction to Fluid Dynamics. Cambridge University Press.

Behrendt, L. and others 2020. PhenoChip: A single-cell phenomic platform for high-throughput photophysiological analyses of microalgae. Science Advances **6:** eabb2754.

Bein, A. and others 2018. Microfluidic organ-on-a-chip models of human intestine. Cell Mol Gastroenterol Hepatol **5:** 659-668.

Bianchi, D., T. S. Weber, R. Kiko, and C. Deutsch. 2018. Global niche of marine anaerobic metabolisms expanded by particle microenvironments. Nature Geoscience **11:** 263-268.

Borisov, S. M., T. Mayr, and I. Klimant. 2008. Poly(styrene-block-vinylpyrrolidone) beads as a versatile material for simple fabrication of optical nanosensors. Anal Chem **80:** 573-582.

Chen, H., G. Holst, and E. Gratton. 2015. Modulated CMOS camera for fluorescence lifetime microscopy. Microsc Res Tech **78:** 1075-1081.

Clark, J. L. C., R. Wolf, D. Granger, and Z. Taylor. 1953. Continuous recording of blood oxygen tensions by polarography. J Appl Physiol **6:** 189-193.

Costello, J. H., S. P. Colin, J. O. Dabiri, B. J. Gemmell, K. N. Lucas, and K. R. Sutherland. 2021. The hydrodynamics of jellyfish swimming. Annu Rev Mar Sci **13:** 375-396.

de Beer, D., M. Kühl, N. Stambler, and L. Vaki. 2000. A microsensor study of light enhanced Ca^{2+} uptake and photosynthesis in the reef-building hermatypic coral *Favia* sp.†. Mar Ecol Prog Ser **194:** 75-85.

Drescher, K., R. E. Goldstein, N. Michel, M. Polin, and I. Tuval. 2010. Direct measurement of the flow field around swimming microorganisms. Phys Rev Lett **105:** 168101.

Fabricius-Dyg, J., G. Mistlberger, M. Staal, S. M. Borisov, I. Klimant, and M. Kühl. 2012. Imaging of surface O_2 dynamics in corals with magnetic micro optode particles. Mar Biol **159:** 1621-1631.

Frederiksen, M. S., and R. N. Glud. 2006. Oxygen dynamics in the rhizosphere of *Zostera marina*: A two-dimensional planar optode study. Limnol Oceanogr **51:** 1072-1083.

Garren, M. and others 2014. A bacterial pathogen uses dimethylsulfoniopropionate as a cue to target heat-stressed corals. ISME J **8:** 999-1007.

Gemmell, B. J., S. P. Colin, J. H. Costello, and J. O. Dabiri. 2015. Suction-based propulsion as a basis for efficient animal swimming. Nat Commun **6:** 8790.

Gemmell, B. J., H. Jiang, and E. J. Buskey. 2014. A new approach to micro-scale particle image velocimetry (μPIV) for quantifying flows around free-swimming zooplankton. J Plankton Res **36:** 1396-1401.

Gilpin, W., V. N. Prakash, and M. Prakash. 2017. Vortex arrays and ciliary tangles underlie the feeding–swimming trade-off in starfish larvae. Nat Phys **13:** 380-386.

Glud, R. N., A. Tengberg, M. Kühl, P. O. J. Hall, and I. Klimant. 2001. An *in situ* instrument for planar O_2 optode measurements at benthic interfaces. Limnol Oceanogr **46:** 2073-2080.

Gregory, J. W., K. Asai, M. Kameda, T. Liu, and J. P. Sullivan. 2008. A review of pressure-sensitive paint for high-speed and unsteady aerodynamics. Proc Inst Mech Eng G J Aerosp Eng **222:** 249-290.

Guasto, J. S., R. Rusconi, and R. Stocker. 2012. Fluid mechanics of planktonic microorganisms. Annu Rev Fluid Mech **44:** 373-400.

Kanso, E. A., R. M. Lopes, J. R. Strickler, J. O. Dabiri, and J. H. Costello. 2021. Teamwork in the viscous oceanic microscale. Proceedings of the National Academy of Sciences **118:** e2018193118.

Karthäuser, C. and others 2021. Small sinking particles control anammox rates in the Peruvian oxygen minimum zone. Nat Commun **12:** 3235.

Katija, K., and J. O. Dabiri. 2008. *In situ* field measurements of aquatic animal-fluid interactions using a Self-Contained Underwater Velocimetry Apparatus (SCUVA). Limnol Oceanogr Methods **6:** 162-171.

---. 2009. A viscosity-enhanced mechanism for biogenic ocean mixing. Nature **460:** 624-626.

Katija, K., R. E. Sherlock, A. D. Sherman, and B. H. Robison. 2017. New technology reveals the role of giant larvaceans in oceanic carbon cycling. Science Advances **3:** e1602374.

Kheradvar, A. and others 2010. Echocardiographic particle image velocimetry: A novel technique for quantification of left ventricular blood vorticity pattern. Journal of the American Society of Echocardiography **23:** 86-94.

Khosravi, Y. and others 2020. Use of an oxygen planar optode to assess the effect of high velocity microsprays on oxygen penetration in a human dental biofilms in-vitro. BMC Oral Health **20:** 230.

Kim, H. D., S. J. Yi, and K. C. Kim. 2013. Simultaneous measurement of dissolved oxygen concentration and velocity field in microfluidics using oxygen-sensitive particles. Microfluid Nanofluidics **15:** 139-149.

Kiørboe, T., and U. H. Thygesen. 2001. Fluid motion and solute distribution around sinking aggregates. II. Implications for remote detection by colonizing zooplankters. Mar Ecol Prog Ser **211:** 15-25.

Klimant, I., V. Meyer, and M. Kühl. 1995. Fiber-optic oxygen microsensors, a new tool in aquatic biology. Limnol Oceanogr **40:** 1159-1165.

Koren, K., K. E. Brodersen, S. L. Jakobsen, and M. Kühl. 2015. Optical sensor nanoparticles in artificial sediments – A new tool to visualize O_2 dynamics around the rhizome and roots of seagrasses. Environ Sci Technol **49:** 2286-2292.

Koren, K., S. L. Jakobsen, and M. Kühl. 2016. In-vivo imaging of O_2 dynamics on coral surfaces spray-painted with sensor nanoparticles. Sens. Actuators B Chem. **237:** 1095-1101.

Koren, K., M. Moßhammer, V. V. Scholz, S. M. Borisov, G. Holst, and M. Kühl. 2019. Luminescence lifetime imaging of chemical sensors — A comparison between time-domain and frequency-domain based camera systems. Anal Chem **91:** 3233-3238.

Krishnamurthy, D. and others 2020. Scale-free vertical tracking microscopy. Nat Methods **17:** 1040-1051.

Krzic, U., S. Gunther, T. E. Saunders, S. J. Streichan, and L. Hufnagel. 2012. Multiview light-sheet microscope for rapid *in toto* imaging. Nat Methods **9:** 730-733.

Kühl, M. and others 2020. Substantial near-infrared radiation-driven photosynthesis of chlorophyll *f*-containing cyanobacteria in a natural habitat. eLife **9:** e50871.

Liao, Q. and others 2009. Development of an *in situ* underwater particle image velocimetry (UWPIV) system. Limnol Oceanogr Methods **7:** 169-184.

Markov, D. A., E. M. Lillie, S. P. Garbett, and L. J. McCawley. 2014. Variation in diffusion of gases through PDMS due to plasma surface treatment and storage conditions. Biomed Microdevices **16:** 91-96.

Mayr, T. and others 2009. Light harvesting as a simple and versatile way to enhance brightness of luminescent sensors. Anal Chem **81:** 6541-6545.

Merl, T., and K. Koren. 2020. Visualizing NH_3 emission and the local O_2 and pH microenvironment of soil upon manure application using optical sensors. Environ Int **144:** 106080.

Meysman, F. J. R., O. S. Galaktionov, R. N. Glud, and J. J. Middelburg. 2010. Oxygen penetration around burrows and roots in aquatic sediments. J Mar Res **68:** 309-336.

Mistlberger, G. and others 2010. Multifunctional magnetic optical sensor particles with tunable sizes for monitoring metabolic parameters and as a basis for nanotherapeutics. Adv Funct Mater **20:** 1842-1851.

Moradi, N., B. Liu, M. Iversen, M. M. Kuypers, H. Ploug, and A. Khalili. 2018. A new mathematical model to explore microbial processes and their constraints in

phytoplankton colonies and sinking marine aggregates. Science Advances **4:** eaat1991.

Morris, M. J., J. F. Donovan, J. T. Kegelman, S. D. Schwab, R. L. Levy, and R. C. Crites. 1993. Aerodynamic applications of pressure sensitive paint. AIAA Journal **31:** 419-425.

Moßhammer, M., K. E. Brodersen, M. Kühl, and K. Koren. 2019. Nanoparticle- and microparticle-based luminescence imaging of chemical species and temperature in aquatic systems: a review. Microchim Acta **186:** 126.

Murniati, E., D. Gross, H. Herlina, K. Hancke, R. N. Glud, and A. Lorke. 2016. Oxygen imaging at the sediment-water interface using lifetime-based laser induced fluorescence (τLIF) of nano-sized particles. Limnol Oceanogr Methods **14:** 506-517.

Nelson, H. R., and A. H. Altieri. 2019. Oxygen: the universal currency on coral reefs. Coral Reefs **38:** 177-198.

Nielsen, L. T., and T. Kiørboe. 2021. Foraging trade-offs, flagellar arrangements, and flow architecture of planktonic protists. PNAS **118:** e2009930118.

Pacherres, C. O., S. Ahmerkamp, G. M. Schmidt-Grieb, M. Holtappels, and C. Richter. 2020. Ciliary vortex flows and oxygen dynamics in the coral boundary layer. Sci Rep **10:** 7541.

Pedersen, O., J. Borum, C. M. Duarte, and M. D. Fortes. 1998. Oxygen dynamics in the rhizosphere of *Cymodocea rotundata*. Mar Ecol Prog Ser **169:** 283-288.

Ploug, H. 2001. Small-scale oxygen fluxes and remineralization in sinking aggregates. Limnol Oceanogr **46:** 1624-1631.

Quaranta, M., S. M. Borisov, and I. Klimant. 2012. Indicators for optical oxygen sensors. Bioanal Rev **4:** 115-157.

Raffel, M., C. E. Willert, F. Scarano, C. Kähler, S. T. Wereley, and J. Kompenhans. 2018. Particle image velocimetry: a practical guide, 3rd ed. Springer.

Revsbech, N. P., and B. B. Jørgensen. 1986. Microelectrodes: Their use in microbial ecology. *In* M. K.C. [ed.], Adv Microb Ecol. Springer.

Rusconi, R., M. Garren, and R. Stocker. 2014a. Microfluidics expanding the frontiers of microbial ecology. Annu Rev Biophys **43:** 2.1-2.27.

Rusconi, R., J. S. Guasto, and R. Stocker. 2014b. Bacterial transport suppressed by fluid shear. Nat Phys **10:** 212-217.

Scilipoti, S., K. Koren, N. Risgaard-Petersen, A. Schramm, and L. P. Nielsen. 2021. Oxygen consumption of individual cable bacteria. Science Advances **7:** eabe1870.

Seidel, S., R. W. Maschke, S. Werner, V. Jossen, and D. Eibl. 2021. Oxygen mass transfer in biopharmaceutical processes: Numerical and experimental approaches. Chem Ing Tech **93:** 42-61.

Shapiro, O. H. and others 2014. Vortical ciliary flows actively enhance mass transport in reef corals. PNAS **111:** 13391-13396.

Sheffield, P. J. 1998. Measuring tissue oxygen tension: a review. Undersea Hyperb Med **25:** 179-188.

Son, K., D. R. Brumley, and R. Stocker. 2015. Live from under the lens: exploring microbial motility with dynamic imaging and microfluidics. Nat Rev Microbiol **13:** 761.

Spencer, J. A. and others 2014. Direct measurement of local oxygen concentration in the bone marrow of live animals. Nature **508:** 269-273.

Speth, D. R., M. H. in 't Zandt, S. Guerrero-Cruz, B. E. Dutilh, and M. S. M. Jetten. 2016. Genome-based microbial ecology of anammox granules in a full-scale wastewater treatment system. Nat Commun **7:** 11172.

Stockdale, A., W. Davison, and H. Zhang. 2009. Micro-scale biogeochemical heterogeneity in sediments: A review of available technology and observed evidence. Earth-Sci Rev **92:** 81-97.

Trampe, E. and others 2018. Functionalized bioink with optical sensor nanoparticles for O_2 imaging in 3D–bioprinted constructs. Adv Funct Mater **28:** 1804411.

Volpe, G., I. Buttinoni, D. Vogt, H.-J. Kümmerer, and C. Bechinger. 2011. Microswimmers in patterned environments. Soft Matter **7:** 8810-8815.

Wang, X.-d., and O. S. Wolfbeis. 2014. Optical methods for sensing and imaging oxygen: materials, spectroscopies and applications. Chem Soc Rev **43:** 3666-3761.

Welty, J., C. E. Wicks, R. E. Wilson, and G. L. Rorrer. 2000. Fundamentals of momentum, heat, and mass transfer. Wiley.

Westerweel, J., G. E. Elsinga, and R. J. Adrian. 2013. Particle image velocimetry for complex and turbulent flows. Annu Rev Fluid Mech **45:** 409-436.

Yawata, Y., O. X. Cordero, F. Menolascina, J.-H. Hehemann, M. F. Polz, and R. Stocker. 2014. Competition–dispersal tradeoff ecologically differentiates recently speciated marine bacterioplankton populations. PNAS **111:** 5622-5627.

Yousif, M. Y., D. W. Holdsworth, and T. L. Poepping. 2011. A blood-mimicking fluid for particle image velocimetry with silicone vascular models. Exp Fluids **50:** 769-774.

Zetsche, E.-M., A. I. Larsson, M. H. Iversen, and H. Ploug. 2020. Flow and diffusion around and within diatom aggregates: Effects of aggregate composition and shape. Limnol Oceanogr **65:** 1818-1833.

4.7 Supplementary information

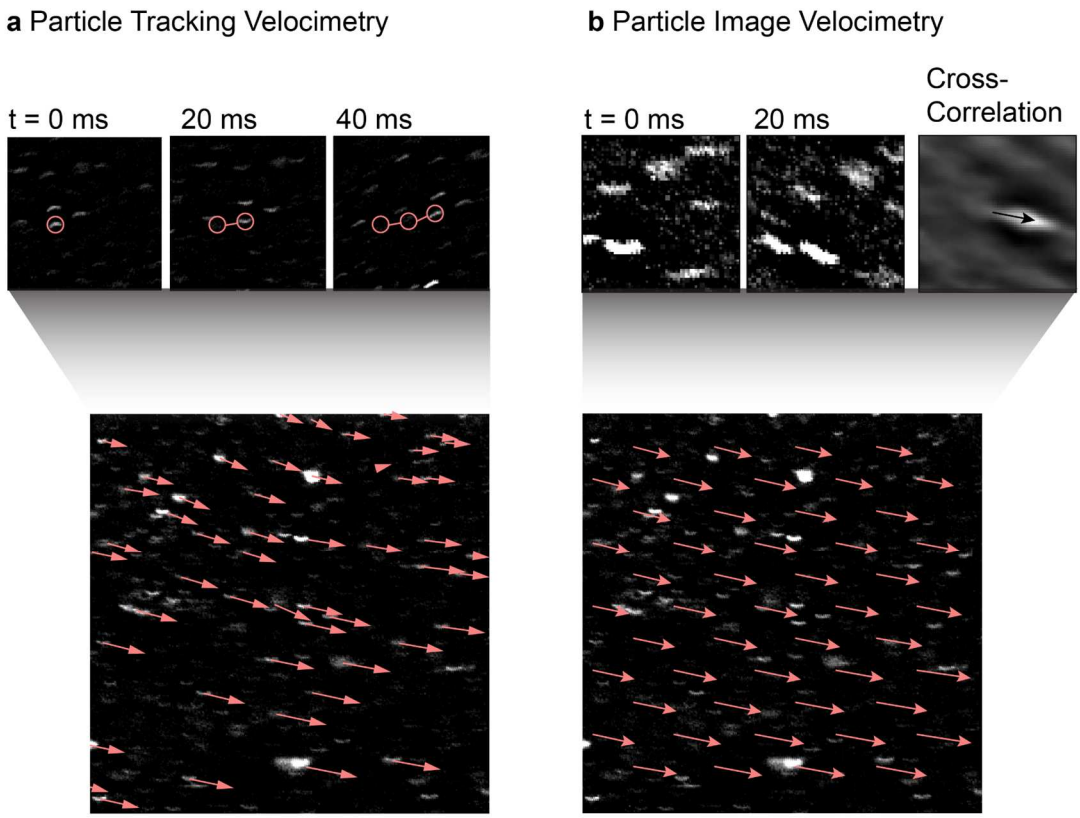

Fig. S4.1 Particle image velocimetry and particle tracking velocimetry applied to the sensPIV dataset. Example of **a** particle tracking velocimetry and **b** particle image velocimetry applied to the coral test-case. For both particle velocimetry methods, the red channel was extracted from the color images and background noise as well as any remaining O_2 signal from small particles was removed by using a gaussian high-pass filter with a 15 px kernel. For particle tracking velocimetry **a**, individual particles were tracked using intensity thresholding and determining the trajectories of the particle (see methods). For particle image velocimetry **b**, the images were decomposed into small interrogation windows and it was ensured that 7-9 individual particles are located within one interrogation window resulting in typical window sizes of 64 px (approx. 115 µm for the coral test-case). Each interrogation window was cross-correlated with the subsequent image to determine the movement of the particles within the window.

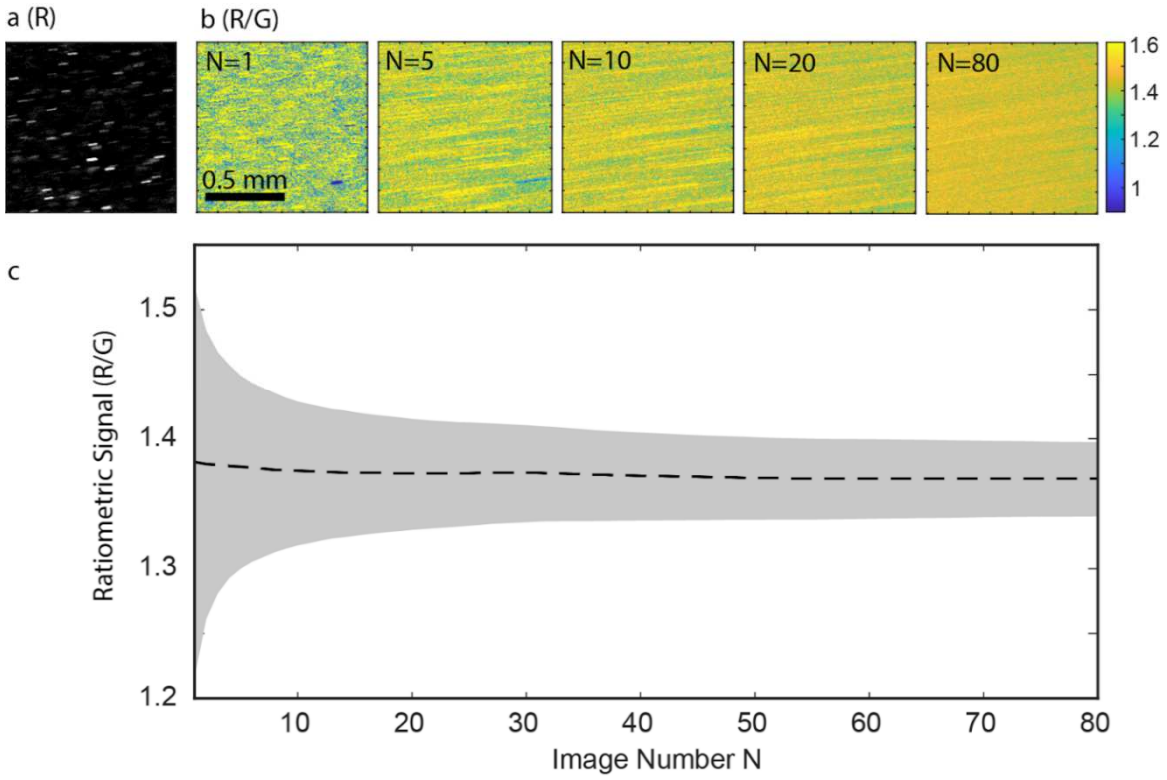

Fig. S4.2 **a** Red fluorescence on which basis the flow field is reconstructed. **b** Ratiometric images (Red/Green) based on which O_2 concentrations are calculated. N represents the number of images which were averaged. **c** Convergence of the ratiometric signal (R/G) based on the averaging of an image ensemble (see also main text). The gray envelope represents the 75% and 25% percentile of values within the test window.

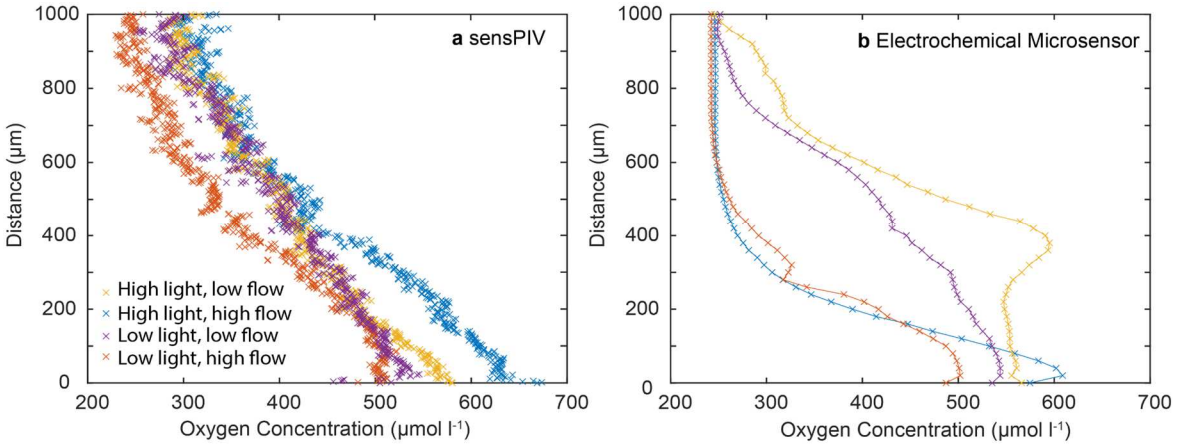

Fig. S4.3. Comparison of sensPIV profile and microsensor profiles: **a** One-dimensional profiles extracted from the 2-dimensional sensPIV data which was recorded within 2 seconds. Four experiments were performed where the coral was exposed to low flow (300 µm s^{-1}), high flow (1500 µm s^{-1}), high light (160 µmol quanta m^{-2} s^{-1}) and low light (80 µmol quanta m^{-2} s^{-1}) conditions. Each data point represents the O_2 value in one pixel which had a spatial extent of 1.8 µm in the presented experiments. **b** O_2 data recorded at the same location as **a** with an electrochemical microsensor at a spatial resolution of 20 µm recorded in 5 min per profile. While overall similar patterns are captured, the microsensor image seems to exhibit stronger gradients. We attribute this to the fact that the sensPIV experiments were performed after the microsensor measurements on the same fragment when O_2 concentration did not reach full stationarity.

Table S4.1. Overview of the applied instruments

Method	**Cameras**	**Light Source**	**Optical Setup**
Luminescence imaging *Microfluidics*	Monochromatic sCmos (Zyla, XX)	Lumencor spectraX	Microscope (Nikon Ti-E microsope)
Ratiometric *Coral Experiment*	RGB cmos (Grashopper, Flir, 1650 Eur, GS3-U3-51S5C-C)	LPS3 (ILA, 3500 Eur)	LED Light sheet optics (Thorlabs / Edmund Optics, 800 Eur)
Rapid Lifetime Imaging *Particle Experiment*	pco.Flim, new generation of multi-tap cameras (50.000 Eur)	LedHUB (Omicron, 7200 Eur)	LED Light sheet optics (Thorlabs / Edmund Optics, 800 Eur)

5

Ciliary currents and symbiont heterogeneity segregate sites of oxygen production and accumulation in the coral boundary layer

Cesar O. Pacherres[1,2]*†, Soeren Ahmerkamp[3,4]†, Klaus Koren[5], Gertraud M. Schmidt-Grieb[1], Claudio Richter[1,2] and Moritz Holtappels[1,4]

1 Alfred Wegener Institute, Helmholtz Centre for Polar and Marine Research, Bremerhaven, Germany

2 University of Bremen, Germany

3 Max Planck Institute for Marine Microbiology, Bremen, Germany

4 Marum, Bremen, Germany

5 Center for Water Technology, Department of Biology, Aarhus University, Denmark.

* Corresponding author

†Authors acknowledge equal contribution to this work

Manuscript ready to be submitted

5.1. Abstract

Most tropical shallow-water corals live in photosymbiosis with dinoflagellate algae (zooxanthellae), where the photosynthetic production of oxygen (O_2) by the zooxanthellae may lead to excess O_2 in the diffusive boundary layer (DBL) above the coral tissue surface. When advection is low, cilia-induced mixing of the coral DBL is vital to remove excess O_2 and prevent photo-inhibition and –damage that may lead to coral bleaching and mortality. Here, we combined particle image velocimetry using O_2-sensitive nanoparticles (sensPIV) with chlorophyll-sensitive hyperspectral imaging to visualize the microscale distribution and dynamics of ciliary flows and O_2 in the coral DBL in relation to the distribution of zooxanthellae in the coral tissue of the reef building coral, *Porites lutea*. Curiously, we found an inverse relation between O_2 and chlorophyll, with patches of high O_2 above the coral mouth areas (low chlorophyll) alternating with areas of low O_2 concentrations at the coral periphery (high chlorophyll). The experimental results are supported by a 2D transport-reaction model of a coral boundary layer. The spatial segregation of chlorophyll and O_2 suggests that ciliary induced vortical flows also cause a lateral redistribution of metabolites in the DBL so that in case of O_2, parts of the surplus can be allocated to areas containing less symbiont densities, thus minimizing oxidative damage and enhancing O_2 fluxes in the DBL. Mass transfer at the coral DBL is, thus, not uniform but spatially complex. The cilia-induced heterogeneity has important implications for how corals cope with oxidative stress.

Author contributions

The experiments for this study were designed by C.O.P., S.A., G.M.S., C.R and M.H. C.O.P. conducted all the experiments and calibrations. C.O.P. and S.A. analyzed the sensPIV and hyperspectral data and generated the result figures. M.H. and S.A worked on the model and its figures. K.K. created and supplied the sensPIV particles necessary for the oxygen experiments. C.O.P., S.A., K.K., G.M.S., C.R. and M.H. contributed to the interpretation of the collected data, and conceived and wrote the manuscript.

5.2. Introduction

Tropical shallow-water scleractinian corals live in photosymbiosis with dinoflagellate algae (zooxanthellae), an association that allows them to recycle essential elements and thrive in nutrient-poor waters (Muscatine 1973). The zooxanthellae are contained in vacuoles (symbiosomes) inside the gastrodermal cells in densities of 10^6 to 10^7 zooxanthellae cm^{-2} (Muscatine et al. 1989) and 1 to 12 zooxanthellae (host cell)$^{-1}$ depending on tissue architecture, light and nutrient availability (Muscatine et al. 1998). Among the zooxanthellae, chlorophyll concentrations can be highly heterogeneous as well, since the algae can adapt to reduced light by increasing the amount of chlorophyll in order to optimize light harvesting. For example, shade-adapted corals can contain up to 4× more Chl *a* µg cm^{-2} compared to light-adapted counterparts (Falkowski and Dubinsky 1981, Dubinsky et al. 1984).

While the coral consumes most of the oxygen (O_2) produced by the zooxanthellae, the surplus diffuses out of the tissue into the coral DBL (Shashar et al. 1993). *In vivo* imaging and microsensor studies found a heterogeneous distribution of O_2 at the tissue surface (Koren et al. 2016) and coral-water interface (also known as Diffusive Boundary Layer – DBL) (Kühl et al. 1995, Al-Horani et al. 2005). In the coral *Galaxea fascicularis* higher photosynthetic rates were found in the middle parts of the corallite septa, tentacles and tissue surrounding the mouth, while the wall of the polyp and the coenosarc showed lower photosynthetic rates. This heterogeneity was attributed to differences in zooxanthellae distribution, and localized higher photosynthetic activity in response to increased metabolic demand (calcification in the top part of the polyp) (Al-Horani et al. 2005), but concurrent respective assessments are so far lacking. For *Favia* sp., spatial variations in O_2, Ca^{2+} and CO_2 within a single polyp were attributed to differences in the light field and variations in the thickness of the DBL (de Beer et al. 2000) which acts as a bottleneck for solute exchange indirectly controlling the photosynthetic rate (Weis et al. 1989, Kühl et al. 1995). While O_2 exchange in the coral tissue and DBL has long been considered passive by means of diffusion (Kühl et al. 1995, Mass et al. 2010), more recent work has shown the importance of ciliary currents enhancing the mass transport of O_2 at the coral surface (Shapiro et al. 2014, Pacherres et al. 2020). Ciliary action was shown to create vortices affecting the O_2 distribution in the DBL and the coupling with the water aloft.

The heterogeneities in zooxanthellae distribution, host activity (e.g. sites of calcification) and ciliary flows are therefore likely to result in a complex patterning of the O_2

microenvironment of the coral, with differential O_2 accumulation and/or consumption and contrasting cellular responses to O_2 levels. Although O_2 is essential for all aerobic organisms, excess O_2 can be detrimental for autophototrophs (Dykens and Shick 1984, Lesser and Shick 1989). Since the photosynthetic apparatus of the zooxanthellae – Rubisco Form II – has a higher affinity to O_2 over CO_2, the excess of the former will cause photorespiration and the production of O_2 radicals (Crawley et al. 2010). This not only entails higher metabolic costs (Shick 1990), but also may cause cellular damage and, ultimately, coral bleaching (Lesser et al. 1990, Lesser 1997, Yakovleva et al. 2009). Therefore, understanding the O_2 dynamics at the coral-water interface is of paramount importance since it has a direct influence on the microenvironment inside the colony and thus on its health and performance. Here, we provide the first simultaneous assessment of the 2D O_2- and flow field in the coral DBL, along with a mapping of chlorophyll concentrations under controlled ambient illumination and flow. We aim to characterize the chlorophyll distribution inside the coral tissue O_2 and relate it with the dynamics at the coral surface, examining the role of ciliary flows in the transport of O_2 away from the tissue surface.

5.3. Results and Discussion

5.3.1. Chlorophyll concentrations in the coral tissue

Using hyperspectral imaging technology (Joyce and Phinn 2003) at a millimetric scale, we analyzed the chlorophyll distribution along the tissue of the coral *Porites lutea*. We observed higher normalized absorbance of 0.8 in the septa and coenosarc, indicating high chlorophyll concentration (Fig. 5.1b - ROI 1; 5.1d - yellow areas). In comparison, normalized absorbance was 0.3 at the mouth openings, indicating low chlorophyll concentration (Fig. 5.1b - ROI 2; 5.1d - blue areas). As the polyps of *Porites* tend to remain partially retracted during the day (Pacherres et al. 2013) in order to enhance planar density and photosynthetic performance of its symbionts (Sebens and DeRiemer 1977, Lasker 1979), it is no surprise that the areas surrounding the mouth opening (septa and coenosarc) contain higher chlorophyll concentrations than the mouth opening itself. Due to the architectural complexity of the coral surface, the μ-metric quantification and distribution of Chlorophyll densities have, only recently been made possible by the application optical techniques (Spicer et al. 2019, Liu et al. 2020) which nevertheless require extensive sample preparation (Liu et al. 2020) or the

short-term removal of culturing water (Spicer et al. 2019). Here, images were taken on a flow though chamber and without disturbing the coral. While, it must be taken into consideration that the results derived from the hyperspectral images provide a map of the Chl *a* distribution near the surface of the coral, with limited resolution deep inside the tissue, the O_2 produced by the near-surface Chlorophyll will be the one immediately diffusing towards the outer surface of the coral and into the DBL, likely explaining the patchy distribution of photo-derived O_2 seen by Koren et al. (2016). If diffusional processes would be the only mechanisms of mass transport at the coral water interface, we would expect a similar heterogeneous O_2 distribution in the coral DBL.

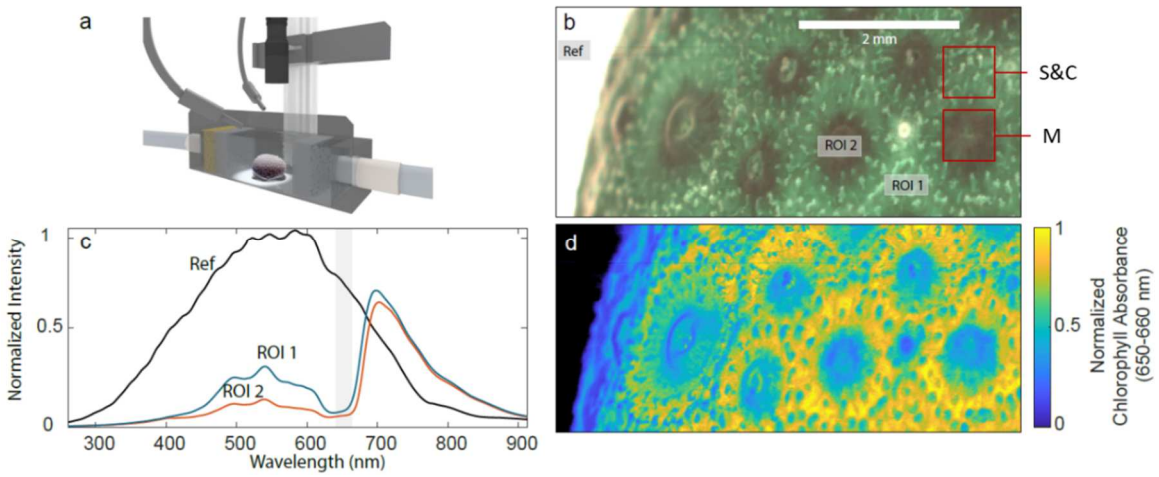

Fig. 5.1. Hyperspectral imaging of zooxanthellae chlorophyll distribution. **a** Experimental set up showing the arrangement of the coral inside the flow-through chamber with the hyperspectral camera and lens on top which were moved horizontally using a linear motor. **b** Processed image of the coral surface showing the Regions Of Interest (ROI) and the external reference area. . Septa and coenosarc (S&C) and mouth opening (M) are marked. **c** Normalized light intensities at the ROIs and reference shown in b. **d** Map of the chlorophyll concentrations inside the coral tissue derived from normalized chlorophyll absorbance.

5.3.2. Flow field and oxygen concentrations at the coral surface

In order to relate the heterogeneous chlorophyll distribution observed inside the tissue with the O_2 dynamics at the DBL, we used O_2-sensitive nanoparticles as seed in a particle image velocimetry system (sensPIV) (Fig. 5.2a). We observed a heterogeneous O_2 distribution along the coral surface. Areas of high O_2 concentrations (hotspots) over the mouth openings of the coral polyps contrasted with areas of lower O_2 concentrations at the periphery of the

polyps (Fig. 5.2d). The patchiness suggests the superposition of two independent processes, as outlined below: passive diffusion of O_2 from the sites of production (zooxanthellae) and active transport of water by ciliary currents.

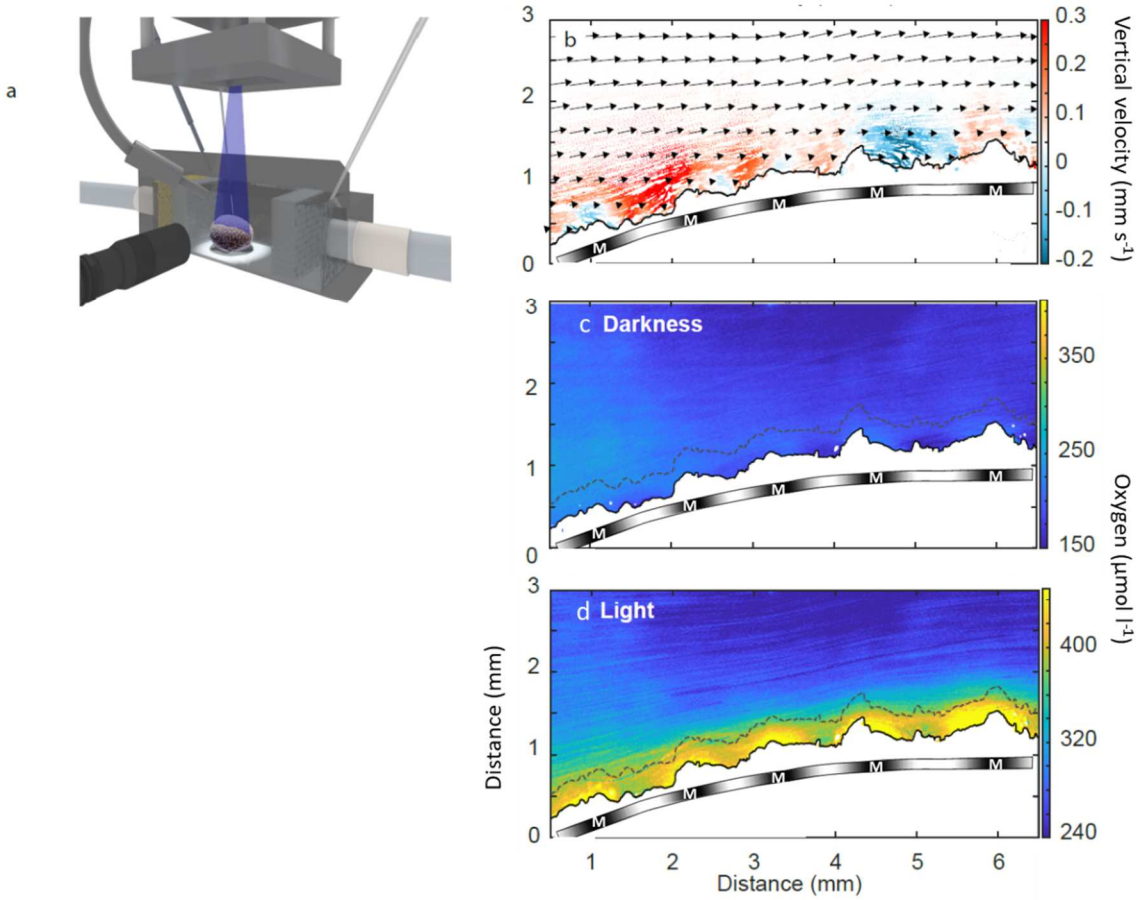

Fig. 5.2. O_2 and flow dynamics inside the DBL of *Porites lutea* measured simultaneously using sensPIV. Flow speed of water was 1300 µm s^{-1} measured at 2 mm from the coral surface. **a** Experimental set up showing the coral colony inside the flow-through chamber with the microsensors and cameras (see also Pacherres et al. 2020). **b** Combined particle image velocimetry (PIV) and particle tracking velocimetry (PTV) of sensPIV particles. Arrows indicate the water flow direction on top of the coral surface. Colored dots represent single tracked particles and the color indicates their vertical velocity. Red and blue depict upward and downward flow of particles respectively. **c** & **d** O_2 concentrations (extracted from the sensPIV signal) inside the DBL of the coral exposed to darkness (c) and light (d). The black and white bar indicates areas of high and low chlorophyll represented by Septa and coenosarc (white) and Mouth (black), respectively.

In all cases (n=6) we found that under the flow conditions of our experiments (300 and 1500 µm s^{-1}), cilia on the surface of the coral generated vortical currents (Fig. 5.2b). At high ambient flow speeds (1500 µm s^{-1}), the average height and width of the vortices were 300 ±

55 µm and 1500 ± 230 µm, respectively. At low ambient flow speeds (300 µm s^{-1}) the corresponding values were 500 ± 50 µm and 1500 ± 220 µm, respectively (Supp. Inf. Fig. S5.1). Inside the vortices, the vertical flow velocities reached up to 300 µm s^{-1} and -200 µm s^{-1} (Fig. 5.2b), in line with previous reports (Shapiro et al. 2014, Pacherres et al. 2020). The vortices' structure was similar to those found in Pacherres et al. (2020) with the upward flow of the vortice facing towards the ambient current while the downward flow was located leeward, suggesting cilia beating against the ambient current. The upward flank of the vortices transported water from the coral polyp periphery aloft (red areas, Fig. 5.2b) while the downward flank was situated somewhat leeward of the polyp mouth opening (blue areas, Fig 5.2b). As a result, the main part of the vortices were situated on top of the mouth opening. In darkness, we found slightly lowered O_2 concentrations in the downwelling areas suggesting respiration (Fig. 5.2c). In the light, we found high O_2 concentrations near the coral surface, with highest values over the mouths and lower values in the periphery (Fig. 5.2d).

5.3.3. Combining oxygen at the DBL and tissue chlorophyll

The O_2 and chlorophyll distributions were inversely related (Fig. 5.3). This surprising finding is in conflict with the current paradigm of an exclusively diffusive transport of O_2 which would predict a positive relation between chlorophyll and O_2. We found the opposite, suggesting a re-distribution of O_2 by cilia-induced vortical currents dominating O_2 transport in *Porites*. The vortices were located above the chlorophyll-poor areas, with their upward flow extending into the adjacent chlorophyll-rich areas. This allows O_2 to be transported laterally from the main production site into the vortex, which itself extends vertically as a bulged interface into the ambient water with lower O_2. In effect, O_2 accumulation in the chlorophyll-rich tissue is alleviated and at the same time, the high O_2 concentration in the vortex increases the concentration gradient towards the ambient water and thus the diffusive flux.

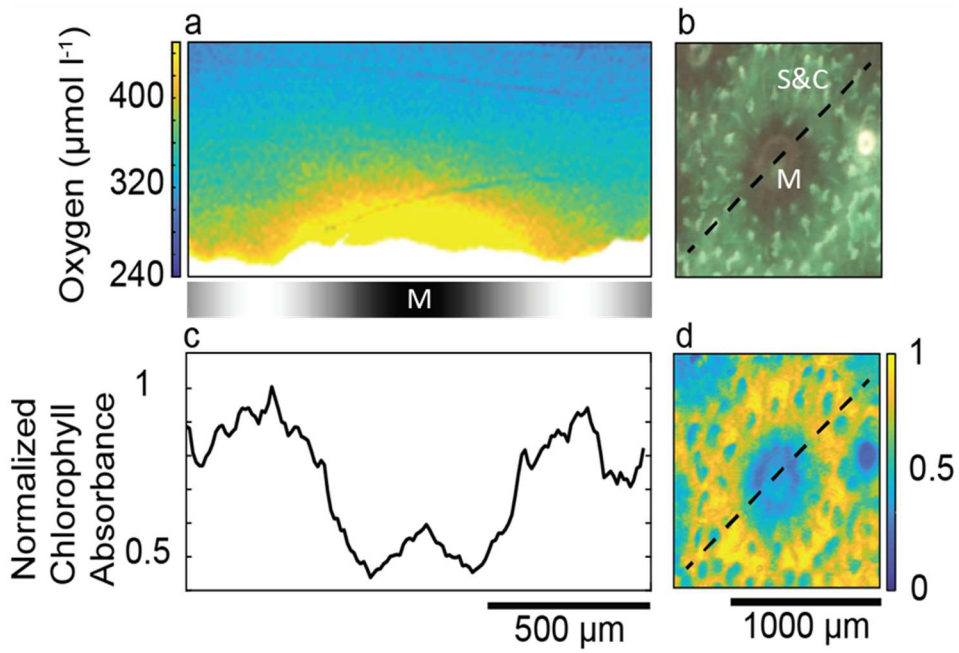

Fig. 5.3. Combined surface O_2 and internal chlorophyll results along the dashed lines of a single polyp of *Porites lutea*. **a** O_2 concentration extracted from the SensPIV results along the dashed line shown in **b**. Black and white panel below indicate different regions of the coral: Septa and coenosarc (white), Mouth (black) (as in Fig 2). **c** Estimate chlorophyll concentrations along the dashed line shown in **d**. Please notice that O_2 distribution and chlorophyll distribution are not from the same locations but are picked as representative examples. S&C = septa and coenosarc, M = mouth. Scale bars are applicable for the respective vertical panels.

5.3.4. Simulations of the boundary layer dynamics of P. lutea

To investigate the relation between tissue chlorophyll and the diffusive and advective flux of photosynthetic O_2, we simulated the effects of diffusion and ciliary flow along the coral surface by means of a simplified planar two-layer model. The lower layer has a thickness of 100 µm, representing the tissue of *P. lutea* in which the zooxanthellae are located and transport is limited to diffusion (dotted line in Fig. 5.4a). The heterogeneously distributed zooxanthellae produce O_2 at a constant rate, assuming constant light regime and no photoinhibition. The layer above represents the water column in which the cilia stir the boundary layer under flow conditions. The ciliary flow is driven by a moving boundary with horizontal velocity components that oscillate in both directions along the surface at an amplitude (maximum ciliary flow) that was adjusted to c_{vel} = 150 µm s^{-1}, similar to previous measurements (Shapiro et al., 2014). The undisturbed flow velocity in the chamber was set to set to 1500 µm s^{-1} similar to the measurements.

The interaction of the flow field and the cilia beating leads to vertical flow speeds of 80-100 µm s^{-1} which are slightly lower than the maximum vertical speeds from the experiments (up to 300 µm, Fig. 5.1b) and the velocities seen in the upward zones of the vortices in Shapiro et al. (2014). At the surface, the opposing horizontal velocities lead to the formation of two stagnation points above which the initially horizontal velocities result in vertical upward and downward directed flows for converging and diverging horizontal surface velocities, respectively. The combination of upward and downward directed flows leads to the formation of vortex structures along the surface of the coral. The horizontal extent of the vortices is largely determined by the boundary conditions, i.e. the wavelength of the oscillating boundary, which was adjusted to δ = 1200 µm, similar to the average size of the calyx of the coral (see details of calyx size in Fig. 5.3b). The specific shape of the vortices leads to two distinct regions within the coral boundary layer, which are determined through the location of the stagnation points along the surface of the coral (Fig 5.4a, red dots and dashed line). The first region (Fig. 5.4a, inserted panel: R1) is characterized through the rotating velocities inside the vortex structure; streamlines within the vortex are closed, indicating no advective exchange with the ambient water. The second region (Fig. 5.4a, inserted panel: R2) is characterized by strong horizontal velocities close to the coral surface that potentially lead to increased vertical concentration gradients enhancing the diffusive exchange with the tissue.

In the simulations, O_2 produced diffuses from the coral tissue in proportion to the observed Chl *a* distribution (Fig. 5.2d). For simplicity, the heterogeneity of O_2 production is simulated by a sinusoidal curve which spatial extent was adjusted to match the experimentally obtained results: highest O_2 production was situated outside the vortex structures, while lowest O_2 production was situated underneath the vortex (Fig. 5.3b). The produced O_2 diffuses through the tissue before reaching the ambient water. Along the tissue surface, diffusive exchange fluxes are highest where O_2 gradients between tissue and the ambient water are strongest. The strongest O_2 gradients occur where O_2 is produced at a higher rate and lower- O_2 ambient water is directed downward at high velocities (Fig. 5.4a, inserted panel: R2). In contrast, O_2 concentrations within the vortex structures are elevated, fed by the upward flow of O_2-enriched water from the tissue surface. While rotating in the vortex, O_2 diffuses across the vortex boundaries into the ambient water so that the downward flow carries less O_2 and can be recharged again (Fig. 5.4a, inserted panel: R1). Both, the model and experiments agree in reproducing the surprising spatial segregation of high O_2 concentrations above low O_2-

production sites and vice versa (Fig 5.4). The measured O_2 distribution exhibits a similar pattern as the simulated O_2 distribution. Five distinct vortices reaching up to 500 µm into the flow field are visible where O_2 concentrations are supersaturated (Fig. 5.4).

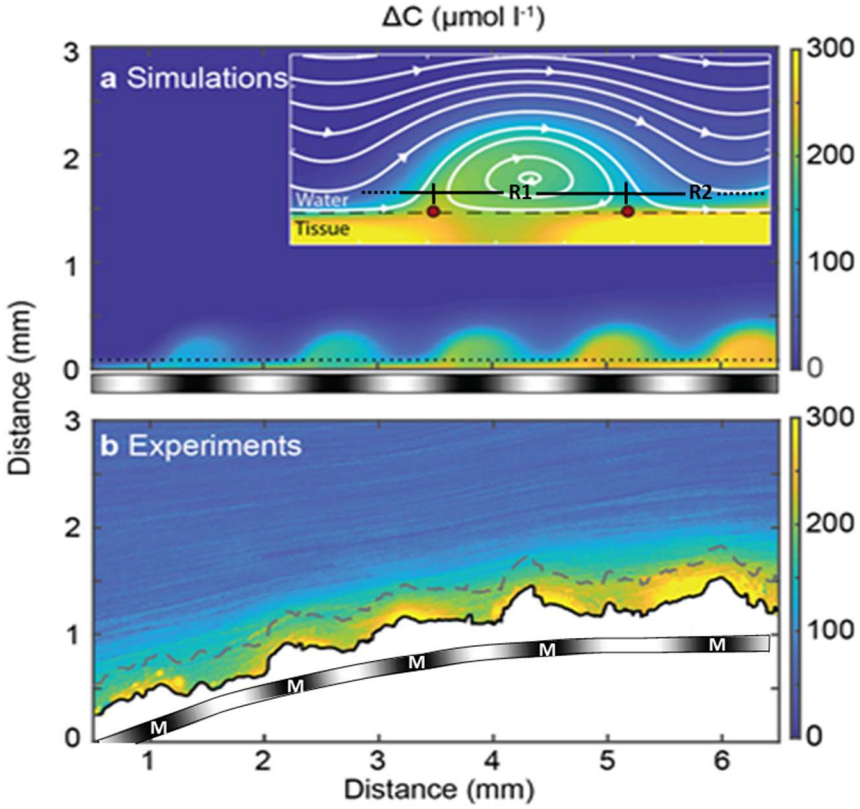

Fig. 5.4. **a** Model results of the O_2 distribution inside the DBL of the coral under the same flow speed of water as in the experiments. Inserted panel in **a** represents the O_2 and flow distribution of a magnified vortex, red dots depict the stagnation points and distinct regions along the surface and coral DBL respectively (see text). **b** Experimental results of the O_2 concentration differences between Light and darkness (180 and 0 µmol quanta m^{-2} s^{-1}). Black and white panel below the O_2 simulations indicate the regions of high photosynthetic activity (white) and low activity (black), equivalent to different regions of the coral measured in the experiments: septa and coenosarc (white) and Mouth (black) (see also Fig. 5.2 and 5.3).

Since it was possible to reproduce the measured phenomena with our model, we used it to test how ciliary flow velocities, photosynthetic inhibition due to O_2-production and heterogeneous versus homogeneous O_2-production affect the O_2 distribution and flux in the coral DBL. We focus on two measures: (i) the average O_2 concentration in the tissue of the coral and (ii) the average fluxes of O_2 out of the tissue. The effect of ciliary flow on the O_2 flux is represented by the Sherwood number, which is the ratio of the mass flux due to

advection (cilia action) to the flux that would occur if only diffusion was the mass transport mechanisms (cilia inhibited) (White 2010). The model shows that O_2 concentration in the tissue is affected by the ciliary flow at speeds of approximately $2 \cdot 10^{-2}$ mm s^{-1} (Fig. 5.5a) and strongly decreases as the ciliary flow increases. In contrast to the O_2 concentration, we did not observe an effect of the ciliary flow on the O_2 fluxes, shown by the constant Sherwood number =1 (Fig. 5.5b). The simple reason is that the tissue layer represents a boundary with a constant flux, i.e. zooxanthellae in the tissue produce O_2 at a constant rate, assuming constant light regime and no photoinhibition. Thus, the ciliary flow mitigates high O_2 concentration but does not increase the flux, as confirmed by Pacherres et al. (2020). If we assume that the tissue layer represents a boundary with a constant O_2 concentration (e.g. Shapiro et al. 2014), the O_2 flux is directly controlled by the flow field, i.e. the amplitude of the ciliary flow. However, such constant O_2 concentration at the tissue surface can only be achieved if the zooxanthellae adjust their O_2 production to the ciliary flow, so that increased transport is compensated by an increased O_2 production. As this is unlikely, we considered a constant-flux boundary condition as the more realistic baseline case.

Photosynthetic activity by zooxanthellae can, however, be inhibited by O_2 accumulation through photorespiration and the formation of reactive oxygen species (ROS) (Finelli et al. 2006, Mass et al. 2010). Photorespiration occurs when O_2 is used as a preferred substrate instead of CO_2, resulting in the loss of energy (Jordan and Ogren 1981), while ROS are formed through photoreduction of O_2 and are believed to directly damage the photosystem II of the chloroplast (Lesser 1996, Roberty et al. 2014). To take this effect into account, we added an O_2 dependent inhibition term to the production term (Eq. 5.7). Under this more realistic representation of the O_2 production through the zooxanthellae, we observed that O_2 fluxes are strongly increased as a result of the overall reduced O_2 concentration in the tissue. Distinct differences between the heterogeneous and homogeneous chlorophyll concentrations become visible (Fig. 5.5c, d). The average O_2 concentration for the tissue with a heterogeneous chlorophyll concentration is further reduced with respect to a homogeneous chlorophyll concentration as the zones of high O_2 production coincide with regions of high horizontal velocities, i.e. strong concentration gradients. This reduces the inhibition of the production term, which imprints on the O_2 fluxes. In summary, the simulation results indicate that the heterogeneous O_2 distribution in the overlying water column is not directly reflecting the heterogeneous chlorophyll concentration inside the tissue, but is instead a result of the specific structure of the cilia induced flow field, further

supporting the observed results (Fig. 5.3). The results further indicate that the heterogeneous distribution of both ciliary flow and O_2 production helps in avoiding photosynthetic inhibition.

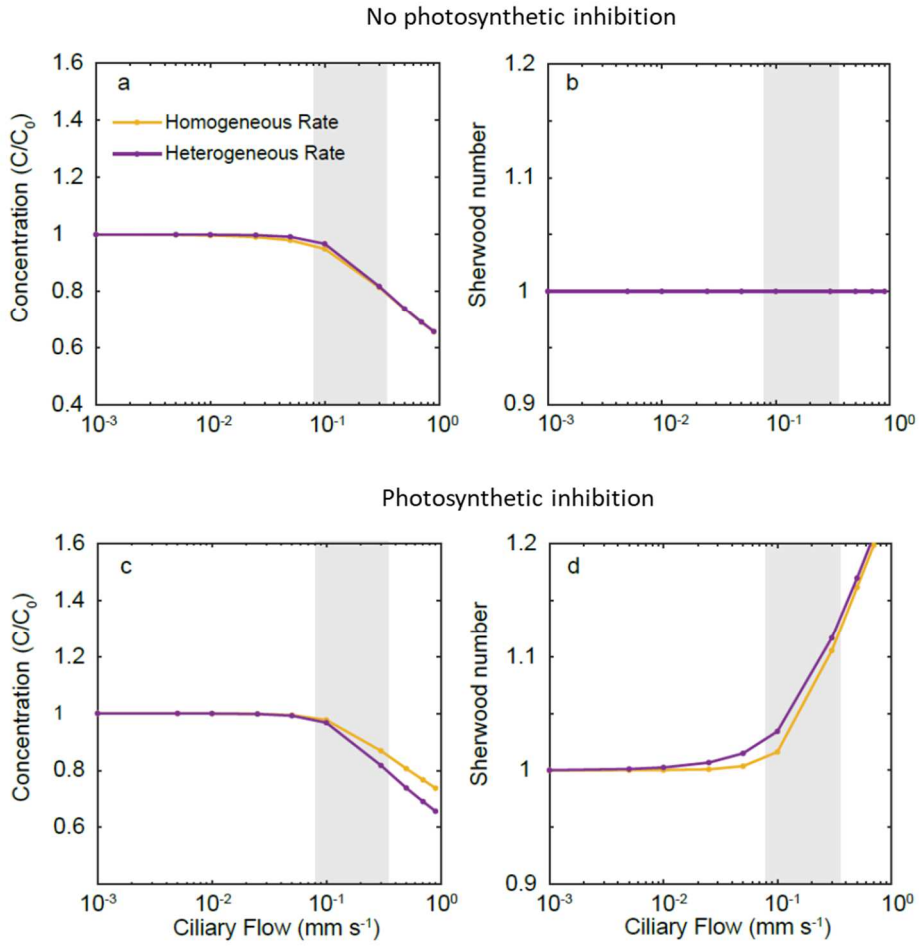

Fig. 5.5. Modeled O_2 concentrations (**a** & **c**) and fluxes, Sherwood number, (**b** & **d**) at the surface of the coral *Porites lutea* under different O_2 production rates of their tissue, homogenous (yellow) and heterogeneous (blue). **a** & **b** show the O_2 concentrations and Sherwood number assuming no inhibitory properties of high O_2 concentrations while **c** & **d** represent the inhibition of photosynthesis with increasing O_2 concentrations. Grey bars indicate the range of the ciliary flow observed within the experiments. C_0 refers to the concentration in absence of cilia beating.

5.3.5. Implications for the coral's resilience to oxidative stress

The coupling of diffusional processes and active transport by ciliary vortices - which lead to the generation of O_2 hotspots at the surface of the coral - may help explain variations in coral response to stress events as it results in different levels of exposure at different scales (cells and polyps). Our model results, when considering the inhibition of photosynthesis by excess

O_2, show a clear influence of ciliary beating in enhancing the O_2 fluxes under the observed heterogeneous O_2 distribution at the coral surface. Ciliary vortices localized at specific areas of excess O_2 production might, therefore, prove beneficial for the coral in the face of oxidative stress, especially under weak currents, which have been found to exacerbate bleaching (Loya et al. 2001, Fifer et al. 2021). It is well known that colonies adjacent to each other, experiencing similar water temperatures, can present different bleaching responses (Cunning et al. 2016), and more so, different regions within the same colony can show differential bleaching severities as well (Putnam et al. 2017). If taken into consideration that the capacity of the organism to adapt to environmental changes depends on its life history exposure to environmental variations (Brown et al. 2002, Pacherres et al. 2013), these heterogeneities might represent a buffering system in the face of environmental stress. Moreover, the presence of different optical micro-niches within the coral tissue have been suggested to act as possible refugia for minor symbiont populations during stress conditions causing bleaching, helping in the repopulation and redistribution of symbionts following the bleaching event (Wangpraseurt et al. 2012, Wangpraseurt et al. 2014). It must also be noted that ciliary vortices are three-dimensional (Supp. Inf. SV5.1), adding even more complexity to the micro-niche distribution in corals and their influence in their physiological processes and response to stress.

The ability of corals to enhance O_2 transport in specific areas (septa and coenosarc) (Fig. 5.2c) might have implications not only in the coral's response to its environment but also in its relationship with bacteria and viruses that inhabit its surface (Ainsworth et al. 2017). The community of prokaryotic and eukaryotic microbes, virus and archaea comprising the coral microbiome is extremely diverse and has been associated not only with diseases (van Oppen et al. 2009, Sweet and Séré 2016) but also with the capacity of corals to resist environmental stress by supporting nutrient acquisition, pathogen defense, genome modification, etc. (Wegley et al. 2007, Gerardo 2013). The ability of cilia to generate chemical microenvironments, such as seen here for the O_2 hotspots, could provide an advantage to certain coral-associated microbes by enhancing the transport of the metabolic compounds necessary for their development. Further research will be needed in order to unveil the consequence of the observed microenvironment creation and the repercussions it might have upon coral-microbe relations and coral health.

5.3.6. Conclusions

Altogether, this study demonstrates that interactions between ciliary flows related to tissue structures (mouth openings, coenosarc) and internal physiological processes (photosynthesis) can give rise to local heterogeneities in the chemical landscape and solute exchange, which will not always align. This has consequences in the ability of corals to react and cope with environmental stressors and to create micro niches on the coral surface potentially affecting coral-microbe interactions and, possibly, coral disease. A 3D exploration of the coral DBL, taking into consideration the different elements that intervene in its shape and characteristics, can be an important next step to reveal further insights into the complex coral-water interface, and better understand the role of the DBL in the coral's relationship with its environment.

5.4. Materials and Methods

5.4.1. Coral fragments

Colonies of the massive coral *Porites lutea*, reared at the aquaria facilities of the Alfred Wegener Institute (AWI) were used as fragment source. They were kept in artificial seawater (salinity 32.6 ± 0.26) (Dupla Marine Premium Reef Salt Natural Balance) under conditions mimicking those found at the depth of their origin (15 m), i.e. 25.2 ± 0.07 °C, a 12-h light-dark cycle, light intensities between 75 and 80 µmol quanta m^{-2} s^{-1} (LI-COR LI-192, USA) and a pH of 7.9 ± 0.09 (YSI, USA). Food was provided in the form of freshly hatched *Artemia* nauplii every second day. Before the start of the experiments, small fragments (2 cm long, 2 cm wide) bearing 60 to 80 polyps were cut out from 4 of the source colonies and allowed to heal for at least one month in the same culturing tanks their original colonies were kept. Survival of the fragments was >90%.

5.4.2. Experimental set-up

For all experiments, the light-sheet-microscopy based flow chamber setup was used (as in Pacherres et al., 2020) (Fig. 5.1a & Fig. 5.2a). The coral fragment was placed in the chamber filled with filtered artificial seawater (FASW) (0.2 µm pore size) from the coral's culturing tank. There, it was allowed to acclimate to the chamber conditions for at least an hour under dark conditions before experiments started. Temperature of the water inside the chamber

was monitored every 30 seconds (Pt100 sensor, PyroScience, Germany). For all experiments, temperature was kept constant at 25 °C ± 0.5. The flow rate of the water inside the chamber was set to be 400 µm s^{-1} measured at 2 mm above the coral tissue. In the case of experiments requiring a light source a fiber optic lamp (Schott 1500, USA) was used in order to maintain constant illumination. In order to standardize respiratory differences due to digestion, all experiments were performed after 2 days of starvation.

5.4.3. Hyperspectral imaging

Chlorophyll concentrations of zooxanthellae inside the tissue of the coral colony were obtained using hyperspectral line-scanning. For that, hyperspectral imaging optics (Wasatch, USA) were used. Briefly, a line is recorded through a long distance microscope lens (Optem Fusion) and directed through a diffraction grid. The resulting light spectrum is aligned with a camera CCD chip (FLIR, blackfly, Canada) along a pixel row of 1288 px. in the visible light range, this results in a spectral resolution of approx. 1 nm. Using a micromanipulator (Pyroscience, Germany) the camera system was slowly moved parallel to the coral surface at a speed of 50 µm s^{-1} to the focused line along the coral fragment while continuously recording images with an exposure time of 400 ms. This resulted in a 3-dimensional tensor or hypercube, i.e. each pixel of the image consists of a spectrum ranging from 400 nm - 700 nm. Horizontal and vertical resolution was 42 and 6 µm per px, respectively. The setup was controlled using serial-interfaces and the Spinnaker Software Development Kit (FLIR Spinnaker SDK) through an in-house developed Python script (Python Software Foundation). The raw images were processed using Matlab (2018b).

Chl *a* pigments reflect green light and absorb light in the blue-violet and orange-red range with peaks at 450-475 nm and around 650-680 nm, respectively. In our hyperspectral line-scanning setup, reflectance spectra were measured, implying that low spectral intensities correspond to a high absorbance and, conversely, high spectral intensities correspond to low absorbance. Therefore, to estimate the absorbance spectra induced by the Chl *a*, we subtracted the integrated wavelengths between 650 nm and 660 nm from the reference light spectrum. To compensate for lower light intensity and 3D structures at the surface of the coral, we normalized the resulting absorbance spectrum by chlorophyll unaffected wavelengths between 550 nm and 560 nm. Therefore, the resulting normalized absorbance value indicates the amount of orange-red light that is absorbed from the incident light, which depends on the amount of Chl *a* in the tissue of the coral.

During the experimental procedure, the coral fragment was placed in the flow-chamber (Fig. 5.1a) and illuminated using a homogenous white light (Schott 1500, USA), intensity reached 160 µmol quanta m^{-2} s^{-1} (LI-COR LI-192, USA). Camera exposure was set to 400 ms. The chamber was placed on top of a white surface, which later served as reference.

5.4.4. SensPIV *measurements*

In order to identify the relative influence of cilia activity on the two dimensional structure of the O_2 DBL at the coral surface, O_2 distributions were compared under light and dark conditions (180 and 0 µmol quanta m^{-2} s^{-1} respectively). To resolve the O_2 and flow field around the coral fragment, we used O_2 sensitive nanoparticles (Koren et al. 2015), which have proven ideal for mapping O_2 concentrations at relevant scales (see Chapter 3 of the thesis). The stock solution contained 2 mg mL^{-1} which was further diluted by a factor of 200. Illumination was achieved using a LED pulsing system (LPS3, ILA_5150, Germany) connected to led light sheet optics similar to the one described by (Willert et al. 2010). The light sheet was approx. 1 mm thick and intensity reached 4500 µmol quanta m^{-2} s^{-1} (LI-COR LI-192, USA) at a wavelength of around 468 nm. One hundred images were captured using a Grasshopper3 camera (FLIR, USA) recording at 20 frames per second (fps) with an exposure time of 50 ms. A long distance custom-made microscope lens (based on the Optem FUSION system, Germany) with a yellow-orange long-pass filter (515 nm, LP515, Midopt, USA) was used for all experiments. To avoid photoinhibition of the zooxanthellae from the intense illumination, light exposure was limited to 5 s for each experiment and LED light was only active during 50 ms illumination of the camera chip. The recorded images were post-processed using custom-built Matlab (MathWorks, R2018b) algorithms to obtain the O_2 concentration signal and a map of the particle movement inside the chamber.

Nanoparticle readings were later compared and calibrated with O_2 profiles, performed before each experiment, using an electrochemical sensor of 10 µm tip diameter (Unisense, Denmark). The profile was recorded 3 min before the images were captured. Values were recorded using the SensorTrace-PRO software (Unisense, Denmark). For each experiment, microelectrodes were 2-point calibrated in O_2-free (bubbling pre-filtered seawater with N_2 gas for 10 min) and air-saturated FASW of known salinity and temperature (Kühl et al. 1995). The tip of the sensor was carefully placed at the surface of the coral. A micromanipulator (Unisense, Denmark) was programmed to move the sensor up in 20 µm

steps. The range of the vertical profile was 1000 µm. At each step, dissolved O_2 was measured one time with a sampling interval of 2 s.

To directly relate the O_2 production of the coral colony with the chlorophyll concentration inside the coral tissue we carefully pinpoint the area of the coral observed through the camera and later extracted the chlorophyll concentrations from the same area out of the hyperspectral images.

5.4.5. Model formulation

The cilia beating of corals generates a complex flow pattern, which is reproduced using numerical simulations which were performed in Comsol (Comsol Multiphysiscs). The flow field is given by the laminar Navier-Stokes equations:

$$\rho(u \,.\nabla)u = \, -\nabla\rho + \mu\nabla^2 u \qquad \text{[Eq. 5.1]}$$

Where u is the velocity vector, p the pressure, μ dynamic viscosity and ∇ the del-operator. The continuity equation for incompressible fluids reads:

$$\nabla \,.\, u = 0 \qquad \text{[Eq. 5.2]}$$

The O_2 distribution was calculated solving the advection-diffusion equations:

$$D\nabla^2 C = u \,.\nabla C \qquad \text{[Eq. 5.3]}$$

According to the model proposed by Shapiro (2014), the cilia-induced currents were simulated assuming oscillating horizontal velocity components at the coral surface:

$$u_x = c_{vel} \,.\sin\left(\frac{2\pi}{\delta}x\right) \qquad \text{[Eq. 5.4]}$$

where x is the horizontal distance, c_{vel} the maximum ciliate beating velocity and δ is the characteristic length scale of the vortices, see text for values and explanation. Volumetric rates of O_2 production in the tissue were simulated based on three scenarios:

(i) constant rates through-out the tissue were assumed, as a consequence of an homogeneous chlorophyll distribution along the coral tissue with an O_2 production rate R_C of 20 µmol L^{-1} s^{-1}:

$$R = R_C \qquad \text{[Eq. 5.5]}$$

(ii) the rates were assumed to be heterogeneous, a product of the clustering of chlorophyll at certain areas of the tissue:

$$R_H = R_C\left(1 + \sin\left(\frac{2\pi x}{\delta}\right)\right) \quad \text{[Eq. 5.6]}$$

(iii) rates were assumed to be heterogeneous and inhibited at high O_2 concentrations.

$$R_{inh} = R_H \frac{K_m}{K_m + C} \quad \text{[Eq. 5.7]}$$

where K_m = 400 µmol L^{-1} is the inhibition constant. The mathematical model allowed us to simulate O_2 concentrations and fluxes (Sherwood number) inside the DBL in the presence of constant and heterogeneous O_2 production rates by the coral. The Sherwood number (*Sh*) is the ratio of the mass flux in presence of cilia induced advection to the flux in absence of cilia induced advection (White 2010). We evaluated the results as a function of the magnitude of ciliary flow speeds, which in our understanding can be taken as a reflection of the amount of cilia present in an area.

Acknowledgements

We thank Esther Lüdtke and Ulrike Holtz for their help with the culturing of the coral colonies. This research was conducted in the frame of the Ph.D. project of Cesar O. Pacherres at the University of Bremen and the Alfred Wegener Institute (AWI). It was supported and financed by AWI and FONDECYT, initiative from the *Consejo Nacional de Ciencia, Tecnología e Innovación Tecnológica* (CONCYTEC), *Perú*. *Contrato* 086-2016-FONDECYT and the AWI (PoF4.6: Marine and Polar Life). MPI Bremen provided logistic and instrumental support. S.A. acknowledges funding from the Max Planck Society (MPG) for the "Multiscale Approach on the Role of Marine Aggregates (MARMA)" project.

5.5. References

Ainsworth, T. D., A. J. Fordyce, and E. F. Camp. 2017. The other microeukaryotes of the coral reef microbiome. Trends Microbiol **25:** 980-991.

Al-Horani, F. A., T. Ferdelman, S. M. Al-Moghrabi, and D. de Beer. 2005. Spatial distribution of calcification and photosynthesis in the scleractinian coral *Galaxea fascicularis*. Coral Reefs **24:** 173-180.

Brown, B., R. Dunne, M. Goodson, and A. Douglas. 2002. Experience shapes the susceptibility of a reef coral to bleaching. Coral Reefs **21:** 119-126.

Crawley, A., D. I. Kline, S. Dunn, K. Anthony, and S. Dove. 2010. The effect of ocean acidification on symbiont photorespiration and productivity in *Acropora formosa*. Glob. Change Biol. **16:** 851-863.

Cunning, R., R. Ritson-Williams, and R. D. Gates. 2016. Patterns of bleaching and recovery of *Montipora capitata* in Kāne'ohe Bay, Hawai'i, USA. Mar Ecol Prog Ser **551:** 131-139.

de Beer, D., M. Kühl, N. Stambler, and L. Vaki. 2000. A microsensor study of light enhanced Ca^{2+} uptake and photosynthesis in the reef-building hermatypic coral *Favia* sp.†. Mar Ecol Prog Ser **194:** 75-85.

Dubinsky, Z., P. G. Falkowski, J. W. Porter, L. Muscatine, and D. C. Smith. 1984. Absorption and utilization of radiant energy by light- and shade-adapted colonies of the hermatypic coral *Stylophora pistillata*. Proc R Soc B **222:** 203-214.

Dykens, J. A., and J. M. Shick. 1984. Photobiology of the symbiotic sea anemone, *Anthopleura elegantissima*: Defenses against photodynamic effects, and seasonal photoacclimatization. Biol Bull **167:** 683-697.

Falkowski, P. G., and Z. Dubinsky. 1981. Light-shade adaptation of *Stylophora pistillata*, a hermatypic coral from the Gulf of Eilat. Nature **289:** 172-174.

Fifer, J., B. Bentlage, S. Lemer, A. G. Fujimura, M. Sweet, and L. J. Raymundo. 2021. Going with the flow: How corals in high-flow environments can beat the heat. Mol Ecol **30:** 2009-2024.

Finelli, C. M., B. S. T. Helmuth, N. D. Pentcheff, and D. S. Wethey. 2006. Water flow influences oxygen transport and photosynthetic efficiency in corals. Coral Reefs **25:** 47-57.

Gerardo, Nicole M. 2013. The give and take of host-microbe symbioses. Cell Host Microbe **14:** 1-3.

Jordan, D. B., and W. L. Ogren. 1981. Species variation in the specificity of ribulose biphosphate carboxylase/oxygenase. Nature **291:** 513-515.

Joyce, K. E., and S. R. Phinn. 2003. Hyperspectral analysis of chlorophyll content and photosynthetic capacity of coral reef substrates. Limnol Oceanogr **48:** 489-496.

Koren, K., K. E. Brodersen, S. L. Jakobsen, and M. Kühl. 2015. Optical sensor nanoparticles in artificial sediments – A new tool to visualize O_2 dynamics around the rhizome and roots of seagrasses. Environ Sci Technol **49:** 2286-2292.

Koren, K., S. L. Jakobsen, and M. Kühl. 2016. In-vivo imaging of O_2 dynamics on coral surfaces spray-painted with sensor nanoparticles. Sens. Actuators B Chem. **237:** 1095-1101.

Kühl, M., Y. Cohen, T. Dalsgaard, B. B. Jørgensen, and N. P. Revsbech. 1995. Microenvironment and photosynthesis of zooxanthellae in scleractinian corals studied with microsensors for O_2, pH and light. Mar Ecol Prog Ser **117:** 159-172.

Lasker, H. R. 1979. Light dependent activity patterns among reef corals: *Montastrea cavernosa*. Biol Bull **156:** 196-211.

Lesser, M. P. 1996. Elevated temperatures and ultraviolet radiation cause oxidative stress and inhibit photosynthesis in ymbiotic dinoflagellates. Limnol Oceanogr **41:** 271-283.

---. 1997. Oxidative stress causes coral bleaching during exposure to elevated temperatures. Coral Reefs **16:** 187-192.

Lesser, M. P., and J. M. Shick. 1989. Effects of irradiance and ultraviolet radiation on photoadaptation in the zooxanthellae of *Aiptasia pallida* primary production, photoinhibition, and enzymic defenses against oxygen toxicity. Mar Biol **102:** 243-255.

Lesser, M. P., W. R. Stochaj, D. W. Tapley, and J. M. Shick. 1990. Bleaching in coral reef anthozoans: effects of irradiance, ultraviolet radiation, and temperature on the activities of protective enzymes against active oxygen. Coral Reefs **8:** 225-232.

Liu, C., S. H. Cheng, and S. Lin. 2020. Illuminating the dark depths inside coral. Cell Microbiol **22:** e13122.

Loya, Y., K. Sakai, K. Yamazato, Y. Nakano, H. Sambali, and R. van Woesik. 2001. Coral bleaching: the winners and the losers. Ecol Lett **4:** 122-131.

Mass, T., A. Genin, U. Shavit, M. Grinstein, and D. Tchernov. 2010. Flow enhances photosynthesis in marine benthic autotrophs by increasing the efflux of oxygen from the organism to the water. PNAS **107:** 2527-2531.

Muscatine, L. 1973. Nutrition of corals p. 77-115. *In* O. A. Jones and R. Endean [eds.], Biology and Geology of Coral Reefs. Academic Press.

Muscatine, L., P. G. Falkowski, Z. Dubinsky, P. A. Cook, L. R. McCloskey, and D. C. Smith. 1989. The effect of external nutrient resources on the population dynamics of zooxanthellae in a reef coral. Proc R Soc B **236:** 311-324.

Muscatine, L., C. Ferrier-Pagès, A. Blackburn, R. D. Gates, G. Baghdasarian, and D. Allemand. 1998. Cell-specific density of symbiotic dinoflagellates in tropical anthozoans. Coral Reefs **17:** 329-337.

Pacherres, C. O., S. Ahmerkamp, G. M. Schmidt-Grieb, M. Holtappels, and C. Richter. 2020. Ciliary vortex flows and oxygen dynamics in the coral boundary layer. Sci Rep **10:** 7541.

Pacherres, C. O., G. M. Schmidt, and C. Richter. 2013. Autotrophic and heterotrophic responses of the coral *Porites lutea* to large amplitude internal waves. J. Exp. Biol. **216:** 4365-4374.

Putnam, H. M., K. L. Barott, T. D. Ainsworth, and R. D. Gates. 2017. The vulnerability and resilience of reef-building corals. Curr Biol **27:** R528-R540.

Roberty, S., B. Bailleul, N. Berne, F. Franck, and P. Cardol. 2014. PSI Mehler reaction is the main alternative photosynthetic electron pathway in *Symbiodinium* sp., symbiotic dinoflagellates of cnidarians. New Phytol **204:** 81-91.

Sebens, K. P., and K. DeRiemer. 1977. Diel cycles of expansion and contraction in coral reef anthozoans. Mar Biol **43:** 247-256.

Shapiro, O. H. and others 2014. Vortical ciliary flows actively enhance mass transport in reef corals. PNAS **111:** 13391-13396.

Shashar, N., Y. Cohen, and Y. Loya. 1993. Extreme diel fluctuations of oxygen in diffusive boundary layers surrounding stony corals. Biol Bull **185:** 455-461.

Shick, J. M. 1990. Diffusion limitation and hyperoxic enhancement of oxygen consumption in zooxanthellate sea anemones, zoanthids, and corals. Biol Bull **179:** 148-158.

Spicer, G. L. C. and others 2019. Measuring light scattering and absorption in corals with Inverse Spectroscopic Optical Coherence Tomography (ISOCT): a new tool for non-invasive monitoring. Sci Rep **9:** 14148.

Sweet, M. J., and M. G. Séré. 2016. Ciliate communities consistently associated with coral diseases. J Sea Res **113:** 119-131.

van Oppen, M. J. H., J.-A. Leong, and R. D. Gates. 2009. Coral–virus interactions: A double-edged sword? Symbiosis **47:** 1-8.

Wangpraseurt, D., A. Larkum, P. Ralph, and M. Kühl. 2012. Light gradients and optical microniches in coral tissues. Frontiers in Microbiology **3:** 1-9.

Wangpraseurt, D. and others 2014. The in situ light microenvironment of corals. Limnol Oceanogr **59:** 917-926.

Wegley, L., R. Edwards, B. Rodriguez-Brito, H. Liu, and F. Rohwer. 2007. Metagenomic analysis of the microbial community associated with the coral *Porites astreoides*. Environ Microbiol **9:** 2707-2719.

Weis, V. M., G. J. Smith, and L. Muscatine. 1989. A "CO_2 supply" mechanism in zooxanthellate cnidarians: role of carbonic anhydrase. Mar Biol **100:** 195-202.

White, F. M. 2010. Fluid mechanics 7th ed. Mcgraw-Hill

Willert, C., B. Stasicki, J. Klinner, and S. Moessner. 2010. Pulsed operation of high-power light emitting diodes for imaging flow velocimetry. Meas Sci Technol **21:** 075402.

Yakovleva, I. M., A. H. Baird, H. H. Yamamoto, R. Bhagooli, M. Nonaka, and M. Hidaka. 2009. Algal symbionts increase oxidative damage and death in coral larvae at high temperatures. Mar Ecol Prog Ser **378:** 105-112.

5.7. Supplementary information

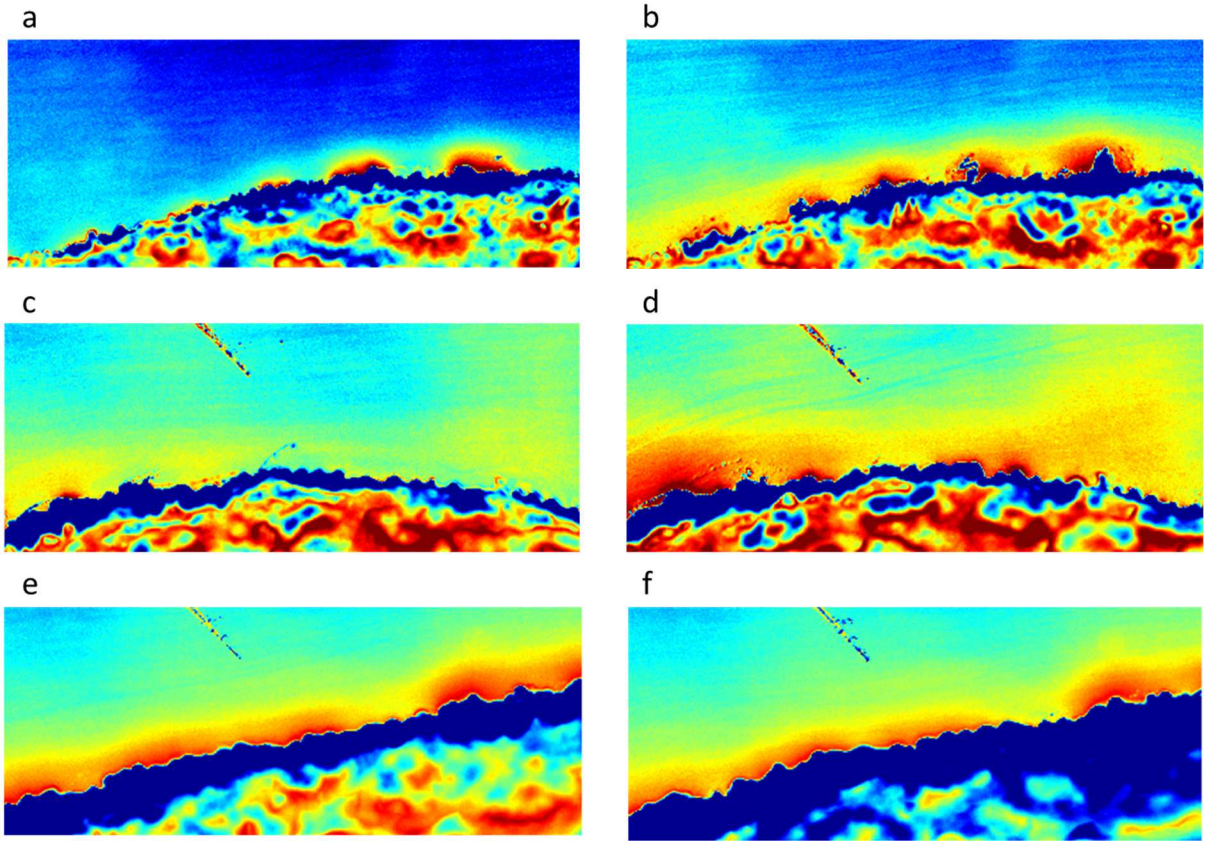

Fig. S5.1. SensPIV images of the 3 coral replicas under 2 different flow speeds of water, 300 and 1500 µm s^{-1} (right and left columns respectively). **a** & **b** Replica 1; **c** & **d** Replica 2 and **e** & **f** Replica 3.

6

The role of cilia in coral suspension feeding

Cesar O. Pacherres[1,2,*], Soeren Ahmerkamp[3,4], Moritz Holtappels[1,4], Gertraud M. Schmidt-Grieb[1] and Claudio Richter[1,2]

1 Alfred Wegener Institute, Helmholtz Centre for Polar and Marine Research, Bremerhaven, Germany

2 University of Bremen, Germany

3 Max Planck Institute for Marine Microbiology, Bremen, Germany

4 Marum, Bremen, Germany

* Corresponding author

Manuscript in preparation

6.1 Abstract

Corals have long been considered passive suspension feeders with stinging tentacles capturing large plankton advected by the currents. Although tentacle feeding is inefficient at low Reynolds numbers, corals have been shown to defy hydrodynamics and retain also the smallest ultraplankton (<5 µm), suggesting other pathways such as passive entrapment by mucus covering the tentacles. Using microscopic particle image velocimetry, we here show that the common scleractinian coral *Porites lutea* is an active suspension-feeder that generates feeding currents to capture small suspended particles (5 µm). We found that cilia-induced vortices extending up to 300 µm aloft entrained particle-rich free-stream waters into the coral boundary layer, where the particles were filtered by the mucus layer intercepting the vortices. The process resulted in particle aggregations in the coral mucus with 3.4 times higher particle trapping rates per minute in corals with active cilia compared to cases in which their cilia activity had been arrested. Cilia have long been believed to play a role in tentacle feeding – as sensory stimuli receptors for the discharge of nematocysts. We carried out incubation experiments with suspended *Artemia* nauplii (737 µm average length) to test if relaxation of the cilia affected feeding on these large food items (2× vortex diameter). We found that corals with active cilia were able to capture an average of 2.9 times more prey than when their cilia were inhibited (42 vs. 14 ind. h^{-1}). Our results highlight the role of cilia in enhancing Pico: <2 µm; ultra: <5 µm and mesozooplankton food capture in corals and show the need to review the classic classification of these important organisms as merely passive suspension feeders.

Author contributions

C.O.P., S.A., G.M.S., M.H. and C.R. designed the setup for the experiments. C.O.P. conducted all the experiments. S.A. provided the Matlab algorithm for particle counting. C.O.P. extracted, analyzed the data and created all figures. C.O.P. and C.R. contributed to the interpretation of the collected data, and conceived and wrote the manuscript.

6.2 Introduction

Tropical shallow water scleractinian corals live in nutrient-poor waters, nevertheless they sustain one of the richest ecosystems on earth (Stoddart 1969). This nutrient paradox is partly explained by the symbiotic association between corals and the endozoic algae (zooxanthellae) living inside their tissue, which supply a great part of their metabolic requirements (Muscatine 1973, Muscatine and Porter 1977). However, while most of the energy demand of the coral-zooxanthellae association (or holobiont) is covered by autotrophy, i.e. translocation of the photosynthate of the zooxanthellae, the material demand of the holobiont depends, to a stronger degree, on heterotrophy, i.e. the accrual and metabolism of organic matter (OM). The OM food is taken up by the coral host, by means of suspension feeding, to replenish the losses of inorganic nitrogen, phosphorus, and other nutrients that cannot be adequately supplied by their symbiotic algae (Farrant et al. 1987, Anthony 1999).

Suspension feeding is defined as the capture and ingestion of food particles suspended in the water (Hentschel and Shimeta 2008). The process of suspension feeding can be divided into four stages: (1) transport of water past the suspension feeding structures, (2) trapping of suspended food elements, (3) transport of captured elements from the suspension feeding structures to the mouth, (4) ingestion (Werner 1959). A further classification of suspension feeders is based on the means employed on the first stage. Passive suspension feeders depend on ambient water flow to supply food particles to their feeding structures, whereas active suspension feeders create their own feeding currents to enhance the supply of food particles (Hentschel and Shimeta 2008). All corals are considered passive suspension-feeders (Muscatine 1973) as they depend on ambient currents to drive water past their feeding structures, i.e. nematocyst-bearing stinging tentacles and/or mucus filaments, employing an array of different techniques depending on the size of its suspended prey (Yonge 1940, Jørgensen 1966, Muscatine 1973, Anthony 1999). Mesozooplankton, by virtue of its large size and mass (>200 µm diameter), possesses the inertia needed to short-cut the flow lines around the tentacles, impact the coral surface and trigger nematocyst discharge, as the mechanistic basis for an efficient capture by the tentacles (Ben-Ari et al. 2018). The process likely involves a complex of cilia and microvilli as sensory organelles, as identified for sea anemones but not explicitly proven in corals (Watson and Hessinger 1989). This sieving technique is, however, inefficient for the small ultra-plankton (groups with sizes <5 µm, that include small flagellates and bacteria; Cushing et al. 1958), since the viscous forces

overwhelm the inertial forces at low Reynolds numbers and particles no longer escape the streamlines to cause physical impact (Vogel 1996). Incubation studies have demonstrated an uptake of pico- and nanoplankton (<2µm, <20µm; (Sorokin 1973b, Bak et al. 1998, Houlbrèque et al. 2004b) which appears to defy hydrodynamics, invoking other passive capture mechanisms – notably involving coral mucus (Carpenter 1910, Muscatine 1973, Naumann et al. 2009).

Mucus filaments are secreted by specialized cells called mucocytes, located in the coral tissue at different densities, accounting for as much as 90% of the area in some parts of its surface (Marshall and Wright 1993, Goldberg 2002, Brown and Bythell 2005). Corals use mucus not only to slough off inorganic particles settling on their surface, but also to trap food items and later transport them to their mouth openings (Yonge 1930, Stafford-Smith and Ormond 1992, Stafford-Smith 1993). While it was noted early that epidermal cilia are present in all corals (Mariscal and Bigger 1977) and are involved in the transport of food and waste particles, cilia were long considered unimportant in the coral's capture of food (Carlgren 1905, Carpenter 1910, Yonge 1928). This notion was overturned by Lewis and Pierce (1975) who proposed that the cilia played a role in lifting the mucus layer and exposing the sticky strands to the ambient currents, thus facilitating the scavenging of particles to be subsequently drawn into the mouth. Lewis and Price (1976) maintained, however, that "no discrete feeding currents are present in corals" and that the scavenging was a passive process at the mercy of ambient currents. The application of microscopic Particle Image Velocimetry (mPIV) revealed the presence of ciliary vortices in the coral *Pocillopora damicornis* enhancing the dissipation of excess oxygen in stagnant water (Shapiro et al. 2014). Pacherres et al. (2020) showed that these vortices were present in another common coral, *Porites lutea*, and importantly, that the features prevailed under varying flow conditions. We here suggest that vortical flows not only alleviate excess oxygen stress but may also play a role in enhancing the ability of corals to prey upon a food source that in spite of being abundant might be unavailable to passive suspension feeders – ultra plankton.

The aim of this study is to understand the relative roles of cilia and their generated vortices in coral's suspension feeding, using the reef building coral *P. lutea* as a model. A mPIV set-up with a LED light sheet was used to observe the ciliary vortices interacting with the mucus on the coral surface, and determine if the coral's ability to capture suspended ultra-plankton-sized particles (5 µm) depended on its cilia activity. In addition, incubation experiments were

conducted with suspensions of brine shrimp (*Artemia* sp.*)* naupii (~740 µm length) as mesozooplankton food source, in order to quantify the capture rate of corals with and without cilia activity.

6.3 Materials and Methods

6.3.1 Coral fragments

Experiments were carried out on the massive coral *Porites lutea* reared at the aquaria facilities of the Alfred Wegener Institute (AWI) under conditions mimicking those found at the depth of their origin (15 m). Corals were kept in artificial seawater (salinity 32.6 ± 0.26, YSI, USA) (Dupla Marin Premium Reef Salt Natural Balance) at 25.2 ± 0.07 °C on a 12-h light-dark cycle. Light intensities fluctuated between 75 and 80 µmol quanta m^{-2} s^{-1} (LI-COR LI-192, USA) and pH was kept at 7.9 ± 0.09 (YSI, USA). Food was provided in the form of freshly hatched *Artemia* nauplii every second day. Before the start of the experiments small fragments, (2 cm long, 2 cm wide) bearing 60 to 80 polyps were cut out from 2 of the source colonies and allowed to heal for at least one month in the same culturing tanks their original colonies were kept. Survival of the fragments was >90%.

6.3.2 **Artemia** *culturing*

Artemia sp. eggs (ERDMANN, Germany) were cultured at 23 °C under constant light 100 µmol quanta m^{-2} s^{-1} (LI-COR LI-192, USA) for 2 days in order to obtain viable nauplii, average size was 737 ± 12.2 µm (n=5). Salinity ranged 32.5 – 33 (YSI, USA). Individuals were counted and separated under the stereo microscope before the start of the experiments.

6.3.3 Experimental set up

mPIV and mucus production

We used the light-sheet-microscopy based flow chamber setup described in Pacherres et al. (2020) (Fig. 6.1a-c). The coral fragment was placed in the chamber filled with Filtered Artificial Sea Water (FASW) (0.2 pore size) from the coral´s culturing tank. It was allowed to acclimate to the chamber conditions under a low flow regime (water replacement in the chamber every 2 minutes) for at least one hour under dark conditions before experiments started. Temperature of the water inside the chamber was monitored every 30 seconds (Pt100

sensor, PyroScience, Germany) positioned at the outlet of the chamber. For all experiments, temperature was kept constant at 24 °C ± 0.5.

To track the fate of ultraparticles (<5 µm) as they interact with the mucus filaments produced by the coral, water inside the flow through system was seeded with such particles (Exc: 468 nm, Emi: 530 nm) (Applied Microspheres, The Netherlands). Particle density was adjusted to approx. 60×10^6 particles L^{-1}. Illumination was achieved using a LED Pulsing System PIV V3 (ILA_5150, Germany) connected to led light sheet optics (Willert et al. 2010). The light sheet was 1 mm thick and intensity reached 5500 µmol quanta m^{-2} s^{-1} (LI-COR LI-192, USA) at a wavelength of around 468 nm. Images were captured using a ILA.PIV.µEYE camera (ILA_5150, Germany) recording pictures at 25 frames per second (fps) with an exposure time of 26 ms. A long distance microscope lens (Optem FUSION, Germany) with a bandpass filter of 532 nm was used for all experiments.

Feeding experiments

Eight *Porites lutea* fragments were placed in individual beakers (80mm diameter, VWR, USA) filled with artificial filtered seawater (FASW) (total volume: 180 mL). Beakers were placed on a magnetic stirring table (IKA-WERKE, RO15, Germany) set up at low level (rotation speed: 100 rpm). Water temperature inside the beakers was constant and remained at 24 °C ± 0.5 (PyroScience, Germany) throughout the experiment's duration.

For all experiments (ultraparticles or *Artemia*) involving the arrest of the coral's cilia activity, we used the fully reversible ATPase inhibitor sodium orthovanadate dissolved in FASW at a concentration of 0.1 mM (Na_3VO_4; Sigma Aldrich) (Gibbons et al. 1978, Shapiro et al. 2014). Corals were placed inside the chemical solution for one hour before adding the suspended element. Chemical remained in solution for the duration of the experiments.

6.3.4 Experimental design

Particle trapping by mucus

We aimed to obtain both, profiling and areal views of the coral-water interface in order to get both, a mechanistic understanding and quantitative data of particle retention. In both configurations, the focus of the camera was on the particles illuminated by the light sheet. For the profiling view, we used the standard configuration (Pacherres et al. 2020) where the coral was placed at the center of the chamber with the PIV light sheet illuminating the coral

from above, perpendicular to the axis of the camera, and the plane of the light sheet intersecting the highest part of the colony (Fig. 6.1a-b). This configuration helped us highlight the profile of the coral surface and recognize the vertical extension of the vortices and how the particles carried by them interacted with the mucus filaments over time (their generated images were not used for particle trapping quantification). In the areal view configuration, we kept the camera in place and moved the plane of the light sheet from its medio-sagittal position towards the camera until the plane of light no longer intersected with the coral and came to be fixed at about 100 µm from the coral surface. This allowed us to view the polyps on the side of the coral from above (Fig. 6.1c-d). This arrangement helped us visualize the mucus layer covering the coral and allowed the precise quantification of the particles being trapped by the mucus per unit area. In this case, image frames were processed using custom-built Matlab (MathWorks, R2018b) algorithms to obtain number of not moving particles (trapped by mucus) inside a specific area (1 mm^2) each minute of the experiment. Videos were created using the free software FFmpeg (Mplayer).

A total of 8 coral fragments were used for all experiments, four for each cilia activity (active and arrested). Each fragment was viewed under both PIV-light configurations (profiling, areal) at different days. Experiments started (time 0) immediately after the suspended particles were introduced into the system. Using a custom build Python algorithm controlling both the camera trigger and the PIV light generator, 100 images were captured every minute for a total of 60 min, with a capture frame rate of 25 fps. Light exposure from the PIV LED was limited to 4 s for every PIV measurement interval to avoid photoinhibition and bleaching of the coral. For all experiments, water flow inside the chamber was 1300 µm s^{-1}, measured 2 mm above the coral surface. This corresponds to the boundary flow velocities expected in a turbulent flow environment of 1-2 cm s^{-1} (Van Driest 1956) typical of the flow velocities measured in the immediate vicinity of coral colonies (Chang et al. 2009, Fifer et al. 2021).

For the interpretation of the results, we assume that the presence of the chemical used to arrest cilia activity had no influence on the ability of the coral to secret mucus. Sodium orthovanadate acts by inhibiting enzyme activity in the protein complex that trigger cilia movement (dynein) (Gibbons et al. 1978), and therefore would have no influence on mucocyte response. Previous experiments have shown its effective use in cilia arrestment without compromising other aspects of the coral physiology, e.g. photosynthesis (Pacherres et al. 2020).

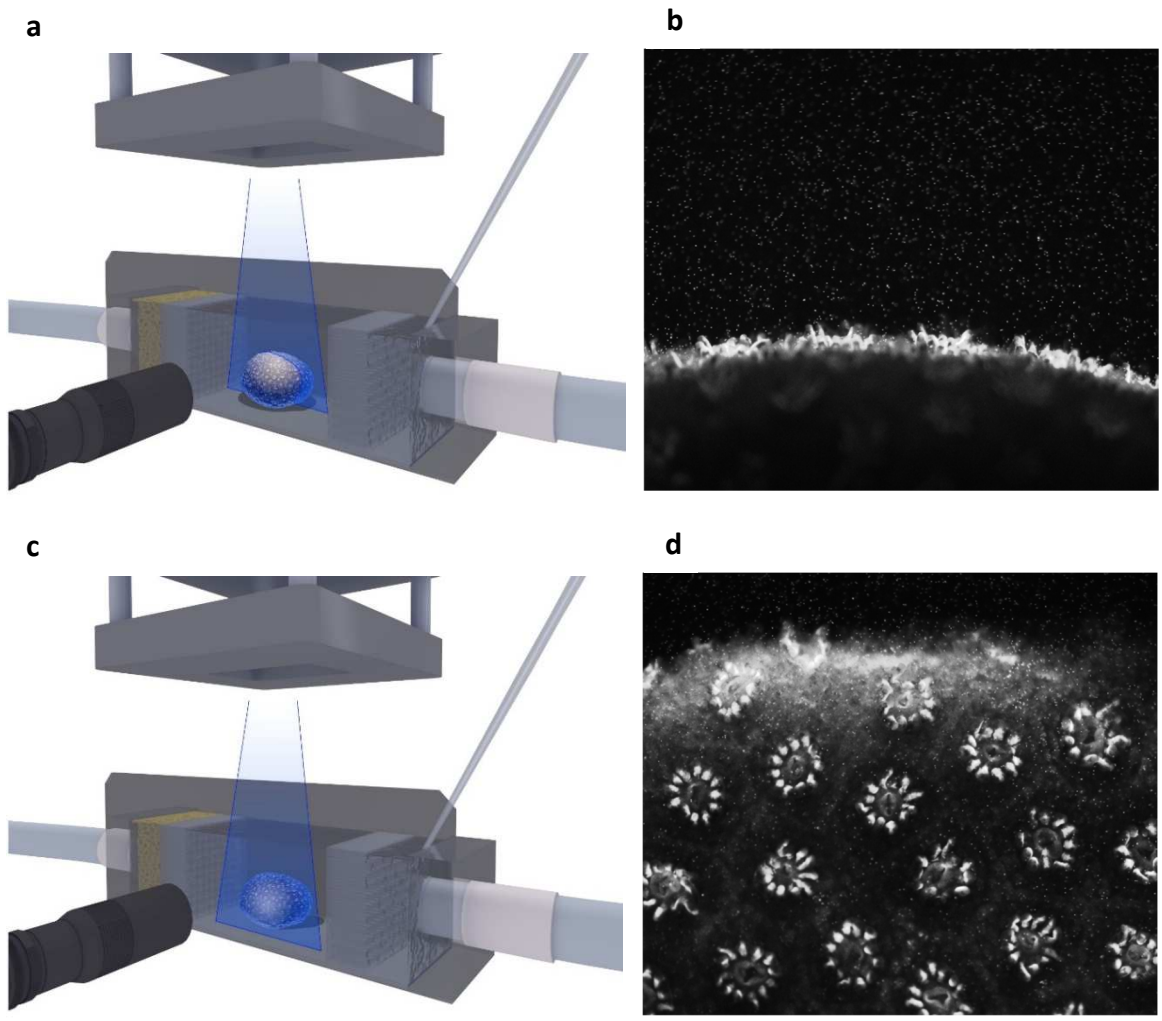

Figure 6.1. Experimental set-up showing the flow through chamber and the coral placed in two different positions allowing different views of the water surrounding the colony and the particles in it. **a** & **b**: coral was positioned at the center of the chamber fully under the PIV light-sheet permitting a side view of the coral water interface. **c** & **d**: coral was positioned towards the back of the chamber (behind the PIV light -sheet) which allowed a full view of the layer of water next to the colony, in this case the light sheet and the camera were illuminating and focused on the layer of water around 200 µm from the coral surface.

Artemia *feeding*

Corals were placed in their respective beakers, 4 of them containing FASW while the other 4 contained FASW with inhibitor (Supp. Inf. Fig. S6.1). Corals remained in their respective incubation beakers for one hour, in order to acclimate to the new conditions. Before the start of the experiment, 8 times 100 *Artemia* nauplii were separated and placed on the beakers containing the coral colonies. Incubations lasted for 1.5 hours. Once the time had passed, corals were removed and all *Artemia* left in each beaker were counted. Corals were returned

to their culturing tanks and 2 days later, the procedure was repeated, alternating the water conditions (corals that were non-arrested on the first experimental day, went to the chemical treatment on the second day). All experiments were performed in the dark.

6.4 Results

6.4.1 Particle trapping by mucus

Mucus filaments were secreted by the coral regardless of cilia activity. As time passed, the filaments joined together forming mucus nets (Fig. 6.2). The fate of the filaments and/or part of the net varied considerably: some filaments were lost to the water column, while others were transformed into mucus balls (Supp. Inf. Fig. S6.2) and ingested and/or disposed-of (Fig. 6.2; Supp. Inf. SV.6.1, SV.6.2).

The PIV experiment revealed that cilia beating generated a vortices up to 300 µm in height which intercepted the mucus filaments (Supp. Inf. SV.6.1, SV.6.2). Over time, the mucus filaments collected particles and were transformed into particle-rich mucus balls (Fig. 6.2a-c). Under arrested cilia activity, we observed laminar flow conditions in the boundary layer of the coral, with water flowing parallel to the tissue surface. Here, mucus filaments appeared less dense with particles and mucus balls (if present) took longer to develop (Fig. 6.2b-d).

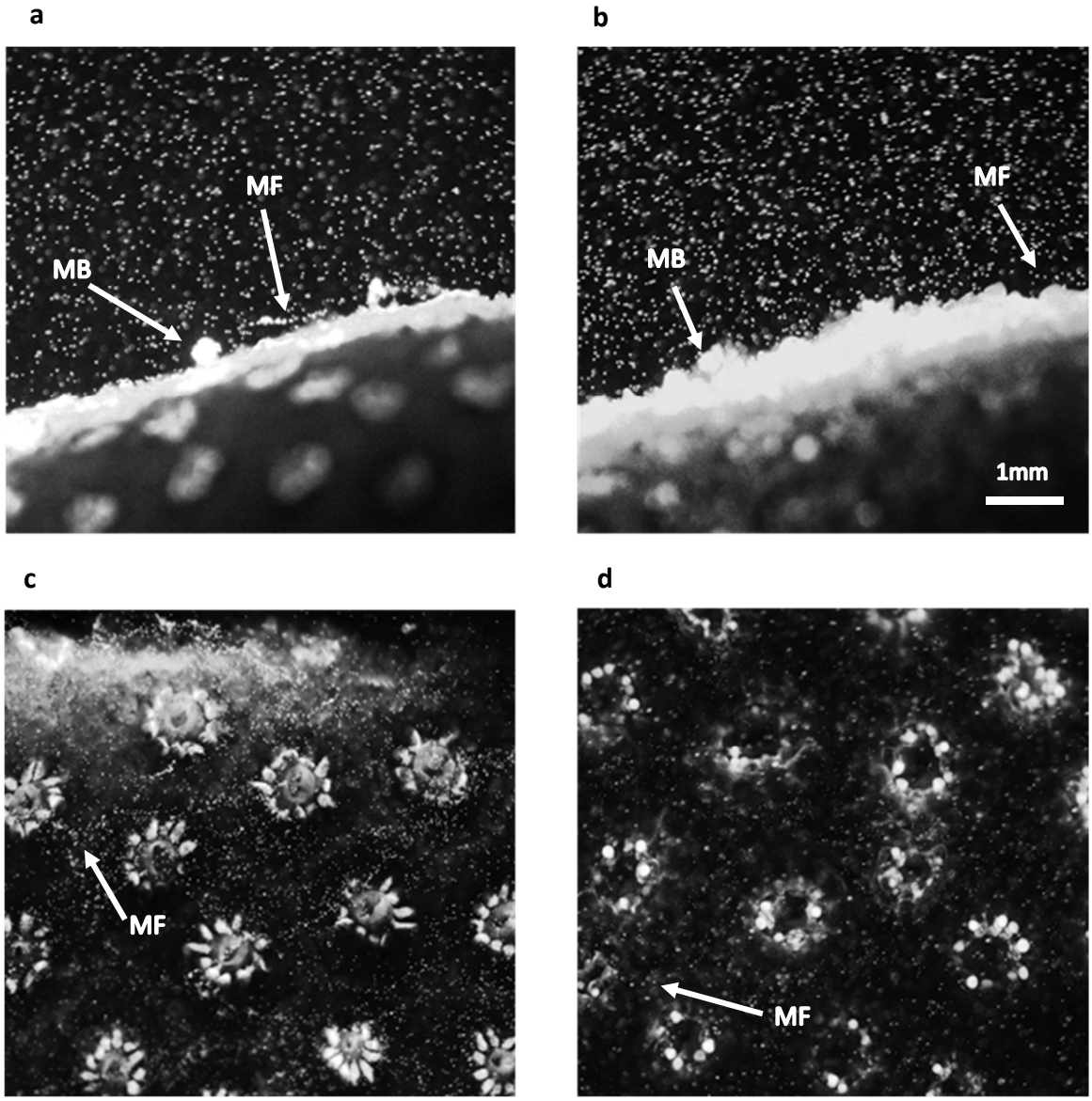

Figure 6.2. Two views of the coral water interface and the particles trapped by mucus filaments at the surface of the coral *Porites lutea* under active (**a** & **c**) and arrested (**b** & **d**) cilia activity. All 4 images were extracted from min 50 of the experimental period. Mucus filament (MF), Mucus ball (MB).

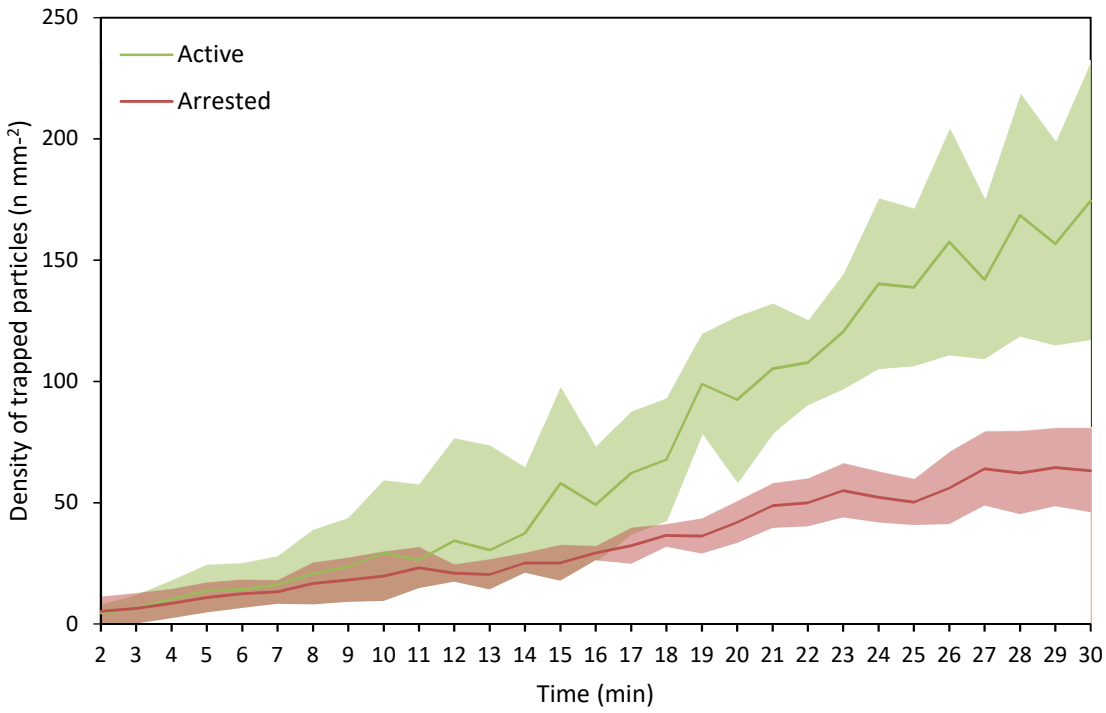

Figure 6.3. Temporal evolution of the density of particles trapped by mucus filaments excreted by the coral *Porites lutea* under active and arrested cilia activity. Values are plotted at 1 min intervals over the first 30 min of the experimental period. Solid lines represents the mean values, shadows the SD of the mean.

The capture rates (n mm^{-2} min^{-1}) by the mucus filaments (i.e. the slope of the curves in Fig. 6.3) was significantly higher in active compared to arrested corals, especially from min 10 to 30 (ANOVA, $P < 0.05$, Supp. Inf. Table S6.1). During the first 10 minutes of the experiments, while particles mixed in the water, corals detected their presence and commenced their mucus production, the number of particles getting trapped in the mucus were similar between active and arrested states (Fig. 6.3). After this 10 min lag phase, differences in particle capture rate became evident with 8.08 and 2.53 n mm^{-2} min^{-1} for active and arrested states, respectively (R^2= 0.968 and 0.962 for active and arrested), equivalent to a factor 3.2 increase due to cilia activity. Standard deviation values under active cilia were higher than their arrested counterparts due to two main reasons: (1) mucus filaments loaded with particles sometimes moved away from the area under analysis towards the polyp mouths and became part of a mucus ball; (2) were lost to the water column a phenomenon that was particularly more common after min 30 (Fig S6.3).

6.4.2 **Artemia** *feeding*

Corals with active cilia movement had significantly higher capture rates compared to when their cilia were inhibited (Fig. 6.4, One-way ANOVA, $P < 0.05$, Supp. Inf. Table S6.2). Mean capture rate of *Artemia* nauplii by corals colonies reached 41.9 ± 8.7 ind. h^{-1} compared to 14 ± 6.1 ind. h^{-1} under active and arrested cilia activity respectively. The highest capture rate was 51 ind. h^{-1} with active cilia compared to 23 ind. h^{-1} when arrested, while the lowest values were 29 and 5 ind. h^{-1} under active and arrested states, respectively. On average, corals decreased their capture rate by 27.6 ± 9.8 ind. h^{-1} when cilia was arrested. The swimming behavior of the *Artemia* individuals was not affected by the presence of the inhibitor.

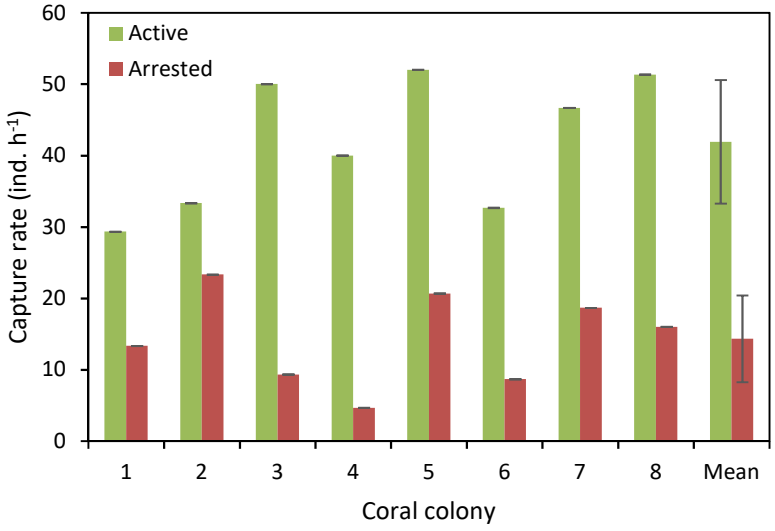

Figure 6.4. Capture rate (individuals h^{-1}) of *Artemia* nauplii by small colonies (n=8) (2 cm^2) of the coral *Porites lutea* under arrested and active cilia activity. Mean and SD are shown in the last column.

6.5 Discussion

The present is the first comprehensive study to evaluate the role of cilia in the capturing success of a reef building coral exposed to small and large particles. Moreover, it provides the first mechanistic explanation for ultraplankton retention in corals, by demonstrating that their capacity to capture suspended ultraparticles was boosted by the presence of ciliary vortices. Earlier studies have shown the ability of vortical flows in enhancing the exchange of oxygen (Shapiro et al. 2014) and alleviate oxidative stress (Pacherres et al. 2020). Here,

we demonstrate that they can also improve feeding on the abundant, but minute, particles suspended in the water column. Corals are known to use mucus filaments as means to capture fine particle matter which will be eventually ingested (Muscatine 1973, Ferrier-Pagès and Gattuso 1998). Our results showed that the beating of cilia at the surface of the coral generated vortices which moved water containing particles towards the mucus-covered coral surface, thus increasing particle entrapment (Fig. 6.5). The ability of corals to create a feeding current to trap small planktonic particles may have important consequences in the functional classification of these important organisms, placing them as active filter feeders together with i.a. sponges, acidians and bivalves. Additionally, corals used ciliary currents to shape mucus filaments into particle-enriched mucus balls and transport them into their mouth openings where they were ingested, a mechanism seen as well in early studies (Yonge 1930, Lewis and Price 1976). Nevertheless, and even though we were able to observe the ingestion of these mucus balls, the coral subsequently rejected them (Fig.S6.2). We attribute this behavior to the indigestible nature of the synthetic particles used. As reported by Yonge (1930), tentacles and mesenterial filaments have the ability to discern the nutritional nature of the particles embedded in the mucus, rejecting and eventually shedding those carrying non-nutritive elements.

Cilia also appear to play a strong role in the capture of large plankton prey as demonstrated in the *Artemia* incubations, where the deactivation of cilia caused a decrease in the capture rate of the coral colony. We see two interpretations for the observed capture differences. One is that the ciliary currents increased the transport of *Artemia* to the coral surface, which we believe unlikely given the scales with the *Artemia* being much larger (~737 µm) in comparison with the average height of the vortices (~300 µm) (see Fig. 6.5). Moreover, zooplankton can perform vigorous escape responses when facing a predator (Singarajah 1969). Copepods for example, are able to reach swimming speeds up to 500 body lengths s^{-1} (Strickler 1975) to dart away from the predator stimulus. If the same is applied in the case of the *Artemia* nauplii used in our experiments that avoidance swimming speed might reach up 3.7 x 10^5 µm s^{-1}, surpassing by several orders of magnitude the speeds inside the ciliary vortices (up to 400 µm s^{-1}) (Pacherres et al. 2020) proving them ineffective as a zooplankton capture mechanism. The second possible reason for the observed results is the deactivation of the machinery involved in zooplankton capture caused by the chemical used to arrest cilia activity. In order to capture mesozooplankton (>200 µm diameter), corals are equipped with clusters of stinging cells (nematocysts) found mostly along their tentacles. Planktonic prey

coming in contact with these structures trigger nematocysts discharge of toxins incapacitating the prey (Ben-Ari et al. 2018). Observations in sea anemones have shown that ciliary organelles, located in supporting cells adjacent to the nematocysts, have a sensory function associated with the reception of chemical and mechanical stimuli prior to their discharge (Mariscal 1974, Watson and Hessinger 1989, Cannon and Wagner 2003). Here, by adding sodium orthovanadate to arrest cilia activity, we might have effectively deactivated an important mechanical stimuli receptor, partially weakening the coral response to its suspended planktonic prey, but at the same time highlighting its role in the capture of large plankton elements.

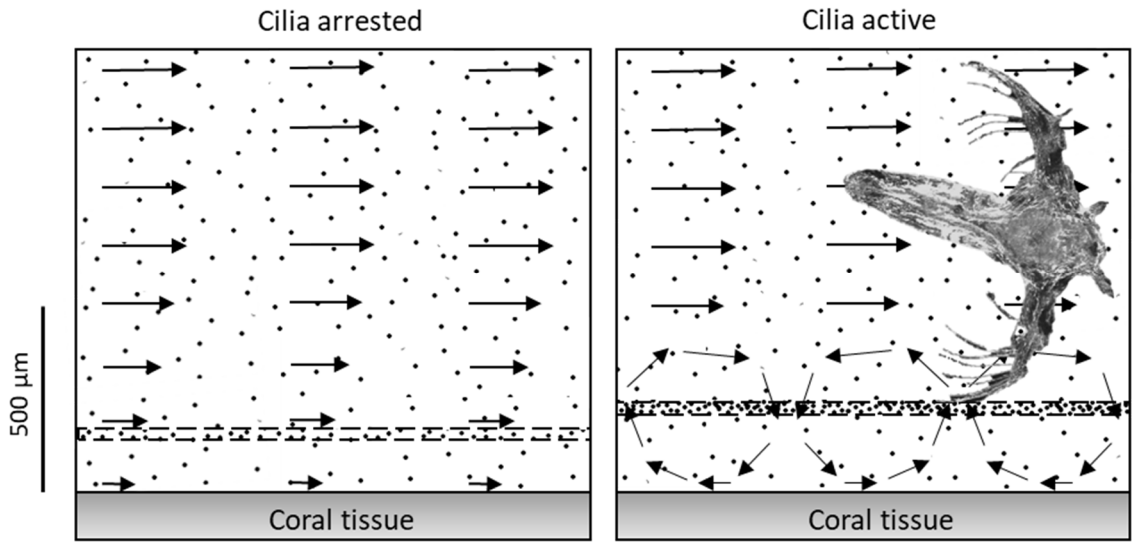

Figure 6.5. Schematic representation of the particle transport and mucus location within the coral-water interface (boundary layer). When cilia are arrested the flow field close to the coral tissue is undisturbed (Left panel), suspended ultraparticles in the water column will move along the flow lines being passively trapped in the mucus filaments (enclosed dashed area). Under active cilia activity (right) revolving vortices translocate water parcels increasing the encounter rate of suspended particles with mucus filaments. Size and orientation of inserted arrows represent differences in water flow velocity and direction. An *Artemia* nauplii is as well in the frame depicting its comparable size with the vortices (see size bar on the left).

Altogether, the results presented here highlight the ability of these evolutionary preserved organelles to intervene in almost all the stages of the coral`s suspension feeding process (Werner 1959, LaBarbera 1981). (1) They create vortices in the lower BL transporting particle-rich water aloft to the coral surface and into the mucus filaments which act as feeding

structures (Fig. 6.3). (2) They are indirectly involved in the trapping of suspended large elements (Fig. 6.4) as stimuli receptors prior to nematocysts discharge. (3), they contribute to the folding of mucus strings and sheaths into mucus balls enriched with particles, and the transport of these larger items (Supp. Inf. Fig. S6.2) along with zooplankton prey towards the mouth openings where they are to be ingested (Lewis and Price 1976). Furthermore, the ability of corals to use the currents created by cilia beatings to enhance the trapping of suspended ultraparticles by mucus, and by doing so creating their own feeding current, call for the need to review the standard classification of corals as merely passive suspension feeders.

6.6 References

Anthony, K. R. N. 1999. Coral suspension feeding on fine particulate matter. J Exp Mar Biol Ecol **232:** 85-106.

Bak, R. P. M., M. Joenje, I. de Jong, D. Y. M. Lambrechts, and G. Nieuwland. 1998. Bacterial suspension feeding by coral reef benthic organisms. Mar Ecol Prog Ser **175:** 285-288.

Ben-Ari, H., M. Paz, and D. Sher. 2018. The chemical armament of reef-building corals: inter- and intra-specific variation and the identification of an unusual actinoporin in *Stylophora pistilata*. Sci Rep **8:** 251.

Brown, B. E., and J. C. Bythell. 2005. Perspectives on mucus secretion in reef corals. Mar Ecol Prog Ser **296:** 291-309.

Cannon, Q., and E. Wagner. 2003. Comparison of discharge mechanisms of cnidarian cnidae and myxozoan polar capsules. Rev Fish Sci **11:** 185-219.

Carlgren, O. 1905. Über die Bedeutung der Flimmerbewegung für den Nahrungstransport bei den Actinarien und Madreporarien. Biol. Zbl. **25:** 308-322.

Carpenter, F. W. 1910. Feeding reactions of the rose coral (*Isophyllia*). Proc Am Acad Arts Sci **46:** 149-162.

Chang, S., C. Elkins, M. Alley, J. Eaton, and S. Monismitha. 2009. Flow inside a coral colony measured using magnetic resonance velocimetry. Limnol Oceanogr **54:** 1819-1827.

Cushing, D. H., G. F. Humphrey, K. Banse, and T. Laevastu. 1958. Report of the committee on terms and equivalents. Rapp. P.-V. Réun. Cons. perm. int. Explor. Mer **144:** 15-16.

Farrant, P. A., M. A. Borowitzka, R. Hinde, and R. J. King. 1987. Nutrition of the temperate Australian soft coral *Capnella gaboensis*. Mar Biol **95:** 575-581.

Ferrier-Pagès, C., and J. P. Gattuso. 1998. Biomass, production and grazing rates of pico- and nanoplankton in coral reef waters (Miyako island, Japan). Microb Ecol **35:** 46-57.

Fifer, J., B. Bentlage, S. Lemer, A. G. Fujimura, M. Sweet, and L. J. Raymundo. 2021. Going with the flow: How corals in high-flow environments can beat the heat. Mol Ecol **30:** 2009-2024.

Gibbons, I. R. and others 1978. Potent inhibition of dynein adenosinetriphosphatase and of the motility of cilia and sperm flagella by vanadate. PNAS **75:** 2220-2224.

Goldberg, W. M. 2002. Feeding behavior, epidermal structure and mucus cytochemistry of the scleractinian *Mycetophyllia reesi*, a coral without tentacles. Tissue Cell **34:** 232-245.

Hentschel, B. T., and J. Shimeta. 2008. Suspension Feeders, p. 3437-3442. *In* S. E. Jørgensen and B. D. Fath [eds.], Encyclopedia of Ecology. Academic Press.

Houlbrèque, F., E. Tambutté, C. Richard, and C. Ferrier-Pagès. 2004b. Importance of a micro-diet for scleractinian corals. Mar Ecol Prog Ser **282:** 151-160.

Jørgensen, C. B. 1966. Biology of suspension feeding. Pergamon Press.

LaBarbera, M. 1981. Water flow patterns in and around three species of articulate brachiopods. J Exp Mar Biol Ecol **55:** 185-206.

Lewis, J. B., and W. S. Price. 1975. Feeding mechanisms and feeding strategies of Atlantic reef corals. J Zool (Lond) **176:** 527-544.

---. 1976. Patterns of ciliary currents in Atlantic reef corals and their functional significance. J Zool (Lond) **178:** 77-89.

Mariscal, R. N. 1974. Scanning electron microscopy of the sensory surface of the tentacles of sea anemones and corals. Zeitschrift für Zellforschung und Mikroskopische Anatomie **147:** 149-156.

Mariscal, R. N., and C. H. Bigger. 1977. Possible ecological significance of octocoral epithelial ultrastructure. Proc 3rd Int Coral Reef Symp **1:** 127-134.

Marshall, A. T., and O. P. Wright. 1993. Confocal laser scanning light microscopy of the extra-thecal epithelia of undecalcified scleractinian corals. Cell Tissue Res **272:** 533-543.

Muscatine, L. 1973. Nutrition of corals p. 77-115. *In* O. A. Jones and R. Endean [eds.], Biology and Geology of Coral Reefs. Academic Press.

Muscatine, L., and J. W. Porter. 1977. Reef corals: Mutualistic symbioses adapted to nutrient-poor environments. Bioscience **27:** 454-460.

Naumann, M. S., C. Richter, M. el-Zibdah, and C. Wild. 2009. Coral mucus as an efficient trap for picoplanktonic cyanobacteria: implications for pelagic–benthic coupling in the reef ecosystem. Mar Ecol Prog Ser **385:** 65-76.

Pacherres, C. O., S. Ahmerkamp, G. M. Schmidt-Grieb, M. Holtappels, and C. Richter. 2020. Ciliary vortex flows and oxygen dynamics in the coral boundary layer. Sci Rep **10:** 7541.

Shapiro, O. H. and others 2014. Vortical ciliary flows actively enhance mass transport in reef corals. PNAS **111:** 13391-13396.

Singarajah, K. V. 1969. Escape reactions of zooplankton: The avoidance of a pursuing siphon tube. J Exp Mar Biol Ecol **3:** 171-178.

Sorokin, Y. I. 1973b. On the feeding of some scleractinian corals with bacteria and dissolved organic matter. Limnol Oceanogr **18:** 380-385.

Stafford-Smith, M. G. 1993. Sediment–rejection efficiency of 22 species of Australian scleractinian corals. Mar Biol **115:** 229-243.

Stafford-Smith, M. G., and R. F. G. Ormond. 1992. Sediment–rejection mechanisms of 42 species of Australian scleractinian corals. Mar. Freshw. Res. **43:** 683-705.

Stoddart, D. R. 1969. Ecology and morphology of recent coral reefs. Biol Rev **44:** 433-498.

Strickler, J. R. 1975. Swimming of planktonic cyclops species (Copepoda, Crustacea): Pattern, movements and their control, p. 599-613. *In* T. Y. T. Wu, C. J. Brokaw and C. Brennen [eds.], Swimming and Flying in Nature: Volume 2. Springer US.

Van Driest, E. R. 1956. On turbulent flow near a wall. AIAA J. **23:** 1007-1011.

Vogel, S. 1996. Life in moving fluids, 2nd ed. Princeton Univ. Press.

Watson, G., and D. Hessinger. 1989. Cnidocyte mechanoreceptors are tuned to the movements of swimming prey by chemoreceptors. Science **243:** 1589-1591.

Werner, B. 1959. Das Prinzip des endlosen schleimfilters beim Nahrungserwerb wirbelloser Meerestiere. Internationale Revue der gesamten Hydrobiologie und Hydrographie **44:** 181-215.

Willert, C., B. Stasicki, J. Klinner, and S. Moessner. 2010. Pulsed operation of high-power light emitting diodes for imaging flow velocimetry. Meas Sci Technol **21:** 075402.

Yonge, C. M. 1928. Feeding mechanisms in the invertebrates. Biol Rev **3:** 21-76.

---. 1930. Studies on the physiology of corals: I. Feeding mechanisms and food. Scientific Reports / Great Barrier Reef Expedition 1928-29. **1:** 13-57.

---. 1940. The Biology of reef–building corals. Scientific Reports / Great Barrier Reef Expedition 1928-29. **1:** 352-391.

6.7 Supplementary information

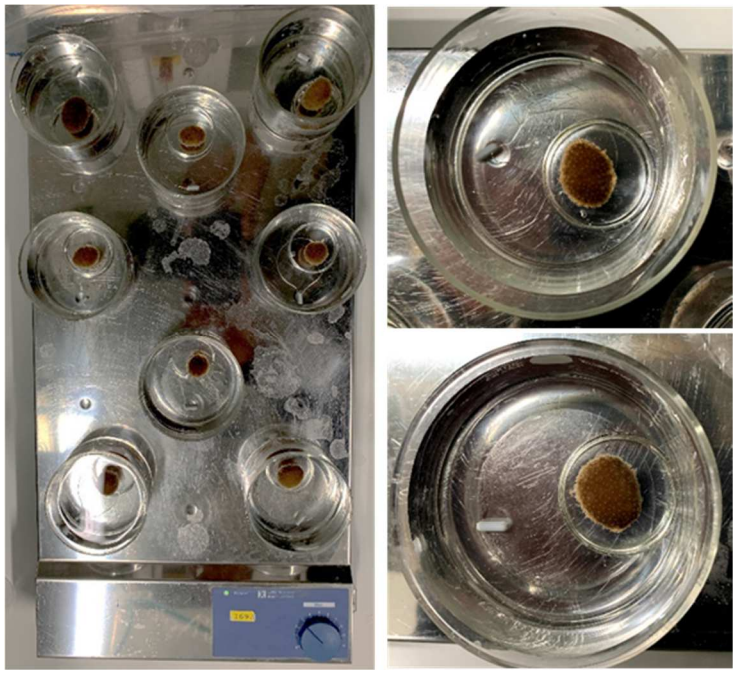

Figure S6.1. Experimental set-up for the feeding experiments involving *Artemia* nauplii.

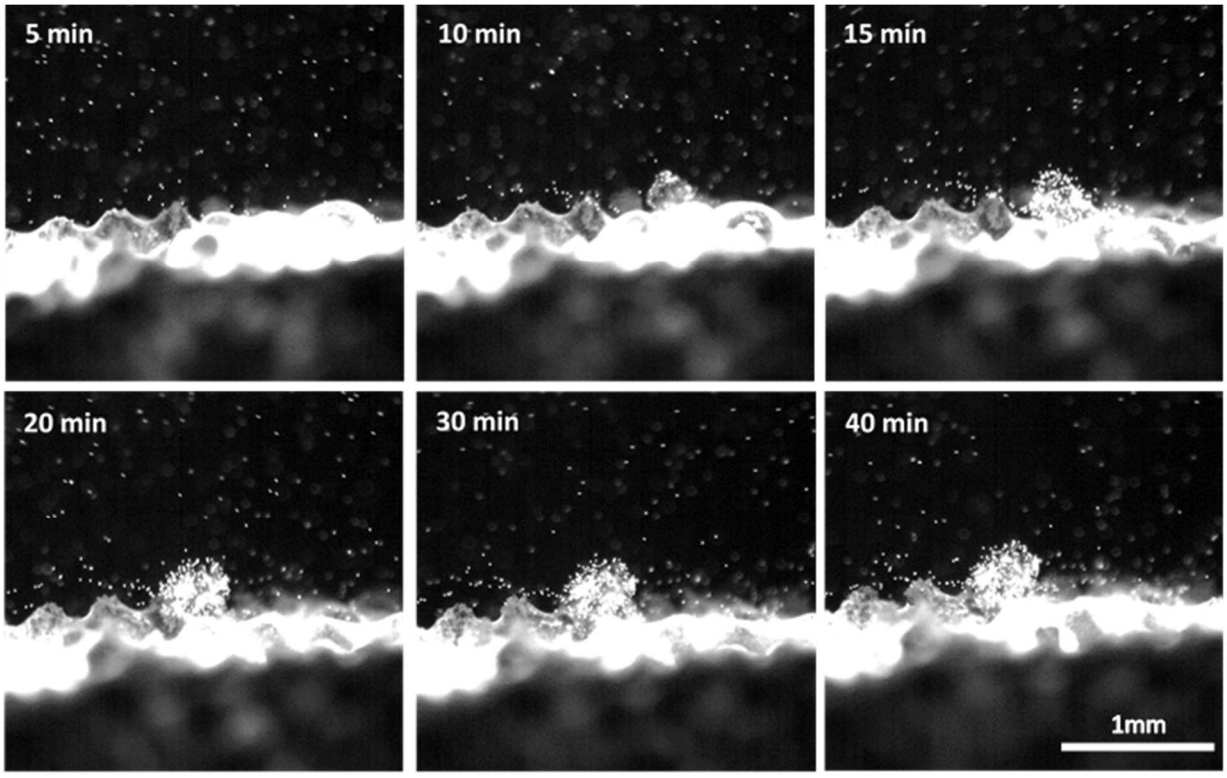

Figure S6.2. Image sequence of the formation of a mucus ball enriched with particles under active cilia activity.

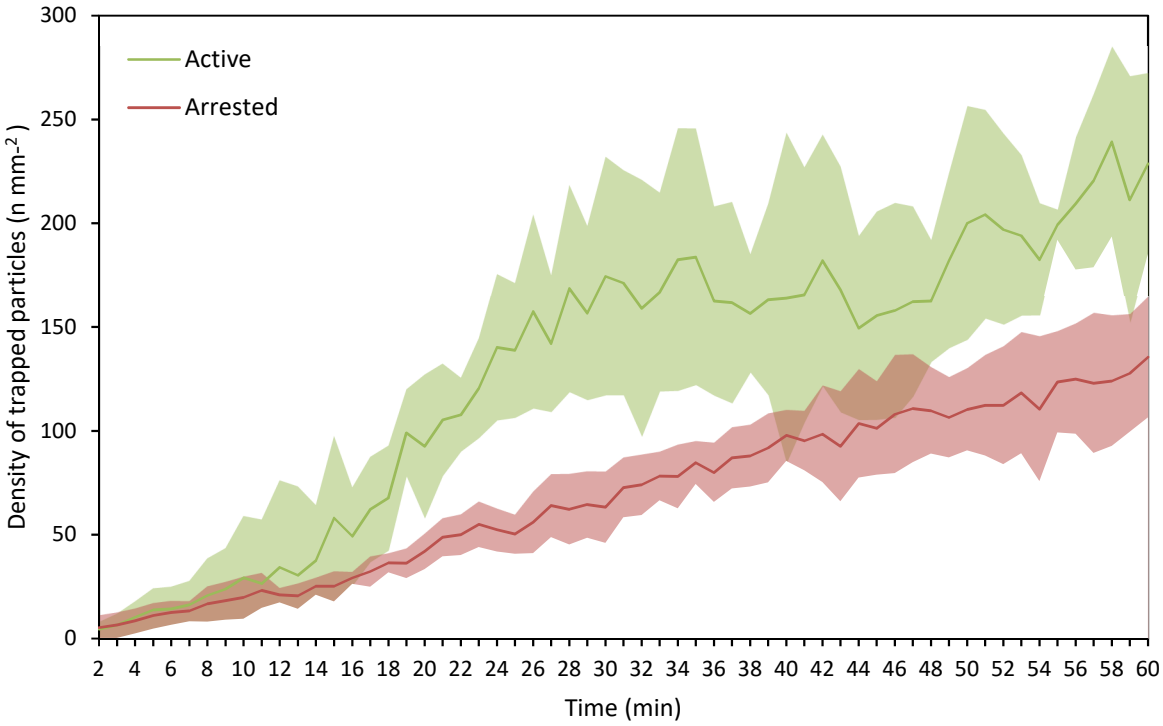

Figure S6.3. Number of particles trapped by mucus filaments excreted by the coral *Porites lutea* under active and arrested cilia activity plotted at 1 min intervals over the entire experimental period (60 min). Solid lines represents the mean number of trapped particles over a 1 mm^2 area of coral surface. Shadow represents the SD of the mean.

Table S6.1. ANOVA results comparing the slopes of the capture rate of suspended particles (5 µm) of different colonies of *Porites lutea* with active and arrested cilia activity during the first 30 min of the experiments.

Source of variation	Sum of squares	d.f.	Mean square	*F*	*P*
Cilia activity	47413	1	47413	319.299	<2.20E-16
Colony	9781	3	3260	21.957	7.22E-12

Table S6.1. Oneway-ANOVA results on the capture rates of *Artemia* nauplii (ind. min^{-1}) of different colonies of *Porites lutea* with active and arrested cilia activity.

Source of variation	Sum of squares	d.f.	Mean square	*F*	*P*
Cilia activity	3043.36	1	3043.36	47.67	7.27E-06
Colony	512.86	7	73.26	1.34	0.3523

7

Discussion and Conclusions

At the time of the start of this thesis the roles of cilia and their generated vortices upon the physico-chemical processes around corals were starting to be recognized. While it was noted early last century that epidermal cilia are present in all corals and are responsible for the transport of food and waste particles, their involvement in the coral's hydrodynamical processes were only discovered last decade. In this chapter I will discuss the outcome of my research project which aimed to unveil the role which ciliary vortices play on the dynamics of the coral boundary layer. I could demonstrate that the massive coral *Porites lutea* is able to utilize these vortical currents to advantageously modify its oxygen DBL and to enhance its prey capture abilities; two mechanisms that might help the coral overcome not only external but also internal pressures.

7.1 Feedback to the proposed research questions

Q.1. How do ciliary vortices behave under various flow and light conditions?

Ciliary vortices were present at the surface of the coral regardless of the flow speed in the water column. Vortex height, however, was dependent on the imposed flow speed, reaching heights of up to 500 μm under low flows (400 μm s^{-1}) and 250 μm under high flows (1300 μm s^{-1}). Light had no influence on the generated vortices as they were present under oxygen production (light) and consumption (dark). These vortices had a direct impact upon the DBL, enhancing mass transport and changing oxygen concentrations at the tissue surface, thus alleviating oxygen extremes seen under arrested ciliary action. (**Chapter 3**).

Q.2. By thinning the DBL, what happens with the diffusive flux and how is the coral profiting on the effects of a reduced DBL thickness?

I found no increase in the diffusive flux when comparing corals with active and arrested cilia activities. For the case of active cilia, I observed a two layered boundary consisting of a vortex layer with an enhanced mass transport coefficient due to diffusive-advective transport, and a diffusive boundary layer above (upper DBL) with a determinable molecular diffusion coefficient. I found that the oxygen diffusion flux measured at the upper DBL under active cilia activity was similar to the one measured in arrested corals. A reduction of the DBL under a constant flux entailed a decrease in the concentration difference between the coral surface and the environment, as seen in the presented results (**Chapter 3**). Thus, the benefit of vortex mixing is mainly the reduction of oxygen gradients at the immediate surface of the coral which in turn will promote the efflux of oxygen out of the tissue reducing the detrimental consequences of oxygen accumulation, i.e. production of reactive oxygen species and subsequent bleaching of the coral. Modelled results showed that ciliary vortices are able to enhance oxygen transport at the vortex layer specially when assuming toxicity from increase oxygen accumulation and heterogeneous oxygen concentrations coming out of the tissue (**Chapter 5**).

Q.3. Is the removal of oxygen by ciliary vortices homogeneous along the surface of the coral?

No, results showed highly heterogeneous oxygen concentrations at the coral surface caused by different features of the vortices. First, the revolving nature of the vortices implied that areas within the vortex were intrinsically different, i.e. under light, the upward flow of the vortex carried oxygen rich waters from the surface to the upper DBL, while the downward flow carried water containing less oxygen towards the tissue surface (**Chapter 3**). Second, I observed that cilia were not stirring the entire DBL homogeneously but rather organized their beating to increase the upward transport of oxygen along certain areas of the coral surface (**Chapter 4** and **5**). The strongest oxygen gradients occur where oxygen is produced at a higher rate (septa and coenosarc) and lower-oxygen ambient water is directed downward at high velocities. In contrast, oxygen concentrations within the vortex structures (located on top of the mouth openings) are elevated, fed by the upward flow of oxygen-enriched water from the tissue surface. While rotating in the vortex, oxygen diffuses across the vortex boundaries into the ambient water so that the downward flow carries less oxygen and can be recharged again. This pattern created a series of oxygen accumulation hotspots located at the coral mouth openings (**Chapter 5**).

Q.4. Are ciliary vortices at the tissue surface related to the amount of chlorophyll inside the tissue?

Yes, results showed that high chlorophyll areas (septa and coenosarc) were situated outside the vortex structures, while low chlorophyll areas (mouth openings) were situated underneath the vortex suggesting the coupling of ciliary beatings with these areas of high chlorophyll as means to ventilate them (**Chapter 5**). This mechanism caused a patchiness in the distribution of oxygen at the DBL, a pattern that did not match the chlorophyll distribution. Oxygen was always believed to directly reflect the photosynthetic rate of the tissue below. Results however, showed that this might not always be the case, as internal and external processes of diffusion are coupled with the coral's ability to actively transport water masses (and oxygen) by means of ciliary vortices, and consequently alleviate oxygen accumulation inside the tissue (**Chapter 4** and **5**).

Q.5. Are the vortices able to transport not only dissolved chemical elements but small particles as well, effectively intervening in the coral's heterotrophic nutrition?

Yes, cilia-induced vortices extending up to 300 µm from the coral surface can transport particle-rich waters into the coral boundary layer. There the particles were filtered by the mucus layer intercepting the vortices, this process resulted in particle aggregations within the coral mucus. More importantly, it resulted in a 3.4 times higher particle trapping rates in corals with active cilia compared to cases in which their cilia activity had been arrested. Clearly, this represents a first mechanistic explanation of ultraplankton capture by corals and call for the need to review the standard classification of corals as merely passive suspension feeders (**Chapter 6**).

7.2 General discussion and perspectives

7.2.1. Cilia and the coral-symbiont relationship

Corals are sessile organisms, commonly perceived to be subjected to the physicochemical conditions of their environment, interacting with it through a diffusion boundary layer (DBL). Therefore, any factor that alters the conditions of the DBL will indirectly have an effect on the coral and its symbionts. In my research I proved that corals are not entirely at the mercy of unpredictable external water currents ruling over DBL processes. On the contrary, they possess the ability to disturb the lower DBL through the generation of vortices created by the beating of epidermal cilia (**Chapter 3, 4, 5**). These small surface currents will enhance the transport of elements, effectively changing the dynamics of the DBL and impacting one of the holobiont's most important metabolic processes, its photosynthesis.

The coral's relationship with its endosymbiont is highly complex, dating back millions of years, providing corals with the tools to withstand environmental changes across millennia (Stolarski et al. 2011). Nevertheless, this relationship comes with its costs. The coral animal must deal with a byproduct of the photosynthetic process, namely oxygen, which in high quantities can become toxic (Lesser et al. 1990, Lesser 1997, Yakovleva et al. 2009). Lacking respiratory organs, corals were believed to exclusively rely on passive diffusion to get rid of excess oxygen form its surface and tissue, a process which can be extremely slow and thus limiting (Shick 1990, Carpenter and Patterson 2007). However, in **Chapter 3** I

could prove that, under realistic scenarios of external flow and light, corals are able to overcome this limitation by generating a series of vortices with the beating of the cilia organelles covering its tissue. These vortices will effectively transport oxygen away from the coral towards the upper DBL improving the conditions at the surface and promoting the efflux of oxygen out of the tissue. This mechanism is of particular importance when taking into consideration that chlorophyll distribution is not homogeneous along the coral tissue and oxygen production will be concentrated at certain areas of the tissue (**Chapter 4** and **5**). Consequently, the ventilation of these highly productive areas by ciliary beating could alleviate oxygen accumulation and thus, its toxic properties that might lead to the expulsion of the symbiont by the animal host (Lesser 1997), thus creating more favorable living conditions. This proves that corals are not passive oxyconformers; rather, they actively change their chemical environment as part of a homeostatic control mechanism that potentially plays a crucial role in the coral's relationship with its symbionts (**Chapter 3**).

By altering water motion, ciliary beatings might also affect rates of nutrient delivery and the export of other metabolic byproducts. To further investigate this, I performed first calculations on the transport effect of protons (**Chapter 3**). I found that cilia activity would mitigate proton depletion, maintaining a reduced pH compared to higher pH values expected under arrested cilia, which in turn might favor corals' calcification rates. Similarly, an efficient acquisition of Dissolved Inorganic Carbon (DIC) by the zooxanthellae is key to the health of the coral holobiont, as the amount of DIC fixed by the symbiont will determine the transfer of photosynthetic products transfer to the hosts (Gibbin et al. 2020, Roberty et al. 2020). Even though oceanic concentrations of DIC are generally high, DIC can be a source of limitation for the primary production of the zooxanthellae (Herfort et al. 2008). The role of cilia, in the cases when conditions determine DIC as a limiting element for photosynthesis, will require further research as it might prove to be important for the overall health of the coral colony. Additional investigations will be needed as well to study the response of cilia activity to different boundary conditions under elevated heat, increased pH, or high particle concentrations and evaluate their role in alleviating those stress scenarios.

Overall, I clearly show the ability of ciliary vortices to boost transport of solutes and I emphasize the subsequent advantages of this process. I also pointed out that this process is not equal across the entire coral surface as it strongly depended on the vortex geometry (**Chapter 3**) and location of the vortices along the coral tissue (**Chapter 4** and **5**). This heterogeneity will give rise to contrasting levels of cellular exposure to the chemical

environment and may cause heterogeneous cellular responses along the coral holobiont. On the other hand, it must be taken into consideration that the coral tissue itself possess different optical properties that generates internal microenvironments which have been suggested to act as zooxanthellae refugia during light-related bleaching conditions (Wangpraseurt et al. 2012, Wangpraseurt et al. 2014). Corals are found to be differentially sensitive to environmental changes like high temperature or ocean acidification with some species or even colonies being more susceptible than others (Cunning et al. 2016). It has been hypothesized that the development of a distinct microenvironment within the DBL contributes to this differential response (Loya et al. 2001, Chan et al. 2016). Thus, by changing the shape and processes along the DBL, ciliary action might represent the missing link in order to understand corals' heterogeneous responses to stress. The complex relationships between symbionts and host, as well as the internal and external heterogeneities of the coral microenvironments might, very well, provide the source for buffering and acclimatization, and thus resilience to environmental pressures. A next step would be to explore the interactions between the aforementioned internal and external heterogeneities performing combined observations with the same coral.

I have outlined above, that an external heterogeneous chemical microenvironment (**Chapter 4** and **5**) may result in a range of different cellular responses at the coral and symbiont levels; however, those might not only be the ones affected. The observed heterogeneous distribution of oxygen and ciliary action might also intervene in the coral's relationship with its associated microbial community. The role of the coral's microbiome (bacteria, fungi, archaea and viruses) upon the organism performance remains largely unexplored. Yet there are first indications that microorganisms might be important in terms of nitrogen fixation, sulfur cycling and the competitive exclusion of pathogens (Bourne et al. 2016, Hernandez-Agreda et al. 2017) and by this contribute to the coral's well-being. In addition, functional diversity of microbial communities differs within the coral itself, responding to the specific characteristics of the chemical microenvironment (Sweet et al. 2011). Spatial physicochemical heterogeneities at the coral surface (**Chapter 5**) might, therefore, also affect coral-microbiome landscape at µ-metric scale. Future studies on the capacity of the coral to shape its microbiome and possibly optimize its performance by a heterogeneous vortex generation, will allow us to better understand symbiotic processes and responses to environmental conditions.

The possible occasional arrestment of cilia beating by different stressors requires as well in-depth understanding, since elemental accumulation or depletion at tissue level will have detrimental consequences on the coral's physiological processes. Unpublished observations while conducting the experiments for this thesis suggested that the coral itself could sometimes suppress cilia beating, opening the question as of whether the coral is able to modulate its ciliary response and intensity and the triggers for this behavior. Finally, for the different experiments comprising this thesis, I used *Porites lutea* as a model organism. *Porites* is a massive coral, characterized by tick tissue and relatively small polyps (Lough and Barnes 2000). The questions that now arise are several: How do ciliary beating alter the DBL dynamics in other scleractinian coral morphs? Will branching corals with thin tissues and big polyps interact differently with the generated vortices caused by cilia? What will be the effect of ciliary beatings in other corals' microenvironment generation? How will these mechanisms contribute to the acclimatization and adaptation of coral reefs to an accelerated anthropogenic climate change? These questions will require further research in order to understand, in depth, the extent of the role of cilia in the physiological processes of corals.

7.2.2. Cilia and coral heterotrophy

Before this thesis, the involvement of cilia and their generated vortices in the feeding success of corals was thought to be restricted to a) the facilitation the movement of mucus towards or away from the mouth and b) the function as sensors to detect prey triggering the nematocyst discharge. In **Chapter 6**, I showed that vortical flows also play an important role in the trapping of ultraplankton particles (<5 µm) by mucus filaments. These results provide the first mechanistic explanation for ultraplankton retention in corals, a strategy that explains their proven ability to effectively feed on this minute, but highly abundant, energy source (Houlbrèque et al. 2004b, Houlbrèque et al. 2006). Cyanobacteria, in particular, are considered responsible for 80 to 90% of the total carbon fixation in oligotrophic tropical waters (Stockner 1988, Partensky et al. 1999) with abundances of more than 50,000 cells/mL (Flombaum et al. 2013). The coral's ability to profit from this highly abundant prey will be of extreme importance. On the one hand, it can constitute an additional energy source to fuel corals' metabolism and on the other it can become the coral's only nutrient source in the face of environmental stressors (Grottoli et al. 2006, Towle et al. 2015), which can cause corals to expel the symbionts from their tissues (Glynn et al. 1985). While the loss of photosynthesis entails a metabolic crisis for most bleached corals, there are promising reports of full recovery in cases where 100 % of the daily metabolic energy could be covered

by planktonic sources (Grottoli et al. 2006, Palardy et al. 2008). Similarly, episodic periods of low light, due to increased turbidity, can force corals to shift from autotrophy to a more heterotrophic supply of energy (Anthony and Fabricius 2000) to compensate from the diminished supply coming from the symbionts. The coral's ability to enhance the capture of a highly abundant food source will, therefore, have important implications when facing the aforementioned environmental stressors.

The role of cilia in the capture of large zooplankton prey, was indirectly seen as well, when their deactivation caused corals to capture less individuals of *Artemia* nauplii (**Chapter 6**). The cilia's function as sensory organelles prior to nematocyst discharge is well described in the case of sea anemones in which they are located in cnidocyte-supporting cell complexes (Watson and Hessinger 1989). It is therefore no surprise that, in the case of corals, the deactivation of cilia beating decreased their capacity to sense as well as react to swimming plankton in their vicinity and thus, resulted in capturing less prey (**Chapter 6**).

Cilia and their vortices play an important role in the coral's heterotrophic nutrition, as they will help the coral to interact more efficiently with its planktonic prey regardless of its size. Considering this, it is of paramount importance to understand the different environmental factors that might trigger natural cilia arrestment as they might have ramifications beyond that of elemental transport and will affect corals' heterotrophic pathway. Furthermore, the creation of feeding currents by cilia beating challenges the coral's current functional classification within the ecosystem (**Chapter 6**). Corals have long being considered passive suspension feeders that rely on external currents to move water across their feeding structures. However, the results presented here supports their classification as filter feeders together with mollusks and sponges. This new classification will allow a better understanding of the trophic players in the coral reef ecosystem and help identify biodiversity changes to environmental alterations and develop better conservation strategies.

7.3 Concluding remarks

My thesis has focused on the study of the vortices created by the coral's epidermal cilia. I have shown that the ability of these vortices to translocate water masses from the tissue surface to the upper water column, and *vice versa*, influenced several aspects of the coral holobiont. These vortices provided the coral with a tool to prevent the toxicity that may come

with oxygen accumulation while, at the same time, helped them break the barrier imposed by a diffusion-controlled BL. Moreover these vortices not only transported chemical elements but also small particles, consequently impacting upon the coral's ability to feed on small food elements like bacteria or flagellates. These findings open several questions regarding the role of ciliary vortices as buffers for environmental stress as well as their role in the coral's heterotrophic capacity.

Finally, to reveal the mechanisms that support resilience in and around corals at a µ-metric scale is of extreme importance if we want to fully understand coral reefs and assess their acclimatization and adaptation potentials. In the face of anthropogenic climate change, the need to rapidly understand reef's response at a larger scale many times neglects the underlying small mechanisms leading to that reaction. However, only an in-depth understanding of the fundamental ecophysiological process of these organisms will improve our ability to successfully develop models that project the response of corals to environmental change. Coral reefs are, basically, the result of cellular level processes inside the coral animal which rely on the intricate interactions between the animal and its algae symbiont (Putnam et al. 2017), a complex system that is, at the same time, modulated by external BL dynamics. Ciliary vortices have the ability to alter these dynamics and therefore their importance. Within this thesis, I developed and advanced high-resolution methods to visualize and study the coral's surrounding, I highlighted its heterogeneous nature and provided a first glimpse into the complex interaction between ciliary flows and the coral's internal and external microenvironment. These mechanistic processes might be critical for the coral as they can mediate its stress response in the face of a rapidly changing environment.

7.4 References

Anthony, K. R. N., and K. E. Fabricius. 2000. Shifting roles of heterotrophy and autotrophy in coral energetics under varying turbidity. J Exp Mar Biol Ecol **252:** 221-253.

Bourne, D. G., K. M. Morrow, and N. S. Webster. 2016. Insights into the coral microbiome: Underpinning the health and resilience of reef ecosystems. Annu Rev Microbiol **70:** 317-340.

Carpenter, L. W., and M. R. Patterson. 2007. Water flow influences the distribution of photosynthetic efficiency within colonies of the scleractinian coral *Montastrea annularis* (Ellis and Solander, 1786); implications for coral bleaching. J Exp Mar Biol Ecol **351:** 10-26.

Chan, N. C. S., D. Wangpraseurt, M. Kühl, and S. R. Connolly. 2016. Flow and coral morphology control coral surface ph: Implications for the effects of ocean acidification. Front Mar Sci **3**.

Cunning, R., R. Ritson-Williams, and R. D. Gates. 2016. Patterns of bleaching and recovery of *Montipora capitata* in Kāne'ohe Bay, Hawai'i, USA. Mar Ecol Prog Ser **551:** 131-139.

Flombaum, P. and others 2013. Present and future global distributions of the marine Cyanobacteria *Prochlorococcus* and *Synechococcus*. PNAS **110:** 9824-9829.

Gibbin, E., G. Banc-Prandi, M. Fine, A. Comment, and A. Meibom. 2020. A method to disentangle and quantify host anabolic turnover in photosymbiotic holobionts with subcellular resolution. Commun Biol **3:** 14.

Glynn, P. W., E. C. Peters, and L. Muscatine. 1985. Coral tissue microstructure and necrosis: relation to catastrophic coral mortality in Panamá. Dis Aquat Org **1:** 29-37.

Grottoli, A. G., L. J. Rodrigues, and J. E. Palardy. 2006. Heterotrophic plasticity and resilience in bleached corals. Nature **440:** 1186-1189.

Herfort, L., B. Thake, and I. Taubner. 2008. Bicarbonate stimulation of calcification and photosynthesis in two hermatypic corals. J Phycol **44:** 91-98.

Hernandez-Agreda, A., R. D. Gates, and T. D. Ainsworth. 2017. Defining the core microbiome in corals' microbial soup. Trends Microbiol **25:** 125-140.

Houlbrèque, F., B. Delesalle, J. Blanchot, Y. Montel, and C. Ferrier-Pagès. 2006. Picoplankton removal by the coral reef community of La Prévoyante, Mayotte Island. Aquat Microb Ecol **44:** 59-70.

Houlbrèque, F., E. Tambutté, C. Richard, and C. Ferrier-Pagès. 2004b. Importance of a micro-diet for scleractinian corals. Mar Ecol Prog Ser **282:** 151-160.

Lesser, M. P. 1997. Oxidative stress causes coral bleaching during exposure to elevated temperatures. Coral Reefs **16:** 187-192.

Lesser, M. P., W. R. Stochaj, D. W. Tapley, and J. M. Shick. 1990. Bleaching in coral reef anthozoans: effects of irradiance, ultraviolet radiation, and temperature on the activities of protective enzymes against active oxygen. Coral Reefs **8:** 225-232.

Lough, J. M., and D. J. Barnes. 2000. Environmental controls on growth of the massive coral Porites. J Exp Mar Biol Ecol **245:** 225-243.

Loya, Y., K. Sakai, K. Yamazato, Y. Nakano, H. Sambali, and R. van Woesik. 2001. Coral bleaching: the winners and the losers. Ecol Lett **4:** 122-131.

Palardy, J. E., L. J. Rodrigues, and A. G. Grottoli. 2008. The importance of zooplankton to the daily metabolic carbon requirements of healthy and bleached corals at two depths. J Exp Mar Biol Ecol **367:** 180-188.

Partensky, F., W. R. Hess, and D. Vaulot. 1999. *Prochlorococcus*, a marine photosynthetic prokaryote of global significance. Microbiol Mol Biol Rev **63:** 106–127.

Putnam, H. M., K. L. Barott, T. D. Ainsworth, and R. D. Gates. 2017. The vulnerability and resilience of reef-building corals. Curr Biol **27:** R528-R540.

Roberty, S., E. Béraud, R. Grover, and C. Ferrier-Pagès. 2020. Coral productivity is co-limited by bicarbonate and ammonium availability. Microorganisms **8:** 640.

Shick, J. M. 1990. Diffusion limitation and hyperoxic enhancement of oxygen consumption in zooxanthellate sea anemones, zoanthids, and corals. Biol Bull **179:** 148-158.

Stockner, J. G. 1988. Phototrophic picoplankton: An overview from marine and freshwater ecosystems. Limnol Oceanogr **33:** 765-775.

Stolarski, J., M. V. Kitahara, D. J. Miller, S. D. Cairns, M. Mazur, and A. Meibom. 2011. The ancient evolutionary origins of Scleractinia revealed by azooxanthellate corals. BMC Evol Biol **11:** 316.

Sweet, M. J., A. Croquer, and J. C. Bythell. 2011. Bacterial assemblages differ between compartments within the coral holobiont. Coral Reefs **30:** 39-52.

Towle, E. K., I. C. Enochs, and C. Langdon. 2015. Threatened caribbean coral is able to mitigate the adverse effects of ocean acidification on calcification by increasing feeding rate. PLoS ONE **10:** e0123394.

Wangpraseurt, D., A. Larkum, P. Ralph, and M. Kühl. 2012. Light gradients and optical microniches in coral tissues. Frontiers in Microbiology **3:** 1-9.

Wangpraseurt, D. and others 2014. The in situ light microenvironment of corals. Limnol Oceanogr **59:** 917-926.

Watson, G., and D. Hessinger. 1989. Cnidocyte mechanoreceptors are tuned to the movements of swimming prey by chemoreceptors. Science **243:** 1589-1591.

Yakovleva, I. M., A. H. Baird, H. H. Yamamoto, R. Bhagooli, M. Nonaka, and M. Hidaka. 2009. Algal symbionts increase oxidative damage and death in coral larvae at high temperatures. Mar Ecol Prog Ser **378:** 105-112.

Acknowledgments

To thank all the people who have, in one way or another, contributed to this thesis just won't be easy, I apologize if I forget somebody.

To the reviewers of this thesis, Prof. Richer, Prof. Kühl, Dr. Zetsche, and the evaluation committee, Prof. Harder and Dr. Kunzmann. Thanks for the time invested and the helpful comments and discussion both on the thesis and the defense.

Palabras que señalen el grado de **amor** y **gratitud** que le tengo **a mi familia** jamás existirán. **Mamá, Papá**, **Hermana**, **Dani**, sin ustedes no estaría escribiendo estas líneas. Sin su apoyo incondicional y constante nada de esto sería realidad, simplemente **GRACIAS**.

A mis segundas madres: Bene y Rede todo esto es por ustedes. Abuela Rede, puede que no llegaras a ver a tu nieto convertirse en Doctor, pero guardo en mi corazón la esperanza de que en alguna parte estas cuidándome y sonriendo conmigo.

Gaby, gracias por recibirme en tu casa, por preocuparte por mí y siempre estar al pendiente de mi bienestar. Gracias por hacerme parte de tu familia.

To Claudio, my supervisor, thanks for trusting in me, in my work and in my abilities as a scientist. I sincerely hope the collaboration that started almost 12 years ago, back when I was a master student in the ISATEC, will continue regardless of what the future holds.

Moritz and Soeren, I believe this thesis would be completely different without your involvement. Thanks for jumping into this crazy project, for the prompt help and advice.

Gerti, thanks for your feedback and support, and for putting your concerns about my psychological well-being above those of work. Marlene and Krissi, thank you for your help and advice, for giving parts of this thesis a read and improve it with your comments.

Esther und Ulrike, danke, dass ihr euch um meine Korallen gekümmert und mir geholfen habt, sie gesund und glücklich zu halten, damit ich mit ihnen experimentieren kann. Esther, danke für die Schokolade und die netten Gespräche, ich schätze deine Freundschaft und Hilfe.

Thanks to the team at AWI: Jürgen, Ulla, Horst, Julian, for your help with scientific, and administrative problems. Nils in particular thank you for your advice and fresh ideas, for the ice creams and the walks.

Mario, danke für deine Hilfe und Begleitung, dafür, dass du diese Reise geteilt hast, auch wenn es nur für eine Weile war. Danke für die schönen Skizzen und die Hilfe bei den 3D-Diagramme meines Versuchsaufbaus. Einige der Abbildungen in dieser Arbeit würden ohne deine Beteiligung ganz anders aussehen.

Nur and Thomy, my fellow PhD companions, gracias por su apoyo, por compartir las risas y lágrimas producto de esta montaña rusa que es el doctorado, sin ustedes los días en el AWI hubieran sido muy distintos y mucho más grises.

Cote, amiga mía, lo que significa tu amistad es algo que jamás podré expresar en palabras. Gracias por el apoyo incondicional, el paño de lágrimas y las risas. Tenerte de compañera de piso este último año fue la cereza de estos casi 5 años.

A “La Pandilla”, chicos ha sido un honor conocerlos y compartir estos años juntos en Bremen, por todas las fiestas, los asados, las risas, los viajes en tren, gracias a todos y cada uno de ustedes, en especial a las “noches de miércoles”, Miri, Mariano, Elena, Santi, Graciana y Daniele, gracias por todas las risas y sobre todo por el apoyo que me brindaron.

Yure, Migue, Gon, gracias por su amistad, las cerves y los consejos.

Pierrick, je ne peux pas exprimer ce que ton soutien signifie, surtout cette dernière année, je sais que cela n'a pas été facile, mais je te remercie infiniment pour chaque mot de soutien, chaque câlin, merci de me garder sain d'esprit et en vie.

And finally to you COVID, you have affected the development of this thesis perhaps more than anybody, for good or bad, thank you.

Cover design: Gianfranco Zegarra

General bibliography

Abe, S., K. Okamoto, and H. Madarame. 2004. The development of PIV–PSP hybrid system using pressure sensitive particles. Meas Sci Technol **15:** 1153-1157.

Abelson, A., T. Miloh, and Y. Loya. 1993. Flow patterns induced by substrata and body morphologies of benthic organisms, and their roles in determining availability of food particles. Limnol Oceanogr **38:** 1116-1124.

Ahmerkamp, S. and others 2017. Regulation of benthic oxygen fluxes in permeable sediments of the coastal ocean. Limnol Oceanogr **62:** 1935-1954.

Ainsworth, T. D., A. J. Fordyce, and E. F. Camp. 2017. The other microeukaryotes of the coral reef microbiome. Trends Microbiol **25:** 980-991.

Al-Horani, F. A., S. M. Al-Moghrabi, and D. de Beer. 2003. Microsensor study of photosynthesis and calcification in the scleractinian coral, *Galaxea fascicularis*: active internal carbon cycle. J Exp Mar Biol Ecol **288:** 1-15.

Al-Horani, F. A., T. Ferdelman, S. M. Al-Moghrabi, and D. de Beer. 2005. Spatial distribution of calcification and photosynthesis in the scleractinian coral *Galaxea fascicularis*. Coral Reefs **24:** 173-180.

Alldredge, A. L., and J. M. King. 2009. Near-surface enrichment of zooplankton over a shallow back reef: implications for coral reef food webs. Coral Reefs **28:** 895-908.

Altieri, A. H., S. B. Harrison, J. Seemann, R. Collin, R. J. Diaz, and N. Knowlton. 2017. Tropical dead zones and mass mortalities on coral reefs. PNAS **114:** 3660-3665.

Anderson, D. M., W. L. Prell, and N. J. Barratt. 1989. Estimates of Sea Surface Temperature in the Coral Sea at the Last Glacial Maximum. Paleoceanography **4:** 615 - 627.

Andrews, J. C., and P. Gentien. 1982. Upwelling as a source of nutrients for the Great Barrier Reef ecosystems: A solution to Darwin's question? Mar Ecol Prog Ser **8:** 257-269.

Anthony, K. R. N. 1999. Coral suspension feeding on fine particulate matter. J Exp Mar Biol Ecol **232:** 85-106.

Anthony, K. R. N., and K. E. Fabricius. 2000. Shifting roles of heterotrophy and autotrophy in coral energetics under varying turbidity. J Exp Mar Biol Ecol **252:** 221-253.

Baird, A. H., J. R. Guest, and B. L. Willis. 2009. Systematic and biogeographical patterns in the reproductive biology of scleractinian corals. Annu Rev Ecol Evol Syst **40:** 551-571.

Bak, R. P. M., M. Joenje, I. de Jong, D. Y. M. Lambrechts, and G. Nieuwland. 1998. Bacterial suspension feeding by coral reef benthic organisms. Mar Ecol Prog Ser **175:** 285-288.

Barott, K. L., and F. L. Rohwer. 2012. Unseen players shape benthic competition on coral reefs. Trends Microbiol **20:** 621-628.

Barry, P. H., and J. M. Diamond. 1984. Effects of unstirred layers on membrane phenomena. Physiol. Rev. **64:** 763-872.

Batchelor, G. K. 2000. An Introduction to Fluid Dynamics. Cambridge University Press.

Bayne, B. L. 1985. Response to environmental stress: tolerance, resistance and adaptation, p. 331 - 349. *In* J. S. Gray and M. E. Christiansen [eds.], Marine Biology of Polar Regions and Effects of Stress in Marine Organisms: Proceedings of the 18th European Marine Biology Symposium, University of Oslo, Norway. John Wiley & Sons.

Beck, J. W. and others 1992. Sea-surface temperature from coral skeletal strontium/calcium ratios. Science **257:** 644-647.

Behrendt, L. and others 2020. PhenoChip: A single-cell phenomic platform for high-throughput photophysiological analyses of microalgae. Science Advances **6:** eabb2754.

Bein, A. and others 2018. Microfluidic organ-on-a-chip models of human intestine. Cell Mol Gastroenterol Hepatol **5:** 659-668.

Ben-Ari, H., M. Paz, and D. Sher. 2018. The chemical armament of reef-building corals: inter- and intra-specific variation and the identification of an unusual actinoporin in *Stylophora pistilata*. Sci Rep **8:** 251.

Bianchi, D., T. S. Weber, R. Kiko, and C. Deutsch. 2018. Global niche of marine anaerobic metabolisms expanded by particle microenvironments. Nature Geoscience **11:** 263-268.

Borisov, S. M., T. Mayr, and I. Klimant. 2008. Poly(styrene-block-vinylpyrrolidone) beads as a versatile material for simple fabrication of optical nanosensors. Anal Chem **80:** 573-582.

Boudreau, B. P. 1997. Diagenetic models and their implementation, 1st ed. Springer.

Bourne, D. G., K. M. Morrow, and N. S. Webster. 2016. Insights into the coral microbiome: Underpinning the health and resilience of reef ecosystems. Annu Rev Microbiol **70:** 317-340.

Brandl, S. J. and others 2019. Demographic dynamics of the smallest marine vertebrates fuel coral reef ecosystem functioning. Science **364:** 1189-1192.

Brennen, C., and H. Winet. 1977. Fluid mechanics of propulsion by cilia and flagella. Annu Rev Fluid Mech **9:** 339-398.

Brokaw, C. J. 2009. Thinking about flagellar oscillation. Cell Motility **66:** 425-436.

Brown, B., R. Dunne, M. Goodson, and A. Douglas. 2002. Experience shapes the susceptibility of a reef coral to bleaching. Coral Reefs **21:** 119-126.

Brown, B. E. 1997. Adaptations of reef corals to physical environmental stress, p. 221-299. *In* J. H. S. Blaxter and A. J. Southward [eds.], Adv Mar Biol. Academic Press.

Brown, B. E., and J. C. Bythell. 2005. Perspectives on mucus secretion in reef corals. Mar Ecol Prog Ser **296:** 291-309.

Brown, B. E., R. P. Dunne, T. P. Scoffin, and M. D. A. Le Tissier. 1994. Solar damage in intertidal corals. Mar Ecol Prog Ser **105:** 219-230.

Brown, B. E., M. D. A. Le Tissier, and J. C. Bythell. 1995. Mechanisms of bleaching deduced from histological studies of reef corals sampled during a natural bleaching event. Mar Biol **122:** 655-663.

Cannon, Q., and E. Wagner. 2003. Comparison of discharge mechanisms of cnidarian cnidae and myxozoan polar capsules. Rev Fish Sci **11:** 185-219.

Carlgren, O. 1905. Über die Bedeutung der Flimmerbewegung für den Nahrungstransport bei den Actinarien und Madreporarien. Biol. Zbl. **25:** 308-322.

Carpenter, F. W. 1910. Feeding reactions of the rose coral (*Isophyllia*). Proc Am Acad Arts Sci **46:** 149-162.

Carpenter, L. W., and M. R. Patterson. 2007. Water flow influences the distribution of photosynthetic efficiency within colonies of the scleractinian coral *Montastrea annularis* (Ellis and Solander, 1786); implications for coral bleaching. J Exp Mar Biol Ecol **351:** 10-26.

Chamberlain, J. J. A., and R. R. Graus. 1975. Water flow and hydromechanical adaptations of branched reef corals. Bull Mar Sci **25:** 112-125.

Chan, N. C. S., D. Wangpraseurt, M. Kühl, and S. R. Connolly. 2016. Flow and coral morphology control coral surface ph: Implications for the effects of ocean acidification. Front Mar Sci **3**.

Chang, S., C. Elkins, M. Alley, J. Eaton, and S. Monismitha. 2009. Flow inside a coral colony measured using magnetic resonance velocimetry. Limnol Oceanogr **54:** 1819-1827.

Chen, H., G. Holst, and E. Gratton. 2015. Modulated CMOS camera for fluorescence lifetime microscopy. Microsc Res Tech **78:** 1075-1081.

Clark, J. L. C., R. Wolf, D. Granger, and Z. Taylor. 1953. Continuous recording of blood oxygen tensions by polarography. J Appl Physiol **6:** 189-193.

Clayton, W. S., Jr, and H. R. Lasker. 1982. Effects of light and dark treatments on feeding by the reef coral *Pocillopora damicornis* (Linnaeus). J Exp Mar Biol Ecol **63:** 269-279.

Coles, S. L., and Y. H. Fadlallah. 1991. Reef coral survival and mortality at low temperatures in the Arabian Gulf: new species-specific lower temperature limits. Coral Reefs **9:** 231-237.

Costello, J. H., S. P. Colin, J. O. Dabiri, B. J. Gemmell, K. N. Lucas, and K. R. Sutherland. 2021. The hydrodynamics of jellyfish swimming. Annu Rev Mar Sci **13:** 375-396.

Crawley, A., D. I. Kline, S. Dunn, K. Anthony, and S. Dove. 2010. The effect of ocean acidification on symbiont photorespiration and productivity in *Acropora formosa*. Glob. Change Biol. **16:** 851-863.

Cunning, R., R. Ritson-Williams, and R. D. Gates. 2016. Patterns of bleaching and recovery of *Montipora capitata* in Kāne'ohe Bay, Hawai'i, USA. Mar Ecol Prog Ser **551:** 131-139.

Cushing, D. H., G. F. Humphrey, K. Banse, and T. Laevastu. 1958. Report of the committee on terms and equivalents. Rapp. P.-V. Réun. Cons. perm. int. Explor. Mer **144:** 15-16.

Cussler, E. L. 2007. Diffusion: Mass transfer in fluid systems, 3rd ed. Cambridge University Press.

D'Elia, C. F. 1977. The uptake and release of dissolved phosphorus by reef corals. Limnol Oceanogr **22:** 301-315.

Dade, W. B., A. J. Hogg, and B. P. Boudreau. 2001. Physics of flow above the sediment-water interface, p. 4-43. *In* B. P. Boudreau and B. B. Jørgensen [eds.], The benthic boundary layer: transport processes and biogeochemistry. Oxford University Press.

de Beer, D., M. Kühl, N. Stambler, and L. Vaki. 2000. A microsensor study of light enhanced Ca^{2+} uptake and photosynthesis in the reef-building hermatypic coral *Favia* sp.†. Mar Ecol Prog Ser **194:** 75-85.

de Goeij, J. M. and others 2013. Surviving in a marine desert: The sponge loop retains resources within coral reefs. Science **342:** 108-110.

Dennison, W. C., and D. J. Barnes. 1988. Effect of water motion on coral photosynthesis and calcification. J Exp Mar Biol Ecol **115:** 67-77.

Drescher, K., R. E. Goldstein, N. Michel, M. Polin, and I. Tuval. 2010. Direct measurement of the flow field around swimming microorganisms. Phys Rev Lett **105:** 168101.

Dubinsky, Z., P. G. Falkowski, J. W. Porter, L. Muscatine, and D. C. Smith. 1984. Absorption and utilization of radiant energy by light- and shade-adapted colonies of the hermatypic coral *Stylophora pistillata*. Proc R Soc B **222:** 203-214.

Dykens, J. A., and J. M. Shick. 1984. Photobiology of the symbiotic sea anemone, *Anthopleura elegantissima*: Defenses against photodynamic effects, and seasonal photoacclimatization. Biol Bull **167:** 683-697.

Eppard, R. A., G. J. Highison, and R. W. Mead. 1989. Scanning electron microscopy of epithelial surfaces of the sea anemone *Acontiophorum niveum* (Phylum Cnidaria): Class anthozoa. J Morphol **200:** 63-69.

Fabricius-Dyg, J., G. Mistlberger, M. Staal, S. M. Borisov, I. Klimant, and M. Kühl. 2012. Imaging of surface O_2 dynamics in corals with magnetic micro optode particles. Mar Biol **159:** 1621-1631.

Fabricius, K. E. 2006. Effects of irradiance, flow, and colony pigmentation on the temperature microenvironment around corals: Implications for coral bleaching? Limnol Oceanogr **51:** 30-37.

Falkowski, P. G., and Z. Dubinsky. 1981. Light-shade adaptation of *Stylophora pistillata*, a hermatypic coral from the Gulf of Eilat. Nature **289:** 172-174.

Farrant, P. A., M. A. Borowitzka, R. Hinde, and R. J. King. 1987. Nutrition of the temperate Australian soft coral *Capnella gaboensis*. Mar Biol **95:** 575-581.

Fautin, D., and R. N. Mariscal. 1991. Cnidaria: Anthozoa, p. 267-358. *In* F. W. Harrison and J. A. Westfall [eds.], Microscopic anatomy of invertebrates: Placozoa, Porifera, Cnidaria and Ctenophora. Microscopic anatomy of invertebrates. Wiley-Liss.

Ferrier-Pagès, C., and J. P. Gattuso. 1998. Biomass, production and grazing rates of pico- and nanoplankton in coral reef waters (Miyako island, Japan). Microb Ecol **35:** 46-57.

Ferrier-Pagès, C. and others 2013. In situ assessment of the daily primary production of the temperate symbiotic coral *Cladocora caespitosa*. Limnol Oceanogr **58:** 1409-1418.

Ferrier-Pagès, C. and others 2011. Summer autotrophy and winter heterotrophy in the temperate symbiotic coral *Cladocora caespitosa*. Limnol Oceanogr **56:** 1429-1438.

Ferrier-Pagès, C., C. Rottier, E. Beraud, and O. Levy. 2010. Experimental assessment of the feeding effort of three scleractinian coral species during a thermal stress: Effect on the rates of photosynthesis. J Exp Mar Biol Ecol **390:** 118-124.

Ferrier-Pagès, C., J. Witting, E. Tambutté, and K. P. Sebens. 2003. Effect of natural zooplankton feeding on the tissue and skeletal growth of the scleractinian coral *Stylophora pistillata*. Coral Reefs **22:** 229-240.

Fifer, J., B. Bentlage, S. Lemer, A. G. Fujimura, M. Sweet, and L. J. Raymundo. 2021. Going with the flow: How corals in high-flow environments can beat the heat. Mol Ecol **30:** 2009-2024.

Finelli, C. M., B. S. T. Helmuth, N. D. Pentcheff, and D. S. Wethey. 2006. Water flow influences oxygen transport and photosynthetic efficiency in corals. Coral Reefs **25:** 47-57.

Flombaum, P. and others 2013. Present and future global distributions of the marine Cyanobacteria *Prochlorococcus* and *Synechococcus*. PNAS **110:** 9824-9829.

Frederiksen, M. S., and R. N. Glud. 2006. Oxygen dynamics in the rhizosphere of *Zostera marina*: A two-dimensional planar optode study. Limnol Oceanogr **51:** 1072-1083.

Gardella, D. J., and P. J. Edmunds. 1999. The oxygen microenvironment adjacent to the tissue of the scleractinian *Dichocoenia stokesii* and its effects on symbiont metabolism. Mar Biol **135:** 289-295.

---. 2001. The effect of flow and morphology on boundary layers in the scleractinians *Dichocoenia stokesii* (Milne-Edwards and Haime) and *Stephanocoenia michilini* (Milne-Edwards and Haime). J Exp Mar Biol Ecol **256:** 279-289.

Garren, M. and others 2014. A bacterial pathogen uses dimethylsulfoniopropionate as a cue to target heat-stressed corals. ISME J **8:** 999-1007.

Gemmell, B. J., S. P. Colin, J. H. Costello, and J. O. Dabiri. 2015. Suction-based propulsion as a basis for efficient animal swimming. Nat Commun **6:** 8790.

Gemmell, B. J., H. Jiang, and E. J. Buskey. 2014. A new approach to micro-scale particle image velocimetry (μPIV) for quantifying flows around free-swimming zooplankton. J Plankton Res **36:** 1396-1401.

Genin, A., and L. Karp. 1994. Effects of flow on competitive superiority in scleractinian corals. Limnol Oceanogr **39:** 913-924.

Gerardo, Nicole M. 2013. The give and take of host-microbe symbioses. Cell Host Microbe **14:** 1-3.

Gibbin, E., G. Banc-Prandi, M. Fine, A. Comment, and A. Meibom. 2020. A method to disentangle and quantify host anabolic turnover in photosymbiotic holobionts with subcellular resolution. Commun Biol **3:** 14.

Gibbons, I. R. and others 1978. Potent inhibition of dynein adenosinetriphosphatase and of the motility of cilia and sperm flagella by vanadate. PNAS **75:** 2220-2224.

Gilpin, W., M. S. Bull, and M. Prakash. 2020. The multiscale physics of cilia and flagella. Nat Rev Phys **2:** 74-88.

Gilpin, W., V. N. Prakash, and M. Prakash. 2017. Vortex arrays and ciliary tangles underlie the feeding–swimming trade-off in starfish larvae. Nat Phys **13:** 380-386.

Glud, R. N., A. Tengberg, M. Kühl, P. O. J. Hall, and I. Klimant. 2001. An *in situ* instrument for planar O_2 optode measurements at benthic interfaces. Limnol Oceanogr **46:** 2073-2080.

Glynn, P. W. 1983. Extensive 'bleaching' and death of reef corals on the pacific coast of Panamá. Environ Conserv **10:** 149-154.

Glynn, P. W., E. C. Peters, and L. Muscatine. 1985. Coral tissue microstructure and necrosis: relation to catastrophic coral mortality in Panamá. Dis Aquat Org **1:** 29-37.

Goldberg, W. M. 2002. Feeding behavior, epidermal structure and mucus cytochemistry of the scleractinian *Mycetophyllia reesi*, a coral without tentacles. Tissue Cell **34:** 232-245.

Goreau, T. F., N. I. Goreau, and C. M. Yonge. 1971. Reef corals: Autotrophs or heterotrophs? Biol Bull **141:** 247-260.

Gregory, J. W., K. Asai, M. Kameda, T. Liu, and J. P. Sullivan. 2008. A review of pressure-sensitive paint for high-speed and unsteady aerodynamics. Proc Inst Mech Eng G J Aerosp Eng **222:** 249-290.

Grigg, R., J. Polovina, and M. Atkinson. 1984. Model of a coral reef ecosystem. Coral Reefs **3:** 23-27.

Grottoli, A. G., L. J. Rodrigues, and J. E. Palardy. 2006. Heterotrophic plasticity and resilience in bleached corals. Nature **440:** 1186-1189.

Guasto, J. S., R. Rusconi, and R. Stocker. 2012. Fluid mechanics of planktonic microorganisms. Annu Rev Fluid Mech **44:** 373-400.

Haas, A., M. Al-Zibdah, and C. Wild. 2009. Effect of inorganic and organic nutrient addition on coral–algae assemblages from the Northern Red Sea. J Exp Mar Biol Ecol **380:** 99-105.

Harland, A. D., and P. S. Davies. 1995. Symbiont photosynthesis increases both respiration and photosynthesis in the symbiotic sea anemone *Anemonia viridis*. Mar Biol **123:** 715-722.

Helmuth, B., and K. Sebens. 1993. The influence of colony morphology and orientation to flow on particle capture by the scleractinian coral *Agaricia agaricites* (Linnaeus). J Exp Mar Biol Ecol **165:** 251-278.

Helmuth, B. S. T., K. P. Sebens, and T. L. Daniel. 1997. Morphological variation in coral aggregations: branch spacing and mass flux to coral tissues. J Exp Mar Biol Ecol **209:** 233-259.

Hentschel, B. T., and J. Shimeta. 2008. Suspension Feeders, p. 3437-3442. *In* S. E. Jørgensen and B. D. Fath [eds.], Encyclopedia of Ecology. Academic Press.

Herfort, L., B. Thake, and I. Taubner. 2008. Bicarbonate stimulation of calcification and photosynthesis in two hermatypic corals. J Phycol **44:** 91-98.

Hernandez-Agreda, A., R. D. Gates, and T. D. Ainsworth. 2017. Defining the core microbiome in corals' microbial soup. Trends Microbiol **25:** 125-140.

Hill, R., U. Schreiber, R. Gademann, A. W. D. Larkum, M. Kühl, and P. J. Ralph. 2004. Spatial heterogeneity of photosynthesis and the effect of temperature-induced bleaching conditions in three species of corals. Mar Biol **144:** 633-640.

Hoegh-Guldberg, O., and G. J. Smith. 1989. Influence of the population density of zooxanthellae and supply of ammonium on the biomass and metabolic characteristics of the reef corals *Seriatopora hystrix* and *Stylophora pistillata*. Mar Ecol Prog Ser **57:** 173-186.

Hondzo, M., T. Feyaerts, R. Donovan, and B. L. O'Connor. 2005. Universal scaling of dissolved oxygen distribution at the sediment-water interface: A power law. Limnol Oceanogr **50:** 1667-1676.

Hossain, M. M., and A. E. Staples. 2019. Passive vortical flows enhance mass transport in the interior of a coral colony. Phys Fluids **31:** 061701.

---. 2020. Mass transport and turbulent statistics within two branching coral colonies. Fluids **5:** 153.

Houlbrèque, F., B. Delesalle, J. Blanchot, Y. Montel, and C. Ferrier-Pagès. 2006. Picoplankton removal by the coral reef community of La Prévoyante, Mayotte Island. Aquat Microb Ecol **44:** 59-70.

Houlbrèque, F., and C. Ferrier-Pagès. 2009. Heterotrophy in tropical scleractinian corals. Biol Rev (Camb) **84:** 1-17.

Houlbrèque, F., E. Tambutté, D. Allemand, and C. Ferrier-Pagès. 2004a. Interactions between zooplankton feeding, photosynthesis and skeletal growth in the scleractinian coral *Stylophora pistillata*. J. Exp. Biol. **207:** 1461-1469.

Houlbrèque, F., E. Tambutté, and C. Ferrier-Pagès. 2003. Effect of zooplankton availability on the rates of photosynthesis, and tissue and skeletal growth in the scleractinian coral *Stylophora pistillata*. J Exp Mar Biol Ecol **296:** 145-166.

Houlbrèque, F., E. Tambutté, C. Richard, and C. Ferrier-Pagès. 2004b. Importance of a micro-diet for scleractinian corals. Mar Ecol Prog Ser **282:** 151-160.

Jimenez, I. M., M. Kühl, A. W. D. Larkum, and P. J. Ralph. 2011. Effects of flow and colony morphology on the thermal boundary layer of corals. J R Soc Interface **8:** 1785-1795.

Jokiel, P. L. 1978. Effects of water motion on reef corals. J Exp Mar Biol Ecol **35:** 87-97.

Jones, R., P. Bessell-Browne, R. Fisher, W. Klonowski, and M. Slivkoff. 2016. Assessing the impacts of sediments from dredging on corals. Mar Pollut Bull **102:** 9-29.

Jones, R. J., and O. Hoegh-Guldberg. 2001. Diurnal changes in the photochemical efficiency of the symbiotic dinoflagellates (*Dinophyceae*) of corals: photoprotection, photoinactivation and the relationship to coral bleaching. Plant Cell Environ **24:** 89-99.

Jordan, D. B., and W. L. Ogren. 1981. Species variation in the specificity of ribulose biphosphate carboxylase/oxygenase. Nature **291:** 513-515.

Jørgensen, B. B. 2001. Life in the diffusive boundary layer, p. 348-373. *In* B. P. Boudreau and B. B. Jørgensen [eds.], The benthic boundray layer: Transport processes and biogeochemistry. Oxford University Press.

Jørgensen, B. B., and D. J. Des Marais. 1990. The diffusive boundary layer of sediments: Oxygen microgradients over a microbial mat. Limnol Oceanogr **35:** 1343-1355.

Jørgensen, B. B., and N. P. Revsbech. 1985. Diffusive boundary layers and the oxygen uptake of sediments and detritus1. Limnol Oceanogr **30:** 111-122.

Jørgensen, C. B. 1966. Biology of suspension feeding. Pergamon Press.

Jorissen, H., C. Skinner, R. Osinga, D. de Beer, and M. M. Nugues. 2016. Evidence for water-mediated mechanisms in coral - algal interactions. Proc R Soc B **283:** 20161137.

Joyce, K. E., and S. R. Phinn. 2003. Hyperspectral analysis of chlorophyll content and photosynthetic capacity of coral reef substrates. Limnol Oceanogr **48:** 489-496.

Kanso, E. A., R. M. Lopes, J. R. Strickler, J. O. Dabiri, and J. H. Costello. 2021. Teamwork in the viscous oceanic microscale. Proceedings of the National Academy of Sciences **118:** e2018193118.

Karthäuser, C. and others 2021. Small sinking particles control anammox rates in the Peruvian oxygen minimum zone. Nat Commun **12:** 3235.

Katija, K., and J. O. Dabiri. 2008. *In situ* field measurements of aquatic animal-fluid interactions using a Self-Contained Underwater Velocimetry Apparatus (SCUVA). Limnol Oceanogr Methods **6:** 162-171.

---. 2009. A viscosity-enhanced mechanism for biogenic ocean mixing. Nature **460:** 624-626.

Katija, K., R. E. Sherlock, A. D. Sherman, and B. H. Robison. 2017. New technology reveals the role of giant larvaceans in oceanic carbon cycling. Science Advances **3:** e1602374.

Kheradvar, A. and others 2010. Echocardiographic particle image velocimetry: A novel technique for quantification of left ventricular blood vorticity pattern. Journal of the American Society of Echocardiography **23:** 86-94.

Khosravi, Y. and others 2020. Use of an oxygen planar optode to assess the effect of high velocity microsprays on oxygen penetration in a human dental biofilms in-vitro. BMC Oral Health **20:** 230.

Kim, H. D., S. J. Yi, and K. C. Kim. 2013. Simultaneous measurement of dissolved oxygen concentration and velocity field in microfluidics using oxygen-sensitive particles. Microfluid Nanofluidics **15:** 139-149.

Kim, P., K. W. Kwon, Park, Min Cheol , S. H. Lee, S. M. Kim, and K. Y. Suh. 2008. Soft Lithography for Microfluidics: a Review. Biochip Journal **2:** 1-11.

Kiørboe, T., and U. H. Thygesen. 2001. Fluid motion and solute distribution around sinking aggregates. II. Implications for remote detection by colonizing zooplankters. Mar Ecol Prog Ser **211:** 15-25.

Klimant, I., V. Meyer, and M. Kühl. 1995. Fiber-optic oxygen microsensors, a new tool in aquatic biology. Limnol Oceanogr **40:** 1159-1165.

Koren, K., K. E. Brodersen, S. L. Jakobsen, and M. Kühl. 2015. Optical sensor nanoparticles in artificial sediments – A new tool to visualize O_2 dynamics around the rhizome and roots of seagrasses. Environ Sci Technol **49:** 2286-2292.

Koren, K., S. L. Jakobsen, and M. Kühl. 2016. In-vivo imaging of O_2 dynamics on coral surfaces spray-painted with sensor nanoparticles. Sens. Actuators B Chem. **237:** 1095-1101.

Koren, K., M. Moßhammer, V. V. Scholz, S. M. Borisov, G. Holst, and M. Kühl. 2019. Luminescence lifetime imaging of chemical sensors — A comparison between time-domain and frequency-domain based camera systems. Anal Chem **91:** 3233-3238.

Kraines, S., Y. Suzuki, K. Yamada, and H. Komiyama. 1996. Separating biological and physical changes in dissolved oxygen concentration in a coral reef. Limnol Oceanogr **41:** 1790-1799.

Krishnamurthy, D. and others 2020. Scale-free vertical tracking microscopy. Nat Methods **17:** 1040-1051.

Krzic, U., S. Gunther, T. E. Saunders, S. J. Streichan, and L. Hufnagel. 2012. Multiview light-sheet microscope for rapid *in toto* imaging. Nat Methods **9:** 730-733.

Kühl, M., Y. Cohen, T. Dalsgaard, B. B. Jørgensen, and N. P. Revsbech. 1995. Microenvironment and photosynthesis of zooxanthellae in scleractinian corals studied with microsensors for O_2, pH and light. Mar Ecol Prog Ser **117:** 159-172.

Kühl, M. and others 2020. Substantial near-infrared radiation-driven photosynthesis of chlorophyll *f*-containing cyanobacteria in a natural habitat. eLife **9:** e50871.

LaBarbera, M. 1981. Water flow patterns in and around three species of articulate brachiopods. J Exp Mar Biol Ecol **55:** 185-206.

---. 1984. Feeding currents and particle capture mechanisms in suspension feeding animals. Am Zool **24:** 71-84.

Laland, K. N., and K. Sterelny. 2006. Perspective: Seven reasons (not) to neglect niche construction. Evolution **60:** 1751-1762.

Langdon, C., and M. J. Atkinson. 2005. Effect of elevated pCO_2 on photosynthesis and calcification of corals and interactions with seasonal changes in temperature/irradiance and nutrient enrichment. J. Geophys. Res. **110:** 1-16.

Lasker, H. R. 1979. Light dependent activity patterns among reef corals: *Montastrea cavernosa*. Biol Bull **156:** 196-211.

Lea, D. W., D. K. Pak, and H. J. Spero. 2000. Climate impact of late quaternary equatorial pacific sea surface temperature variations. Science **289:** 1719-1724.

Lesser, M. P. 1996. Elevated temperatures and ultraviolet radiation cause oxidative stress and inhibit photosynthesis in ymbiotic dinoflagellates. Limnol Oceanogr **41:** 271-283.

---. 1997. Oxidative stress causes coral bleaching during exposure to elevated temperatures. Coral Reefs **16:** 187-192.

Lesser, M. P., and J. M. Shick. 1989. Effects of irradiance and ultraviolet radiation on photoadaptation in the zooxanthellae of *Aiptasia pallida* primary production, photoinhibition, and enzymic defenses against oxygen toxicity. Mar Biol **102:** 243-255.

Lesser, M. P., M. Slattery, M. Stat, M. Ojimi, R. D. Gates, and A. Grottoli. 2010. Photoacclimatization by the coral *Montastraea cavernosa* in the mesophotic zone: light, food, and genetics. Ecology **91:** 990-1003.

Lesser, M. P., W. R. Stochaj, D. W. Tapley, and J. M. Shick. 1990. Bleaching in coral reef anthozoans: effects of irradiance, ultraviolet radiation, and temperature on the activities of protective enzymes against active oxygen. Coral Reefs **8:** 225-232.

Levy, O., Z. Dubinsky, and Y. Achituv. 2003. Photobehavior of stony corals: responses to light spectra and intensity. J. Exp. Biol. **206:** 4041-4049.

Levy, O., Z. Dubinsky, K. Schneider, Y. Achituv, D. Zakai, and M. Y. Gorbunov. 2004. Diurnal hysteresis in coral photosynthesis. Mar Ecol Prog Ser **268**.

Levy, O., L. Mizrahi, N. E. Chadwick-Furman, and Y. Achituv. 2001. Factors controlling the expansion behavior of *Favia favus* (Cnidaria: Scleractinia): Effects of light, flow, and planktonic prey. Biol Bull **200:** 118-126.

Lewis, J. B., and W. S. Price. 1975. Feeding mechanisms and feeding strategies of Atlantic reef corals. J Zool (Lond) **176:** 527-544.

---. 1976. Patterns of ciliary currents in Atlantic reef corals and their functional significance. J Zool (Lond) **178:** 77-89.

Liao, Q. and others 2009. Development of an *in situ* underwater particle image velocimetry (UWPIV) system. Limnol Oceanogr Methods **7:** 169-184.

Liu, C., S. H. Cheng, and S. Lin. 2020. Illuminating the dark depths inside coral. Cell Microbiol **22:** e13122.

Lough, J. M. 1994. Climate variation and El Niño-Southern Oscillation events on the Great Barrier Reef: 1958 to 1987. Coral Reefs **13:** 181-185.

Lough, J. M., and D. J. Barnes. 2000. Environmental controls on growth of the massive coral Porites. J Exp Mar Biol Ecol **245:** 225-243.

Loya, Y., K. Sakai, K. Yamazato, Y. Nakano, H. Sambali, and R. van Woesik. 2001. Coral bleaching: the winners and the losers. Ecol Lett **4:** 122-131.

Manton, I., and B. Clarke. 1952. An electron microscope study of the spermatozoid of *sphagnum*. J Exp Bot **3:** 265-275.

Mariscal, R. N. 1974. Scanning electron microscopy of the sensory surface of the tentacles of sea anemones and corals. Zeitschrift für Zellforschung und Mikroskopische Anatomie **147:** 149-156.

Mariscal, R. N., and C. H. Bigger. 1977. Possible ecological significance of octocoral epithelial ultrastructure. Proc 3rd Int Coral Reef Symp **1:** 127-134.

Markov, D. A., E. M. Lillie, S. P. Garbett, and L. J. McCawley. 2014. Variation in diffusion of gases through PDMS due to plasma surface treatment and storage conditions. Biomed Microdevices **16:** 91-96.

Marshall, A. T., and O. P. Wright. 1993. Confocal laser scanning light microscopy of the extra-thecal epithelia of undecalcified scleractinian corals. Cell Tissue Res **272:** 533-543.

Mass, T., A. Genin, U. Shavit, M. Grinstein, and D. Tchernov. 2010. Flow enhances photosynthesis in marine benthic autotrophs by increasing the efflux of oxygen from the organism to the water. PNAS **107:** 2527-2531.

Mayr, T. and others 2009. Light harvesting as a simple and versatile way to enhance brightness of luminescent sensors. Anal Chem **81:** 6541-6545.

Merl, T., and K. Koren. 2020. Visualizing NH_3 emission and the local O_2 and pH microenvironment of soil upon manure application using optical sensors. Environ Int **144:** 106080.

Meysman, F. J. R., O. S. Galaktionov, R. N. Glud, and J. J. Middelburg. 2010. Oxygen penetration around burrows and roots in aquatic sediments. J Mar Res **68:** 309-336.

Mistlberger, G. and others 2010. Multifunctional magnetic optical sensor particles with tunable sizes for monitoring metabolic parameters and as a basis for nanotherapeutics. Adv Funct Mater **20:** 1842-1851.

Mitchell, D. R. 2007. The evolution of eukaryotic cilia and flagella as motile and sensory organelles, p. 130-140. Eukaryotic membranes and cytoskeleton: Origins and evolution. Springer New York.

Mitchison, T. J., and H. M. Mitchison. 2010. How cilia beat. Nature **463:** 308-309.

Moradi, N., B. Liu, M. Iversen, M. M. Kuypers, H. Ploug, and A. Khalili. 2018. A new mathematical model to explore microbial processes and their constraints in phytoplankton colonies and sinking marine aggregates. Science Advances **4:** eaat1991.

Morris, M. J., J. F. Donovan, J. T. Kegelman, S. D. Schwab, R. L. Levy, and R. C. Crites. 1993. Aerodynamic applications of pressure sensitive paint. AIAA Journal **31:** 419-425.

Moßhammer, M., K. E. Brodersen, M. Kühl, and K. Koren. 2019. Nanoparticle- and microparticle-based luminescence imaging of chemical species and temperature in aquatic systems: a review. Microchim Acta **186:** 126.

Murniati, E., D. Gross, H. Herlina, K. Hancke, R. N. Glud, and A. Lorke. 2016. Oxygen imaging at the sediment-water interface using lifetime-based laser induced fluorescence (τLIF) of nano-sized particles. Limnol Oceanogr Methods **14:** 506-517.

Muscatine, L. 1973. Nutrition of corals p. 77-115. *In* O. A. Jones and R. Endean [eds.], Biology and Geology of Coral Reefs. Academic Press.

Muscatine, L., P. G. Falkowski, Z. Dubinsky, P. A. Cook, L. R. McCloskey, and D. C. Smith. 1989. The effect of external nutrient resources on the population dynamics of zooxanthellae in a reef coral. Proc R Soc B **236:** 311-324.

Muscatine, L., C. Ferrier-Pagès, A. Blackburn, R. D. Gates, G. Baghdasarian, and D. Allemand. 1998. Cell-specific density of symbiotic dinoflagellates in tropical anthozoans. Coral Reefs **17:** 329-337.

Muscatine, L., and J. W. Porter. 1977. Reef corals: Mutualistic symbioses adapted to nutrient-poor environments. Bioscience **27:** 454-460.

Naganuma, T. 1996. Calanoid copepods: Linking lower-higher trophic levels by linking lower-higher Reynolds numbers. Mar Ecol Prog Ser **136:** 311-313.

Nakamura, T., and R. van Woesik. 2001. Water-flow rates and passive diffusion partially explain differential survival of corals during the 1998 bleaching event. Mar Ecol Prog Ser **212:** 301-304.

Nakamura, T., R. van Woesik, and H. Yamasaki. 2005. Photoinhibition of photosynthesis is reduced by water flow in the reef-building coral *Acropora digitifera*. Mar Ecol Prog Ser **301:** 109-118.

Nakamura, T., H. Yamasaki, and R. van Woesik. 2003. Water flow facilitates recovery from bleaching in the coral *Stylophora pistillata*. Mar Ecol Prog Ser **256:** 287-291.

Naseer, A., and B. G. Hatcher. 2000. Assessing the integrated growth response of coral reefs to monsoon forcing using morphometric analysis of reefs in Maldives. Proc 9th Int Coral Reef Symp **1:** 75-80.

Naumann, M. S., C. Richter, M. el-Zibdah, and C. Wild. 2009. Coral mucus as an efficient trap for picoplanktonic cyanobacteria: implications for pelagic–benthic coupling in the reef ecosystem. Mar Ecol Prog Ser **385:** 65-76.

Nelson, H. R., and A. H. Altieri. 2019. Oxygen: the universal currency on coral reefs. Coral Reefs **38:** 177-198.

Nielsen, D. A., K. Petrou, and R. D. Gates. 2018. Coral bleaching from a single cell perspective. ISME J **12:** 1558-1567.

Nielsen, L. T., and T. Kiørboe. 2021. Foraging trade-offs, flagellar arrangements, and flow architecture of planktonic protists. PNAS **118:** e2009930118.

Niggl, W., A. F. Haas, and C. Wild. 2010. Benthic community composition affects O_2 availability and variability in a Northern Red Sea fringing reef. Hydrobiologia **644:** 401-405.

Nilsson, G. E., S. Östlund-Nilsson, and P. L. Munday. 2010. Effects of elevated temperature on coral reef fishes: Loss of hypoxia tolerance and inability to acclimate. Comp Biochem Physiol A **156:** 389-393.

Nowell, A. R. M., and P. A. Jumars. 1984. Flow environments of aquatic benthos. Annu Rev Ecol Syst **15:** 303-328.

Odling-Smee, F. J., K. N. Laland, and M. W. Feldman. 1996. Niche construction. Am Nat **147:** 641-648.

Ong, R. H., A. J. C. King, B. J. Mullins, and M. J. Caley. 2019. The effect of small-scale morphology on thermal dynamics in coral microenvironments. J Therm Biol **86:** 102433.

Pacherres, C. O., S. Ahmerkamp, G. M. Schmidt-Grieb, M. Holtappels, and C. Richter. 2020. Ciliary vortex flows and oxygen dynamics in the coral boundary layer. Sci Rep **10:** 7541.

Pacherres, C. O., G. M. Schmidt, and C. Richter. 2013. Autotrophic and heterotrophic responses of the coral *Porites lutea* to large amplitude internal waves. J. Exp. Biol. **216:** 4365-4374.

Palardy, J. E., L. J. Rodrigues, and A. G. Grottoli. 2008. The importance of zooplankton to the daily metabolic carbon requirements of healthy and bleached corals at two depths. J Exp Mar Biol Ecol **367:** 180-188.

Pandolfi, J. M. 1996. Limited membership in pleistocene reef coral assemblages from the Huon Peninsula, Papua New Guinea: Constancy during global change. Paleobiology **22:** 152-176.

Partensky, F., W. R. Hess, and D. Vaulot. 1999. *Prochlorococcus*, a marine photosynthetic prokaryote of global significance. Microbiol Mol Biol Rev **63:** 106–127.

Patterson, M. R. 1984. Patterns of whole colony prey capture in the octocoral, *Alcyonium siderium*. Biol Bull **167:** 613-629.

---. 1991. The effects of flow on polyp-level prey capture in an octocoral, *Alcyonium siderium*. Biol Bull **180 1:** 93-102.

---. 1992. A mass transfer explanation of metabolic scaling relations in some aquatic invertebrates and algae. Science **255:** 1421-1423.

Patterson, M. R., and K. P. Sebens. 1989. Forced convection modulates gas exchange in cnidarians. PNAS **86:** 8833-8836.

Patterson, M. R., K. P. Sebens, and R. Randolph Olson. 1991. *In situ* measurements of flow effects on primary production and dark respiration in reef corals. Limnol Oceanogr **36:** 936-948.

Pearson, P. N., and M. R. Palmer. 2000. Atmospheric carbon dioxide concentrations over the past 60 million years. Nature **406:** 695-699.

Pedersen, O., J. Borum, C. M. Duarte, and M. D. Fortes. 1998. Oxygen dynamics in the rhizosphere of *Cymodocea rotundata*. Mar Ecol Prog Ser **169:** 283-288.

Ploug, H. 2001. Small-scale oxygen fluxes and remineralization in sinking aggregates. Limnol Oceanogr **46:** 1624-1631.

Porter, J. W. 1976. Autotrophy, heterotrophy, and resource partitioning in caribbean reef-building coral. Am Nat **110:** 731-742.

Putnam, H. M., K. L. Barott, T. D. Ainsworth, and R. D. Gates. 2017. The vulnerability and resilience of reef-building corals. Curr Biol **27:** R528-R540.

Quaranta, M., S. M. Borisov, and I. Klimant. 2012. Indicators for optical oxygen sensors. Bioanal Rev **4:** 115-157.

Raffel, M., C. E. Willert, F. Scarano, C. Kähler, S. T. Wereley, and J. Kompenhans. 2018. Particle image velocimetry: a practical guide, 3rd ed. Springer.

Ralph, P. J., U. Schreiber, R. Gademann, M. Kühl, and A. W. D. Larkum. 2005. Coral photobiology studied with a new imaging pulse amplitude modulated fluorometer. J Phycol **41:** 335-342.

Reidenbach, M. A., S. G. Monismith, J. R. Koseff, G. Yahel, and A. Genin. 2006. Boundary layer turbulence and flow structure over a fringing coral reef. Limnol Oceanogr **51:** 1956-1968.

Revsbech, N. P., and B. B. Jørgensen. 1986. Microelectrodes: Their use in microbial ecology. *In* M. K.C. [ed.], Adv Microb Ecol. Springer.

Rinkevich, B., and Y. Loya. 1984. Does light enhance calcification in hermatypic corals? Mar Biol **80:** 1-6.

Roberty, S., B. Bailleul, N. Berne, F. Franck, and P. Cardol. 2014. PSI Mehler reaction is the main alternative photosynthetic electron pathway in *Symbiodinium* sp., symbiotic dinoflagellates of cnidarians. New Phytol **204:** 81-91.

Roberty, S., E. Béraud, R. Grover, and C. Ferrier-Pagès. 2020. Coral productivity is co-limited by bicarbonate and ammonium availability. Microorganisms **8:** 640.

Roder, C., L. Fillinger, C. Jantzen, G. M. Schmidt, S. Khokiattiwong, and C. Richter. 2010. Trophic response of corals to large amplitude internal waves. Mar Ecol Prog Ser **412:** 113-128.

Ruppert, E. E., R. S. Fox, and B. R. D. 2004. Invertebrate zoology: A functional evolutionary approach, 7th ed. Thomson, Brooks/Cole.

Rusconi, R., M. Garren, and R. Stocker. 2014a. Microfluidics expanding the frontiers of microbial ecology. Annu Rev Biophys **43:** 2.1-2.27.

Rusconi, R., J. S. Guasto, and R. Stocker. 2014b. Bacterial transport suppressed by fluid shear. Nat Phys **10:** 212-217.

Schiller, C., and G. J. Herndl. 1989. Evidence of enhanced microbial activity in the interstitial space of branched corals: possible implications for coral metabolism Coral Reefs **7:** 179-184.

Schlichting, H., and K. Gersten. 2017. Boundary-layer Theory, 9th ed. Springer -Verlag.

Schmidt, G. M., N. Phongsuwan, C. Jantzen, C. Roder, S. Khokiattiwong, and C. Richter. 2012. Coral community composition and reef development at the Similan Islands, Andaman Sea, in response to strong environmental variations. Mar Ecol Prog Ser **456:** 113-126.

Schreiber, U., U. Schliwa, and W. Bilger. 1986. Continuous recording of photochemical and non-photochemical chlorophyll fluorescence quenching with a new type of modulation fluorometer. Photosynth. Res. **10:** 51-62.

Scilipoti, S., K. Koren, N. Risgaard-Petersen, A. Schramm, and L. P. Nielsen. 2021. Oxygen consumption of individual cable bacteria. Science Advances **7:** eabe1870.

Sebens, K. P., and K. DeRiemer. 1977. Diel cycles of expansion and contraction in coral reef anthozoans. Mar Biol **43:** 247-256.

Sebens, K. P., S. P. Grace, B. Helmuth, E. J. Maney Jr, and J. S. Miles. 1998. Water flow and prey capture by three scleractinian corals, *Madracis mirabilis, Montastrea cavernosa* and *Porites porites*, in a field enclosure. Mar Biol **131:** 347-360.

Sebens, K. P., and A. S. Johnson. 1991. Effects of water movement on prey capture and distribution of reef corals. Hydrobiologia **226:** 91-101.

Sebens, K. P., K. S. Vandersall, L. A. Savina, and K. R. Graham. 1996. Zooplankton capture by two scleractinian corals *Madracis mirabilis* and *Montastrea cavernosa*, in a field enclosure. Mar Biol **127:** 303-317.

Seidel, S., R. W. Maschke, S. Werner, V. Jossen, and D. Eibl. 2021. Oxygen mass transfer in biopharmaceutical processes: Numerical and experimental approaches. Chem Ing Tech **93:** 42-61.

Shapiro, O. H. and others 2014. Vortical ciliary flows actively enhance mass transport in reef corals. PNAS **111:** 13391-13396.

Shapiro, O. H., E. Kramarsky-Winter, A. R. Gavish, R. Stocker, and A. Vardi. 2016. A coral–on–a–chip microfluidic platform enabling live-imaging microscopy of reef-building corals. Nat Commun **7:** 10860.

Shashar, N., Y. Cohen, and Y. Loya. 1993. Extreme diel fluctuations of oxygen in diffusive boundary layers surrounding stony corals. Biol Bull **185:** 455-461.

Shashar, N., S. Kinane, P. L. Jokiel, and M. R. Patterson. 1996. Hydromechanical boundary layers over a coral reef. J Exp Mar Biol Ecol **199:** 17-28.

Sheffield, P. J. 1998. Measuring tissue oxygen tension: a review. Undersea Hyperb Med **25:** 179-188.

Shick, J. M. 1990. Diffusion limitation and hyperoxic enhancement of oxygen consumption in zooxanthellate sea anemones, zoanthids, and corals. Biol Bull **179:** 148-158.

Shick, J. M., W. I. Brown, E. G. Dolliver, and S. R. Kayar. 1979. Oxygen uptake in sea anemones: Effects of expansion, contraction, and exposure to air and the limitations of diffusion. Physiol Zool **52:** 50-62.

Singarajah, K. V. 1969. Escape reactions of zooplankton: The avoidance of a pursuing siphon tube. J Exp Mar Biol Ecol **3:** 171-178.

Son, K., D. R. Brumley, and R. Stocker. 2015. Live from under the lens: exploring microbial motility with dynamic imaging and microfluidics. Nat Rev Microbiol **13:** 761.

Sorokin, Y. I. 1973a. Microbial aspects of the productivity of coral reefs, p. 17-46. *In* O. A. Jones and R. Endean [eds.], Biology and Geology of Coral Reefs. Academic Press.

Sorokin, Y. I. 1973b. On the feeding of some scleractinian corals with bacteria and dissolved organic matter. Limnol Oceanogr **18:** 380-385.

Spencer, J. A. and others 2014. Direct measurement of local oxygen concentration in the bone marrow of live animals. Nature **508:** 269-273.

Speth, D. R., M. H. in 't Zandt, S. Guerrero-Cruz, B. E. Dutilh, and M. S. M. Jetten. 2016. Genome-based microbial ecology of anammox granules in a full-scale wastewater treatment system. Nat Commun **7:** 11172.

Spicer, G. L. C. and others 2019. Measuring light scattering and absorption in corals with Inverse Spectroscopic Optical Coherence Tomography (ISOCT): a new tool for non-invasive monitoring. Sci Rep **9:** 14148.

Stafford-Smith, M. G. 1993. Sediment–rejection efficiency of 22 species of Australian scleractinian corals. Mar Biol **115:** 229-243.

Stafford-Smith, M. G., and R. F. G. Ormond. 1992. Sediment–rejection mechanisms of 42 species of Australian scleractinian corals. Mar. Freshw. Res. **43:** 683-705.

Stockdale, A., W. Davison, and H. Zhang. 2009. Micro-scale biogeochemical heterogeneity in sediments: A review of available technology and observed evidence. Earth-Sci Rev **92:** 81-97.

Stocking, J. B., J. P. Rippe, and M. A. Reidenbach. 2016. Structure and dynamics of turbulent boundary layer flow over healthy and algae-covered corals. Coral Reefs **35:** 1047-1059.

Stockner, J. G. 1988. Phototrophic picoplankton: An overview from marine and freshwater ecosystems. Limnol Oceanogr **33:** 765-775.

Stoddart, D. R. 1969. Ecology and morphology of recent coral reefs. Biol Rev **44:** 433-498.

Stolarski, J., M. V. Kitahara, D. J. Miller, S. D. Cairns, M. Mazur, and A. Meibom. 2011. The ancient evolutionary origins of Scleractinia revealed by azooxanthellate corals. BMC Evol Biol **11:** 316.

Strickler, J. R. 1975. Swimming of planktonic cyclops species (Copepoda, Crustacea): Pattern, movements and their control, p. 599-613. *In* T. Y. T. Wu, C. J. Brokaw and C. Brennen [eds.], Swimming and Flying in Nature: Volume 2. Springer US.

Summers, K. E., and I. R. Gibbons. 1971. Adenosine triphosphate–induced sliding of tubules in trypsin-treated flagella of sea-urchin sperm. PNAS **68:** 3092-3096.

Sweet, M. J., A. Croquer, and J. C. Bythell. 2011. Bacterial assemblages differ between compartments within the coral holobiont. Coral Reefs **30:** 39-52.

Sweet, M. J., and M. G. Séré. 2016. Ciliate communities consistently associated with coral diseases. J Sea Res **113:** 119-131.

Talley, L. 2011. Descriptive physical oceanography, 6th ed. Academic Press.

Tambutté, E., P. Ganot, A. A. Venn, and S. Tambutté. 2020. A role for primary cilia in coral calcification? Cell Tissue Res.

Towle, E. K., I. C. Enochs, and C. Langdon. 2015. Threatened caribbean coral is able to mitigate the adverse effects of ocean acidification on calcification by increasing feeding rate. PLoS ONE **10:** e0123394.

Trampe, E. and others 2018. Functionalized bioink with optical sensor nanoparticles for O_2 imaging in 3D–bioprinted constructs. Adv Funct Mater **28:** 1804411.

Ulstrup, K. E., R. Hill, and P. J. Ralph. 2005. Photosynthetic impact of hypoxia on in hospite zooxanthellae in the scleractinian coral *Pocillopora damicornis*. Mar Ecol Prog Ser **286:** 125-132.

Van Driest, E. R. 1956. On turbulent flow near a wall. AIAA J. **23:** 1007-1011.

van Oppen, M. J. H., J.-A. Leong, and R. D. Gates. 2009. Coral–virus interactions: A double-edged sword? Symbiosis **47:** 1-8.

van Woesik, R., A. Irikawa, R. Anzai, and T. Nakamura. 2012. Effects of coral colony morphologies on mass transfer and susceptibility to thermal stress. Coral Reefs **31:** 633-639.

Veron, J. E. N. 1995. Corals in space and time, 1st ed. UNSW Press.

---. 2000. Corals of the world. Australian Institute of Marine Science.

---. 2011. Corals: Biology, skeletal deposition, and reef-building, p. 275-281. *In* D. Hopley [ed.], Encyclopedia of modern coral reefs: Structure, form and process. Springer Netherlands.

Vogel, S. 1996. Life in moving fluids, 2nd ed. Princeton Univ. Press.

Volpe, G., I. Buttinoni, D. Vogt, H.-J. Kümmerer, and C. Bechinger. 2011. Microswimmers in patterned environments. Soft Matter **7:** 8810-8815.

Wall, M., G. M. Schmidt, P. Janjang, S. Khokiattiwong, and C. Richter. 2012. Differential impact of monsoon and large amplitude internal waves on coral reef development in the Andaman Sea. PLoS ONE **7:** e50207.

Wan, K. Y. 2018. Coordination of eukaryotic cilia and flagella. Essays Biochem **62:** 829 - 838.

Wang, J., L. Zhao, and H. Wei. 2012. Variable diffusion boundary layer and diffusion flux at sediment-water interface in response to dynamic forcing over an intertidal mudflat. Chin. Sci. Bull. **57:** 1568-1577.

Wang, X.-d., and O. S. Wolfbeis. 2014. Optical methods for sensing and imaging oxygen: materials, spectroscopies and applications. Chem Soc Rev **43:** 3666-3761.

Wangpraseurt, D., A. Larkum, P. Ralph, and M. Kühl. 2012. Light gradients and optical microniches in coral tissues. Frontiers in Microbiology **3:** 1-9.

Wangpraseurt, D. and others 2014. The in situ light microenvironment of corals. Limnol Oceanogr **59:** 917-926.

Warner, M. E., W. K. Fitt, and G. W. Schmidt. 1996. The effects of elevated temperature on the photosynthetic efficiency of zooxanthellae in hospite from four different species of reef coral: a novel approach. Plant Cell Environ **19:** 291-299.

Watson, G., and D. Hessinger. 1989. Cnidocyte mechanoreceptors are tuned to the movements of swimming prey by chemoreceptors. Science **243:** 1589-1591.

Wegley, L., R. Edwards, B. Rodriguez-Brito, H. Liu, and F. Rohwer. 2007. Metagenomic analysis of the microbial community associated with the coral *Porites astreoides*. Environ Microbiol **9:** 2707-2719.

Weis, V. M., G. J. Smith, and L. Muscatine. 1989. A "CO_2 supply" mechanism in zooxanthellate cnidarians: role of carbonic anhydrase. Mar Biol **100:** 195-202.

Welty, J., C. E. Wicks, R. E. Wilson, and G. L. Rorrer. 2000. Fundamentals of momentum, heat, and mass transfer. Wiley.

Werner, B. 1959. Das Prinzip des endlosen schleimfilters beim Nahrungserwerb wirbelloser Meerestiere. Internationale Revue der gesamten Hydrobiologie und Hydrographie **44:** 181-215.

Westerweel, J., G. E. Elsinga, and R. J. Adrian. 2013. Particle image velocimetry for complex and turbulent flows. Annu Rev Fluid Mech **45:** 409-436.

White, F. M. 2010. Fluid mechanics 7th ed. Mcgraw-Hill

Wijgerde, T., C. I. F. Silva, V. Scherders, J. van Bleijswijk, and R. Osinga. 2014. Coral calcification under daily oxygen saturation and pH dynamics reveals the important role of oxygen. Biology Open **3:** 489-493.

Wijgerde, T., P. Spijkers, E. Karruppannan, J. A. J. Verreth, and R. Osinga. 2012. Water flow affects zooplankton feeding by the scleractinian coral *Galaxea fascicularis* on a polyp and colony level. J Mar Biol **2012:** 854849.

Wild, C., M. Huettel, A. Klueter, S. G. Kremb, M. Y. M. Rasheed, and B. B. Jørgensen. 2004. Coral mucus functions as an energy carrier and particle trap in the reef ecosystem. Nature **428:** 66-70.

Willert, C., B. Stasicki, J. Klinner, and S. Moessner. 2010. Pulsed operation of high-power light emitting diodes for imaging flow velocimetry. Meas Sci Technol **21:** 075402.

Yakovleva, I. M., A. H. Baird, H. H. Yamamoto, R. Bhagooli, M. Nonaka, and M. Hidaka. 2009. Algal symbionts increase oxidative damage and death in coral larvae at high temperatures. Mar Ecol Prog Ser **378:** 105-112.

Yawata, Y., O. X. Cordero, F. Menolascina, J.-H. Hehemann, M. F. Polz, and R. Stocker. 2014. Competition–dispersal tradeoff ecologically differentiates recently speciated marine bacterioplankton populations. PNAS **111:** 5622-5627.

Yonge, C. M. 1928. Feeding mechanisms in the invertebrates. Biol Rev **3:** 21-76.

---. 1930. Studies on the physiology of corals: I. Feeding mechanisms and food. Scientific Reports / Great Barrier Reef Expedition 1928-29. **1:** 13-57.

---. 1940. The Biology of reef–building corals. Scientific Reports / Great Barrier Reef Expedition 1928-29. **1:** 352-391.

Yonge, C. M., M. J. Yonoe, and A. G. Nicholls. 1932. Studies on the physiology of corals: VI. The relationship between respiration in corals and the production of oxygen by their zooxanthellae. Scientific Reports / Great Barrier Reef Expedition 1928-29. **1:** 213-251.

Yousif, M. Y., D. W. Holdsworth, and T. L. Poepping. 2011. A blood-mimicking fluid for particle image velocimetry with silicone vascular models. Exp Fluids **50:** 769-774.

Zetsche, E.-M., A. I. Larsson, M. H. Iversen, and H. Ploug. 2020. Flow and diffusion around and within diatom aggregates: Effects of aggregate composition and shape. Limnol Oceanogr **65:** 1818-1833.

Versicherung an Eides Statt

Ich, _____
(Vorname, Name, Anschrift, Matr.-Nr.)

versichere an Eides Statt durch meine Unterschrift, dass ich die vorstehende Arbeit selbständig und ohne fremde Hilfe angefertigt und alle Stellen, die ich wörtlich dem Sinne nach aus Veröffentlichungen entnommen habe, als solche kenntlich gemacht habe, mich auch keiner anderen als der angegebenen Literatur oder sonstiger Hilfsmittel bedient habe.
Ich versichere an Eides Statt, dass ich die vorgenannten Angaben nach bestem Wissen und Gewissen gemacht habe und dass die Angaben der Wahrheit entsprechen und ich nichts verschwiegen habe.
Die Strafbarkeit einer falschen eidesstattlichen Versicherung ist mir bekannt, namentlich die Strafandrohung gemäß § 156 StGB bis zu drei Jahren Freiheitsstrafe oder Geldstrafe bei vorsätzlicher Begehung der Tat bzw. gemäß § 161 Abs. 1 StGB bis zu einem Jahr Freiheitsstrafe oder Geldstrafe bei fahrlässiger Begehung.

_____
Ort, Datum, Unterschrift

Declaration on the contribution of the candidate to a multi-author article/manuscript, which is included as a chapter in the submitted doctoral thesis

Chapter 3: Ciliary vortex flows and oxygen dynamics in the coral boundary layer

Contribution of the candidate in % of the total work load (up to 100% for each of the following categories):

Experimental concept and design:	ca. 80%
Experimental work and/or acquisition of (experimental) data:	ca. 100%
Data analysis and interpretation:	ca. 80%
Preparation of Figures and Tables:	ca. 90%
Drafting of the manuscript:	ca. 80%

Chapter 4: sensPIV: Simultaneous visualization of flow fields and oxygen concentrations to unravel metabolic exchange fluxes

Contribution of the candidate in % of the total work load (up to 100% for each of the following categories):

Experimental concept and design:	ca. 15%
Experimental work and/or acquisition of (experimental) data:	ca. 30%
Data analysis and interpretation:	ca. 20%
Preparation of Figures and Tables:	ca. 20%
Drafting of the manuscript:	ca. 20%

Chapter 5: Ciliary currents and symbiont heterogeneity segregate sites of oxygen production and accumulation in the coral boundary layer

Contribution of the candidate in % of the total work load (up to 100% for each of the following categories):

Experimental concept and design:	ca. 80%
Experimental work and/or acquisition of (experimental) data:	ca. 90%
Data analysis and interpretation:	ca. 70%
Preparation of Figures and Tables:	ca. 80%
Drafting of the manuscript:	ca. 60%

Chapter 6: The role of cilia in coral suspension feeding

Contribution of the candidate in % of the total work load (up to 100% for each of the following categories):

Experimental concept and design:	ca. 80%
Experimental work and/or acquisition of (experimental) data:	ca. 100%
Data analysis and interpretation:	ca. 90%
Preparation of Figures and Tables:	ca. 100%
Drafting of the manuscript:	ca. 90%

Date: 29 / 07 / 2021

Signatures:

ALFRED-WEGENER-INSTITUT
HELMHOLTZ-ZENTRUM FÜR POLAR- UND MEERESFORSCHUNG

THE ROLE OF CILIARY VORTICES ON THE CORAL'S OXYGEN EXCHANGE AND FOOD CAPTURE

Dr. Thesis

Author: Cesar Omar Pacherres Reaño

1st Examiner: Prof. Dr. Claudio Richter
Bentho-Pelagic Processes, Alfred Wegener Institute
Bremerhaven, Germany

2nd Examiner: Prof. Dr. Michael Kühl
Marine Biological Laboratory, University of Copenhagen
Helsingør, Denmark

3rd Examiner: Dr. Eva-Maria Zetsche
Ludwig-Maximilians-Universität München
Munich, Germany

The present study was carried out from January 2017 to July 2021 at the Alfred-Wegener-Institute, Helmholtz Center for Polar and Marine Research (AWI), Bremerhaven, Germany. Additional logistical support was given by the Max Planck Institute for Marine Microbiology, Bremen, Germany. It was financed by the AWI and FONDECYT, initiative from the *Consejo Nacional de Ciencia, Tecnología e Innovación Tecnológica* (CONCYTEC), *Perú.*

Date of the doctoral colloquium: 22.09.2021

CONCYTEC | FONDECYT
Becas y financiamiento del Concytec